# Evolving plate boundaries in the Aegean–Anatolian region

*Ali Değer Özbakır*

UTRECHT STUDIES IN EARTH SCIENCES
No. 199

Members of the dissertation committee:

Prof. dr. Giovanni Bertotti
Faculty of Civil Engineering and Geosciences, TU Delft
Delft, The Netherlands

Prof. dr. Douwe van Hinsbergen
Department of Earth Sciences, Universiteit Utrecht
Utrecht, The Netherlands

Prof. dr. Liviu Matenco
Department of Earth Sciences, Universiteit Utrecht
Utrecht, The Netherlands

Prof. dr. Thomas Meier
Institute of Geosciences, Christian-Albrechts-Universität Kiel
Kiel, Germany

Prof. dr. Wim Spakman
Department of Earth Sciences, Universiteit Utrecht
Utrecht, The Netherlands

The research in this thesis was carried out at:

Tectonophysics group
Department of Earth Sciences
Faculty of Geosciences
Universiteit Utrecht
Utrecht, The Netherlands

ISBN: 978-90-6266-557-0
Printed in the Netherlands by Ipskamp


*Cover illustration: Photo of the Aegean region from the International Space Station, photo credit NASA*

# Evolving plate boundaries in the Aegean–Anatolian region

Evoluerende plaatgrenzen in het Egeïsch - Anatolisch gebied
(met een samenvatting in het Nederlands)

Proefschrift

ter verkrijging van de graad van doctor aan de Universiteit Utrecht op gezag van de rector magnificus, prof.dr. H.R.B.M Kummeling, ingevolge het besluit van het college voor promoties in het openbaar te verdedigen op vrijdag 22 november 2019 des middags te 4.15 uur

door

**Ali Değer Özbakır**

geboren op 26 juli 1980
te İstanbul, Turkije

**Promotor:** Prof. dr. J. Trampert

**Copromotor:** Dr. R.M.A. Govers

For Burcu

# Contents

# Chapter 1

# Introduction

## 1.1 Fragmentation of oceanic slabs

Tectonic plates are bounded by plate boundaries, which accommodate plate relative motions during substantial geological periods (Kearey *et al.*, 2008). The plate tectonic history of our planet shows however that plate boundaries become inoperative at some point (Molnar, 1988). For example, the completion of oceanic subduction eventually leaves an inactive suture between plates that originally were separate (Şengör, 1990). The Mediterranean region represents the plate boundary zone between two major plates, Africa and Eurasia, which is undergoing final closure (Dewey *et al.*, 1989). A bewildering recognition was that, in the western Mediterranean region, young oceanic basins were formed by slab rollback in a land-locked context (Le Pichon, 1982; Jolivet and Faccenna, 2000; Wortel and Spakman, 2000). Further complexity of the region's tectonics can partly be understood as the result of fragmentation of the plate boundaries into ephemeral segments, particularly in the eastern Mediterranean regions of Greece and Anatolia. This thesis is about these ephemeral plate boundary segments in the eastern Mediterranean.

Why is it relevant to understand a relatively small tectonic region like the Mediterranean? The motivation lies in the concept of Uniformitarianism that was first developed by James Hutton in 1788, and made popular in the 19th century by Charles Lyell: "the present is the key to the past" (Oldroyd, 1996). The processes that take place in the Mediterranean were potentially also happening in collision zones that today are in a more advanced stage of closure (e.g., Himalaya's), or where closure is complete (e.g., Appalachians). The need for information/analogies from similar regions like the Mediterranean derives from the fact that closure processes themselves eradicate potential geological observations, like underthrusting, erosion, and overprinting. So, our understanding of the Mediterranean is helpful for the interpretation of collision processes from the remaining sparse observations in historical collision zones.

An important theme in the context of the eastern Mediterranean thus is slab fragmentation. Fragmentation breaks a slab into two fragments along a more or less vertical plane (e.g. Rosenbaum *et al.*, 2008; Wortel *et al.*, 2009). In the cases where slab fragmentation has been documented, it refers to the breaking of the shallowest part of the slab only,

i.e., the deeper part remains intact. One reason for slab fragmentation is asynchronous collision or collision of a continental terrane with a continental overriding plate. Fragmentation allows the resulting slab fragments to subduct at a reduced dissipation rate, typically at a substantially lower subduction speed for the colliding segment and a higher speed with the oceanic segment. Fragmentation creates new free slab edges and results in continual active tearing of the subducting plate near the trench. The differential subduction may eventually become apparent as Subduction-Transform-Edge-Propagator (STEP) Faults in or between the surface plate(s). Govers and Wortel (2005) propose that there are quite a few STEP Faults in the Mediterranean region: near Gibraltar, Calabria, the Pannonian basin, and to the west and east of the Hellenic slab.

An active STEP involves tearing of a plate where one part is subducted and an adjacent part remains at the free surface of the Earth (Govers and Wortel, 2005) (Figure 1.1). Following subduction, the slab thus has a lateral edge. The part of the plate that remains at the surface is juxtaposed to the overriding plate by transcurrent motion along the plate boundary that separates the two plates. As argued by Govers and Wortel (2005), the relative motion along this plate boundary may differ strongly from transform faults, which is why Baes *et al.* (2011) gave it a separate name; "STEP Fault".

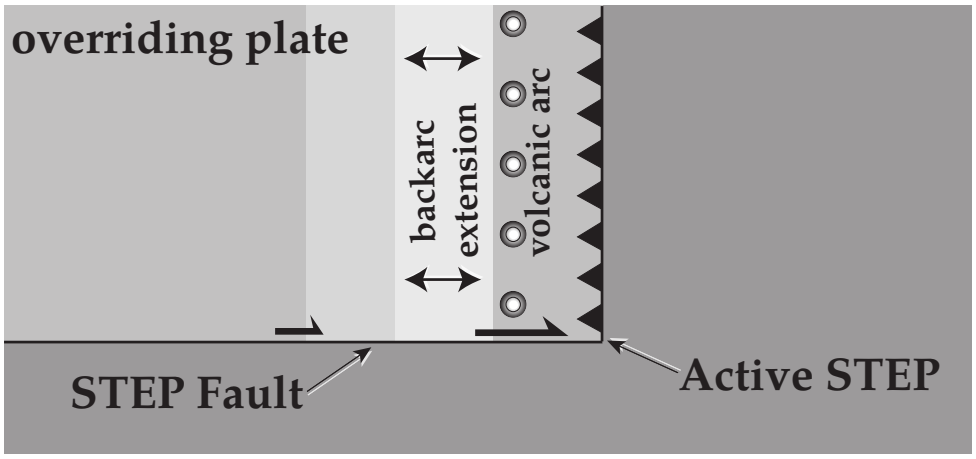


**Figure 1.1:** Schematic illustration of STEP fault.

Another way of forming STEP Faults may result from slab break-off. The Mediterranean also is the, by now classical, location of progressive slab break-off below central Italy (Wortel and Spakman, 2000). Slab tearing in this case occurs along a more or less horizontal fault to separate the deeper part of the slab from the shallower slab. Referring to late Miocene break-off of the western segment of the Apennines-Maghrebides slab beneath northern Algeria, Wortel et al. (2009) discuss scenarios for how this may have resulted

in a lateral edge along the southern Ionian slab. The resulting active STEP facilitated continued subduction and rollback towards the east of the remaining Apennines slab, and the creation of an east-west oriented STEP Fault along its southern edge between northern Sicily and the Tyrrhenian Sea. The STEP Fault along the Apulia escarpment may also have derived from break-off, in this case of the central segment of the Apennines slab beneath central Italy, that transformed into the northern lateral edge along the Ionian slab.

The role of slab fragmentation (and slab break-off) is to separate parts of the surface plate that are easily subductable, like old oceanic lithosphere, from parts that resist subduction, like buoyant continental lithosphere. In this perspective, slab fragmentation facilitates the removal from the surface of remaining oceanic lithosphere segments. Fragmentation thus minimizes the amount of oceanic lithosphere that remains in collision zones. It is important to note the difference between oceanic crust and oceanic lithosphere; oceanic crust as partially represented in ophiolites constitutes only a minor part of the oceanic lithosphere thickness, and may or may not be obducted due to fragmentation. Slab fragmentation likely is more relevant in a nearly closed oceanic basin than in an open ocean, full subduction, context, as we can conclude from the long trenches of most of the present-day subduction systems worldwide.

## 1.2 Imprints of recent plate boundary reorganizations in the eastern Mediterranean

The tectonic evolution of the Balkan-Anatolia region is the response to the overall closure of the Neo-Tethys ocean and regional back-arc basins. This closure occurred diachronously, starting in the Late Cretaceous in the Dinarides and Albanides, until the Miocene in eastern Anatolia. Major crustal sutures separate juxtaposed terranes in the present-day record; 1) the Vardar-Intra Pontides suture between the Istanbul - Rhodope - Strandja terrane in the north and the Pelagonian- Pontides/Sakarya terranes in the south; 2) the Izmir–Ankara–Erzincan suture between the Pontides terrane in the north and the Taurides/Central Anatolian Core Complex in the south; 3) The Bitlis suture separates the Taurides in the north and Arabia in the south.

Three major plate reorganizations occurred after the formation of Anatolian plate. The first phase is marked by the Bitlis – Zagros collision and slab detachment beneath the

East Anatolian High Plateau (Şengör *et al.*, 2008) and subsequent slab fragmentation below central Anatolia in Early Miocene (Bartol and Govers, 2014). The North Anatolian Fault (NAF) initiated in middle-Miocene times (Şengör *et al.*, 2005) and further developed on the pre-existing İzmir-Ankara-Erzincan Suture zone. Concomitantly, the central and east Anatolian plateaus uplifted and a surge of volcanism occurred (Keskin, 2003; Şengör *et al.*, 2005; Bartol and Govers, 2014). The deformation intensified during L. Miocene – Pliocene in response to the migration of the Cyprus slab to its present location (Govers and Fichtner, 2016) and mid-Pliocene initiation of East Anatolian Fault (Şaroğlu *et al.*, 1992; Hubert-Ferrari *et al.*, 2007, 2009). With the formation of the East Anatolian Fault (EAF), Anatolia began its westwards journey (Ketin, 1948), with respect to stable Eurasia, away from the Arabia collision zone in the eastern Turkey and Zagros, towards the Hellenic subduction zone to the southwest (McClusky *et al.*, 2000; Reilinger *et al.*, 2006). This period is also known as the Neotectonic period of Anatolia. Finally during L. Miocene – E. Pliocene modern Pliny-Strabo STEP fault formed (Özbakır *et al.*, 2013).

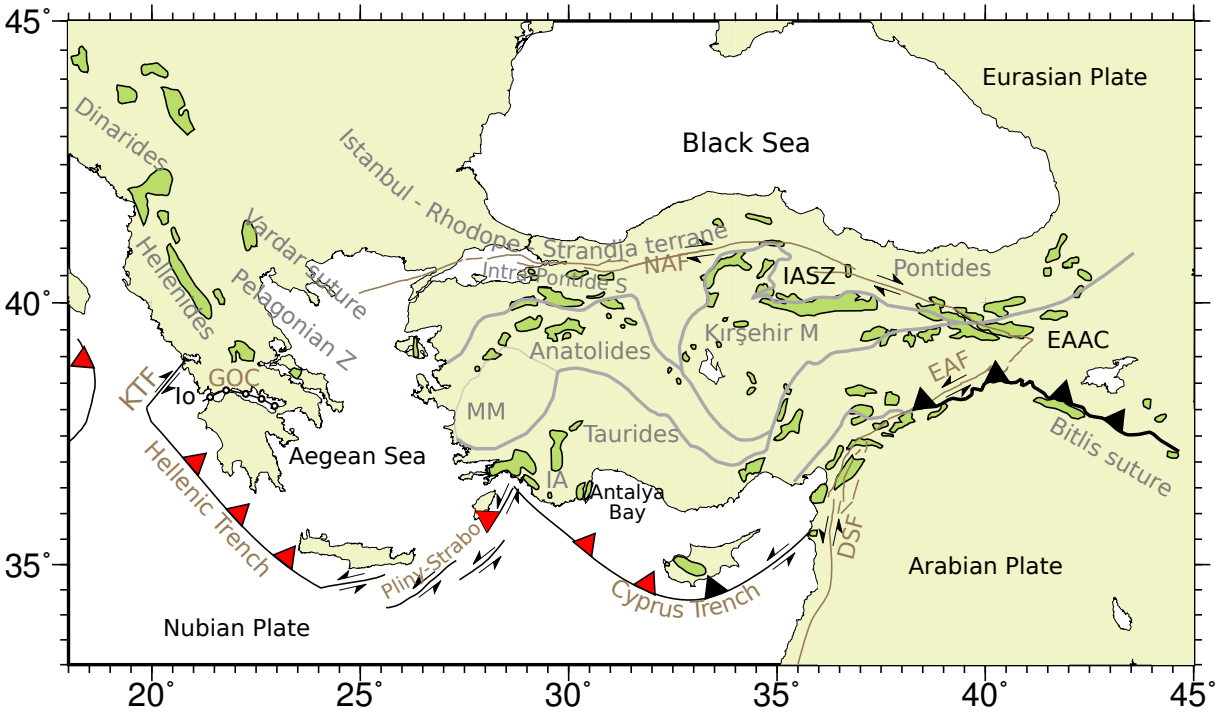


**Figure 1.2:** Tectonic setting of the eastern Mediterranean region. Abbreviations, DSF: Dead Sea Fault, EAAC: East Anatolian Accretionary Complex, EAF: East Anatolian Fault, GOC: Gulf of Corinth, IA: Isparta Angle, IASZ: Izmir Ankara Suture Zone, MM: Menderes Massif, NAF: North Anatolian Fault; KTF: Kefalonia Transform Fault; Io: Ionian Islands.

Along the Dinarides, subduction was active from Early Cretaceous to Oligocene (Handy *et al.*, 2015; Le Breton *et al.*, 2017). Continued convergence led to the foreland-propagating

nappes in the Hellenides (Underhill, 1989). The entry of continental Adriatic lithosphere in the Western Hellenic Subduction Zone initiated slab detachment under the Dinarides from the Oligocene onward (Wortel and Spakman, 1992; Schefer *et al.*, 2011; Handy *et al.*, 2015; Van Unen *et al.*, 2019). In the northern Hellenides, tightening of the orogen continues today, whereas in southern Hellenides, the thrust front has jumped to the subduction boundary south of Ionian islands in Pliocene times (Royden and Papanikolaou, 2011).

Currently, only the Hellenic slab is still actively subducting, mostly by rollback. The overriding plate shows backarc extension in the Aegean region and western Turkey. To the south of Anatolia, the west Cyprus slab segment is located beneath Antalya basin and Isparta Angle (Biryol *et al.*, 2011). Separate from that in the uppermost mantle is the (east) Cyprus slab segment below Cyprus. Both Cyprus slab segments appear to have largely stalled.

## 1.3 Methodology

Our understanding of these processes has increased greatly since the 90's of the previous century. Improvements in two research fields have particularly driven these innovations, structural seismology and kinematic geodesy. This thesis heavily uses the results from these disciplines. Tomographic studies have evolved, and continue to evolve, by using increasingly larger parts of seismograms to image Earth structure. The most recent studies have arrived at a resolution where it starts to become possible to connect the seismic velocities to regional geological features.

Geodetic studies have evolved from pioneering ephemeral GNSS (Global Navigation Satellite System, including the United States' Global Positioning System (GPS), the European Union's Galileo system, and the Russian GLONASS system), Doris and VLBI based sparse measurement networks to affordable and dense networks of GNSS instruments. The interpretation of both the tomographically imaged structures, and of the GNSS velocity models is however neither trivial, nor unique.

## 1.4 Thesis Outline

In the next chapters of my thesis, I investigate the plate boundary configuration, nature of the subducting slab and upper-plate deformation along the Hellenic – Cyprus subduction zones. Each chapter is devoted to a specific and often enigmatic sub-region in the plate boundary zone: Pliny – Strabo trenches, Anaximander mountains and the Isparta Angle, and Kefalonia Transform Fault (Figure 1.3).

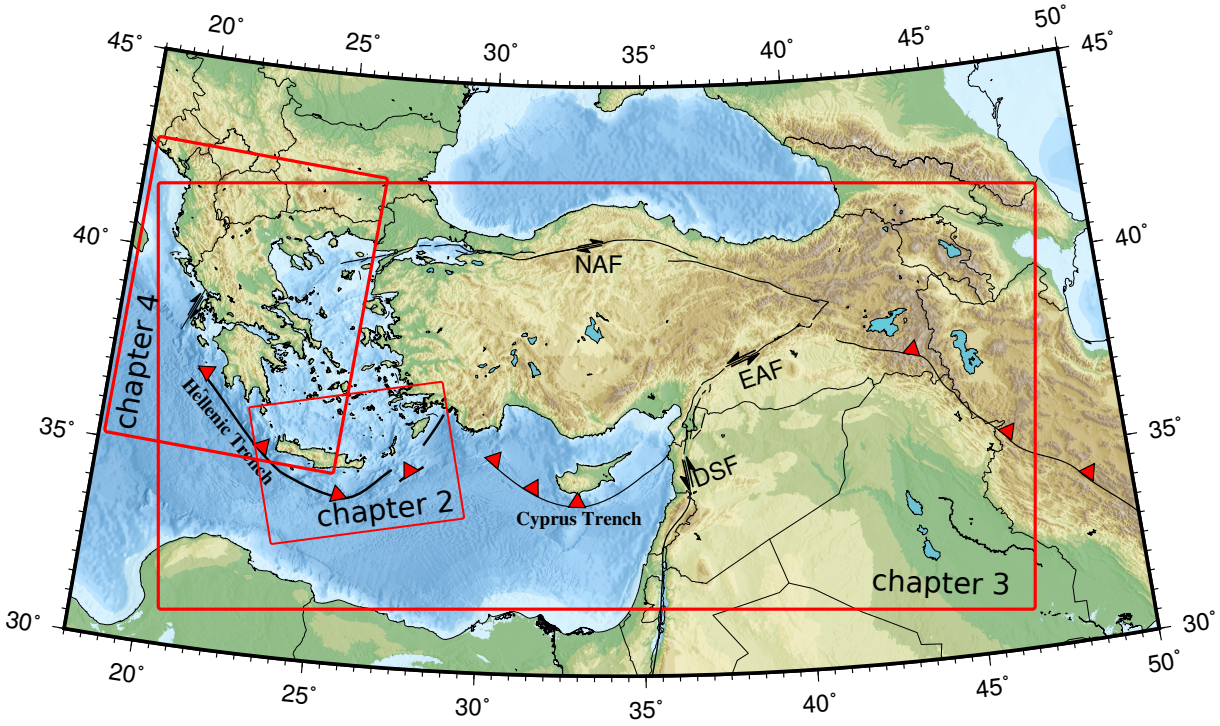


**Figure 1.3:** Roadmap to the thesis

In Chapter 2, published as Özbakır *et al.* (2013), I investigate the Pliny – Strabo "trenches", which have long been an enigmatic feature of Hellenic trench region. We address the genetic link between this deformation zone and the deeper structure and processes. Tearing of the subducting and retreating African lithosphere at the eastern end of the Hellenic trench has been known for some time and it still is an active research topic. The expression of such a tear at the Earth's surface above the tear, however, has hardly been explored. Our work involves an integrative analysis of information from several earth science disciplines, geological as well as geophysical.

In Chapter 3, published as Özbakır *et al.* (2017) I investigate the active faults in the

Anatolia – Aegean region. The Anatolia - Aegean region has been on the fore-front of geodynamics community. The region has come into existence by the accretion of (semi-)rigid blocks to the southern margin of the Eurasian plate and has undergone intense deformation. Furthermore, sub-lithospheric processes have contributed to the overall dynamics and thus shaped the style of deformation. The geodynamics involved is complex within a relatively small geographical scale. Plate boundary region from the Hellenic Arc to the Cyprus Arc is one of the major gap of knowledge in this realm. My work focuses on deformation mechanisms in and around the Anatolian – Aegean region with the aim to constrain the nature and the location of plate boundary in the transition region from the Hellenic Arc to the Cyprus Arc. To this end we use finite element method to calculate displacements and derivative fields. In addition, we address the sensitivity of the overriding plate deformation in response to the plate boundary nature and model slip rates of major faults.

In Chapter 4, which is a manuscript in preparation for submission, we study slab tears, which are a common phenomena of irregular active margins and/or convergence with lateral variation of oceanic or continental lithospheres. Western termination of Hellenic subduction zone is tentatively proposed to be a STEP, whose surface expression overlap with the Kefalonia Fault. Although the velocity structure of the western termination of the Aegean subduction zone has been focus of many seismological studies, evidences of tearing are ambiguous for the uppermost mantle due to poor volumetric resolution of the top 150 km. We use a Full Waveform Tomographic model of Fichtner *et al.* (2013) to study the earth structure and plate boundary segmentation in this region.

# Chapter 2

# Pliny – Strabo trench region: a large shear zone resulting from slab tearing[1]


## Abstract

The eastern part of the Hellenic subduction zone is composed of the Pliny and Strabo "trenches" that have been regarded as a zone of convergence between the subducting African lithosphere and the overriding Anatolian–Aegean plate. In the Pliny and Strabo "trenches", the oblique relative plate motion is generally thought to be accommodated by a typical strain partitioning consisting of strike–slip and convergence components. Notwithstanding the occurrence of strike–slip motion parallel with the Pliny – Strabo "trenches", trench-normal thrusting is not observed so far. Therefore, we conducted a detailed analysis to investigate the deformation mechanisms of the eastern part of the Hellenic Trench system. Our analyses of offshore faulting and mechanisms of earthquakes in the overriding Aegean lithosphere show that the region of the Pliny and Strabo "trenches" obeys the mechanics of the sinistral shear zone model of Tchalenko (1970). We propose that the trench perpendicular convergence is taken up by the Rhodes fold and thrust belt, which has been postulated off the southeast coast of Rhodes. Several regional P-wave tomography results give indications of a slow seismic anomaly under this zone, which is interpreted as a tear between the Hellenic and Cyprus subduction zones. The primary reason for such tear and its propagation is the ongoing rollback of the subducted part of the African lithosphere, also referred to as "the Aegean slab". Our work elucidates the surface expression of this tearing process in the form of the development of a shear zone between the Aegean lithosphere in the NW and the African lithosphere in the SE, the Pliny – Strabo Shear Zone.


[1]This chapter published as:
Ali D. Özbakır, A.M.C. Şengör, M.J.R. Wortel, R. Govers (2013). Pliny – Strabo trench region: a large shear zone resulting from slab tearing. Earth and Planetary Science Letters 375:188-195.

## 2.1 Introduction

The Hellenic subduction zone accommodates the convergence between the African plate and an internally deforming Anatolian–Aegean block (or Scholle) in the eastern Mediterranean (McKenzie, 1970; Dewey and Şengor, 1979) (Fig. 2.1). The plate boundary is well-defined between the Kephalonia Fault and eastern Crete (Fig. 2.1). Farther to the east, however, it is wider and deformation is distributed along multiple complex structures (Shaw and Jackson, 2010). It is the purpose of this paper to investigate the nature of the deformation of this eastern plate boundary zone and to place it into the context of the plate tectonic evolution of the region.

Key elements of the plate boundary region considered are the Pliny and Strabo "trenches" (Emery *et al.*, 1966) and the Ptolemy "trench", which are organized in an en-echelon fashion with an average strike of N60E (Le Pichon *et al.*, 1979; Leite and Mascle, 1982; Mascle *et al.*, 1982) (Fig. 2.1). Whereas the Ptolemy and Pliny "trenches" are more pronounced in the southwest, the Strabo "trench" is more continuous and better developed in the northeast (Le Pichon *et al.*, 1979; Jongsma, 1977).

The relative motion between the Hellenic (fore-) arc and the African plate is calculated by combining GPS velocities and MORVEL (Reilinger *et al.*, 2006; DeMets *et al.*, 2010) for the GPS stations near the eastern Hellenic Trench region (Fig. 2.1). The relative motion vectors have an azimuth of $\sim$ N196E, i.e., at an angle of $\sim 45^\circ$ with the strike of the "trenches". Various authors therefore proposed that the Pliny - Strabo plate boundary zone shows strain partitioning (e.g. Huchon *et al.*, 1982; Le Pichon *et al.*, 1995). Consistency of slip vectors from thrust earthquakes (Shaw and Jackson, 2010) and the direction of relative motion implies that the Pliny - Strabo "trenches" are accommodating the oblique Africa–Aegean convergence. Left-lateral strike–slip motion on both "trenches" has been well documented by marine geophysical studies (Le Pichon *et al.*, 1979; Leite and Mascle, 1982; Mascle *et al.*, 1982) and focal mechanism solutions (Bohnhoff *et al.*, 2005, Fig.3a; Shaw and Jackson, 2010). Thrust faults with slip vectors perpendicular to the Pliny - Strabo "trenches", however, have not been observed so far (Shaw and Jackson, 2010) and that raises the question as to how and where the trench-perpendicular convergence is accommodated. We explore this dilemma by studying the nature of the strain associated with the plate boundary zone, using published seismic and seismicity data. Despite the Ptolemy "trench" being part of the eastern Hellenic fore-arc, lack of focal mechanism solutions belonging to the Aegean lithosphere in the vicinity of Ptolemy "trench" limits our analysis to the Pliny - Strabo "trenches" area.

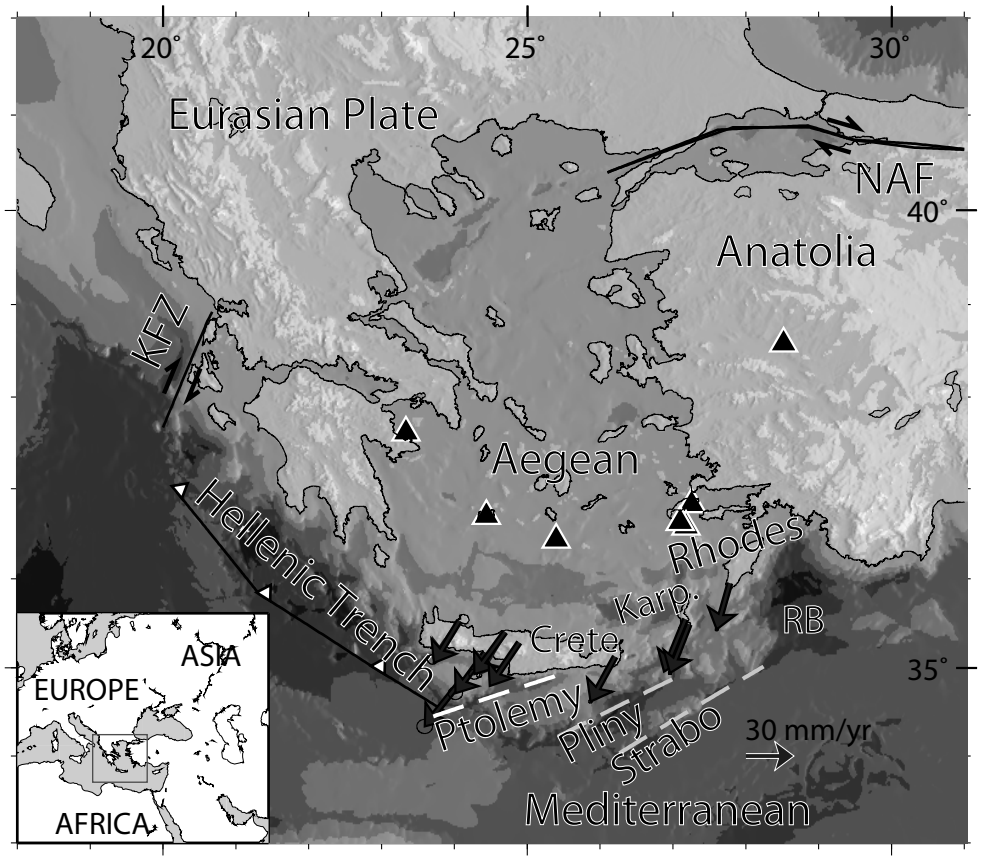


**Figure 2.1:** Bathymetry and the elements of eastern Mediterranean geodynamics. Arrows show the Aegean velocity field with respect to Africa. Dashed-lines indicate Ptolemy, Pliny and Strabo "trenches"; Triangles are volcanoes. NAF: North Anatolian fault; Karp.: Island of Karpathos; KFZ: Kephalonia fault zone; RB: Rhodes basin.

Tearing of the subducting and retreating African lithosphere, somewhat confusingly often referred to as "the Aegean slab", at the eastern end of the Hellenic trench has been known for some time and it still is an active research topic (Barka and Reilinger, 1997; de Boorder *et al.*, 1998; Govers and Wortel, 2005; Biryol *et al.*, 2011). The surface expression of such a tearing process, however, has hardly been explored, Russo's (2012) study being one of the exceptions. The tear is the first-order evidence for the link between the surface deformation and the slab at depth and most of the attempts to relate surface deformation to a slab tear comes from the eastern Hellenic Arc (e.g. seismic anisotropy studies, Brun and Sokoutis, 2010; Endrun *et al.*, 2011; Hatzfeld *et al.*, 2001; Özeren, 2012). Zachariasse *et al.* (2008) relate the evolution of vertical motions on Crete and Karpathos to a slab tear below the eastern Hellenic fore-arc. Dilek and Altunkaynak (2009) studied the evolution

and southward migration of the alkaline volcanism in western Turkey and associated this volcanism with the tearing along the cusp between Cyprus and Hellenic trenches, which is a well-resolved feature in tomograms (Biryol *et al.*, 2011; Spakman *et al.*, 1993; Piromallo and Morelli, 2003). However, so far, the surface faulting has not been related to the large scale picture. In this respect, Govers and Wortel (2005) drew attention to the role of the regional geodynamical setting, which largely controls whether the overriding plate responds to roll-back and slab tearing by extension or by advection in a (quasi-) rigid mode. From the overriding plate's response and the nature of the plate interaction in the region, a variety of surface expressions may arise. Because its lithospheric scale regional context, with oblique convergence, is relatively well-known, the Pliny - Strabo "trenches" region provides favorable conditions for an analysis of one of the possible expressions.

The results of our work position the Pliny - Strabo Shear Zone as one of the best documented expressions so far of the surface deformation associated with a Subduction Transform Edge Propagator (a STEP, a tear fault or a hinge fault; a proper definition will be given in Section 2.3). It involves an integrative analysis of information from several earth science disciplines, geological as well as geophysical. We present it as a novel contribution to the understanding of the relation between deep processes and (near-) surface deformation, a key topic in geodynamic research.

## 2.2 Data and analysis

Distributed *and* localized strike slip phenomena are ubiquitous in the region. We base our analysis on the correspondence of model shear zone structures to observations. Orientations and sense of motion of the model shear zone according to Tchalenko (1970) and Naylor *et al.* (1986) are shown in Fig. 2.2C. En-echelon shears (Riedels or R) and their conjugates (anti-Riedels or R′) develop in the early stages of deformation. The maximum shortening ($\varepsilon_3$) and extensional axes ($\varepsilon_1$) are determined by the bisector of the acute and obtuse angles between R and R′ shears, respectively. Shortening structures (S) develop perpendicularly to the $\varepsilon_3$-axis and extensional structures (E) such as normal faults, tension gashes and possibly dykes develop perpendicularly to the $\varepsilon_1$-axis. After the deformation is distributed within the grid formed by R and R′ shears, secondary P and X shears form in the later stages of deformation. P shears connect pairs of R shears, while R′ shears become passive. Finally, X shears form as antithetic faults to P shears. If the shear zone is also shortened across its strike, all R′, R and E structures will have higher angles and all X, P and S structures flatter angles to the main strike of the shear

zone (see, for example, Ramsay and Huber (1983)).

### 2.2.1 Shallow marine seismic reflection data

Fig. 2.2A shows mapped faults between western Crete and Rhodes including the area of the Pliny - Strabo "trenches" (south and southeast Crete: Mascle *et al.* (1982); south of Karpathos: Mascle *et al.* (1986); Rhodes basin: Woodside *et al.* (2000)). Blue, green and red identify thrust, strike–slip and normal faulting, respectively. Faults generally strike NNE to ESE and regional datasets show only slight variations about this trend; orange and gray distributions are calculated from maps by Ten Veen *et al.* (2004) and Mascle *et al.* (1986), respectively (Fig. 2.2A (all)).

Strike-slip faults in this region are mostly sinistral (Leite and Mascle, 1982; Woodside *et al.*, 2000) and strike in well-defined NE to ENE directions (Fig. 2.2B). Furthermore, the HEAT-4 site (Fig. 2.2A) displays evidence that these sinistral faults are connected with N10W (Le Pichon *et al.*, 1979) or N40W (Peters and Huson, 1985) orientated dextral strike-slip faults. Normal faults are the most common faults in the region (Fig. 2.2B). They are not concentrated in a narrow azimuth interval but strike in a broad directional spread from NNE to ESE. Thrusts are the least common type of faulting and they strike mainly in an ESE direction (Fig. 2.2B). Folds are more common than thrusts and their strikes are compatible with that of the thrusts.

Model predicted elements of a N60E trending sinistral shear zone are drawn in Fig. 2.2C (Tchalenko, 1970; Naylor *et al.*, 1986). The strike–slip fault orientations of our analysis are compatible with Riedel Shears (R) and/or P shears. Furthermore, N10W or N40W dextral strike–slip faults are closely associated with Anti-Riedel shears (R′) and/or X shears (Fig. 2.2C). NNE to NE striking normal faults are compatible with theoretical extension directions (E), while fold and thrust orientations agree with the direction of shortening structures (Fig. 2.2C). We could not associate ENE to ESE striking normal faults to elements of the Tchalenko shear zone model but these directions better agree with those of faults as observed in the fore-arc to the west. Also they may be related to the formation of pull-apart basins formed by coupled X and R shears. Overall, the offshore faulting data fit closely with an ideal sinistral shear zone parallel to the trend of Pliny–Strabo "trenches".

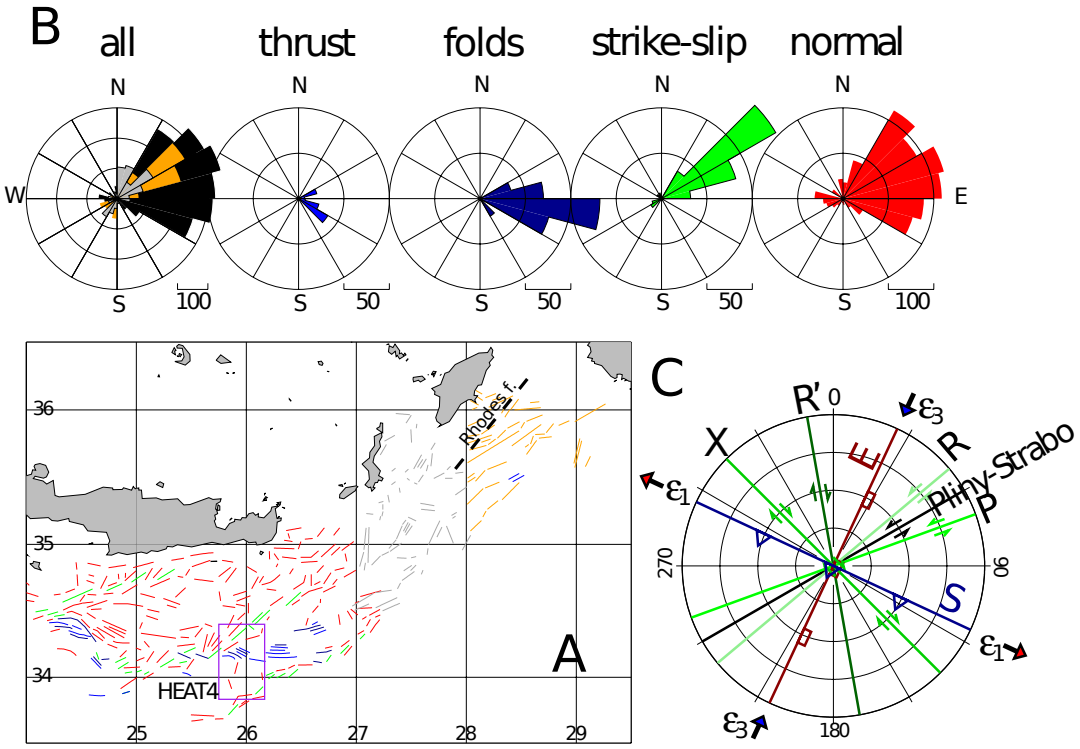


**Figure 2.2:** Analysis of faulting and folding. (A) Mapped offshore faults. Colored line segments indicate sinistral strike–slip (green), normal faulting (red), and folding–thrusting (blue) (Mascle *et al.*, 1982, 1986; Woodside *et al.*, 2000). Faults with reliable strikes and unclear sense of motion are colored in gray and orange, respectively (data from Mascle *et al.* (1986) and Ten Veen *et al.* (2004), respectively). HEAT project site 4 shown within purple frame. (B) Polar histograms of the observed faults and folds. First histogram shows all types faulting by Mascle *et al.* (1982) (black), Mascle *et al.* (1986) (gray) and Ten Veen *et al.* (2004) (orange). Other histograms show direction of faulting for identified faults. (C) Faulting with sense of motions and strain directions according to the Tchalenko (1970) and Naylor *et al.* (1986) shear zone model

### 2.2.2 Focal Mechanism Solutions

We use focal mechanisms of significant earthquakes (Mw$\geq$ 5.0) within the Aegean lithosphere (<42 km depth) as compiled by Shaw and Jackson (2010). Seismic faulting occurs predominantly by strike–slip and thrusting (Fig. 2.3). Here, no thrust faults with strikes parallel to the Pliny–Strabo "trenches" exist (Shaw and Jackson, 2010). This inference agrees with our shear zone interpretation of the offshore faulting data (Fig. 2.2B (thrusts)) with the possible exception of a major fault southeast of Rhodes that has been interpreted as a large, but aseismic thrust (Woodside *et al.*, 2000, Fig. 6a). In Fig. 2.3B, we consider the correlation between focal mechanisms and the Tchalenko shear zone model. Fig. 2.3B clearly shows that one or both of the focal planes correspond to an element of the model

sinistral shear zone (Fig. 2.3A, bottom right).

The correspondence between mechanisms 2, 8, and 9 and the sinistral shear zone is not immediately obvious and these mechanisms are indicated with an asterisk in Fig. 2.3. Mechanism 2 is probably a rotated and shortened R′. The R′ fractures are early locked and rotate into a position that favors shortening on them (Tchalenko, 1970). Mechanisms 8 and 9 are here interpreted as products of an X-shear coupled with two R shears, one at the top and one at the bottom. X-shears start opening up as a pull apart with a slight right-lateral shear along its bounding normal faults. This is precisely what is seen on the fault-plane solutions corroborating an old truism: not all earthquakes are nucleated on pristine rock. Often they employ pre-existing structures. When many faults work close to each other, they move not necessarily following the ideal stress orientations. Mechanism 14 is either a very steep normal fault or a low-angle extensional detachment fault. Overall, we find that focal mechanisms are in agreement with our interpretation of a wide, sinistral, Pliny–Strabo plate boundary zone.

### 2.2.3 How our findings fit the conclusions of previous work

For Crete, Ten Veen and Kleinspehn (2003) showed sinistral movements on ENE–WSW faults and an overall NW–SE extension, which they referred to as wrench tectonics, and which are compatible with our findings for the broad shear zone on the Hellenic fore-arc. This wrench tectonics is dated as post-medial Pliocene to early Pleistocene (Peterek and Schwarze, 2004). Wrench tectonics has been proposed for the Hellenic fore-arc region but without any clear evidence and a detailed analysis (e.g. Chaumillon and Mascle, 1997). Active normal faults in Karpathos and Rhodes document NW–SE extension (Mascle *et al.*, 1986), yet the extensional deformation is not significant for the Rhodes Basin, except for the superficial normal faulting (Hall *et al.*, 2009). These observations are consistent with our interpretation of the Pliny–Strabo shear zone (Fig. 2.2C).

## 2.3 Results

### 2.3.1 Subduction–Transform–Edge–Propagator (STEP) fault zone

From the previous analysis, we conclude that the relative velocity component parallel to the Pliny–Strabo "trenches" is accommodated in the Pliny–Strabo plate boundary region. To appreciate the significance of this observation, it is imperative to consider the evolution of the retreating African slab ("the Aegean slab") in the regional context. Specifically

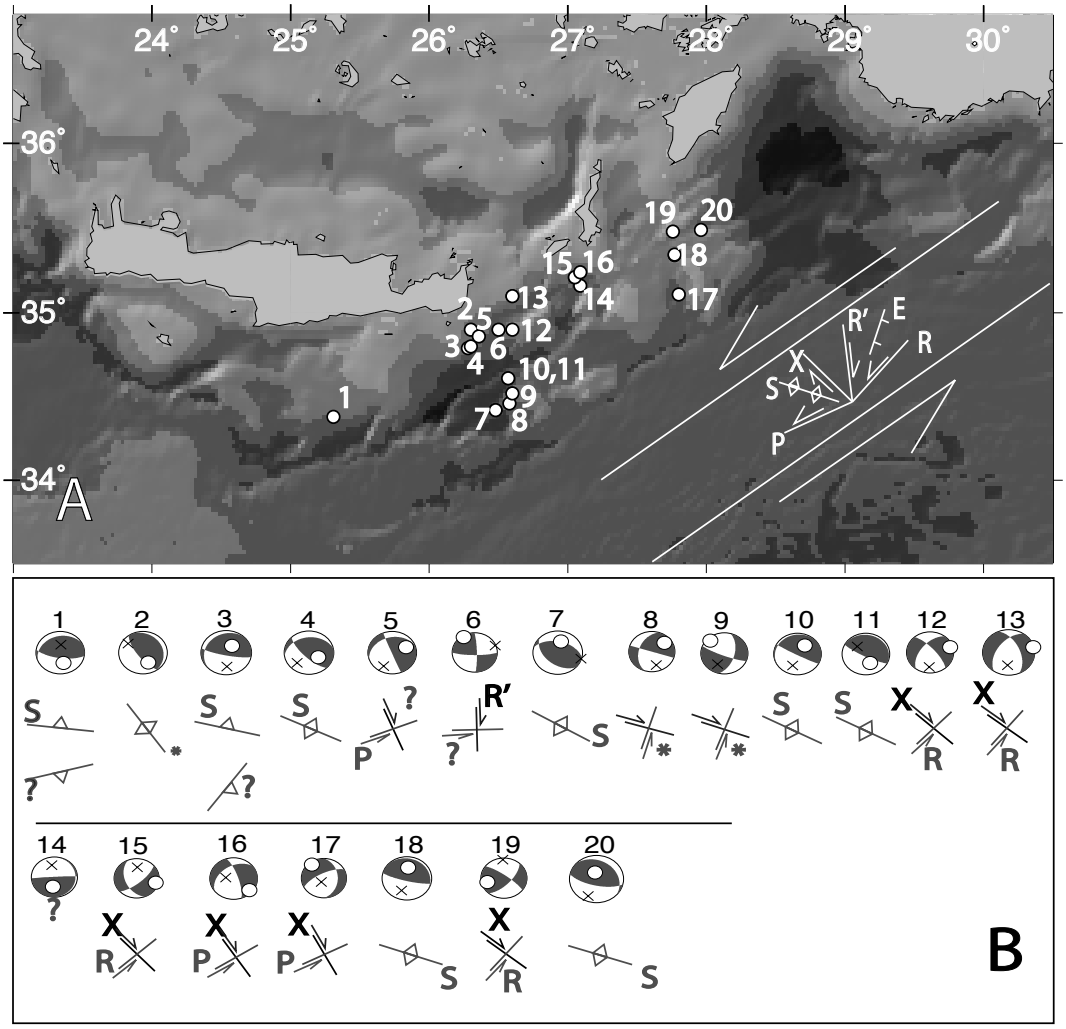


**Figure 2.3:** Analysis of the seismicity. (A) Locations of earthquakes analyzed. Elements of the Tchalenko model are shown to the SE from the actual shear zone for clarity. The position of the schematic shear zone is arbitrary, as a visual guide. (B) Fault mechanism solutions (data from Shaw and Jackson (2010)) and their correlation with an element of a N60E striking sinistral shear zone. Circles and crosses on each beach-ball represent the T and P axes, respectively. Mechanisms in which the correspondence between the sinistral shear zone is not immediately obvious are indicated with an asterisk and discussed in the text.

important is the observation from seismic tomography that the slab has an edge here (Wortel and Spakman, 2000; Biryol *et al.*, 2011). Following Wilson (1965), Isacks *et al.* (1968) and Şengör (1983), Govers and Wortel (2005) argue that continued subduction requires tearing of the subducting plate. The region of active tearing is referred to as a Subduction-Transform-Edge-Propagator or STEP. The (typically wide) deformation zone that remains at the surface in the wake of the active STEP is referred to as the "STEP fault" (Fig. 2.4) (see also Baes *et al.* (2011)). We propose that the Pliny–Strabo plate

boundary zone is part of the STEP fault surface expression associated with STEP activity at the edge of the retreating African slab. As a result of its immaturity, strain has not localized onto a single fault, i.e., it is probably a wide deformation zone at all depths (Şengör, 1983). Hence, the Pliny– Strabo "trenches" do likely correspond to linked Riedel and P shears in the context of a wider plate boundary zone.

Plate boundaries that have been stable for a long time are narrower than plate boundaries that have been subject to recent change, as can be observed in the results of Kreemer *et al.* (2003). We therefore infer that new plate boundaries largely develop to become more localized with increasing strain.

Becker *et al.* (2010) observed low microseismic activity in between the Ptolemy and Pliny "trenches". This observation indicates that the STEP fault is localized on the Ptolemy "trench" only near the active STEP, i.e. here the deformation zone is not broad as in the Pliny–Strabo "trenches".

### 2.3.2 Where is the convergence accommodated?

As we already pointed out, the African and the Anatolian–Aegean plates are juxtaposed along the PSSZ and the observed deformation mainly occurs in the overriding Aegean lithosphere. Our analysis shows that the surface deformation and the seismicity pertain only to the strike–slip motion to the SE of Rhodes. The component of the relative motion between Africa and the Anatolia–Aegean plate perpendicular to the PSSZ (Fig. 2.1) implies the convergence to be accommodated somewhere. Nevertheless, no shortening directions are reported from earthquakes located within a possible plate interface (Shaw and Jackson, 2010).

Sodoudi *et al.* (2006) imaged a NW dipping lithosphere–asthenophere boundary at the eastern Hellenic arc on a NW–SE cross-section near Rhodes by using receiver functions. However, this interface may correspond to the curved section of the amphitheater shaped Hellenic slab (Hatzfeld and Martin, 1992). Shaw and Jackson (2010) anticipate a relatively shallow north-dipping interface as a possible candidate. It is possible that such a north-dipping slab belongs to the northward dipping subducting African lithosphere to the west of the tear.

We propose that shortening and/or thrusting occurs along a NW dipping deformation zone that is located in the NE continuation of the PSSZ. There, i.e., in the Rhodes basin,

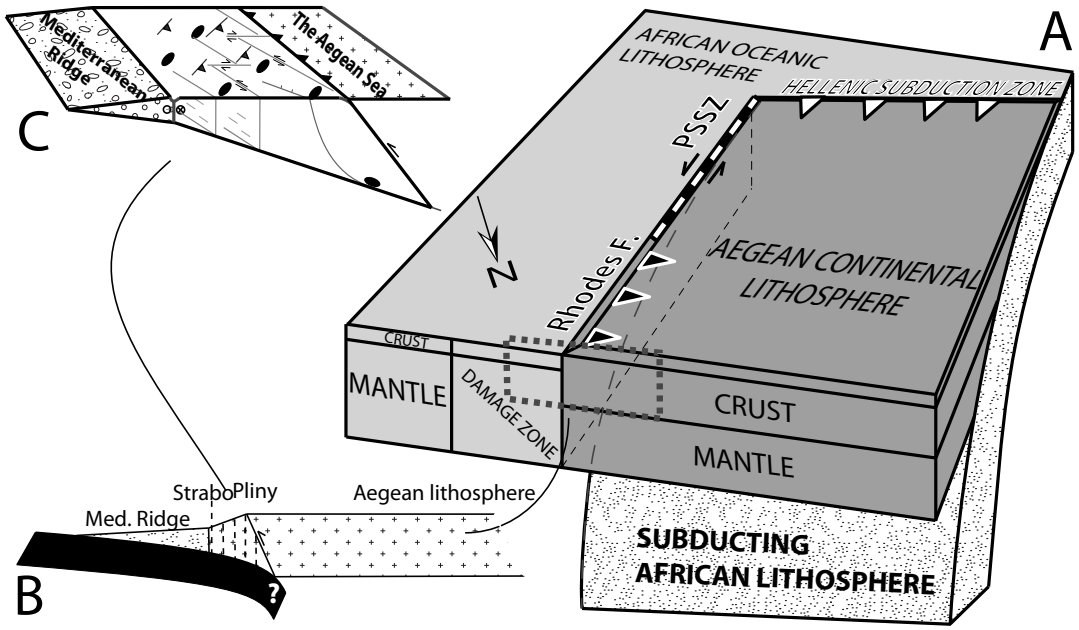


**Figure 2.4:** (A) Block diagram schematically indicating the structure of the eastern part of the Hellenic subduction zone (modified from Baes *et al.* (2011)). The structure indicated in (A) can be seen as a schematic indication of the starting situation upon which the effect of compression should be superimposed. Triangles with white and black fill indicate subduction and thrusting, respectively. The dents next to the Rhodes fold and thrust belt (Rhodes F.) indicate extent of the shear zone. (B) More detailed (albeit still schematic) representation of the geometry of the plate boundary region of the eastern part of the Hellenic arc within the (approximately) rectangular box indicated in (A). (C) Predicted styles of deformation along the Pliny–Strabo Shear Zone.

Hall *et al.* (2009) found evidence in the bathymetry and shallow seismics for folding and thrusting (Fig. 2.5). A NW dipping thrust fault has been tentatively identified in reflection profiles off the SE coast of Rhodes (Woodside *et al.*, 2000, Fig.6a; Ocakoğlu, 2012), which may be linked to vertical motions observed in Rhodes (Kontogianni *et al.*, 2002). Furthermore, mud volcanoes, which are associated with compression and subduction zones (Kopf, 2002) are mapped in the whole outer arc (Huguen *et al.*, 2001, 2006), including the Pliny–Strabo trenches and the southern margin of the Rhodes basin –although the existence of mud volcanoes might be due to the thin-skinned tectonics. We believe that it is as yet unclear whether convergence here is localized along a discrete interface or distributed over a wider shear zone. Given sufficient convergence, this deformation zone may develop into subduction initiation of the African lithosphere (SE) under the Aegean (NW). The inherited damage zone formed during STEP propagation is a key element in assisting the process of subduction initiation (Baes *et al.*, 2011). Further to the SW, available shallow seismic sections perpendicular to PSSZ show no evidence for shortening accommodated by NW dipping thrust faults (e.g Jongsma, 1977; Leite and Mascle, 1982;

Chaumillon and Mascle, 1997; Huguen *et al.*, 2001). One explanation would be that here the evidence would be invisible due to the coverage by the Mediterranean Ridge. We prefer the alternative interpretation that, due to the progressive development of the STEP fault, more convergence has occurred perpendicular to the STEP fault in the (older) NE than in the (more recently developed) SW.

Strain can be partitioned in most diverse ways depending on the convergence angle, thermal regime of the arc/forearc systems, the behavior of the mantle below arcs and inherited structures from old convergence or tearing. Our conclusion rests mainly on the last, markedly different from a typical strain-partitioning hypothesis (e.g. Fitch, 1972, *sensu* Sumatra), as applied to the eastern Hellenic Arc by Le Pichon *et al.* (1995) and Shaw and Jackson (2010).

## 2.4 Discussion

The recent study by Baes *et al.* (2011) indicates that subduction initiation is a likely response to (a component of) convergence perpendicular to a recently formed STEP fault. Such a STEP fault will possibly allow for the down-bending of the free edge of the surface part of the African lithosphere under the Aegean. Rhodes basin is an enigmatically deep basin (∼4 km depth) possibly foundered in post-Miocene times (Woodside *et al.*, 2000), where the convergence might involve under-thrusting of the oceanic Rhodes basin beneath the Aegean lithosphere.

Rhodes Basin consists of a broad NE–SW trending strike–slip zone with predominant compression inferred from kilometer scale thrust relief (Hall *et al.*, 2009) and superficial extension (Ten Veen *et al.*, 2004). A positive flower structure found near the Pliny trench (Woodside *et al.*, 2000) also supports the transpressional regime (see also Ocakoğlu (2012) for the evidences of transtensional and transpressional regime in between Rhodes and the Turkish mainland). Furthermore, high quality shallow seismic sections presented by Hall *et al.* (2009) allow for a pre-Pliocene (Messinian) thrust origin and later Plio-Quaternary sinistral transpression. Moreover the same work shows that the majority of the present-day deformation is accommodated by thrusting, whose strike is compatible with the strike of thrusting required by our model.

Ocakoğlu (2012) used shallow seismic reflection profiles and detailed bathymetry to study the area between the Turkish mainland and the Rhodes Basin. She concluded that trans-

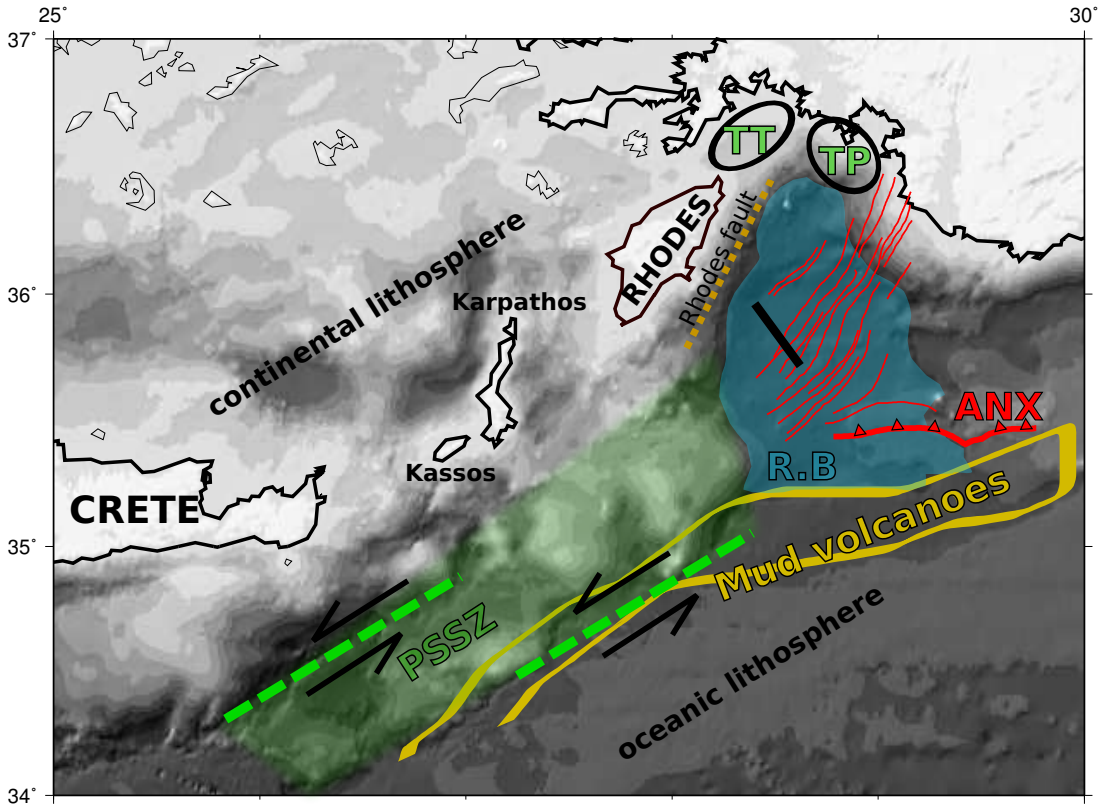


**Figure 2.5:** Summary figure showing the deformation agents near the PSSZ and Rhodes. The green dashed lines and the green transparent area are the PSSZ; yellow ribbon is the extent of the mud volcanism (Huguen *et al.*, 2006); transparent blue region is the Rhodes basin (R.B); dotted orange line segment off the SE coast of Rhodes is the Rhodes fault (after Kontogianni *et al.* (2002)); thick red teethed line indicates the eastern Mediterranean lithosphere underthrusting below Anaximander Mountains (ANX); red thin line segments show Hall *et al.*'s (2009) fold and thrust belt; thick black line segment is the seismic reflection line in which Woodside *et al.* (2000) identified a transpressional fault perpendicular to it; TT and TP refers to the transpression and transtensional zones of Ocakoğlu (2012), with bounding ellipses indicating their extent.

pression and transtensional faults evolved independently, and that they belong to different fault zones. Such an interpretation ignores the fact that this area is a broad deformation zone.

### 2.4.1 Age of the shear zone and evidences for the propagation of STEP

The deformation related to PSSZ has been active since the Pliocene, according to basin analyses, structural interpretations in Crete (Ten Veen and Kleinspehn, 2003; Peterek and Schwarze, 2004; Zachariasse *et al.*, 2008) and vertical motions pattern in Karpathos. Moreover, vertical motions of Pliocene age from Crete, Karpathos (Zachariasse *et al.*,

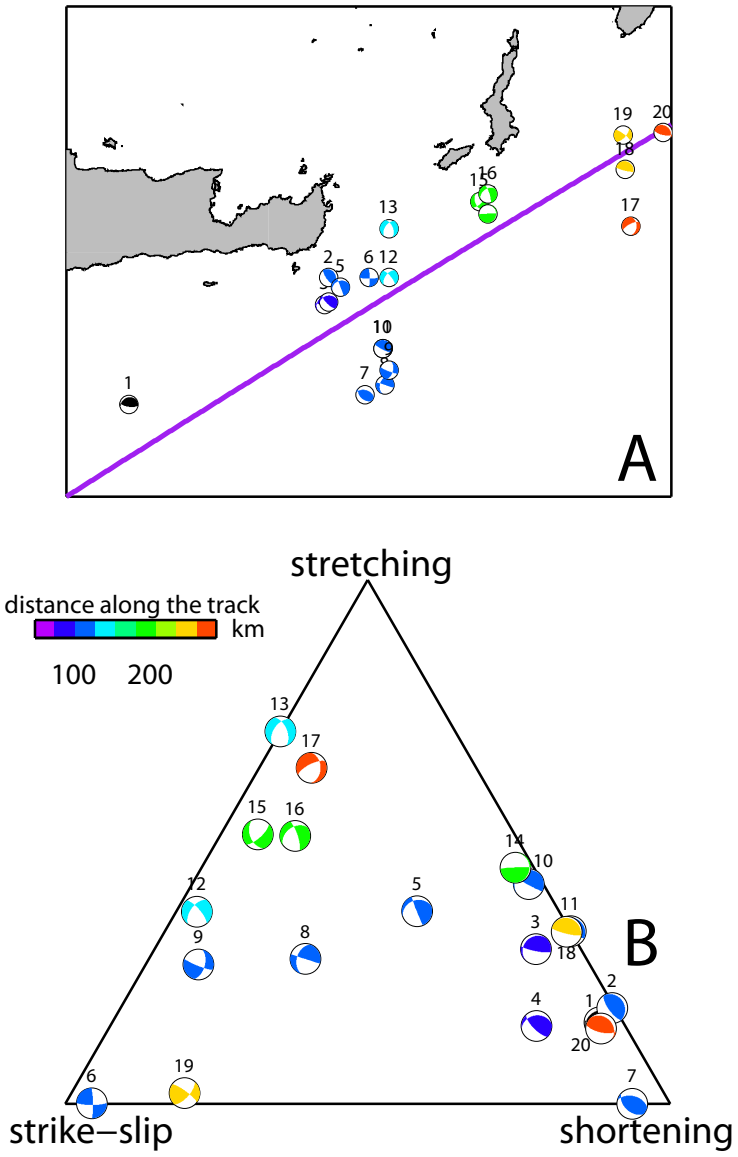


**Figure 2.6:** (A) Focal mechanisms colored according to their distance along the purple line, which roughly shows the strike of PSSZ. The distance is measured from the tip of the active STEP. (B) Ternary diagram of focal mechanisms with color coded spatial distributions.

2008) and Rhodes (Kontogianni *et al.*, 2002) corroborate the mode of propagation of vertical motions as a result of STEP activity (Govers and Wortel, 2005). That uplift of Karpathos occurred simultaneous with that in eastern Crete (within the resolution of the observations) suggests that the STEP propagated fast here. Considering the evolution of the Rhodes basin (after Hall *et al.* (2009)): if indeed the (active) STEP was near Rhodes basin in the Pliocene, then the pre-Pliocene compression is unrelated to STEP activity.

The Rhodes segment has predominantly a fault-perpendicular degree of freedom, whereas PSSZ has a fault-parallel degree of freedom. Different degrees of freedom on the segments which accommodate the Africa–Aegean relative motion facilitates the rotation of the eastern Hellenic Arc. Palaeomagnetic studies document average rates of Plio/Pleistocene anti-clockwise rotations on the islands of Kassos, Karpathos and Rhodes (Duermeijer *et al.*, 2000). However, the resolution of this data is quite low and error margins are high to evaluate whether there is progression in the rates of rotations due to STEP propagation.

### 2.4.2 Trends in focal mechanisms?

Our analysis of focal mechanisms and regional faults supports an overall interpretation of the Pliny–Strabo trench system as a STEP fault. One consequence of the STEP scenario is that the STEP fault system is expected to be younger in the SW than in the NE. The seismicity pattern in Fig. 2.3 shows no evidence of strain localization from SW to the NE. Fig. 2.6 shows focal mechanisms color-coded as a function of the distance from the active tip of the STEP. The ternary plot (Frohlich, 1992, 2001) illustrates that there is no correlation of focal mechanism type with distance along the STEP fault. Thus, although available seismicity data show significant variations in strain along the Pliny–Strabo system, they do not allow us to recognize sub-regions with transtension or transpression, or systematic variations with the (local) age of the STEP fault.

This is noteworthy, but not surprising. Direct evidence for propagating tear faulting through normal faulting focal mechanisms is rare, the STEP at the northern edge of the Tonga slab being a prominent exception (Millen and Hamburger, 1998). The uniquely high convergence rate (of approximately 20 cm/yr Bevis *et al.*, 1995) at the northern part of the Tonga trench–almost an order of magnitude higher than at the Hellenic trench–and the correspondingly high propagation rate of this STEP may well account for this special situation. The lack of expression of a migration aspect in the STEP-fault can further be understood by taking into account the role of the overriding plate, in this case the Aegean lithosphere. STEP faults are the near-surface expressions of the tearing process in the (partially) subducting lithosphere. The nature of the fault, or rather deformation zone, is strongly controlled by the setting of the overriding plate. If the overriding lithosphere can "follow the retreating trench" in a coherent manner, as is the case in the Pliny–Strabo region, the STEP fault will be active along its full length and to first order the fault zone may resemble a transform type of fault zone, without a clear trace of fault propagation. If, however, the overriding lithosphere cannot follow the trench coherently, internal extensional deformation occurs. The locus of extensional deformation may migrate along with

the trench migration and the recent activity along the STEP fault will be concentrated or even limited to the segment above the tip of the migrating STEP tear. The latter scenario can be identified in the Tyrrhenian Sea region, with evidence for highly episodic extension and SE migration of extensional activity from the Vavilov Basin (Early Pliocene) in the central Tyrrhenian Sea to the Marsili Basin (Early Pleistocene) in the southeastern part (Nicolosi *et al.*, 2006; Guillaume *et al.*, 2010).

Since the publication of Özbakır *et al.* (2013), several studies contributed to the understanding of slab geometry in the eastern termination of the Hellenic/Aegean subduction zone (e.g. Sodoudi *et al.*, 2015; Howell *et al.*, 2017; Portner *et al.*, 2018; Bocchini *et al.*, 2018). Here I discuss the consequences of the new observations and insights for our paper.

Sodoudi *et al.* (2015) analyze well-constrained Wadati-Benioff zones dipping into northwesterly directions that outline uninterrupted seismicity from the Pliny-Strabo plate contact to <180 km depth. They are correct by pointing out that existing travel-time tomographic studies have limited resolution in this depth range. Bocchini *et al.* (2018) further refine the Wadati-Benioff zone beneath the Karpathos-Rhodes segment from 40 km down to 180 km depth. They conclude that active subduction occurs beneath the Pliny-Strabo trenches, i.e., they argue against a free edge in the down-going Hellenic/Nubian slab and the interpretation by Özbakır *et al.* (2013) of the Pliny-Strabo shear zone as the corresponding STEP fault.

These new constraints on the Wadati-Benioff zones significantly improve our understanding of the shallow upper mantle below the eastern Aegean region. I believe that these new observations do not contradict the essence of our STEP fault model, but that it will require some modification to account for these new constraints. First about the essence; our 2013 study was based on two pillars, the imaged edge of the Hellenic slab which was resolved in tomographic studies >200 km depth (Biryol *et al.*, 2011; Bijwaard and Spakman, 2000; Piromallo and Morelli, 2003), and the kinematic indicators of surface faulting and mechanisms of near-surface earthquakes. The study of Portner *et al.* (2018) confirms the existence of a slab edge deeper than 200 km. Our kinematic analysis demonstrated a predominant strike-slip component in the relative motion that is accommodated along the Pliny-Strabo trenches, i.e., approximately parallel to the direction relative motion of the Aegean with respect to Nubia (Reilinger *et al.*, 2006; Howell *et al.*, 2017). I therefore still think that the

Pliny-Strabo trenches represent a STEP fault as the surface expression of lithospheric tearing at depth.

The modification of our model derives from the realization that we assumed that the development of the slab edge occurred by efficient tearing at the active STEP (which presently would be located to the south of eastern Crete). The new observations suggest however that the tearing process is relatively slow. Consequence is that the lateral edge of the Hellenic slab is being stretched while sinking below the Pliny-Strabo region. Meanwhile, the overriding Aegean plate continues to track the SSW rollback of the Hellenic trench, resulting in mostly strike-slip motions along the Pliny-Strabo trenches. This interpretation is consistent with both the imaged slab-like Wadati-Benioff zones (Sodoudi *et al.*, 2015; Bocchini *et al.*, 2018), and with down-dip extension (Howell *et al.*, 2017). This modified interpretation of our STEP fault hypothesis is well amendable to further testing.

## 2.5 Conclusions

We show that the offshore shallow seismic reflection and earthquake mechanisms data from the Pliny–Strabo "trenches" region are in excellent agreement with the directions and sense of faulting, and the strain ellipse predicted by the Tchalenko (1970) shear zone model. The "trenches" are part of a shear zone in the Hellenic subduction fore-arc, intensely deformed by STEP fault activity. The Pliny and Strabo "trenches" themselves most likely correspond to linked Riedel shears. The Pliny–Strabo Shear Zone is one of the best-documented deformation zones above a subduction tear so far. The eastern Hellenic arc accommodates the Aegean–Africa convergence in a unique way, which is controlled by the propagating STEP fault, by a shear zone in the PSSZ and a fold and thrust belt in Rhodes basin.

## Acknowledgements

Figures 1-3,5 and 6 are created using GMT software (Wessel and Smith, 1998). ADO is funded by the Netherlands Research Center for Integrated Solid Earth Science (ISES). We thank Jeremy Hall and two anonymous reviewers for their comments which improved the manuscript significantly.

# Chapter 3

# Active faults in the Anatolian–Aegean plate boundary region with Nubia[1]


## Abstract

Convergence of the Africa, Arabia, and Eurasia plates and the westward escape of Anatolia have resulted in an evolving plate boundary zone in the Eastern Mediterranean. The current location and nature of the plate boundary between the Anatolian and the African plate is difficult to trace due to the scattered crustal earthquakes and the absence of deep ones. We examine various types and locations for the plate boundary as constrained by seismicity, seismic reflection studies, tomographic studies, and geodetic measurements and we use a spherical plane stress finite element model to test these possibilities. In our regional model, we impose the convergence of Africa, Arabia, and stable Eurasia by applying GPS-derived velocities in the far-field, as well as the roll-back of the Hellenic trench to solve for regional deformation. Model velocity and stress fields are compared with GPS-derived velocities and stress directions from focal mechanism solutions. We find that the plate boundary via the Pliny and Strabo trenches, the Anaximander Mountains, the Eratosthenes Seamount collisional segment, and the Latakia-Larnaka ridges gives the best fit to the data. The Anaximander Mountains plate boundary has both down-dip and strike-slip motions, and the Latakia segment is pure strike-slip. The Cyprus subduction contact is 42% locked. From a combined analysis of indicators for long-term deformation (predominantly slip-rates on major faults) and model results we infer that this southern plate boundary configuration may have existed since the Late Pliocene.


**Keywords:** Space geodetic surveys, kinematics of crustal deformation, finite element modeling, stress and velocity field of the Anatolia– Aegean region, NAF slip-rates


## 3.1 Introduction

The Anatolian-Aegean region is located in the zone of convergence between the Africa, Arabia, and Eurasia plates (McKenzie, 1972) (Figure3.1). Essentially, the Anatolian -


[1]This chapter is published in Turkish Journal of Earth Sciences as:
Ali D. Özbakır, R. Govers, R. Wortel (2017). Active faults in the Anatolian–Aegean plate boundary region with Nubia. 26, 30-56. DOI:10.3906yer-1603-4

Aegean region has come into existence by the accretion of (semi-)rigid blocks to the southern margin of the Eurasian plate and it has undergone intense deformation. Presently, Anatolia moves westwards with respect to stable Eurasia (Ketin, 1948), from the Arabia collision zone in eastern Turkey and the Zagros region towards the Hellenic subduction zone to the southwest. Some of the regional plate boundaries are well defined: the North Anatolian Fault (NAF) accommodates the motion of Anatolia relative to Eurasia, and the East Anatolian Fault (EAF) accommodates the motion relative to Arabia (McKenzie, 1976; McClusky *et al.*, 2000). The plate boundary along the Hellenic arc is well defined in western Greece, south of the Peloponnese and Crete (Taymaz *et al.*, 1990; Baker *et al.*, 1997; Shaw and Jackson, 2010).

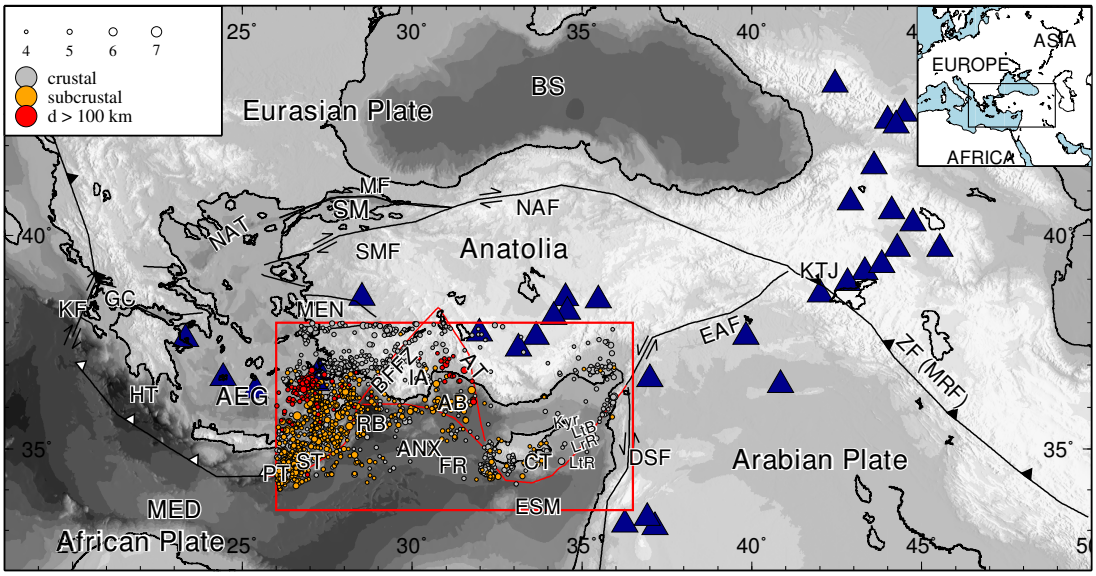


**Figure 3.1:** Tectonic setting of the Eastern Mediterranean. We mainly focus on the location and nature of (possible) plate boundaries (red line segments) in the boxed region. Triangles on faults with black and white filling indicate collision and subduction zones, respectively. Conjugate arrows indicate the strike-slip character of faults; normal faults have no additional labels. Seismicity in the box is shown for the period of 1973–2009 (NEIC, `https://earthquake.usgs.gov/earthquakes/search/`, Last Accessed:02-07-2019). The distinction between crustal and subcrustal earthquakes is based on the Moho depth map of Grad *et al.* (2009). Loci of subcrustal and deep seismicity are Hellenic and Cyprus trenches. Blue triangles indicate active volcanism. Abbreviations: AB, Antalya Basin; AEG, Aegean Sea; ANX, Anaximander Mountains; AT, Aksu Thrust; BFFZ, Burdur Fethiye Fault Zone; BS, Black Sea; CT, Cyprus Trench; DSF, Dead Sea Fault; EAF, East Anatolian Fault; ESM, Eratosthenes Seamount; FR, Florence Rise; GC, Gulf of Corinth; HT, Hellenic Trench; IA, Isparta Angle; KF, Kephalonia Fault; KTJ, Karlıova Triple Junction; Kyr, Kyrenia Ridge; LrT, Larnaka Ridge; LtB, Latakia Basin; LtR, Latakia Ridge; MED, Mediterranean Sea; MEN, Menderes Massif; MF, Marmara Fault; NAF, North Anatolian Fault; NAT, North Aegean Through; PT, Pliny trench; SM, Sea of Marmara; SMF, Southern Marmara Fault; ST, Strabo Trench; ZF, Zagros Fault (Main Recent Fault).

Özbakır *et al.* (2013) recently proposed that the Pliny and Strabo trenches in the eastern part of the Hellenic arc represent the surface expression of a STEP type of plate boundary (Govers and Wortel, 2005), as such referred to as a STEP *fault* (Baes *et al.*, 2011), which is the boundary zone between the nonsubducted African lithosphere and the Aegean lithosphere that overrides the subducted Aegean slab. Continual tear faulting of the African lithosphere at the active STEP separates the subducting lithosphere from the lithosphere at the surface. It was shown that the surface geology documents both strike-slip and convergent tectonics in accordance with a Tchalenko (1970) sinistral shear zone model. The Africa-Aegean velocity component perpendicular to the Pliny-Strabo shear zone was proposed to be accommodated by the Rhodes fold and thrust belt: the outboard part of the Rhodes Basin consists of a broad NE–SW trending strike-slip zone with predominant compression inferred from kilometer scale thrust relief (Hall *et al.*, 2009) and superficial extension (Ten Veen *et al.*, 2004). Although the Pliny-Strabo trenches thus have a small component of convergence on them, most of the relative motion since the Pliocene has been strike-slip (Reilinger *et al.*, 2006; Vernant *et al.*, 2014).

Farther to the east, between Rhodes and Cyprus, the plate boundary is obscure. The broad geographical distribution of earthquakes, lack of deep earthquakes, and discontinuous arc volcanism belonging to the subducting African lithosphere (Figure 3.1) contribute to this uncertainty. In addition, the large separation of GPS stations at opposite sides of the possible plate boundary zone precludes the delineation of this boundary (Figure 3.2A). In short, the location and nature of the plate boundary between Rhodes and Cyprus is unknown. This is the main topic of this paper.

Earthquake epicenters between the longitudes of Rhodes and Cyprus are distributed along bathymetrical highs, basins, and faults, both offshore and onshore, which present potential features to be associated with a plate boundary (red lines in Figure 3.1). These features are the Burdur–Fethiye fault zone (BFFZ), Aksu Thrust (AT), Rhodes basin (RB), Anaximander Mountains (AM), and Florence Rise, which define the margins of a complex tectonic zone known as the Isparta Angle (IA) (Figure 3.1).

The BFFZ constitutes the western limb of the Isparta Angle and it was interpreted as a left-lateral strike-slip fault zone by Price and Scott (1994), Eyidoğan and Barka (1996), and, more recently, Hall *et al.* (2014). Alternatively, the BFFZ is interpreted as a normal fault zone (Koçyiğit *et al.*, 2000; Alçiçek *et al.*, 2006) without significant strike-slip motion. Earthquake focal mechanisms do indeed not support a strike-slip interpretation (Taymaz and Price, 1992), but this may still agree with a STEP fault: relative motions

further away from the active STEP can be zero – this is an aspect that is particular to this type of plate boundary and distinguishes it from a transform fault (Govers and Wortel, 2005). Barka and Reilinger (1997) considered the BFFZ as the on-land extension of the Pliny-Strabo trenches on the basis of the coherence of earthquake slip and GPS-derived velocity vectors. Hall *et al.* (2009, 2014) interpreted offshore seismic reflection data in combination with on-land geology as supporting the connection of the Pliny-Strabo trenches to the BFFZ. Basin and fault analyses near the fault zone indicate that the sinistral motion of the Pliny-Strabo trenches penetrates the southwestern tip of the BFFZ (Alçiçek *et al.*, 2006). The eastern boundary of the Isparta Angle is defined by the Sultan Dağ Thrust (Boray *et al.*, 1985), but the majority of seismic activity is under the Aksu Thrust. Zitter *et al.* (2003) inferred the continuity of the western limb of the Cyprus arc with the Isparta Angle from imaging similar fault types and trends. The first possible plate boundary thus follows the northern perimeter of the Isparta Angle (Figure 3.1).

Another possible location for the plate boundary follows from considering the region south of the Turkish mainland, where bathymetric trends and faults of the Pliny trench have strikes similar to that of the Turkish continental slope (Ten Veen *et al.*, 2004). Furthermore, the post-Miocene deformation age of the Pliny trench also correlates well with the Finike basin, which is located between the Anaximander Mountains and the Turkish continental slope (Ten Veen *et al.*, 2004). This led Ten Veen *et al.* (2004) to propose that the Pliny trench connects with the faults to the north of the Anaximander Mountains. Consistent with this interpretation, Ocakoğlu (2012) found evidence in swath bathymetry and seismic data that the BFFZ and the Pliny-Strabo "trench" system represent different fault systems. Ten Veen *et al.* (2004) interpreted the Anaximander Mountains as a broad sinistral shear zone. The Florence Rise is the broad bathymetrical high to the southeast of the Anaximander Mountains and it separates the Antalya Basin from the region of convergence to the south and southwest (Woodside *et al.*, 2002). Shallow marine seismics (Aksu *et al.*, 2009) show NW-SE trending thrust faults with similar vergences in the region between the Anaximander Mountains and the Florence Rise. This suggests that the present-day plate boundary between Rhodes and Cyprus is located offshore, to the south of Anatolia (Wdowinski *et al.*, 2006).

P-wave tomography under the Isparta Angle region outlines the subducted African plate and the Anatolian lithosphere (Biryol *et al.*, 2011). However, tomographic resolution is insufficient at shallow levels to identify which of the two above alternatives is the plate boundary: near the surface, the boundary zone closely follows the trend of the Strabo "trench", Anaximander Mountains, and Florence Rise. The boundary of the "Western

Cyprus Slab" seismic velocity anomaly roughly corresponds to near-surface features such as the Antalya Bay, Aksu Thrust, BFFZ, and Pliny trench (figures 9 and 10 in Biryol *et al.*, 2011), which may also be the plate boundary.

Thus, for the Rhodes-Cyprus segment two possible plate boundaries can be hypothesized (Figure 3.1): one follows the Aksu Thrust and the BFFZ, forming the outer Isparta Angle, and the other follows the Anaximander Mountains and Antalya Bay. Hereafter, we refer to the boundary along the outer Isparta Angle as NORTH and to the one following the Anaximander Mountains as SOUTH. Our aim is to constrain the location and nature of the plate boundary that is shown with thick red lines in Figure 3.1, and to evaluate for how long approximately this plate boundary has been active.

The two plate boundary configurations have a common segment from the south of Cyprus towards the east. Here, the Eratosthenes Seamount (ESM), a continental fragment on the African plate, is in the process of colliding with the Cyprus arc (Ben-Avraham *et al.*, 1988; Robertson, 1998; Mascle *et al.*, 2000). The degree of coupling between the African plate and Anatolia along the ESM plate boundary segment, however, is not known.

The easternmost segment of the Cyprus arc is composed of a linked fault-and-thrust belt with intervening basins extending to the Levant coast: the Troodos Larnaka culmination in the south and the Kyrenia belt to the north, with the intervening Latakia basin constituting the foreland of the Tauride system (Aksu *et al.*, 2005; Calon *et al.*, 2005). The transition from the Eratosthenes collision zone to a transtensional regime in the Latakia-Larnaka segment was inferred from shallow seismic reflection studies (Vidal *et al.*, 2000). Although the location of this part of the plate boundary between Africa and Anatolia is well constrained, its nature is not.

Our approach is based on the understanding that forces exerted at plate boundaries shape the stress field and, in combination with the rheology, the deformation of the lithosphere (e.g., Warners-Ruckstuhl *et al.*, 2012, 2013) with the plate boundaries' location naturally giving the distribution of the forces involved, the plate boundaries' nature determines their direction and magnitude. We therefore step back and consider Anatolia to be part of a deformation zone with finite discontinuities (plate boundaries and faults) and a north-south extent of hundreds of kilometers. We use mechanical models with either the NORTH or the SOUTH plate boundary geometry to predict the velocity field in Anatolia for comparison with available GPS velocity data. Active faults within Anatolia have been mapped based on their morphological and seismic expressions (Bozkurt, 2001; Emre *et al.*, 2013).

Significant fault slip is possible only on the major fault zones. We therefore will evaluate the improvement in the model compatibility with the GPS-derived velocities when we incorporate these major faults (or shear zones).

The first part of this study deals with the present day and the aim is to determine the preferred southern plate boundary configuration for the present. In the second part we use indicators for the long-term deformation (slip-rates on major faults over many seismic cycles and paleomagnetic rotations) to study the stability of this plate boundary in recent geological time.

## 3.2 Modeling approach

For modeling the Anatolian-Aegean deformation two end-members for the rheology can be assumed. One considers a strong continental lithosphere and assumes the motion of crustal/lithospheric blocks to be coupled through narrow shear zones (e.g., Nyst and Thatcher, 2004; Reilinger *et al.*, 2006; Floyd *et al.*, 2010). The other considers the continental lithosphere to be weak and models it as a thin viscous sheet (e.g., Cianetti *et al.*, 2001; Jimenez-Munt *et al.*, 2003; Özeren and Holt, 2010) or an elastic-plastic crust with a viscous mantle (Fischer, 2006). The former method is known as the block modeling approach, whereas the latter is collectively known as the continuum approach.

Block models are based on rigid crustal blocks that are fully enclosed by faults. They have been successful in describing the surface velocity field with high accuracy and enable calculation of slip-rates on active block bounding faults. However, neither the assumption of an undeforming block nor that of complete closure of the bounding faults appears to be realistic. In most regions that are studied using block models, some parts of the block boundaries are not expressed in the geology, meaning that they have little meaning on time scales of multiple earthquake cycles.

Continuum models are based on the assumption that crustal/lithospheric regions between faults are mechanically weaker than the faults themselves, e.g., thin viscous sheet models (England and McKenzie, 1982). Continuum models relate driving forces (e.g., ridge push, slab pull, gravitational body forces, trench suction) to deformation by varying rheology (Thatcher, 2009). Offsets along plate boundaries and major faults in Anatolia show a significant fraction of the faults and shear zones are as weak as, or weaker than, the rocks separating them. We therefore think that continuum models are not geologically realistic.

Loveless and Meade (2011) presented an elegant methodology that seeks to combine the two perspectives/approaches. They inverted GPS observations to find slip on (predefined) block boundaries and block deformation. Our approach is similar in that we combine the strengths of both modeling approaches. It is different because we do not work with blocks that are fully enclosed by faults because geological observations do not support the existence of these in Anatolia. We only incorporate finite length faults that have been observed from the geology and active tectonics. We solve for stresses and deformation and try to find the minimum number of geologically inferred faults that is required by a given GPS dataset. We use an elastic rheology to capture the continuum deformation, which is consistent with the time scale of a few or more earthquake cycles (henceforth referred to as the geodetic time scale). Implicit in this approach is that deformation associated with small faults is represented by the continuum deformation. Similar to what is observed, e.g., near the eastern end of the Altyn Tagh fault in the Tibetan plateau, distributed deformation is expected here particularly.

## 3.3 Observations

### 3.3.1 GPS-derived velocity field

GPS-derived velocities are the main observational constraint in this study, primarily because of their (very high) accuracy and therefore their sensitivity to the location and nature of the plate boundary. Horizontal velocities have an accuracy of around 1 mm/year on average on a benchmark network with good coverage of the model domain.

In addition to the data from Reilinger *et al.* (2006), we use available GPS-derived velocity data for western Anatolia (Aktuğ *et al.*, 2009), northwestern Arabia (Alchalbi *et al.*, 2010), the western Hellenic Arc (Hollenstein *et al.*, 2008), Greece (Floyd *et al.*, 2010), northern Iran (Masson *et al.*, 2006), Zagros (Hessami *et al.*, 2006), and Macedonia and western Bulgaria (Burchfiel *et al.*, 2006; Kotzev *et al.*, 2006) (see Figure 3.2a) for comparison with the modeled velocity. Reilinger *et al.* (2006) used measurements from before the 1999 İzmit (Mw = 7.4) earthquake, which are not affected by postseismic or coseismic effects. The measurements of Aktuğ *et al.* (2009), however, were collected after the 1999 İzmit and 1999 Düzce (Mw = 7.2) earthquakes. Aktuğ *et al.* (2009) identified the sites that were affected by postseismic and coseismic motions by comparing his velocity results with those of Reilinger *et al.* (2006). Hollenstein *et al.* (2008) used measurements before the Lefkada 2003 (Ms = 6.2), Skyros 2001 (Mw = 6.4), and Strofades 1997 (Ms = 6.4) earthquakes for the velocity calculations. Floyd *et al.* (2010) excluded sites that were affected by Mw

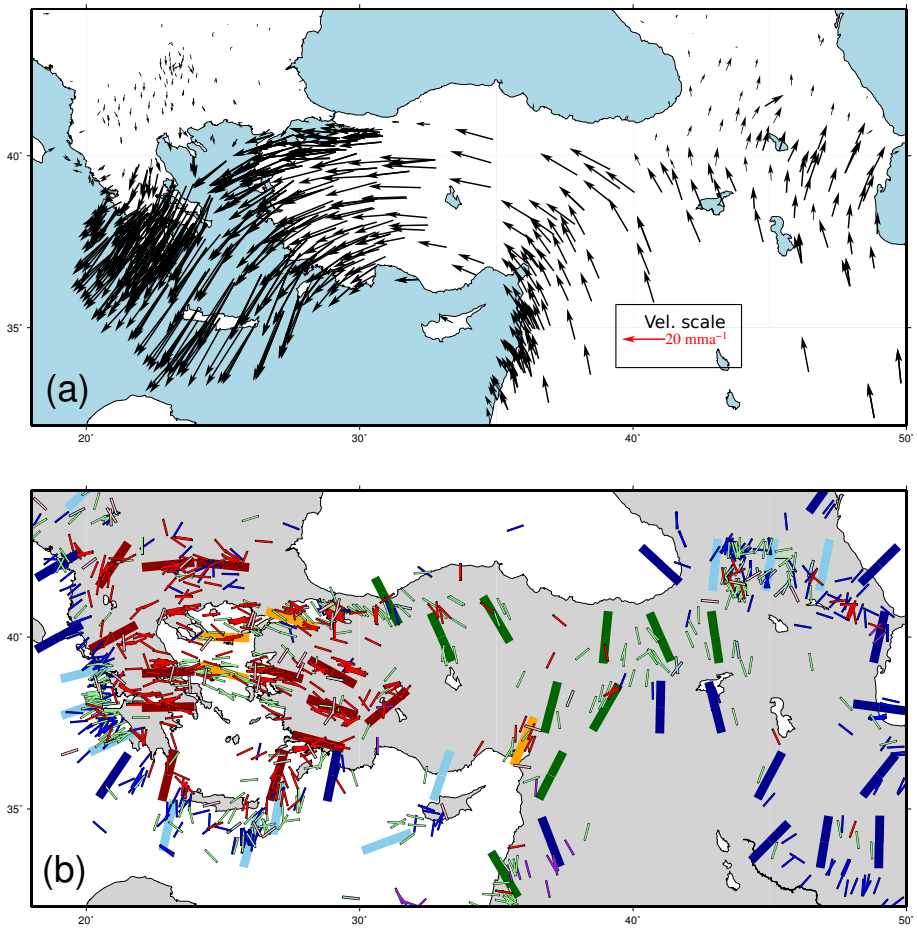


**Figure 3.2:** a) Compilation of GPS velocities (Burchfiel *et al.*, 2006; Hessami *et al.*, 2006; Kotzev *et al.*, 2006; Masson *et al.*, 2006; Reilinger *et al.*, 2006; Hollenstein *et al.*, 2008; Aktuğ *et al.*, 2009; Alchalbi *et al.*, 2010; Floyd *et al.*, 2010). b) "Observed" horizontal stress directions. Bars indicate the direction of maximum compression. Thin bars are taken from the World Stress Map project (Heidbach *et al.*, 2008). Color indicates the stress regime: dark blue for thrusting, light blue for oblique thrusting, green for strike-slip, orange for oblique tension, and red for tension. Wide bars represent spatial averages of the maximum horizontal stress axis, computed with the method of Mardia (1972).

$\geq$ 6 earthquakes during the observation period. Kotzev *et al.* (2006) corrected for the İzmit earthquake coseismic slip at the affected stations. Alchalbi *et al.* (2010), Masson *et al.* (2006), and Hessami *et al.* (2006) did not report of any earthquakes that affected their velocity determinations. Hence, we consider our combined dataset to be unaffected by coseismic and postseismic motions. The GPS velocities likely do reflect the impact of long-term locking of faults. All velocities are specified in an ITRF2000 Eurasia-fixed reference frame. We did not correct the published velocities for relative network rotations. Discrepancies due to different network representations are a few millimeters per year in overlapping stations in the datasets, all of which are within the error ellipses. We removed data with larger standard deviations from the database for overlapping stations.

### 3.3.2 World Stress Map data

World Stress Map (WSM) data provide the direction of the largest horizontal compressive principal stress axis and the stress regime (Heidbach *et al.*, 2008) (Figure 3.2b). Data from various sources and quality are compiled in the WSM. In our domain, 90% of the data were derived from focal mechanism solutions. On average, these are of C-grade quality, corresponding to a 25° angular error for the maximum compressive horizontal stress axis (SHmax). Therefore, WSM data are less accurate than the GPS data. We smoothed the WSM data using the method of Mardia (1972) for comparison with model stresses (see Heidbach *et al.* (2010) and Warners-Ruckstuhl *et al.* (2013) for a detailed explanation of the method). This method finds a smooth and continuous field of stress directions whose difference from observed stress directions is minimized. The choice of search radius does not significantly change the smoothed output field, but it results in lower uncertainties. The directions of maximum compressive stress thus obtained are shown with large bars in Figure 3.2b. A detailed plot for stress observations, smoothed stress field, and stress variances is given in Appendix A.

## 3.4 Model setup

We model the present-day secular velocity field of the Eastern Mediterranean with emphasis on the Anatolia-Aegean region. Since the horizontal extent of the domain is much larger than the vertical (model) dimensions, and because the data have little depth information, the 3D mechanical equilibrium equations can be simplified to 2D by assuming plane stress. We solve these equations with plane stress spherical finite element code GTECTON (Govers and Meijer, 2001).

### 3.4.1 Domain and rheology

The model domain, boundary conditions, and faults for the plate boundary configurations NORTH and SOUTH are shown in Figure 3.3. The lithosphere responds to stresses by elastic, brittle, or viscous deformation. Viscous deformation occurs on many time scales, but mostly on geological time scales. Within our study area significant lateral variations exist in the surface height and topology of the Moho (and other density interfaces). Gravity leads to horizontal forces acting where there are gradients in topography and/or Moho depth, i.e. the forces act in a distributed way rather than as a line force like we assumed

in our (boundary-driven) models so far. As our analysis is based on the fit to surface deformation data, this difference between distributed and line forcing could potentially affect our conclusions significantly. We investigate to what extent our (simple) velocity-driven models correspond to (more realistic yet complicated) models driven by gradients in gravitational potential energy (GPE) in Appendix D.

For the first part of the paper we compare model results with geodetic velocities (acquired on time scales of years to decades). We therefore take the lithosphere to be elastic with faults. Our model domain encompasses both oceanic and continental lithosphere, which have different Young's moduli. In studies focusing on continental areas, Young's modulus values of 70–75 GPa (e.g., Meijer and Wortel, 1996, 1997; Lundgren *et al.*, 1998; Plattner *et al.*, 2009) and for oceanic areas 100–130 GPa (Watts and Zhong, 2000; Got *et al.*, 2008) have been used. Therefore, we assign 75 GPa to continental Arabia, Africa, and Eurasia and use 100 GPa for the Black Sea and the Mediterranean. The Anatolian-Aegean region formed in a context of Cretaceous-Recent subduction of branches of the Neo-Tethys and accretion of intervening ribbon continents (Şengör and Yılmaz, 1981). The entire region is therefore mechanically weak and prone to large deformation. We conducted a priori sensitivity analysis using reference models (Section 3.5) with several different Young's moduli, and we select 25 GPa for the Anatolian-Aegean region. Poisson's ratio is assumed to be 0.3. We used convergence tests to verify that all results shown in this paper are insensitive to further refinement of the finite element grid.

### 3.4.2 Boundary conditions

The northern edge and the northwestern part of the model domain are located in stable Eurasia. As we take stable Eurasia as our reference frame, nodes along these domain edges are fixed in both horizontal directions. The eastern margin of the domain can move in a N-S direction, consistent with ongoing N-S strain in the Zagros and Caucasus (Allen *et al.*, 2004). We force the system by applying GPS-derived velocities in the far-field, i.e. along domain edges in the African and Arabian plates ($v_{ARA}$) (Reilinger *et al.*, 2006). We also impose the relative velocity at the Hellenic trench $v_{RB}$ using the split node technique (Melosh and Raefsky, 1981): since observed relative velocities at the Hellenic trench represent the response to forces due to GPE, trench suction, slab pull, sublithospheric mantle flow, and plate contact resistance, the imposed relative velocity at the trench implicitly accounts for the contribution of GPE forces (and other forces) to the regional kinematics. To avoid double forcing, we do not include body forces in these models.

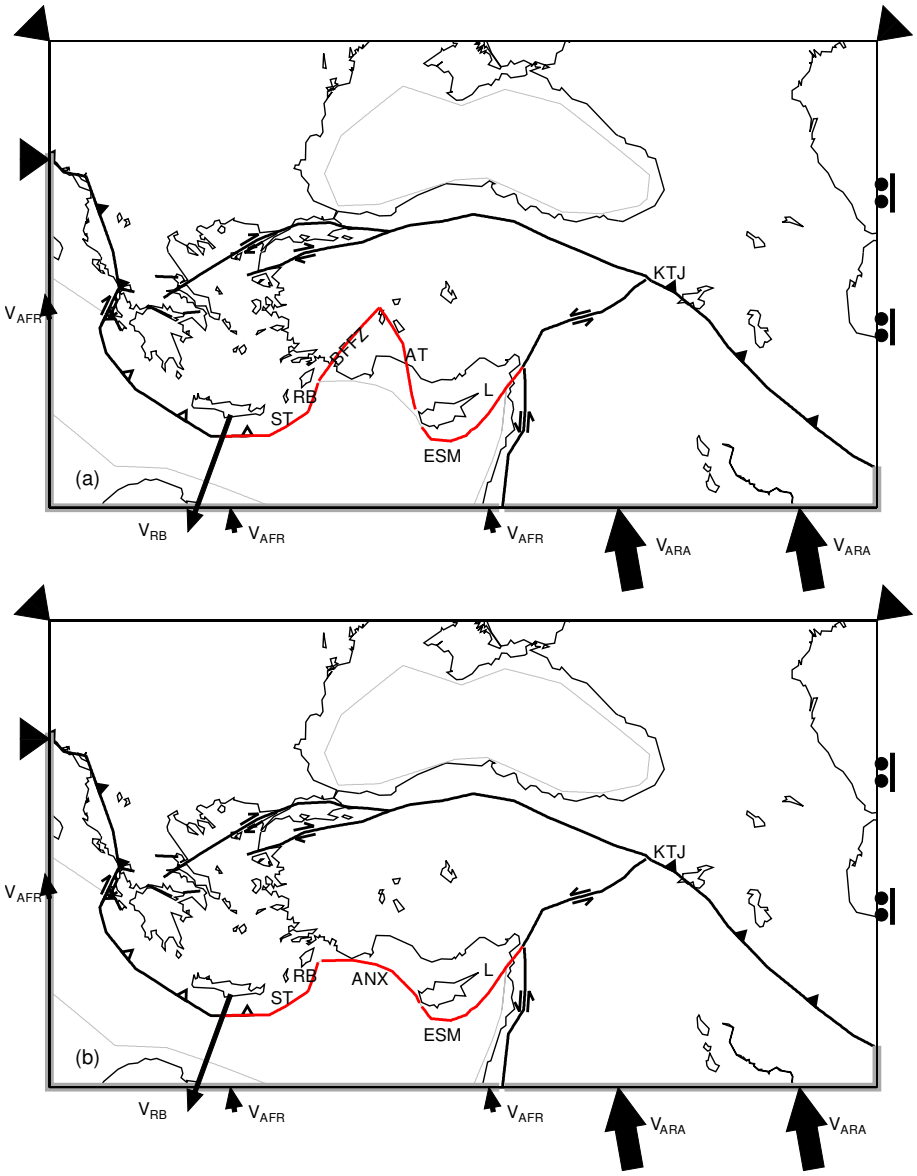


**Figure 3.3:** Model domain, boundary conditions, and known and unknown faults for (a) NORTH and (b) SOUTH model. Known faults are colored black with their sense of slip. Unknown faults are shown in red. The shaded region indicates oceanic lithosphere. GPS-derived velocities are imposed along the African and Arabian margins of the model (thick gray line along the plot frame): $v_{AFR}$ and $v_{ARA}$. $v_{RB}$ is the imposed differential velocity on the plate contact of the Hellenic subduction zone. Rollers on the east boundary correspond to the observation that GPS velocities are oriented approximately north-south here. Solid triangles along the north and NW boundary of the model indicate that here the model is fixed. Abbreviations are the same as in Figure 3.1.

In Section 3.6 we will present models with an alternate choice for the forcing. By their very nature, body forces (and GPE) act on volumes rather than at plate boundaries. In Section 3.6 we therefore will investigate to what extent our (simple) velocity-driven

models correspond to (more complicated) GPE-driven models.

### 3.4.3 Plate boundaries and faults

Plate boundaries and principal (larger) faults are shown in Figure 3.1. The Dead Sea Fault (DSF) takes up the relative motion between the African and the Arabian Plates. The dextral NAF and the sinistral EAF accommodate westward extrusion of Anatolia. Coming from the east, the NAF bifurcates into two branches east of the Sea of Marmara (see Şengör *et al.*, 2005, for a review). The main northern branch continues along the Sea of Marmara and enters the Aegean Sea. Across the North Aegean, the continuation of the NAF manifests itself as a broader shear zone and connects with central Greece via the North Aegean Trough (NAT) and the Sporades (Dewey and Şengor, 1979; Lyberis, 1984). The southern branch of the NAF in the Marmara region has a SW–NE strike and is composed of a set of discrete faults (Şengör *et al.*, 2005). We represent these discrete faults in the model by a single, continuous fault zone. In the west, the Hellenic Arc terminates at the 150-km-wide dextral strike-slip zone including the Kephalonia Fault (KF), which marks the transition from oceanic subduction to continental collision (Baker *et al.*, 1997; Shaw and Jackson, 2010). Following Özbakır *et al.* (2013), we implement the Pliny and Strabo trenches as a single shear zone. The Rhodes Basin consists of a broad NE–SW trending transpressive zone that has the characteristics of a fold and thrust belt (Hall *et al.*, 2009). Therefore, we implement the fold and thrust belt as possibly accommodating both dip-slip and strike-slip motions. Further to the northeast, the Rhodes Fault links the Pliny and Strabo trenches to the Anaximander Mountains.

The selection of active faults in western Anatolia is based on two criteria: the scale of faults and the seismic activity on them. The argument of scale, more specifically, is the condition that the length of a fault is comparable to the crustal thickness in the region. Thus, faults shorter than the crustal thickness or aseismic mapped faults are not incorporated in our analysis. In the course of model development, we implemented some long fault traces such as the Simav fault and Gökova faults. Importantly, some of the fault strands in Western Anatolia are represented in our models as part of a longer fault system rather than by their individual segments. An example is the Bakırçay graben. This graben or the Balıkesir and Havran fault zones are in fact long fault zones, which are included in our model as the southern branch of the NAF. Another example is Alaşehir graben, which is incorporated within the Burdur–Fethiye fault zone.

In our model, we control the nature of faults by a priori imposing whether slip is allowed

in a fault parallel and/or fault normal direction. The "slippery node" formalism (Melosh and Williams, 1989) that we employ has the important property that dynamic stresses in the model determine whether or not such fault slip occurs. Strike-slip faults in the model are assumed to be vertical and frictionless, and fault motion is constrained to be fault-parallel; we do not impose the sense of relative motion. Thrust faults are assumed to be subhorizontal (∼30 degrees) with both fault-normal and fault-parallel motion allowed. In the collision process, horizontal convergence causes an increase of topography. This uplift is controlled by the fault dip and by Airy isostasy: as the height of the orogen increases, the resistance to further growth of the topography increases. To represent this fault-normal resistance in our model, we adopt the formulation of Van Benthem and Govers (2010). Fault-parallel motion on thrust faults is taken to be frictionless. Extensional faults are implemented by only allowing fault-normal motion. Triple junctions are represented by triple overlapping nodes (Plattner *et al.*, 2009).

### 3.4.4 Model evaluation

To quantify the misfit between modeled and observed velocity fields we use the reduced chi-square statistic defined here as:

$$\chi^2 \stackrel{\text{def}}{=} \frac{1}{N - n_T - 1} \sum_{i=1}^{N} \left( \frac{(v_i^{o,x} - v_i^{m,x})^2}{(\sigma_i^x)^2} + \frac{(v_i^{o,y} - v_i^{m,y})^2}{(\sigma_i^y)^2} \right)$$

$v_i^o$ and $v_i^m$ are observed and modeled horizontal velocities at GPS station number $i$ and superscripts $x$, $y$ denote easting and northing components of the velocity vector. $N$ is the number of observations, $n_T$ is the number of model elements, and $\sigma_i$ is the error in the GPS velocity. The number of model elements is the total number of degrees of freedom on model faults, determined as follows. When a fault segment is locked, it has zero degrees of freedom. When a fault segment is allowed to move in one direction (strike-slip, pure normal, or dip-slip), it has one degree of freedom. When a fault segment can move in both strike-slip and dip-slip directions, it has two degrees of freedom. In principle, a large $\chi_R^2$ represents a poor fit. Scaling by one over $N - n_T - 1$ has the consequence that, when two models have the same sum of squares, $\chi_R^2$ will be smaller for the model with fewer constraints $n_T$, i.e. the simpler model. The reduced chi-square statistic thus has the desired property of favoring the simpler over the more complex model when looking for the lowest value. Degrees of freedom (DOFs) of model faults are represented by open/filled triangles and strike-slip symbols in Figures 3.4 and 3.5. Open triangles show the case where both strike-slip and normal motion is allowed. Filled triangles indicate that only

motion perpendicular to the fault strike is allowed, and strike-slip symbols indicate that fault parallel motion is allowed; here, the sense of motion indicated by the strike-slip symbols is meaningless, because this is a model result, not a priori imposed.

## 3.5 Model results and analysis

### 3.5.1 NORTH or SOUTH

In this section, we present model results for the NORTH and SOUTH plate boundary scenarios. We first present two "reference models" based on accepted regional plate boundaries and the two plate boundary scenarios (Figure 3.3). As discussed below, the difference between modeled and observed velocities is larger than the data error in these models. Therefore, we will proceed with more complex models to study how the introduction of additional faults affects the fit to the observations. Importantly, we only introduce faults with clear geological expressions.

#### Reference models NORTH and SOUTH

The NNW-directed motion of Africa towards Anatolia decomposes into plate boundary parallel and normal components. As a starting point, we therefore define reference models where both down-dip and fault parallel motions are allowed along plate boundaries NORTH and SOUTH. Model velocity fields of the reference models are shown in Figures 3.4a and 3.4b. The overall pattern is similar to the GPS observations shown in Figure 3.2a: an increase in the velocity from east to west in a counter-clockwise pattern around a pivot in Cyprus. The difference between the observed and modeled velocity vectors, hereafter referred to as the "residual velocity" vectors or "misfits", gives a better indication of the sensitivity of the velocity field to changes in the unknown faults' nature and geometry. These residual velocities are plotted with black vectors on the misfit maps (Figures 3.4c and 3.4d). The other useful quantity is the fault slip-rate, which shows the direction and magnitude of fault motion in the model. Slip-rates are calculated with respect to the Anatolian-Aegean region and are shown by blue vectors for each of the scenarios.

Both reference models explain the observations in the Arabian plate within confidence limits. Other parts of the eastern model domain show significant misfits, notably in easternmost Turkey, Armenia, and Azerbaijan. A likely reason for this is the uniform free-slip boundary condition on the eastern boundary of the model domain and the absence in the model of fundamental faults in the Caucasus and the Iranian Plateau. However, for our goal of identifying the plate boundary south of Anatolia these are unimportant details; model improvements would lead to a better fit to the GPS observations in the east only. Vice versa, surface deformation in the easternmost part of the domain is practically the same for the NORTH and SOUTH scenarios, indicating that GPS velocities in the easternmost part of our domain are not sensitive to the details of the southern plate boundary of Anatolia. We will therefore not attempt to improve the model fit in the easternmost domain in the rest of this paper.

**Models with additional forcing on the Pliny-Strabo segment**

For both reference models, velocity misfits in western Anatolia and the southeastern Aegean region are large (Figures 3.4c and 3.4d). We therefore need to consider the need for additional drivers of surface deformation (e.g., forces related to the sinking of the Aegean slab, or gravitational collapse of the Aegean lithosphere). In the reference models we imposed the relative velocity along the Hellenic plate contact. In models SOUTH-1 and NORTH-1 we extend the forcing to include the Pliny-Strabo trenches by imposing the GPS-derived relative velocities here as well.

The results (Figures 3.4e and 3.4f) show that residual velocities have decreased in SE Anatolia and its surroundings. We therefore retain the extended forcing in subsequent models. We next investigate changes to the SOUTH and NORTH models individually in an attempt to further improve their fit with the GPS observations.

**SOUTH plate boundary with additional Menderes faults**

For the SOUTH plate boundary, the result in Figure 3.4e shows that the velocity residues are notably reduced in the Aegean Sea and western Turkey. However, near Rhodes and the SW edge of Turkey, misfits are still significant and SSW and S directed. In the vicinity of the Menderes extensional province misfits are oriented E-W. To further improve upon this model we add another important geological element to the model: western Anatolia shows NNE directed extension and the Menderes massif horst-graben system takes up most of the deformation (Şengör, 1987). Thus, we add the Menderes faults as two parallel

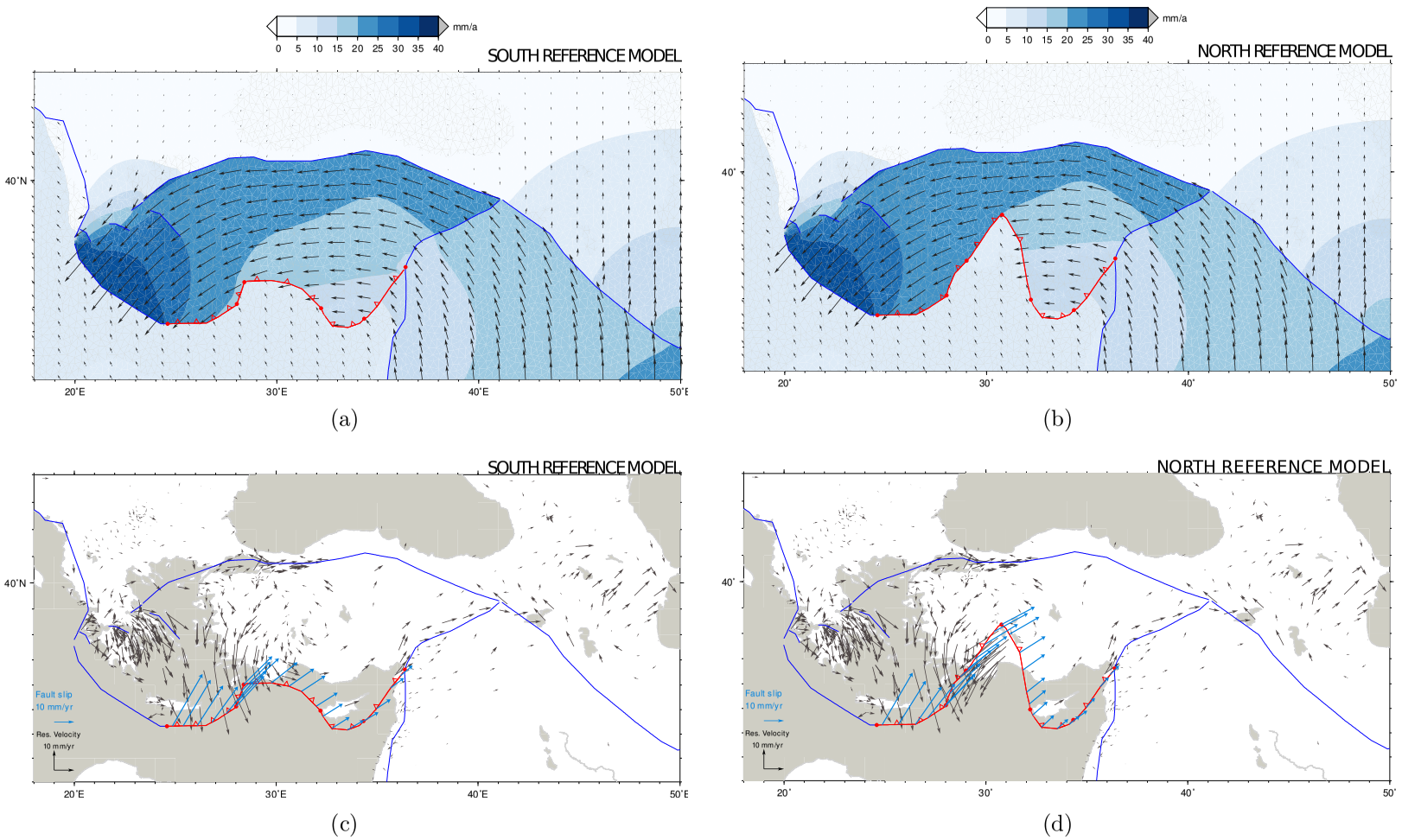


**Figure 3.4:** Model-predicted velocities and velocity misfits (observed minus calculated). The assumed nature of the faults is indicated by filled triangles when only fault-perpendicular motion is allowed and by strike-slip symbols when only fault parallel motion is allowed. Open triangles signify that both strike-slip and fault normal motions are allowed in the model. Blue arrows in the misfit maps (c–g) indicate the resulting fault slip-rate and direction. a) Velocities of the SOUTH reference model; b) velocities of the NORTH reference model; c) velocity misfits of the SOUTH reference model; d) velocity misfits of the NORTH reference model; e) velocity misfits of model SOUTH-1; f) velocity misfits of model SOUTH-2; g) velocity misfits for model NORTH-1; h) velocity misfits for model NORTH-2.

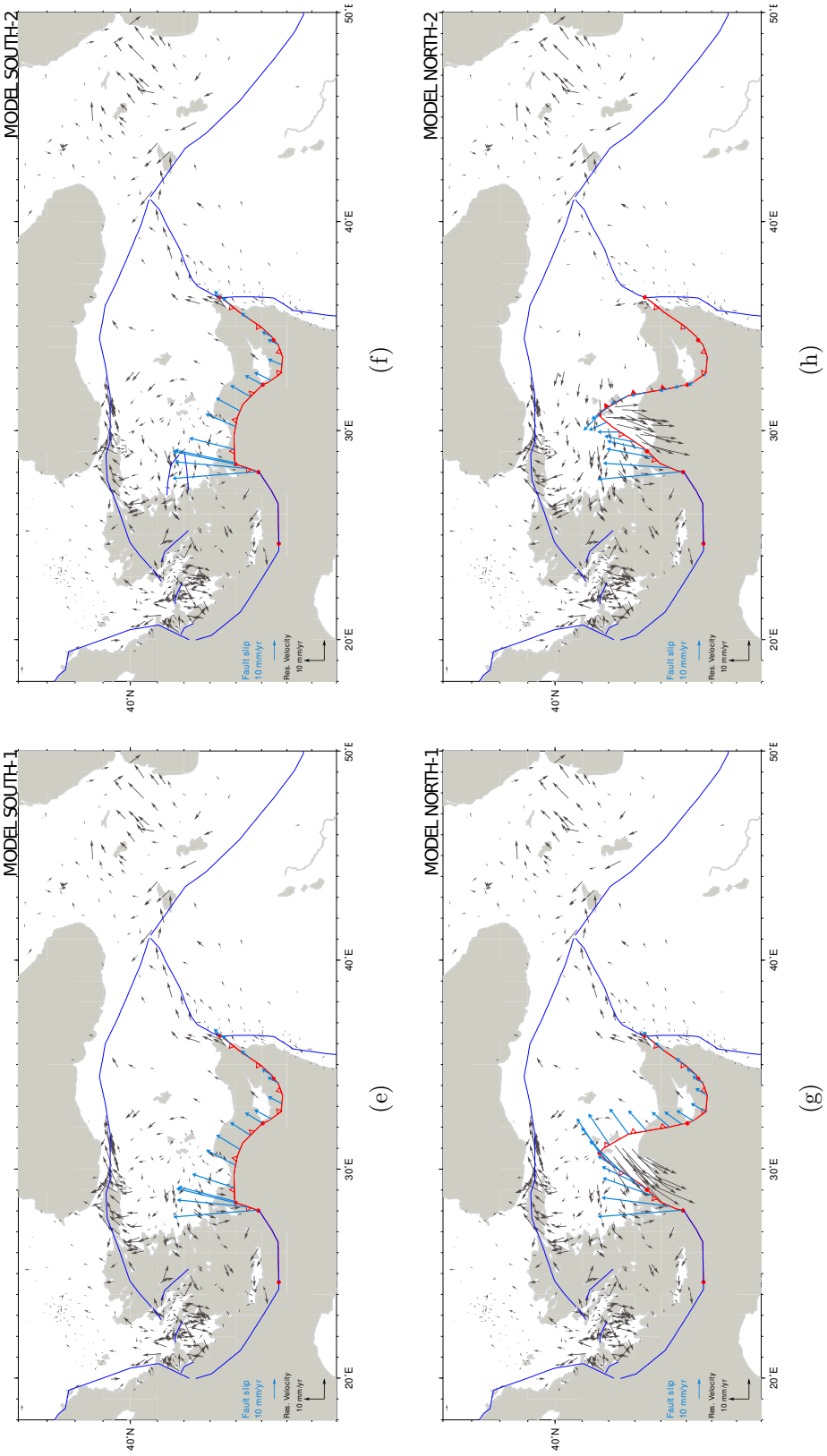
MODEL SOUTH-2
MODEL NORTH-2
MODEL SOUTH-1
MODEL NORTH-1
(f)
(h)
(e)
(g)
40°N
20°E
30°E
40°E
50°E
Fault slip
10 mm/yr
Res. Velocity
10 mm/yr

**Figure 3.4**

dip-slip faults to model SOUTH-2 corresponding to the Menderes and Gediz grabens, to loosen the coupling of NW Turkey from the SW. This modification yields smaller misfits (Figure 3.4f). Below we will seek to further improve the model fit by adding more faults, but the model SOUTH-2 already yields an acceptable fit to the observations in SE Turkey and surroundings.

#### NORTH plate boundary with friction

In the NORTH plate boundary configuration, the Isparta Angle moves with the Africa plate. Misfits in the Isparta Angle are significant in model NORTH-1 (Figure 3.4g). In model NORTH-2 we impose friction on the Aksu fault (E boundary of Isparta Angle) to allow westward push by Anatolia to penetrate into the Isparta Angle (Figure 3.4h). Irrespective of the frictional coupling we impose, the decrease in misfit is insufficient. Unless the Isparta Angle is detached from Africa, we cannot reproduce the GPS observations in the Isparta Angle. That is, there should exist another interface to the south of the Isparta Angle that accommodates the southwestward motion of the Isparta Angle.

#### Plate boundary configuration near southwest Anatolia

In the region closest to the NORTH and SOUTH plate boundaries, misfits for the NORTH model are significantly larger than for the SOUTH model. Geologically relevant possibilities for improvement of the NORTH model come to an end. We therefore conclude that the GPS velocities refute a NORTH plate boundary location. As the GPS observations are made onshore, this does not automatically prove our SOUTH plate boundary configuration to be correct. Below, we therefore seek to further improve the data fit of the SOUTH model to show that it at least is a very likely candidate for the plate boundary configuration.

### 3.5.2 SOUTH models: other regional faults

#### Adding friction on the Cyprus subduction contact: model SOUTH-3

The residual velocity of the Cyprus station is parallel to the direction of model slip vectors in model SOUTH-2 and its magnitude is similar to that of the slip vectors (Figure 3.4f). This residual velocity indicates that the Cyprus trench should have mechanical resistance to underthrusting – thus far we assumed a frictionless interface. Stronger coupling is

likely related to the collision of the ESM at the Cyprus trench (Ben-Avraham *et al.*, 1988; Robertson, 1998; Mascle *et al.*, 2000). In model SOUTH-3 (Appendix B, Figure B.1a), we therefore seek to find the friction value that yields the minimum misfit at the Cyprus trench. In this model, we also restrict relative motion to be trench-perpendicular/down-dip only. The misfit at the Cyprus station and at Turkish stations along the coast facing Cyprus is within the limits of observational error when we select a shear stress of 3 MPa, equivalent to 42% coupling between opposite sides of the fault.

#### Varying the nature of the Rhodes fault: model SOUTH-4

The NNE striking fault bounding the Rhodes basin (RB in Figures 3.1 and 3.3) was thus far taken to accommodate both strike-slip and thrusting. In model SOUTH-4 we allow strike-slip only. The result (Figure B.1b) shows an improved fit to the GPS velocity field. We conclude that this fault is strike-slip only.

#### Pure strike-slip Latakia segment: model SOUTH-5

Thus far, motion on the Latakia Fault segment could be both strike-slip and dip-slip, and it was found to be small and mostly strike-parallel. In model SOUTH-5, we only allow strike-slip to occur on the fault. The result (Figure B.1c) shows that model velocities at nearby GPS stations are practically unaffected by this change (c.f. Figure B.1b). Thus, although we cannot discriminate the two options based on the fit to the data, we prefer a strike-slip interpretation of the Latakia Fault as it is the simpler (fewer DOFs) model, but also because it agrees better with the seismotectonics of the region (Wdowinski *et al.*, 2006).

#### Adding the south branch of the NAF in the west: model SOUTH-6

Inclusion of the southern branch of the NAF as a strike-slip fault into model SOUTH-6 leads to a decrease in chi-square norm from 7.75 to 7.55. The improvement of misfits can be seen in NE Turkey (Figure 3.5). Although, from a statistical point of view, the improvement is not very significant, the slip-rate predictions for the northern branch of the NAF give a better agreement with the geological slip-rate data if we include the southern branch. We will come back to this in Section 3.7.3 below.

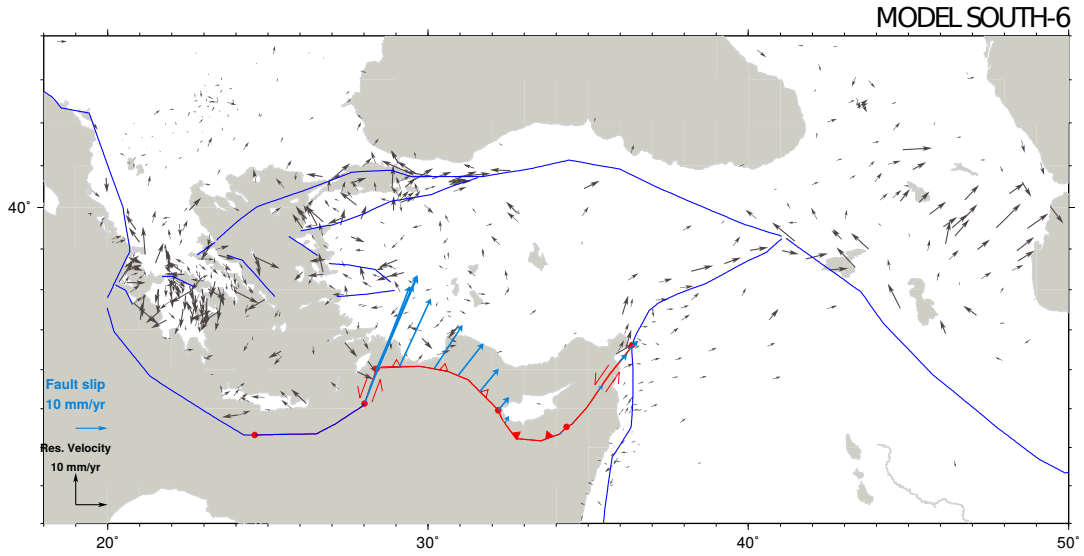


**Figure 3.5:** Velocity misfits (observed minus calculated) for model SOUTH-6. Symbols show the assumed nature of the faults; filled triangles indicate that only fault-perpendicular motion is allowed, strike-slip symbols indicate that only fault parallel motion is allowed. Open triangles indicate that both strike-slip and fault normal motions are allowed in the model. Blue arrows indicate the resulting fault slip-rate and direction.

### Nature of the Burdur-Fethiye fault: models SOUTH-7 and SOUTH-8

With models SOUTH-7 and SOUTH-8 we investigate the imprint of the Burdur-Fethiye fault zone (BFFZ) on the surface velocity field. We implement the BFFZ as a strike-slip (one DOF) fault in both SOUTH-7 and SOUTH-8. In SOUTH-7, the BFFZ is disconnected from the plate boundary; in model SOUTH-8 it is connected to the Rhodes fault. Neither of the models (Figures B.1d and B.1e) results in slip on the BFFZ, so that the match to the GPS observations does not change. We conclude that the BFFZ is effectively locked or inactive at present.

Different from what we find, the block models of Tiryakioğlu *et al.* (2013) and Reilinger *et al.* (2006) require a slip-rate on the BFFZ of up to 11 mm/year to reproduce the regional GPS observations. This illustrates a very important point: model results (including ours) are particularly sensitive to which faults to include or not, and whether the continuum between the faults is allowed to deform. As argued before, we think it is more realistic to add faults step-by-step to our deformation model and verify whether this results in a significant variance reduction. Crustal seismicity is too dispersed around the BFFZ to refute our conclusion that the fault is currently not active.

### Independent Isparta block: model SOUTH-9

At this stage, testing the combination of the NORTH and SOUTH models, i.e. a model that contains the Isparta Angle crustal block, is the logical final step (SOUTH-9). The Isparta Block is bounded by the BFFZ and the Aksu faults. As such, the number of DOFs is the largest in the totality of the models. The misfit map (Figure 3.6) shows that the overall model agreement is more or less the same as in SOUTH-6 and the following models; however, the misfit statistics are slightly unfavorable. Most notable is the fact that inclusion of the Aksu fault does not significantly improve the velocity vectors in its vicinity. We therefore conclude that an independent Isparta block is a less viable option in view of the geodetic observations.

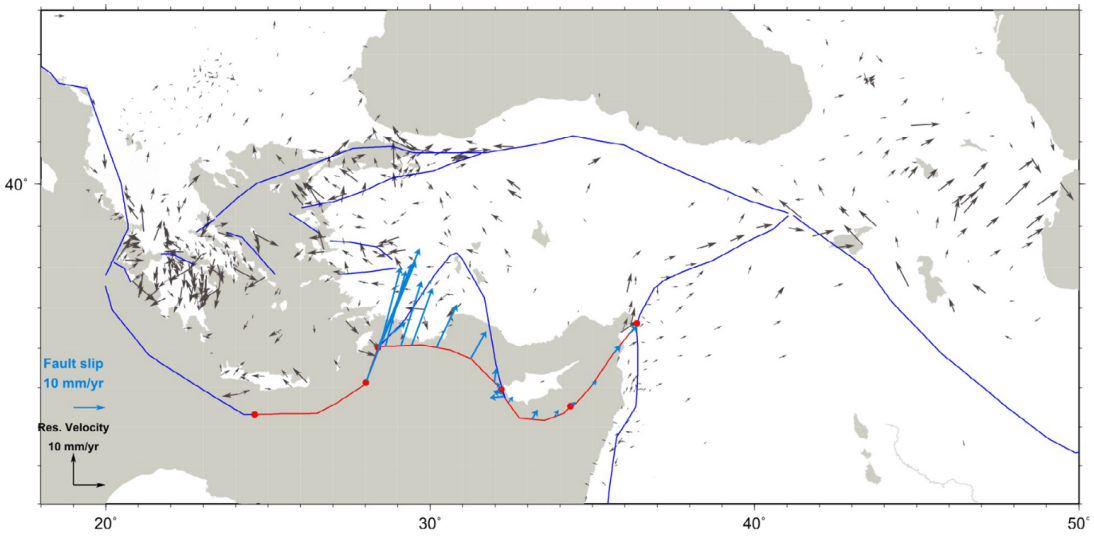


**Figure 3.6:** Velocity misfits (observed minus calculated) for model SOUTH-9, i.e. independent Isparta Block. The symbol explanations are the same as in Figure 3.5 .

### Significance of other regional faults

We further tested models with additional faults with regional significance that may affect the fit to the geodetic data, such as the Simav fault and Gökova faults. The slip-rate on these faults was found to be small and the corresponding improvement negligible. We therefore do not show these results.

### Performance statistics of all models

In Appendix C, Figure C.3 shows the $\chi_R$ statistic as a function of model number for GPS stations in the whole model domain (black circles) and for the box in Figure 3.1 (empty

circles) – this is where the plate boundary configuration has the clearest impact. Model SOUTH-6 (Figure 3.5) is our "best" model from a statistical point of view, although it does not match observations within error in Greece and W Turkey, north of the EAF, and in the eastern part of the model. However, we refrain from trying to further improve this model fit by introducing smaller scale faults because the fit is acceptable near the SOUTH plate boundary. A notable exception is the Dodecanese, where additional, albeit minor, forces result in a more local change in velocity directions.

**Conclusions**

Model SOUTH-6 fits the GPS velocities best. We conclude that: (1) the plate boundary is located to the south of Anatolia. As part of this southern plate boundary (2) the prolongation of the Pliny-Strabo trenches to the NNE is strike-slip; (3) the ∼W-E striking fault from the north of the Rhodes basin, to the Anaximander Mountains, to the W end of Cyprus, is predominantly a thrust contact; and (4) the Cyprus subduction contact is 42% locked. About other regional faults we conclude that: (5) the Burdur-Fethiye fault zone is locked or inactive, (5) the Menderes faults are active, and (6) the observations require the southern strand of the North Anatolia Fault to be active.

### 3.5.3 Match of best fitting model SOUTH-6 to stress observations

WSM stress observations in our region of interest are largely based on focal mechanism data, i.e. they are as representative of the same (short) time scale as the geodetic data that we used to select model SOUTH-6. The stress concentrations shown in Figure 3.7 are the potential areas where intrablock seismic events can be expected. However, these stress concentrations are mainly controlled by geometry because we are not considering a single seismic cycle. That means the model cannot resolve intrablock seismicity in terms of loading history; it can only account for the secular deformation. It is noted that high stresses may result in distributed failure or flow. Such flow phenomena are not modeled in our approach. Here we test the extent to which the stress observations are consistent with the predictions of this model.

Figure 3.7 shows horizontal stress directions as predicted by the model and average directions of maximum compression from the WSM (Figure 3.2b). The fit is remarkably good in Anatolia and Eurasia. Misfits are exclusively clustered along the Hellenic trench and around the Sea of Marmara. For the Hellenic trench, the model does not reproduce

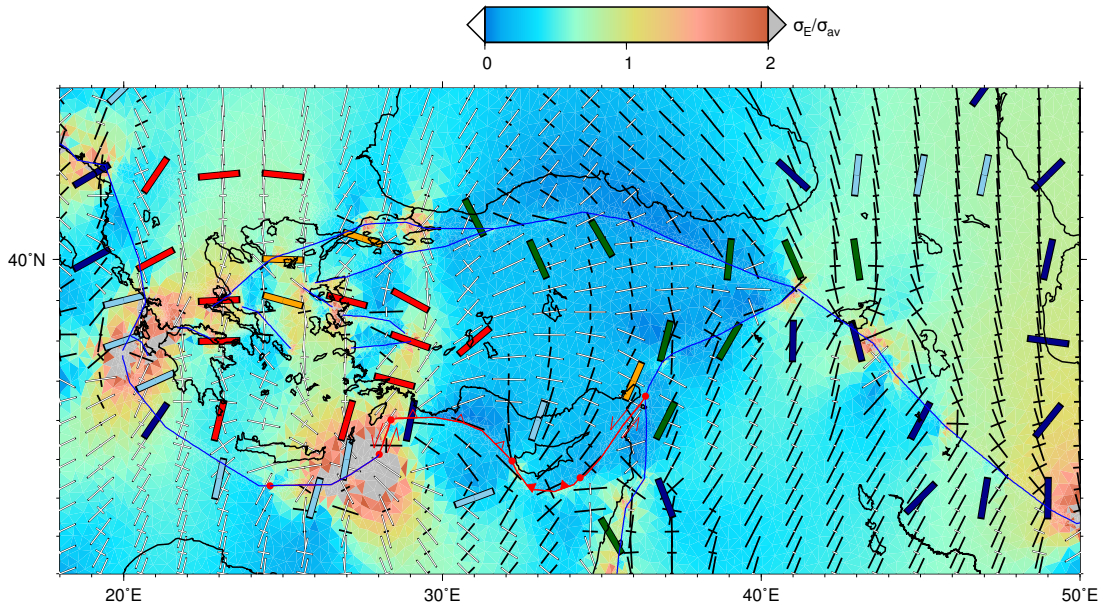


**Figure 3.7:** Stress field for model SOUTH-6. Black and white arrows indicate principal axis directions of horizontal compression and tension, respectively. Color contours indicate effective shear stresses (normalized by the average effective shear stress). Wide bars represent average WSM directions of maximum horizontal compression, with their color indicating the stress regime: dark blue for thrusting, light blue for oblique thrusting, green for strike-slip, orange for oblique tension, and red for tension (Figure 3.2).

trench-normal compression in the accretionary wedge, most likely due to lack of fault friction in our model. It is interesting to note that in the model the Arabian plate interior and central Anatolia display low stress magnitudes; these regions are relatively aseismic. We conclude that available stress direction observations agree with the results of model SOUTH-6.

### 3.5.4 Comparison of model slip-rates with geodetic modeling results from previous studies

Slip-rate is the rate of motion of the fault within a few or many earthquake cycles and thus reflects the short-term rates. Slip-rates can be determined from geodetic methods, such as GPS or InSAR (e.g., McClusky *et al.*, 2000; Wright *et al.*, 2004; Cavalie and Jonsson, 2014), but they always require a model: block-models, elastic or viscoelastic dislocation models, or combined fault/continuum models.

Figure 3.8 shows the compilation of previous slip-rate determinations with upper panel (Figure 3.8a) points to locations where these studies were conducted. The block model study of Meade *et al.* (2002) resulted in a slip-rate of 25.6 mm/year for the western NAF.

Nyst and Thatcher (2004) found 24 mm/year for the Sea of Marmara region with their block model. The Reilinger *et al.* (2006) block model (Figure 3.8b, orange error bars showing the range of values on the y-axis and segment range on the x-axis) has an average of 27.5 mm/year to the west and 25 mm/year to the east of Düzce. McClusky *et al.* (2000) derived a constant value of 24 mm/year for the whole NAF from the GPS data (Figure 3.8b, brown dashed line). In the Sea of Marmara region, the difference between block models and our results (Figure 3.8b, banded graphs for model space and red line for best model SOUTH-6) exceeds ∼5 mm/year. This discrepancy mainly results from the approach in block models to map geodetic velocities onto slip at block boundaries, and to consider residues to result from continuum deformation (e.g., Nyst and Thatcher, 2004): this tends to maximize the fault slip-rate (fault potency rate) and explains why studies that make different choices regarding the partitioning of fault slip and continuum deformation (e.g., Provost *et al.*, 2003; Flerit *et al.*, 2004; Langstaff and Meade, 2013, and this study) consistently find lower fault slip-rates.

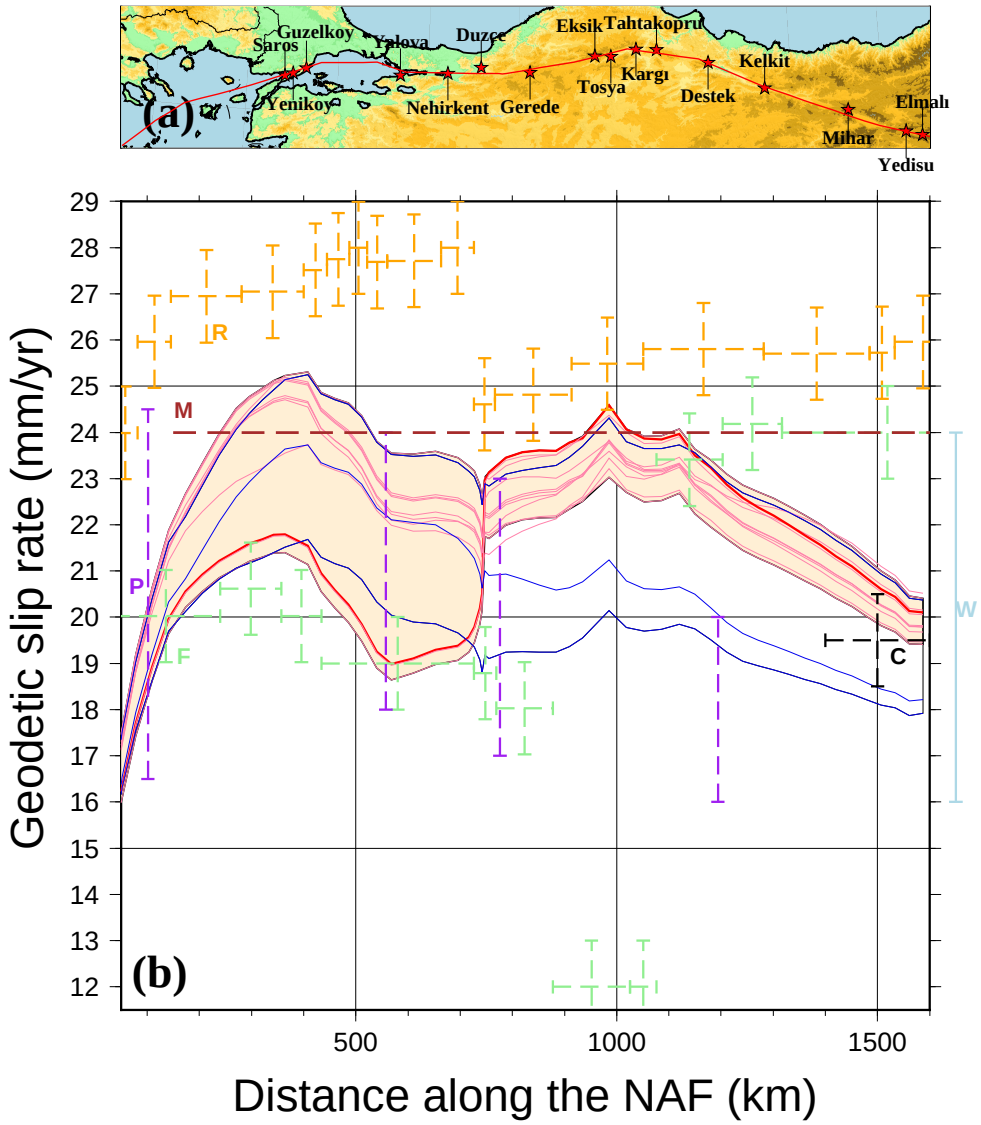


**Figure 3.8:** Comparison of present-day slip-rates on the North Anatolian Fault (NAF) zone with fault slip-rates from our models. a) Shaded relief map of the NAF region locations of geological slip-rate studies (red stars). b) Model slip-rates of SOUTH (orange shaded band) and NORTH (blue hachured band), with individual model slip-rate results shown by red and blue lines, respectively. Thick red line represents our best model (SOUTH-6). Model slip-rates are calculated for the northern branch of the NAF, whose geometry is given nearly parallel to the plot axis shown in panel (a). Brown colored line with label 'M' indicates the rate determined from the Eurasia-Anatolia Euler pole (McClusky *et al.*, 2000). Discrete orange boxes with label 'R' represent the slip-rates from Reilinger *et al.* (2006) block model, where computation error is defined by the height of each box. Light green discrete lines with label 'F' represent Flerit *et al.* (2004) model slip-rates. Purple error bars with label 'P' indicate slip-rates determined from Provost *et al.* (2003). The seismic slip-rate estimates (Table 3.3, light blue bar at the right end of plot area) span a range of 16-24 mm/year for the NAF and represent the slip-rate value for the whole fault zone.

As an alternative to block modeling, Flerit *et al.* (2004) utilized a fracture mechanics approach for the Anatolia deformation, where slip-rates for the NAF (Figure 3.8b, green

error bars showing the range of values on the y-axis and segment range on the x-axis) agree with our results for slip-rate estimates in the Sea of Marmara region, but to the east they predict higher slip-rates. Thus, although in or study we do not constrain a priori where continuum deformation will be taking place as they do, differences appear to be too small to answer which of the methods is superior. Provost *et al.* (2003) applied far-field velocity conditions and the effect of the topography forcing in a 3D model with rheological complexities. Their slip-rate estimates (thick red error bars in Figure 3.8b, purple error bars representing point values) agree with our model results, albeit with much larger uncertainties.

Studies involving seismic moment tensor summation from earthquake catalogues also yield slip-rate estimates for the NAF (Figure 3.8b, light blue error bar at the right end of the plot, indicating range of values: Jackson and McKenzie (1988); Kiratzi (1993); Westaway (1994); Ambraseys (2006), agreeing well with our model results, partly because the range of seismic strain rates is very broad. In Appendix C (Figures C.1 and C.2) we compare modeled slip-rates with results from previous studies for the EAF and DSF. Our model slip-rates for both the EAF and DSF are lower than what previous studies showed, with the exception of seismic slip-rate results. Our results agree well with the range of seismic slip-rates. As explained in Section 3.5.1, we do not attempt to improve the model fit in the easternmost domain in this paper; therefore, slip-rates within this part of the domain may be lower than what elastic block model studies indicate.

In conclusion, our slip-rate results for the NAF thus largely agree with previous work conducted in the region, with the exception of block-model estimates. Considering the 1 mm/year accuracy of the GPS-derived velocity data, variations in model slip-rates are large. This indicates that the overriding plate is sensitive to the southern boundary configuration, although this configuration's role is still subordinate to Hellenic trench and Arabian collisional boundary conditions.

## 3.6 "Geodetic" versus "geological" deformation

### 3.6.1 Context

Deformation after many earthquake cycles usually leaves an expression on the land surface, where the geomorphological features or sediments may be markedly displaced. Determination and dating of such offset markers or sediments yield the geologically determined slip-rates, although the definition of geological slip-rate is vague as long as the time span

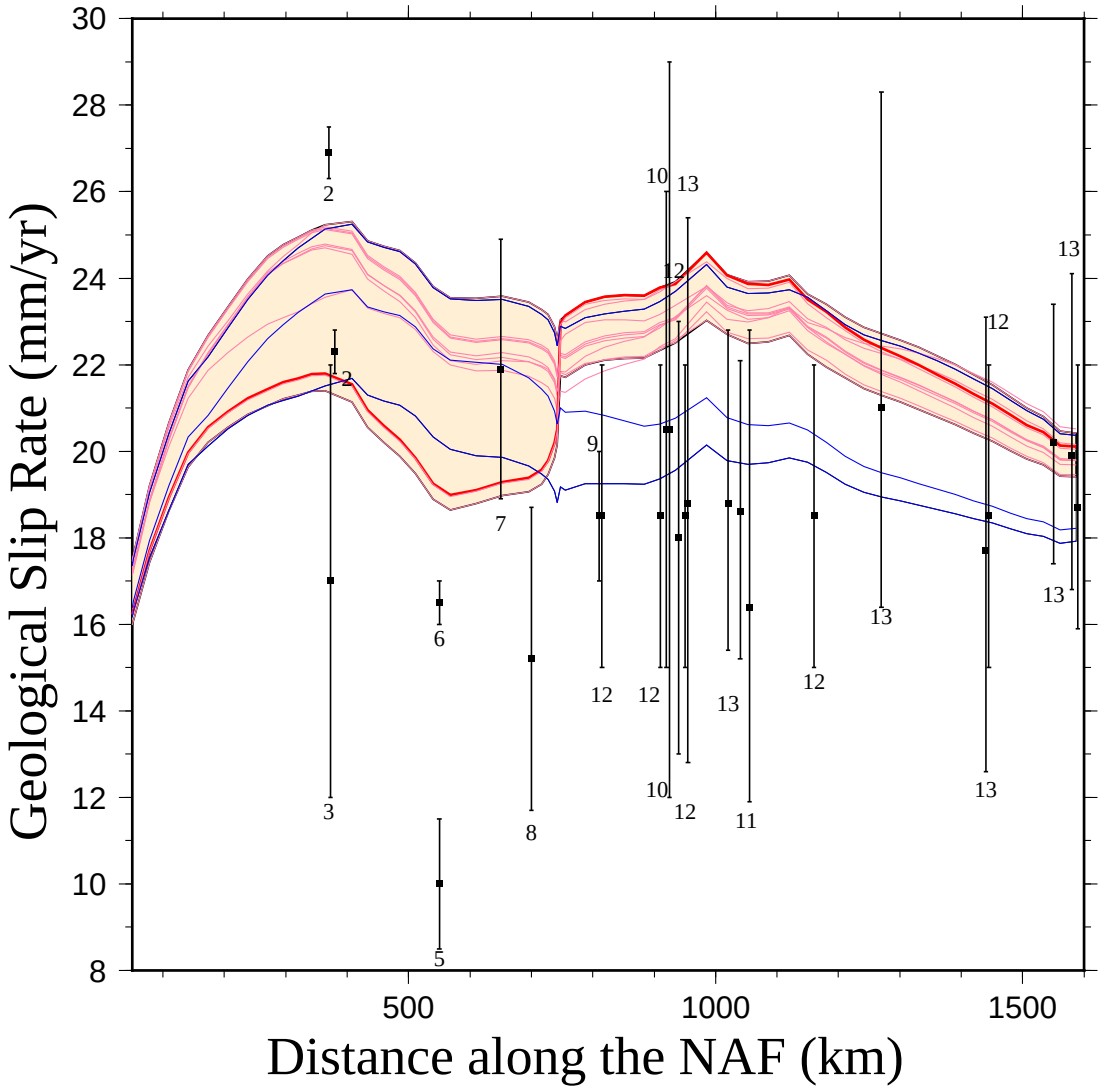


**Figure 3.9:** Comparison of geological slip-rates on the North Anatolian Fault (NAF) zone with fault slip-rates from our models. For location see shaded relief map in Figure 3.8a. Model slip-rates of SOUTH (orange shaded band) and NORTH (blue hachured band), with individual model slip-rate results shown by red and blue lines, respectively. Thick red line represents our best model (SOUTH-6). Model slip-rates are calculated for the northern branch of the NAF, whose geometry is given nearly parallel to the plot axis shown in Figure 3.8a. Observed slip-rates with error bars are labeled by numbers (Table 3.1)

of "many earthquake cycles" is variable; usually a time interval of 1 to 1000 thousand years is implied (e.g., Tapponnier *et al.*, 2001; Thatcher, 2009). Here we compare model slip-rates on the NAF and EAF with respect to geologically determined rates and, as such, discuss the validity of our model results on the scale of geological time. Furthermore, the agreement between geological and geodetic slip-rate is certainly important, because the difference between them is an indication of elastic strain accumulation, which may be released by earthquakes. We present results from the NAF here and leave the discussion

for the DSF and EAF for Appendix C.

### 3.6.2 Slip-rate observations

Geological slip-rate observations represent average displacements divided by time from the early Pliocene-Quaternary until present. For the NAF the majority of the data average many seismic cycles and have a good coverage of the fault zone (Table 3.1 and black error bars in Figure 3.9). The geological slip-rate data have too sparse of a distribution to aid our analysis for the EAF (segments of the fault are indicated in Figure 3.10a). Therefore, we compiled published fault offsets (Table 3.2) and computed first-order estimates for the average slip-rate on the fault by dividing these offsets (Figure 3.10b) by the fault initiation time (2.9 Ma (Hubert-Ferrari *et al.*, 2009) and 1.9 Ma (Herece, 2008)). Resultant slip-rates are shown in Figure 3.10c. This way of calculating slip-rates may underestimate the slip-rate values because faults usually evolve with time and fault segments do not accumulate displacements after the inception of the fault.

### 3.6.3 Comparison of data and models

In Figure 3.9, superimposed on all NORTH and SOUTH model bundles, geological slip-rates of NAF are shown with error bars (see Figure 3.8a for the location map). For the NAF, the best model, SOUTH-6 (thick red line), has a good fit to the data, except in the intervals of 700–900 km and 1000–1200 km. The model overall exhibits higher rates than the geological data. Previous model studies also found that geological rates were too low. The uncertainty in the data is so large that alternative configurations would have been possible. For example, whereas NORTH models show a better fit in the eastern part of the NAF (from 700 km onwards), SOUTH model fits are better in the west. Overall our model results are within the error bars of geologically determined slip-rates along the NAF and we estimate an average slip-rate of 22 mm/year for the fault.

Figure 3.10d shows that model results for the EAF largely agree with the slip-rate data presented in Figure 3.10c, including the northernmost DSF, and if extrapolated further southwest, until Antakya (Seyrek *et al.*, 2007) – the furthermost data point of Figure 3.10c lies outside of the panel. On the other hand, Çetin *et al.*'s (2003) paleoseismological slip-rates between Lake Hazar and Palu are underestimated by all models. The seismic slip-rate estimates (Table 3.3; Figure C.1) span a range of 6–10 mm/year and agree with our slip-rate. Figure 3.11 summarizes the correlation between average geological fault slip-rates and model results for major faults in our domain. Geological estimates

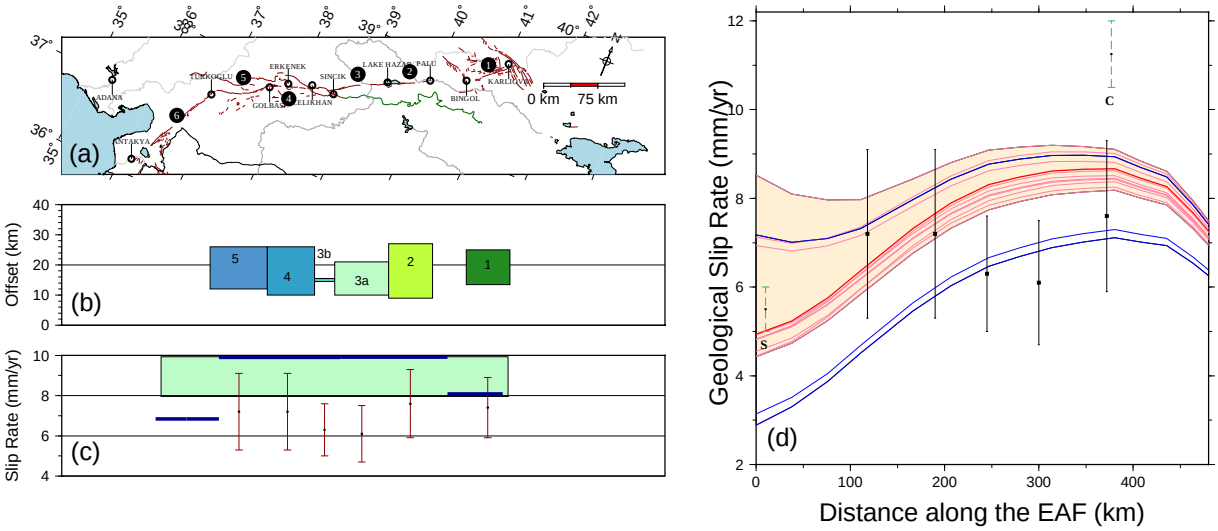


**Figure 3.10:** a) East Anatolian Fault from Karlıova to Antakya (Herece, 2008). Line segments in red show the EAF and green shows Bitlis suture zone. Major rivers in the region are shown in gray. Numbers indicate fault segments: 1. Karlıova - Bingöl, 2. Palu - Lake Hazar, 3. Sincik - Çelikhan , 4. Çelikhan - Gölbaşı, 5. Gölbaşı - Türkoğlu, 6. Türkoğlu - Antakya. b) Measured offsets on the fault, which are tabulated in Table 3.2. Boxes indicate the minimum and maximum estimates. c) Black points with error bars refer to slip-rates obtained from paleoseismology studies listed in Table 3.2. C: (Çetin *et al.*, 2003); S: Seyrek *et al.* (2007) and Karabacak *et al.* (2010). Red points with error bars are the long-term slip-rates of the EAF, calculated from Table 3.2. Light green box indicates the rate determined from the Eurasia-Anatolia Euler pole (McClusky *et al.*, 2000). Discrete line segments are fault parallel slip-rates determined by mechanical models. Dark blue denotes Flerit *et al.* (2004), whereas Reilinger *et al.* (2006) slightly overlies the central segment of Flerit *et al.* (2004) for the whole EAF. Continuous red line with blue circles shows our slip-rate model results. d) Comparison of geological slip-rates on the East Anatolian Fault (EAF) zone with fault slip-rates from our models. For location see Figure 3.10(a). Model slip rates of SOUTH (orange shaded band) and NORTH (blue hachured band), with individual model slip rate results shown in red and blue lines, respectively. Thick red line represents our best model (SOUTH-6).

predominantly reflect average slip-rates from the latest Pliocene-Quaternary until Present. Similar to Reilinger *et al.* (2006), we find good correlation between our model results and geological observations.

### 3.6.4 Vertical axis rotations

Vertical axis rotations are useful for comparison with paleomagnetic observations. Anatolia rotates counter-clockwise with variable rotation rates (Figure 3.12; Piper *et al.*, 2010). Four data points on the Arabian plate show similar rotations coherent with Anatolia (Van Dongen *et al.*, 1967; Nur and Helsley, 1971). The Isparta Angle shows either no rotation or counter-clockwise rotations since the early Miocene (Meijers *et al.*, 2011). Clockwise rotations in western and central Greece pervade to the Peloponnese (Van Hinsbergen *et al.*, 2005) and the westernmost Hellenic trench region. The eastern Hellenic

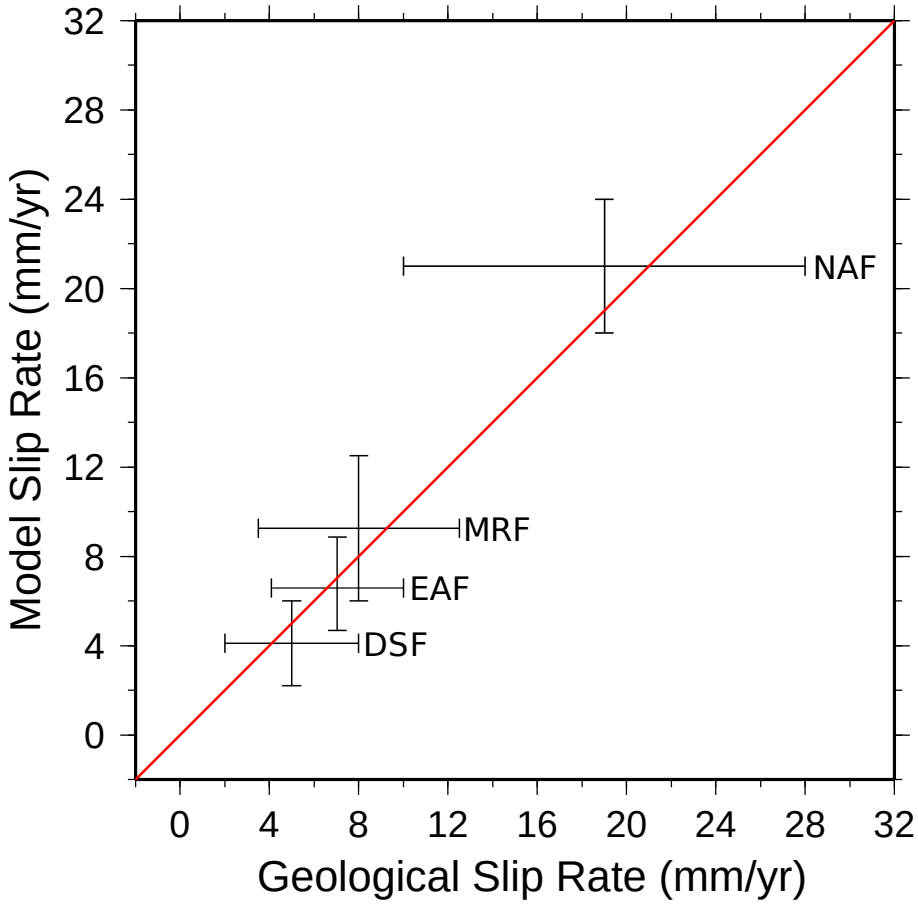


**Figure 3.11:** Spatially averaged geological slip rates vs. slip rates of best model SOUTH-6 for the Dead Sea Fault (DSF), East Anatolian Fault (EAF), Zagros Main Recent Fault (MRF), and North Anatolian Fault (NAF).

trench displays counter-clockwise rotations, similar to Anatolia (Duermeijer *et al.*, 2000). Vertical axis rotations are computed for our preferred SOUTH-6 model, which is elastic. Hence, they are not finite rotations but indicate the potential for rotation to occur on geological time scales. We therefore only compare relative rotations. Our model results show good agreement with the sense of rotation of the data in central Anatolia and the Isparta Angle, mainland Greece, and the Hellenic trench region. Misfits are found in the northwest of Anatolia where the model produces counter-clockwise rotations, whereas data indicate the contrary. This may be due to the nonhomogeneous nature of rotations caused by the active tectonic movements. Furthermore, errors due to the nature of the paleomagnetic data (weak paleomagnetic signal, remagnetization, errors in age determination) result in a scatter of rotations. Overall, model rotations agree with the first-order features of the paleomagnetic data, although the data have large magnitude uncertainties.

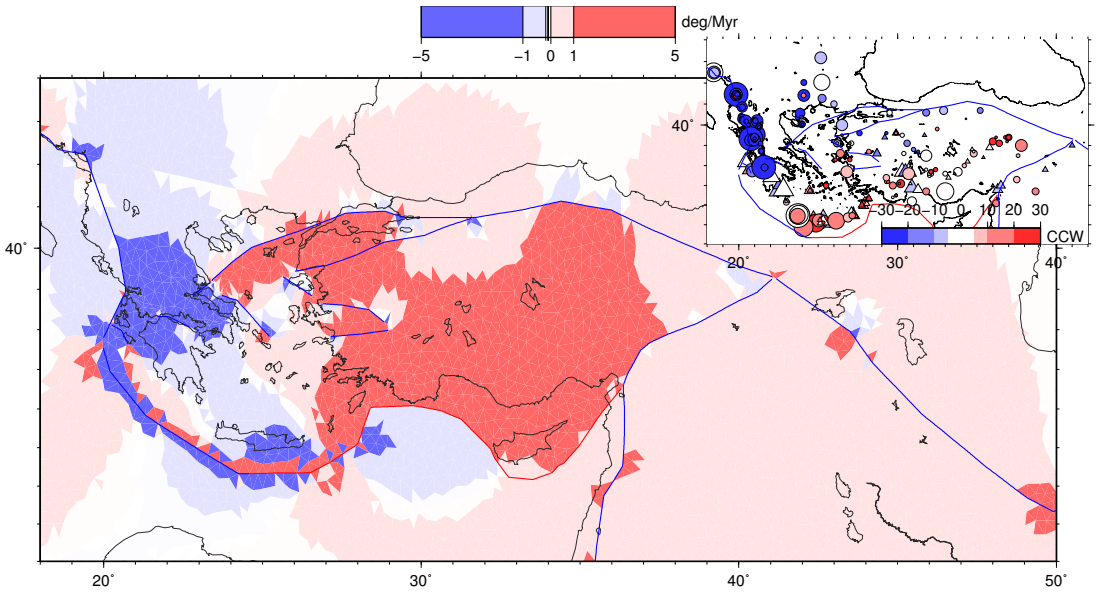


**Figure 3.12:** Vertical axis rotations predicted by model SOUTH-6. The color scale shows the vertical axis rotations in degrees per Myr. Blue and red colors indicate clockwise and counter-clockwise motions, respectively. Inset: Paleomagnetic rotation data (see the main text for references). Circles show pre-Pliocene sampling sites and triangles represent Oligocene and Miocene sample sites. Diameter of symbols are scaled with $\alpha_{95}$ value (larger symbol indicates a more reliable measurement).

## 3.7 Discussion

### 3.7.1 Comparison with block models

Several studies inverted for a block model description of the GPS velocity field (Nyst and Thatcher, 2004; Reilinger *et al.*, 2006; Floyd *et al.*, 2010), whereas we treated the Anatolia–Aegean to be part of a deformation zone, allowing nonrigid behavior. The Anatolia–Aegean region exhibits varying deformation styles and we explain these complex deformation patterns with the least number of faults and blocks. Comparison of RMS error between previous block models and our study is shown in Table 3.4. Our RMS error magnitudes are very similar to the errors of block model studies.

Reilinger *et al.* (2006) argued from their kinematic study that the westward motion and counter-clockwise rotation of Anatolia do not comply with the extrusion process, while the increasing velocities of Anatolia towards the Hellenic trench suggest that slab rollback and accompanying overriding plate motion is a better dynamic explanation. Our model results are at odds with their conclusion. The combined effect of the Arabian push and Hellenic trench pull constitutes the main driving boundary conditions for this deformation zone, as shown by Meijer and Wortel (1996, 1997), and justified by our own model.

Furthermore, Reilinger *et al.* (2006) identified a mismatch between geological and GPS-derived slip-rates for the NAF. The authors attributed the difference to geological surface offsets that do not reflect the full rate at depth due to off-fault shallow deformation. This is a likely explanation. Another contribution to differences between geological and geodetic slip-rates may result from their block approach, which is based on rigid blocks. Hergert and Heidbach (2010) showed that a more appropriate model, which allows internal deformation, accounts for slip-rates in the Marmara segment of the NAF, which are considerably smaller than the block model results and also compatible with the geological rates. In our approach we generalized this finding to the whole of the NAF. We find that the slip-rate estimates are within the error margins of geologically derived slip-rate data.

African and Arabian motion from plate tectonic estimates differed insignificantly from the GPS rate for the past 11 and 22 Myrs, respectively (ArRajehi *et al.*, 2010), although, prior to the Pliocene, active deformation of Anatolia was influenced by different fault geometries. Moreover, the relative motion at the Hellenic trench might have been different (Meijer and Wortel, 1996; Royden and Papanikolaou, 2011). The agreement of our slip-rate model results and the geological data indicates that the mechanical model describes the deformation of this region from the early Pleistocene onwards. Unfortunately, the slip-rate data do not constrain the effect of a variation in the relative plate motion on the Hellenic trench and fault geometries. Using primarily the Aegean dataset Reilinger *et al.* (2010) arrived at the same conclusion concerning the coherence of geological and present-day deformation rates. Our results improve their findings, especially for the NAF and EAF slip-rate estimates.

### 3.7.2 How long has the present-day plate boundary configuration existed?

We consider fault slip-rates as important recorders of changes in the plate boundary configuration. Geological slip-rate data on major regional faults span a variety of ages, from several million years to tens of thousands and even a few hundred years. The compatibility of model results with slip-rates (Figure 3.11) obtained from such a large age spectrum is intriguing. Geological slip-rates are sensitive to two factors: the geometry of the faults and the far-field (plate tectonic) velocities, and both have varied in the recent geological past. First, the NAF is a relatively young feature. The NAF entered the Sea of Marmara at around 200 ka (Le Pichon *et al.*, 2001), implying that the whole strike-slip system acquired its overall geometry after 200 ka. However, deformation related to the NAF predecessor (the wider North Anatolian Shear Zone from which the NAF localized) was

evident in the Sea of Marmara since the late Miocene (Şengör *et al.*, 2005). In fact, prior to 200 ka, the NAF had accumulated more than 90% of its total offset (Şengör *et al.*, 2005) here. Thus, the geometry of the NAF used in this study has been more or less mature for the comparison between the geological and model (geodetic) time scale to be valid. For the EAF, after the initiation of the EAF at around 2.9 (Hubert-Ferrari *et al.*, 2009) or 1.9 Ma (Herece, 2008), the geometry of major faults in the east did not change much.

Geological slip-rates are also sensitive to the plate tectonic velocities and changes therein. According to ArRajehi *et al.* (2010) the present-day Arabia motion with respect to Eurasia obtained from GPS and plate tectonic estimates since the Miocene are consistent within uncertainties. The migration rate of the Hellenic trench has increased since the Oligocene (Royden and Papanikolaou, 2011; Van Hinsbergen and Schmid, 2012), with significant lateral variations from west to east. Slip-rates along the NAF increased also since the middle Miocene (Hubert-Ferrari *et al.*, 2002). The nature and location of the southern plate boundary may thus have existed since a few Myrs, and possibly longer.

## 3.8 Conclusions

Observations of near-surface deformation in and near the Anatolian-Aegean region agree best with an Aegean-Anatolian southern plate boundary via the Pliny-Strabo trench - Anaximander Mountains - ESM collision south of the Cyprus - Latakia ridge. The sense of motion along this boundary is defined by (1) an Anaximander Mountains fault with both strike-slip and dip-slip components and (2) predominant strike-slip along the Latakia segment. The southern plate boundary as preferred for the present day (SOUTH configuration) may have existed since the Late Pliocene.

In addition to well-established faults in Anatolia, the surface deformation requires an inactive Burdur–Fethiye fault zone, active Menderes faults, and an active southern strand of the NAF in NW Turkey

## Acknowledgments

We would like to thank AMC Şengör for valuable discussions, Cengiz Zabcı for providing his PhD thesis and latest slip-rate estimates for the eastern part of the NAF, and Oliver Heidbach for his support in stress field smoothing procedures. We thank Rob Reilinger

and two anonymous reviewers for constructive comments that contributed significantly to improving the manuscript. ADÖ was funded by the Netherlands Research Center for Integrated Solid Earth Sciences (ISES). Figures in this paper were created using GMT Software (Wessel and Smith, 1998).

**Table 3.1:** Compilation of geological slip-rate (slip-rate averaged over a few or more seismic cycles) determinations for the North Anatolian Fault. Ages of structures are reported in thousand years (ka). Numbers in the references column refer to: 1. Armijo *et al.* (1999); 2. Aksoy *et al.* (2010); 3. Meghraoui *et al.* (2012); 4. Schindler (1997); 5. Polonia *et al.* (2004); 6. Dolan (2009); 7. Dikbaş *et al.* (2009); 8. Pucci *et al.* (2008); 9. Kondo *et al.* (2010); 10. Kozacı *et al.* (2007); 11. Kozacı *et al.* (2009); 12.Hubert-Ferrari *et al.* (2002); 13. Zabcı (2012); Gray and white bands separate individual studies in the table. Letter Notes refer to: a: Stratigraphical age and the validity of the correlatable offset markers are disputed by Yaltırak *et al.* (2000) and Şengör *et al.* (2005); b: This measurement is corrected and reinterpreted by Meghraoui *et al.* (2012), which is listed below; c: Dolan (2009) discusses this measurement and reports a faster slip rate for the same location; d: According to Cowgill (2007) and Zabcı (2012), the higher rates of 21±2 reported by Hubert-Ferrari *et al.* (2002) are more reliable for this segment

| **Age (ka)** | **Slip-rate (mm/yr)** | **Location** | **References** |
|---|---|---|---|
| 5000 | 14±1[a] | Ganos | 1 |
| 0.7 | 22.3±0.5[b] | Güzelköy | 2 |
| 0.781 | 26.9±0.6 | | |
| 2.8 | 17.0±0.3 | Yeniköy | |
| 17.5 | 17.7 - 18.9 | Ganos | |
| 20 | 17.9 | | |
| 1 | 17±5 | Güzelköy | 3 |
| 3000-4000 | 15 - 22 | S. of Marmara | 4 |
| 10 | 10±1.5[c] | S. of Marmara | 5 |
| - | 16 - 17 | S. of Marmara | 6 |
| 1 | 21.9±3.0 | Nehirkent/Adapazarı | 7 |
| 21.7±1.9 | 14.0±2.1 | Düzce | 8 |
| 60.1±6.3 | 15.2±3.5 | | |
| 60 | 15.0±3.2 | | |
| 1 | 17 - 20 | Gerede | 9 |
| 2 - 2.5 | 20.5±5.5 | Eksik | 10 |
| | 20.5±8.5 | | |
| 2 - 3 | 18.6±3.4 | Tahtaköprü | 11 |
| | 16.4+6.4/−4.5 | | |
| 10 - 12 | 18.5±3.5 | Eksik&Berçin | 12 |
| 10 - 12 | 18.5±3.5 | Gerede | |
| 10 - 12 | 18.5±3.5 | Destek | |
| 10 - 12 | 18.5±3.5 | Mihar | |
| 1.640±0.06 | 18±5[d] | Üçoluk/Tosya | |
| 2.5±0.3 | 18.7+3.3/−2.8 | Elmalı | 13 |
| 2.7±0.5 | 19.9+4.2/−3.1 | | |
| 3.3±0.3 | 20.2+3.2/−2.8 | Yedisu | |
| 1.6±0.1 | 17.7+5.4/−5.1 | Mihar | |
| 1.3±0.3 | 21.0+7.3/−4.6 | Kelkit V | |
| 4.4±0.5 | 18.8+4.0/−3.4 | Kargı | |
| 1.6+0.1/−0.2 | 18.8+6.6/−6.0 | Tosya | |

**Table 3.2:** Compilation of geological slip-rate (slip-rate averaged over a few or more seismic cycles) determinations for the East Anatolian Fault (EAF). The age of the fault is taken to be bracketed between 1.9 (Herece, 2008) and 2.9 Ma (Hubert-Ferrari *et al.*, 2009). Ages of structures are reported in million years (Ma). Slip-rates are determined by dividing the measured offsets into fault age (1.9–2.9 Ma). Numbers in the references column refer to: 1. Herece (2008); 2. Seymen and Aydin (1972); 3. Dewey *et al.* (1986); 4. Şaroğlu *et al.* (1992); 5. Hubert-Ferrari *et al.* (2009); 6. Arpat and Şaroğlu (1972); 7. Herece and Akay (1992); 8. Turan (1993); 9. Çetin *et al.* (2003); 10. Arpat and Şaroğlu (1975); 11. Hempton (1985); 12. Şaroğlu *et al.* (1987); 13. Parlak (2004); 14. Westaway and Arger (1996); 15. Yönlü *et al.* (2013); 16. Seyrek *et al.* (2007); 17. Karabacak *et al.* (2010). Gray and white bands separate each segment of the EAF system. Numbers in parentheses in the location column are used in Figure 3.10. Letter notes refer to a:cited by Çetin *et al.* (2003); b:Westaway and Arger (1996) measured 17km offset from Hempton (1985)'s map; c:cited by Parlak (2004); d:near Erkenek; e:near Gölbaşı; f:Göksu river offset cited by Westaway and Arger (1996)

| Age (Ma) | Offset (km) | Slip-rate (mm/yr) | Location | References |
|---|---|---|---|---|
| 1.9 | 14.5±1 | 6.0±1.7 | Karlıova - Bingöl (1) | 1 |
| | 15 | 6.3±1.3 | | 2 |
| | 22 | 9.2±1.9 | | 3 |
| 2.88 | 20±5 | 8.3±3.8 | | 4,5 |
| 1.9 | 16.1±1 | 6.7±1.8 | Palu - L Hazar (2) | 1 |
| 1.9 | 15 -23 | 7.9±3.3 | | 2 |
| | 27[a] | 11.3±2.3 | | 6 |
| | 9 | 3.8±0.8 | | 7 |
| | 11 | 4.6±0.9 | | 8 |
| 0.014-0.015 | 0.16-0.175 | 11±0.9 | | 9 |
| 1.9 | 16 | 6.7±1.4 | Hazar - Sincik (3a) | 1 |
| | 10 | 4.2±0.9 | | 7 |
| | 15 | 6.3±1.3 | | 10 |
| | 21(17)[b] | 7.9±2.5 | | 11 |
| | 13[c] | 5.4±1.1 | | 12 |
| | 15 | 6.3±1.3 | Sincik - Çelikhan (3b) | 6 |
| 1.9 | 22.5-26[d] | 10.1±2.8 | Çelikhan - Gölbaşı (4) | 1 |
| | | 4.2±0.9 | | 13 |
| 1.9 | 19-25 | 9.2±3.2 | Gölbaşı - Türkoğlu (5) | 1 |
| 1.9 | 22.5-26[e] | 10.1±2.8 | | 1 |
| 1.9 | 12 | 5.0±1.0 | | 1 |
| | 13[f] | 5.4±1.1 | | 4 |
| 1.9 | 16 | 6.7±1.4 | | 14 |
| | 16.5±1 | 6.9±1.8 | | 15 |
| | | | Türkoğlu - Antakya (6) | |
| | | 5.6±0.5 | Northern DSF (7) | 16 |
| | 7.9±0.3 | 4.9±0.1 | | 17 |

**Table 3.3:** Slip-rate estimates from moment tensor summation. Numbers in the references column refer to: 1. Jackson and McKenzie (1988); 2. Kiratzi (1993); 3. Westaway (1994); 4. Ambraseys (2006); 5. Kuran (1980); 6.Kiratzi and Papazachos (1995). Gray and white bands separate the estimates of NAF from EAF system.

| **Year** | **Slip-rate (mm/yr)** | **Note** | **Location** | **References** |
|---|---|---|---|---|
| 1900-1988 | 25-30 | | NAF | 1 |
| 1850-1988 | 23 | | NAF | 2 |
| 1900-1992 | 30 | | 30°-40°E | 3 |
| 1900-1992 | 8 | Ignoring 1939-1967 | | |
| 1668-1967 | 14.7 | Ignoring 1939-1967 | | |
| 1668-1967 | 16.8 | including Marmara | 26°-40°E | |
| 1668-1967 | 15-17 | Most likely rates | 26°-40°E | |
| 0-2000 | 20±4 | | 26°-31°E | 4 |
| 1850-1988 | 6 | | EAF | 2 |
| | 4.4 | | EAF | 6 |
| 1500-1988 | 6 | | EAF | 3 |
| 995-1980 | 10 | | EAF | 5 |

**Table 3.4:** Comparison of RMS error between previous block models and this study.

| | Number of Blocks | RMS (mm/yr) |
|---|---|---|
| Nyst and Thatcher (2004) | 4 | 3.9 |
| Reilinger *et al.* (2006) | 6 | 3.9 |
| Floyd *et al.* (2010) | 10 | 2.8 |
| | 15 | 2.6 |
| This Study | - | 4.1 |

# Appendix A WSM 2008 data (gray), smoothed stress field (black) and stress variances (orange).

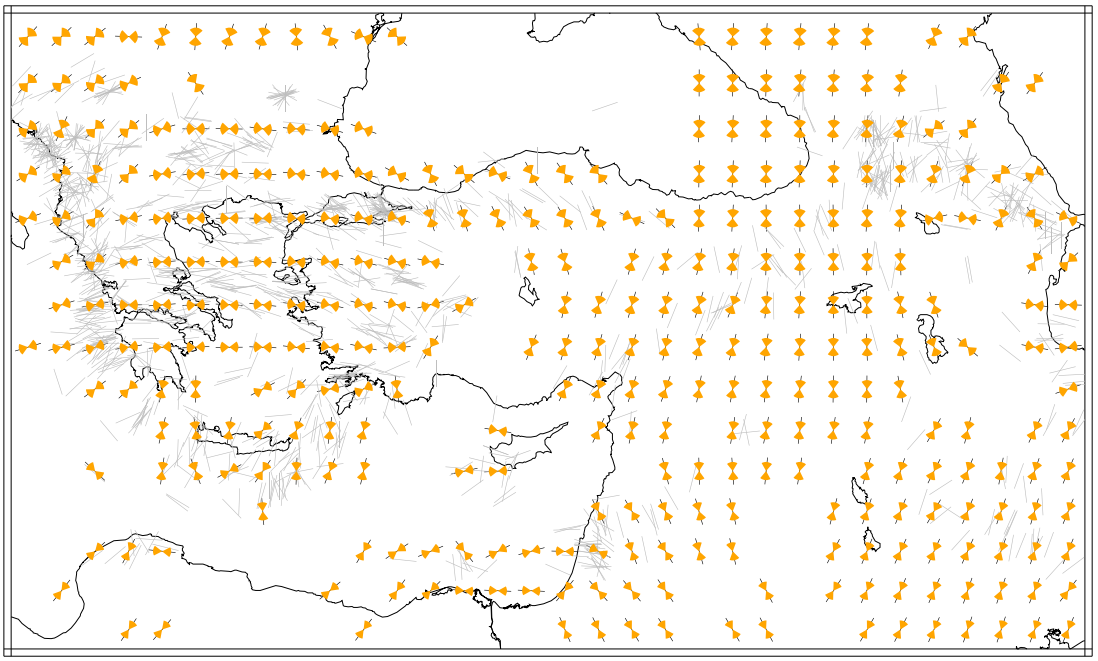

**Figure A.1:** World stress map data, smoothed stress field, and stress variances.

# Appendix B Additional SOUTH model results.

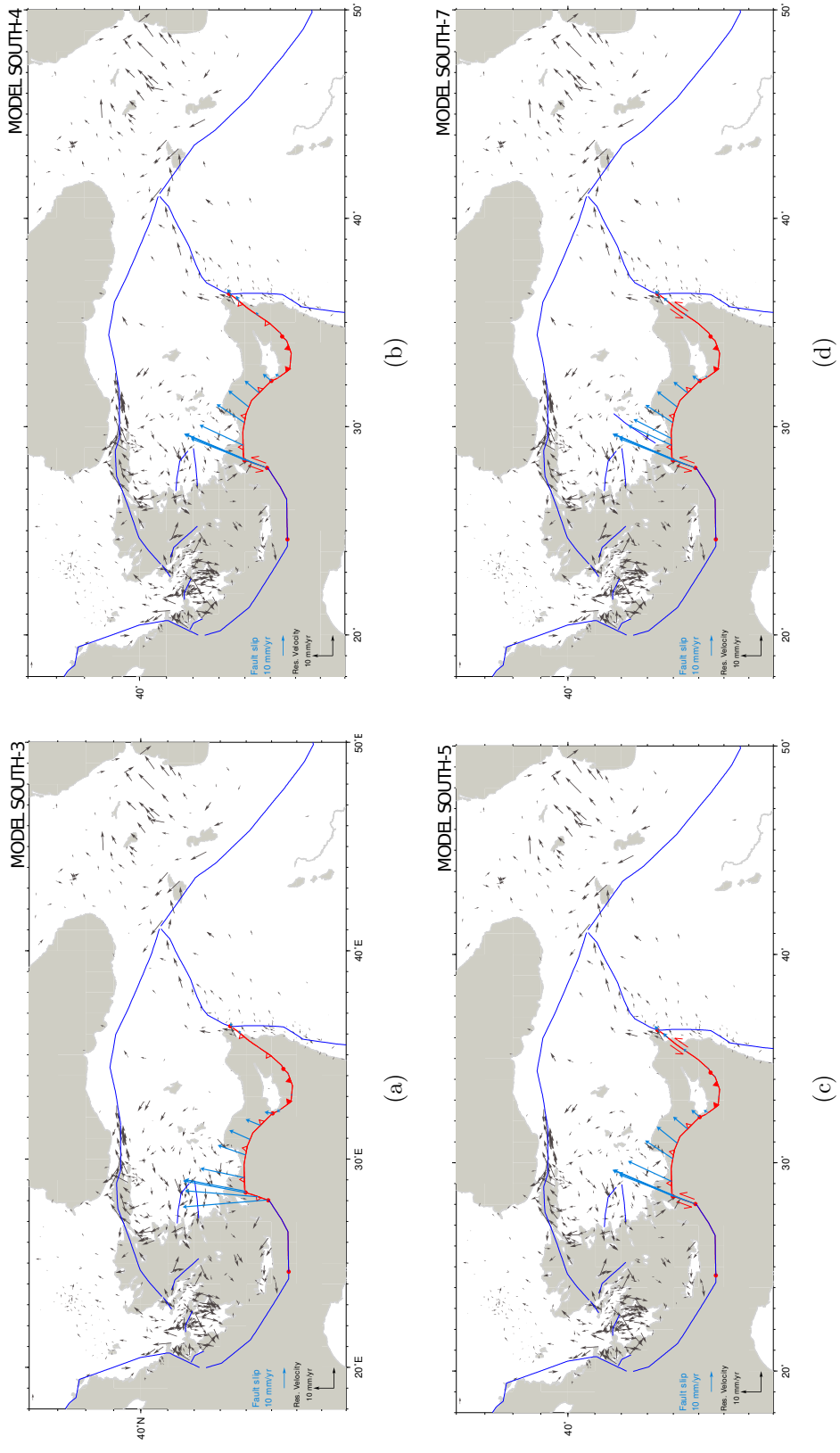


**Figure B.1:** Velocity misfits (observed minus calculated) for a range of SOUTH models. The assumed nature of the faults is indicated on the misfit maps; filled triangles indicate that only fault-perpendicular motion is allowed and strike-slip symbols indicate that only fault parallel motion is allowed. Open triangles indicate that both strike-slip and fault normal motions are allowed in the model. Blue arrows indicate the resulting fault slip-rate and direction. a) Model SOUTH-3 with friction and down-dip relative motion only on the Cyprus trench; b) Model SOUTH-4 with strike-slip only on the Rhodes plate boundary segment; c) Model SOUTH-5 with strike-slip only on the Latakia segment of the plate boundary; d) Model SOUTH-7 with onshore Burdur–Fethiye fault, not connected to Pliny-Strabo trenches; e) Model SOUTH-8 with Burdur–Fethiye fault connected to Pliny-Strabo trenches.

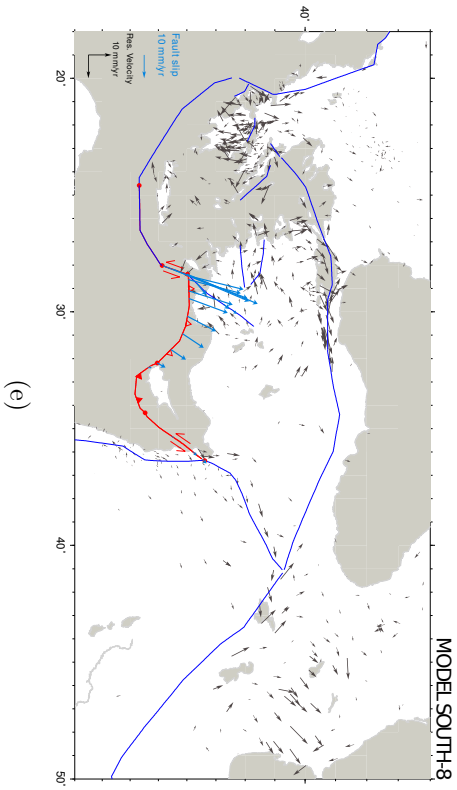
Fault slip
10 mm/yr
Res. Velocity
10 mm/yr
20°
30°
40°
50°
40°
MODEL SOUTH-8

(e)

# Appendix C Geodetic slip-rate model results for EAF and DSF.

Slip-rates for the NORTH and SOUTH model bundles for the EAF and DSF are shown in Figures C.1 and C.2, respectively, with results from previous model studies. For the EAF, model rates span an average of 7 ± 1 mm/year in the east and 6 ± 3 mm/year in the eastern part.

The block model of Reilinger *et al.* (2006), InSAR observations from Cavalie and Jonsson (2014), and the fracture mechanics model of Flerit *et al.* (2004) predict much higher fault slip-rates; none of them, however, agree with the long-term (geological) slip-rate data (Figure 3.10c), which are overestimated by ∼5 mm/year. The seismic slip-rate estimates (Table 3.3, light blue bar at the right end of plot area) span a range of 6–10 mm/year for the EAF and represent a slip-rate value for the whole fault zone, which agrees with our results and with the geological estimates. For the DSF, we predict model slip-rates ranging from 2 mm/year to the south to 5.5 mm/year to the north of the fault system (Figure C.2). The NORTH and SOUTH model bundles have much smaller spread, indicating low sensitivity of the DSF to changing DOFs of southern boundary segments under consideration. Our model rates are smaller than those of other short-time scale studies (Flerit *et al.*, 2004; Reilinger *et al.*, 2006) covering this fault, but they agree with the seismic slip-rate estimates.

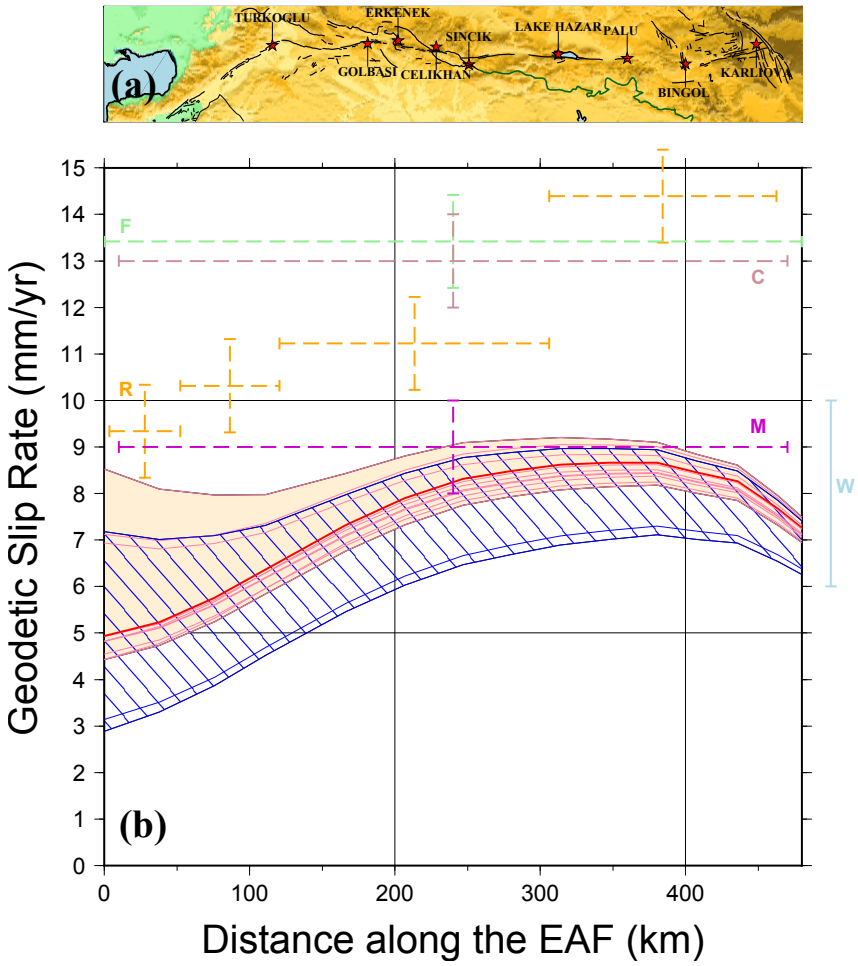


**Figure C.1:** Comparison of geodetic slip-rates with model results for the EAF for SOUTH (orange shaded band) and NORTH (blue hachured band) models, with individual model slip-rate results shown with red and blue lines, respectively. The thick red line represents our best model (SOUTH-6). Error bars indicate previous studies: W: Westaway (1994), M: McClusky *et al.* (2000); F: Flerit *et al.* (2004); R: Reilinger *et al.* (2006); C: Cavalie and Jonsson (2014).

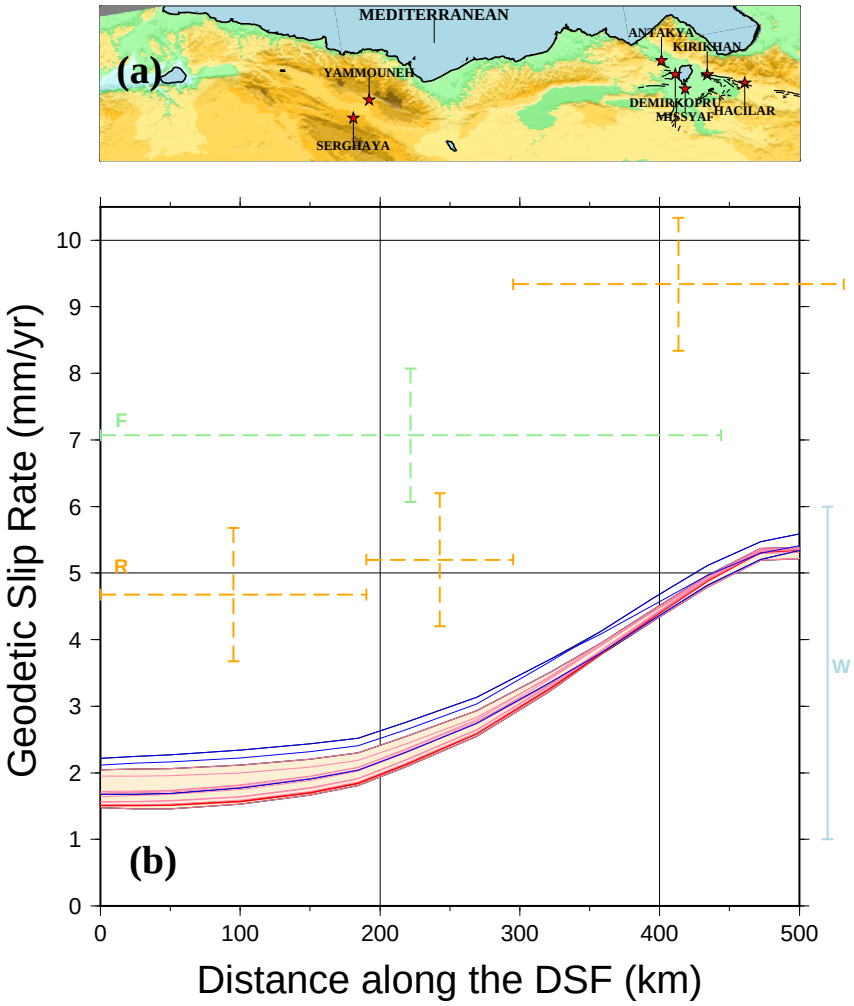


**Figure C.2:** Model slip-rates of the DSF for both SOUTH (orange shaded band) and NORTH (blue hachured band), with individual model slip-rate results shown with red and blue lines, respectively. The thick red line represents the best model (SOUTH-6). Model slip-rates are calculated for the northern branch of the NAF, whose geometry is given nearly parallel to the plot axis shown in the upper panel. Error bars indicate previous studies: W: Westaway (1994), M: McClusky *et al.* (2000); F: Flerit *et al.* (2004); R: Reilinger *et al.* (2006); C: Cavalie and Jonsson (2014).

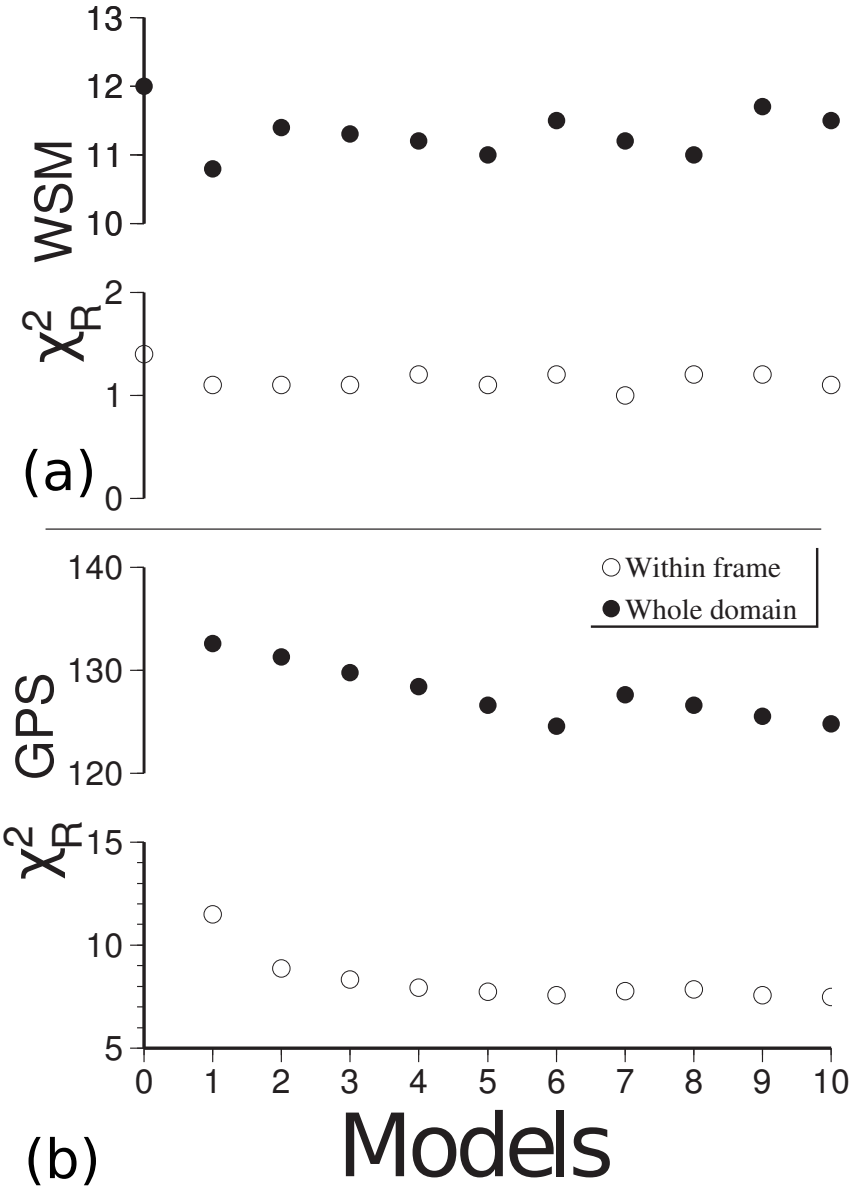


**Figure C.3:** $\chi^2_R$ statistic computed for data points within the whole domain (filled circles) and red frame (empty circles) indicated in Figure 3.1 for a) model stress directions vs. World Stress Map data; b) model velocity predictions vs. GPS-derived velocity data.

# Appendix D Sensitivity of model results to boundary conditions.

In previous models of continental deformation of the Anatolia-Aegean region, GPE is included in some (Cianetti *et al.*, 2001; Jimenez-Munt and Sabadini, 2002; Jimenez-Munt *et al.*, 2003; Fischer, 2006; Özeren and Holt, 2010) and not in others (Meijer and Wortel, 1997; Lundgren *et al.*, 1998; Flerit *et al.*, 2004). All studies match model predictions to (subsets of) available data, but model results (specifically, forces and rheology) differ substantially. For instance, Özeren and Holt (2010) determined pull forces along the Hellenic trench that are about half the magnitude of those obtained by Cianetti *et al.* (2001). Viscosities for the Anatolia region of Fischer (2006) are two orders of magnitude lower than those of Özeren and Holt (2010). Moreover, Jimenez-Munt and Sabadini (2002) inferred that GPE-derived forces are not important for the regional kinematics, which seems at odds with Cianetti *et al.* (2001); Fischer (2006); Özeren and Holt (2010). Such inconsistencies arise from the fact that GPE-based calculations require information about the density layering and mechanical properties of the lithosphere, and this information has significant uncertainties or is even absent in parts of our region of study. Uncertainties in crustal thickness and surface heat flow both contribute to significant uncertainties in the thermal structure of the lithosphere, which translates into significant uncertainties in both the forcing (via density structure) and mechanical properties (via temperature activated viscosity). Another factor contributing to uncertainties in mechanical properties is the (poorly known) composition of the crust. The last unknown is the contribution to the GPE by dynamic topography (e.g., Warners-Ruckstuhl *et al.*, 2012, 2013).

## D.1 Average viscosity

We estimate the vertically averaged viscosity $\eta$ of a lithospheric column by assuming that it behaves as a Newtonian fluid:

$$\eta = \frac{\int_L (\sigma_1 - \sigma_3)\, dz}{\int_L (\dot{\varepsilon}_1 - \dot{\varepsilon}_3)\, dz} \tag{3.1}$$

Here, $(\sigma_1 - \sigma_3)$ is differential stress and $(\dot{\varepsilon}_1 - \dot{\varepsilon}_3)$ is differential strain rate (difference between maximum and minimum eigenvalues of the corresponding tensors), and $L$ is the lithosphere thickness (Ranalli, 1987). A common assumption is that surface strain rates are uniform throughout the lithosphere, such that lithospheric averages follow directly

from differentiating (surface) geodetic velocities:

$$\eta = \frac{\frac{1}{L}\int_L (\sigma_1 - \sigma_3)\, dz}{(\dot{\varepsilon}_1 - \dot{\varepsilon}_3)} \tag{3.2}$$

We use surface differential strain rates for our region from Kreemer *et al.* (2003). Rock strength constitutes an upper limit to the differential stress it may support. An upper limit to average viscosities (and viscosity contrasts) can therefore be derived from the average lithospheric strength map of Tesauro *et al.* (2009) – this defines the numerator. A lower limit to average viscosities can be estimated by assuming that the average differential stress in the domain is small; we assume 1 MPa.

We use a range of viscosities of $3-5\times10^{21}$ Pa s for the Anatolian-Aegean lithosphere in our sensitivity analysis to assess the dependence of model velocity results on the rheology. The Maxwell relaxation time ($\tau_M$) for the highest viscosity domain is 330 kyr. Steady state is generally achieved after $5\tau_M$ (Plattner *et al.*, 2009). Our viscoelastic model reached steady state around $5\tau_M$ and we output the velocities at that time.

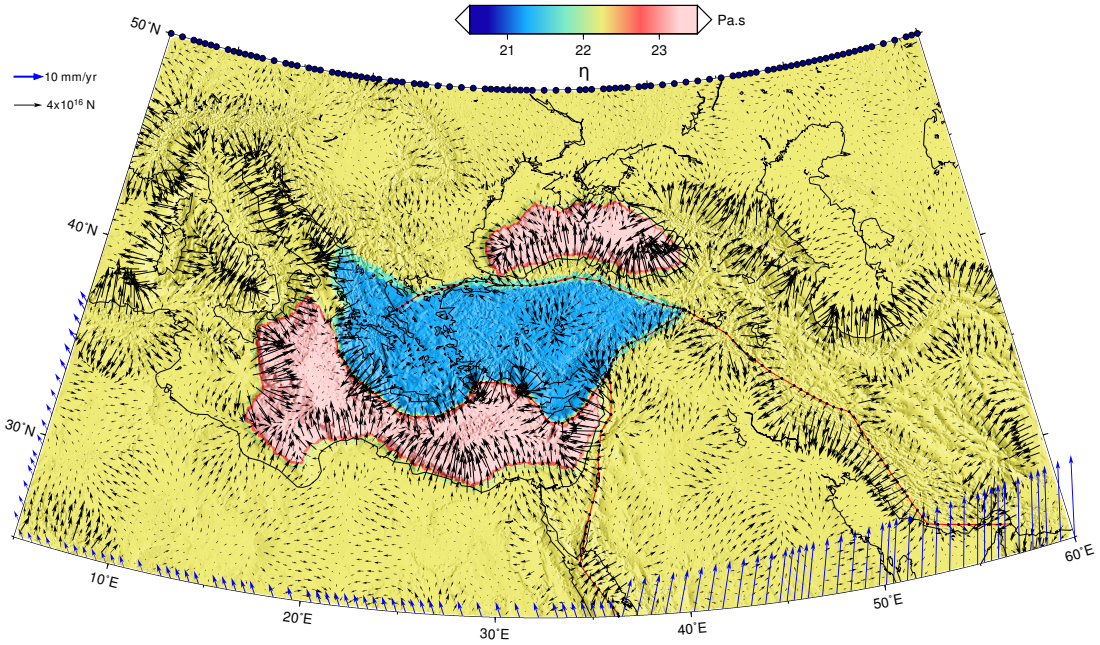


**Figure D.1:** Model domain and boundary conditions (blue arrows) of GPE-driven models. The specific model shown here is for relatively low Aegean-Anatolian viscosity, and for horizontal forces (black arrows) computed with the assumption that the lithosphere is not isostatically compensated. Logarithmic viscosity contours are draped over shaded relief.

## D.2 GPE-derived horizontal forces

GPE forces are applied inside the computational domain. We use the crustal thickness and densities from the CRUST2.0 model (Bassin *et al.*, 2000) and topographical height from the ETOPO2 dataset (2-Minute Gridded Global Relief Data, `http://www.ngdc.noaa.gov/mgg/fliers/06mgg01.html`). The oceanic lithosphere of the Mediterranean is older than 180 Ma (Muller *et al.*, 2008), and hence we assume that the conductive cooling produced a linear geotherm (Stein and Stein, 1992). Mantle lithospheric density profiles are constructed as a function of a linear geotherm for the continental lithosphere. Two different GPE values can be calculated from two end-member density interface topologies: 1) a compensated mantle lithosphere density profile with equalized pressure at the base of the lithosphere and 2) uncompensated pressures at the base. The latter assumption induces about 30%–50% larger forces for this region due to lateral density variations. Ghosh *et al.* (2009) inferred 10%–20% larger forces from their uncompensated global model with respect to the compensated one. Lithospheric thickness is assumed to be 100 km, since there are no cratonic areas in the model domain where the buoyancy from such cratonic roots would affect the GPE calculations.

Given these uncertainties, we investigate end-members for both the GPE-derived forces and for the viscosities in our region of interest. We adopt the plate boundaries and faults of our preferred model (SOUTH-6) from the previous section with one important exception; the Hellenic trench and Pliny-Strabo faults are represented as frictionless faults that can slip in response to model stresses.

Global plate tectonics is driven by body forces, which are manifested within the plates by GPE-derived forces. In a regional model like ours (Figure D.1), boundary conditions ideally would be an accurate representation of GPE-derived forces that surrounding regions exert on the model domain. To determine such boundary conditions is a formidable problem in itself, mostly because the continuity of stresses (and thus forces) across plate boundaries and major faults is strongly modulated by relative details at these discontinuities (e.g., De Franco *et al.*, 2008a,b). Assuming that GPE within the model domain does not significantly affect the velocities of major plates, we impose boundary forces proportional to observed plate velocities along the Africa, Arabia, and Europe margins. Motivated by the results of a recent stress modeling study (Warners-Ruckstuhl *et al.*, 2013) that indicated that GPE forces generated beyond our E and NW domain boundaries are not transmitted into our region of interest, we do not impose forces along these boundaries. A significant difference from the previous models is thus that we do not

impose differential velocities/forces at the Hellenic trench.

## D.3 Results of GPE forcing models

Figure D.2 summarizes the results of our end-member GPE-models. Figure D.2a demonstrates that the misfit is particularly large in the eastern portion of the trench. Here, model SOUTH-6 yields a better (albeit not perfect) match to the observations as a result of additional (subduction-related?) forcing along the Hellenic trench in this model. For the region east of 31°E, Figure D.2b shows an acceptable fit to the GPS velocity magnitudes of the GPE-driven models with low-end viscosities. Importantly, the fit of model SOUTH-6 is equally good, indicating that the representation by edge forces of (distributed) GPE forces does not affect the result. To the west of 31°E, i.e. closer to the Hellenic trench, the misfit between the GPE-driven models and observations is significant. Our conclusion of the previous section, that model SOUTH-6 matches the geodetic observations best, is thus not affected by our choice of boundary conditions in boundary-driven models.

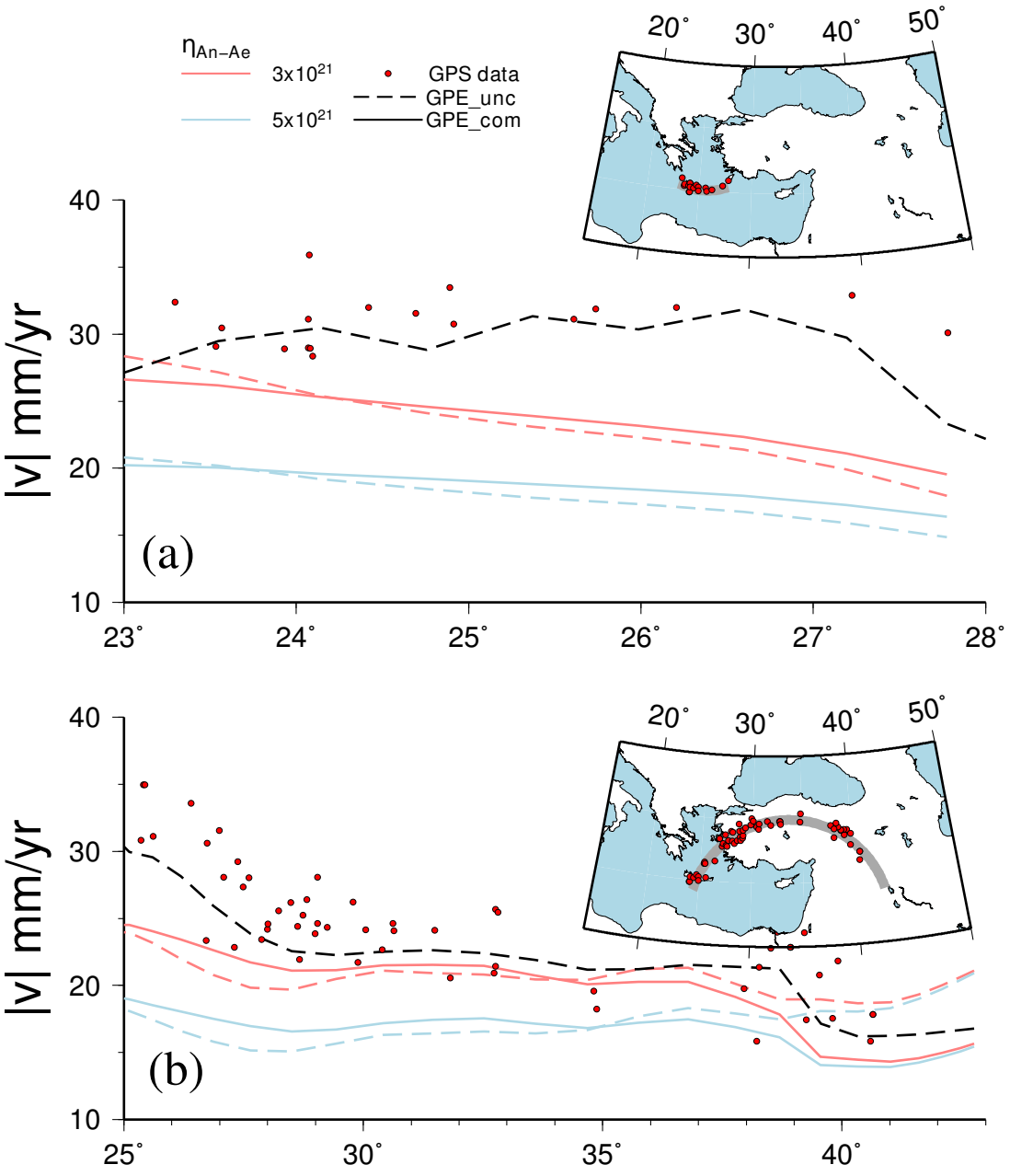


**Figure D.2:** Comparison of observed velocity magnitudes with results of a range of GPE-driven models. Solid lines result from GPE forces derived from isostatically compensated lithosphere, dashed lines from uncompensated lithosphere (see Appendix D for details). Red and blue lines are results of models for relatively low and high viscosities of the Aegean-Anatolian region, respectively. Black dashed lines show velocity magnitudes from model SOUTH-6. a) Velocities in a swath (inset) along the Hellenic trench. b) Velocities along a swath (inset) that is approximately parallel to the relative motion direction of Anatolia with respect to Europe.

# Chapter 4

# The Kefalonia Transform Fault: a STEP in the making[1]

## 4.1 Introduction

Vertical discontinuities have been recognized in various subducted slabs (Figure 4.1; present-day, unless indicated otherwise); including the north Kuriles-Kamchatka slab (Yogodzinski *et al.*, 2001; Levin *et al.*, 2002), Nazca slab (Gutscher *et al.*, 1999; Pesicek *et al.*, 2012; Lynner *et al.*, 2017; Portner *et al.*, 2017), Juan de Fuca/Farallon slab (30 Ma Severinghaus and Atwater, 1990; Sigloch *et al.*, 2008; James *et al.*, 2011), Cocos slab beneath the Trans-Mexican volcanic belt (Dougherty *et al.*, 2012; Dougherty and Clayton, 2014), Izu-Bonin slab (Fryer *et al.*, 2003; Gong *et al.*, 2018; Gvirtzman and Stern, 2004; Miller *et al.*, 2004, 2005, 2006a,b), Japan slab (Obayashi *et al.*, 2009), south Lesser Antilles slab (Russo *et al.*, 1993; Clark *et al.*, 2008; Van Benthem *et al.*, 2013), various Mediterranean slabs (Biryol *et al.*, 2011; Carminati *et al.*, 1998; Jolivet *et al.*, 2013; Spakman *et al.*, 1988; Wortel and Spakman, 2000; de Lis Mancilla *et al.*, 2018), Zagros/Makran slab (Agard *et al.*, 2011), Philippine Sea slab near Taiwan (Lallemand *et al.*, 1997), northern Scotia slab (Forsyth, 1975), eastern Sunda slab (Spakman and Hall, 2010; Widiyantoro *et al.*, 2011), north Tonga slab (Isacks *et al.*, 1969; Millen and Hamburger, 1998), Solomon slab (Neely and Furlong, 2018). Surprisingly, the slab tears evolved into Subduction-Transform-Edge-Propagators (STEPs; Govers and Wortel, 2005) in only very few regions, i.e., the conditions under which STEPs form require other conditions in addition to slab fragmentation. Understanding these conditions is particularly relevant because a vertical tear in a slab seldom leaves a clear tectonic imprint in the crust of the overriding plate. This is different for STEP faults (sensu Baes *et al.*, 2011); their footprint in the tectonic evolution of basins (such as vertical axis rotations, topography build-up, fast trench roll-back) attests to the relevance of STEP activity (e.g., Mediterranean subduction zones, Tonga trench, South Sandwich trench, southern edge of the Lesser Antilles trench, and the western edge of north Sulawesi trench; Govers and Wortel (2005)). We therefore seek to constrain the conditions that facilitate STEP fault initiation in a region where the process may have recently started. Govers and Wortel (2005) suggested that the offshore

[1] A.D. Özbakır, R. Govers, A. Fichtner. *The Kefalonia Transform Fault: a STEP in the making*, manuscript in preparation

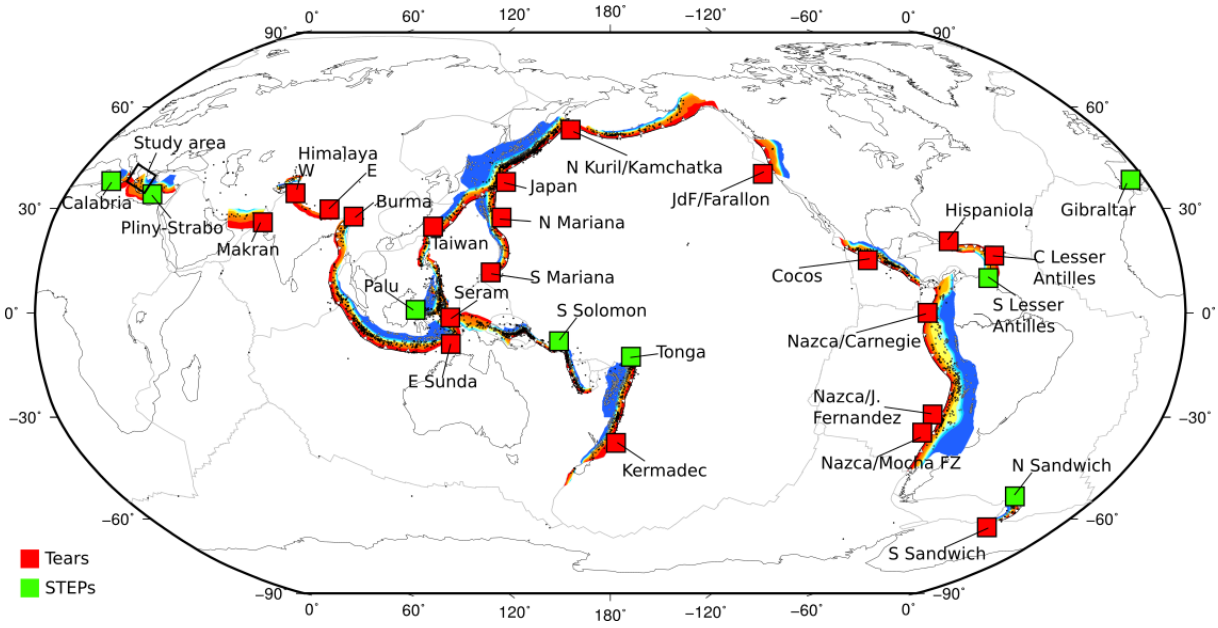


**Figure 4.1:** Global overview of slabs with a vertical tear or a lateral edge that are associated with a STEP fault in the overriding plate ("STEPs"), or not ("Tears"). Slab depth contours (Hayes *et al.*, 2018) are shown in colors, along with plate boundaries from (Bird, 2003) and the intermediate – deep focus earthquake epicenters from the ISC Catalogue (2019) (Weston *et al.*, 2018; Lentas *et al.*, 2019)

Kefalonia Transform Fault (KTF; Figure 4.2) and its on-land continuation constitute a STEP fault. Available geological constraints, discussed below, suggest that the system would be in an infant stage. We study this candidate region for STEP fault initiation in the western Hellenic Subduction Zone.

Here, the active deformation pattern of the overriding Eurasian lithosphere is complex, and its interpretation in terms of the primary drivers non-unique. Likely contributors are rollback of the Hellenic slab and backarc extension, westward motion of Anatolia facilitated by the North Anatolian Fault/North Aegean Trough, strain localization in the Gulf of Corinth, collision in the Dinarides/Albanides, Nubia convergence, mantle convective tractions including dynamic topography, gravitational collapse, and potentially STEP fault activity. In this chapter we do not aim to quantify their relative contributions to the deformation of the overriding plate. Rather, our focus is primarily on the structure of the Hellenic slab near the KTF. The reason is that the interpretation of the deformation of the overriding plate in terms of a STEP fault hinges on the lateral continuity of the slab (Chapter 1, Figure 1.1). In section 4.2 we discuss recent studies of the lateral continuity of the shallow (50-200 km depth) slab and conclude that none of these were conclusive. We present and interpret the results of the regional S-velocity volume of Fichtner *et al.* (2013). As it is based on a tomographic imaging technique that employs complete seismograms

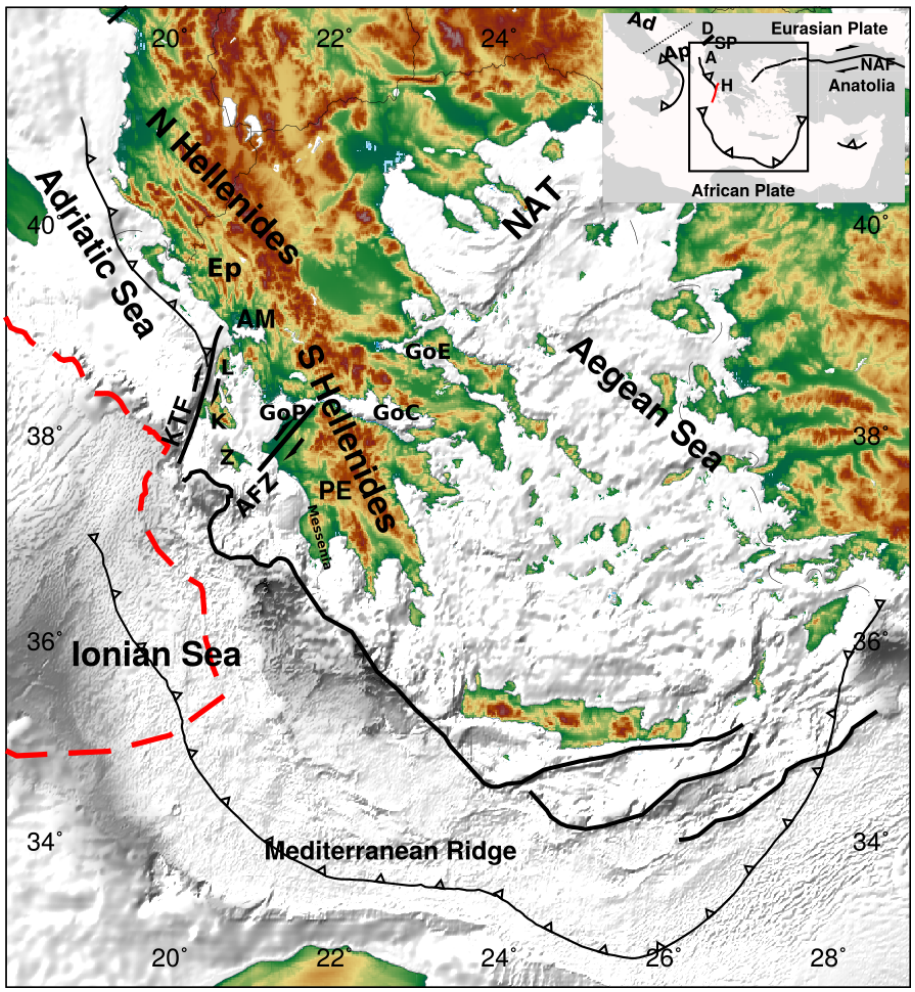


**Figure 4.2:** Topography/bathymetry of the Hellenic subduction zone. The extent of the Ionian oceanic crust is marked by red dashed lines (Chamot-Rooke *et al.*, 2005), thick black lines represent the approximate location of plate contacts and major faults, and the trench physiography is shown with thin barbed black lines. Abbreviations refer to: AM: Amvrakikos Gulf; AFZ: Achaia Fault Zone; Ep: Epirus; GoC: Gulf of Corinth; GoE: Gulf of Evia; GoP: Gulf of Patras; K: Kefalonia; L: Levkas; PE: Peloponnesus; Z: Zakynthos; KTF: Kefalonia Transform Fault; NAT: North Aegean Trough; **Inset** map shows central and eastern Mediterranean subduction/collision zones. A: Albanides, Ad: Adria, Ap: Apulia, D: Dinarides, H: Hellenides, NAF: North Anatolian Fault, SP: Scutari-Pec.

from regional broadband stations, this model captures relevant details in both the crustal and upper-mantle structure between 10 and 200 km depth, where lithosphere–mantle interactions forge tectonic expressions.

The regional context of our study area is typically Mediterranean, of slow Africa-Eurasia convergence and ongoing closure of this land-locked basin (Le Pichon, 1982). Some segments of mostly ephemeral plate boundary segments undergo soft collision (Royden, 1993), while adjacent segments accommodate oceanic subduction with a significant component

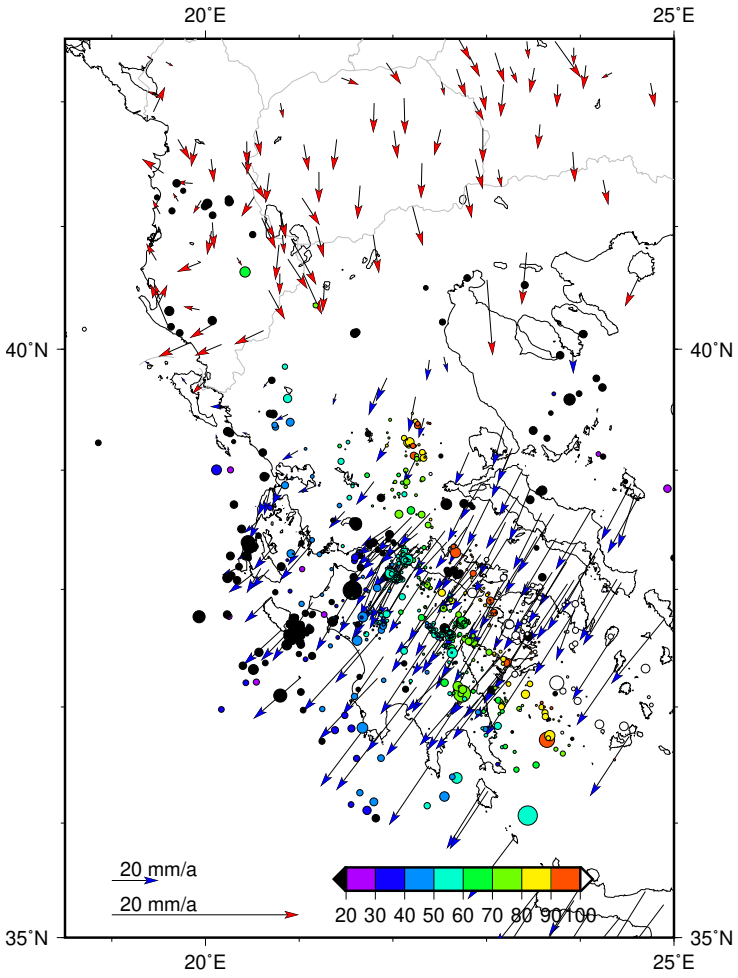


**Figure 4.3:** GNSS-derived horizontal velocity field and seismicity. The velocities are relative to stable Europe, and are compiled from Jouanne *et al.* (2012), Nocquet (2012), and Metois *et al.* (2015). Please note that velocity vectors are 4 times larger for sites north of 40°N to allow better evaluation. Relocated earthquakes for the upper-crust (top 20 km) marked with black circles –symbol size is scaled with the magnitude (Halpaap *et al.*, 2018), while earthquakes deeper than 20 km are colored according to their depth.

of trench rollback. Slab rollback and backarc extension occur at relatively fast rates, and these processes have had a large imprint on the evolution of the Mediterranean region during the last 20 Myr (Wortel and Spakman, 2000). In the eastern Mediterranean, Mio-Pliocene shortening in the external Dinarides in response to the collision of the Adria promontory (of Africa) was limited in southern Montenegro and north Albania (Bega, 2015; Van Unen *et al.*, 2019), and moderate in central Albania (Ustaszewski *et al.*, 2008). The northern Hellenides thrust belt also continues to tighten today. Further to the southeast along the plate boundary, the influence of rollback of the Hellenic slab is noticeable leading to foreland-propagating nappes in the southern Hellenides (Underhill, 1989), where the thrust front has jumped to the subduction boundary south of Ionian is-

lands (Royden and Papanikolaou, 2011). The KTF represents the approximate boundary between these collisional and extensional parts of the Hellenides (Figure 4.3).

This chapter is organized as follows. In section 4.2 we discuss previous studies on the structure and continuity of the Hellenic slab in our study area. We also outline the main results from seismicity studies. In section 4.3 we discuss the data and methods that were used in the tomographic inversion, and for constraining the hypcenters of important earthquakes. Section 4.4 presents the tomographic results and their interpretation. In section 4.5 we connect the tomographically imaged structures to kinematic observations, in particular seismicity, geodetic velocities and vertical motions. Here we conclude that the slab has fragmented and that a proto-STEP fault is active in the overriding plate. The Late Miocene-Pliocene geological history as recorded in the overriding plate is the topic of section 4.6; here we aim to constrain the evolution of the Hellenic slab given what we learned about its structure today. This scenario for the slab fragmentation history and its corresponding imprint on the overriding plate is used in section 4.7 to distill the tectonic conditions that resulted in the formation of the KTF STEP fault, and to globally compare these conditions with those of regions where STEP faults did, and did not, develop.

### 4.1.1 Summary of previous studies

#### Tomographic studies

The velocity structure of the western Hellenic subduction zone was outlined from earlier body-wave tomography studies, which resolved the Hellenic slab in the mantle (Spakman *et al.*, 1988, 1993; Papazachos and Nolet, 1997; Bijwaard and Spakman, 2000; Piromallo and Morelli, 2003). The slab is laterally continuous from Crete to the southern Peloponnesus, extending to lower mantle depths (Spakman *et al.*, 1993; Bijwaard and Spakman, 2000; Piromallo and Morelli, 2003; Zhu *et al.*, 2015). However, the continuity of the slab anomalies for the north-striking segment of the subduction zone is ambiguous, particularly below 150 km. One option is that the slab is horizontally discontinuous between 200 km to 400 km depth beneath the southern Dinarides and Albanides, as far south as the Scutari-Pec fault zone (Spakman *et al.*, 1988; Bijwaard and Spakman, 2000; Amaru, 2007; Koulakov *et al.*, 2009; Zhu *et al.*, 2015). Alternatively, the slab gap is confined to a volume beneath only the northern Dinarides between 150 km and 350 km depth (Piromallo and Morelli, 2003). The absence of high-speed anomalies below the northern Dinarides and its southward progression with depth led Wortel and Spakman (1992) and

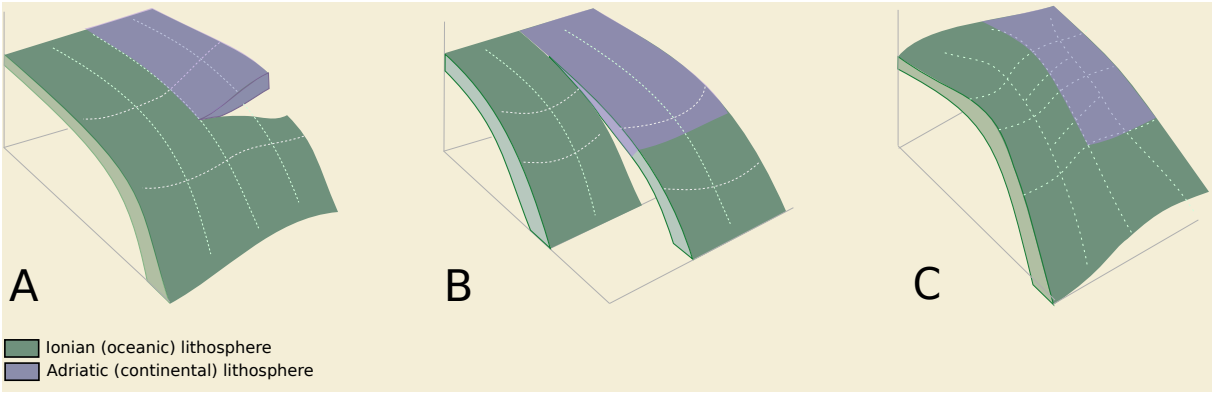


**Figure 4.4:** Previous interpretations of the geometry of the western Hellenic subduction zone. **A.** Slab detachment (horizontal tear) model (Wortel and Spakman, 2000); **B.** STEP (vertical slab tear) model (Govers and Wortel, 2005); **C.** Smooth ramp model (Pearce *et al.*, 2012).

Spakman *et al.* (1993) to propose that here the slab is detached (Figure 4.4A - Lateral tear model). The slab gap below the Dinarides further indicates that there was no recent subduction to the NNE of the Scutari-Pec fault zone in the overriding plate. From this perspective it is surprising that the Scutari-Pec is less tectonically active than the KTF.

Regional scale surface-wave tomography studies beneath east central Greece, illustrated a low-velocity zone at ∼160 km – 200 km depths, whose map projections coincide with the North Aegean Trough and the Central Hellenic Shear Zone, interpreted to be thermally induced (Bourova *et al.*, 2005; Salaün *et al.*, 2012). More recently, for the depth level between 150 km – 250 km depth, Hansen *et al.* (2019) suggested that there is no subducting slab to the north of the Gulf of Patras; the slab is partially disrupted and thinned from the Gulf of Corinth to as far south as the southern shore of the Peloponnesus, while the slab is continuous between the Peloponnesus to Crete. Their model agrees with lateral slab detachment, which migrated as far south as the southern Peloponnesus. Furthermore, beneath the Epirus region, Hansen *et al.* (2019) observed a lithospheric fragment. Whether it is connected to the detached plate or the surface could not be resolved.

### Structural seismology studies

Much research in recent years has focused on investigating the detailed velocity structure of the Hellenic slab at shallow (0 km to ∼150 km) depths to compare with the lithosphere scale faults or tears (e.g., Suckale *et al.*, 2009; Pearce *et al.*, 2012; Sachpazi *et al.*, 2016; Halpaap *et al.*, 2018). Suckale *et al.* (2009) observed the subducted crust using coda waves of teleseismic earthquakes along a N60E-oriented seismic section below the Peloponnesus.

Based on distortion of images from individual scattering modes, they suggest tearing of the Hellenic slab below the large transtensional shear zone in central Greece, called the Central Hellenic Shear Zone (CHSZ), as proposed by Royden and Papanikolaou (2011) (Figure 4.4B – STEP model). Pearce *et al.* (2012) deployed a dense array parallel to and 300 km north of the Peloponnesus seismic line and reanalyzed Suckale *et al.* (2009) data. They distinguished between northern continental and southern oceanic crustal sections. Pearce *et al.* (2012) interpreted the structure between two profiles as a smooth ramp rather than a vertical tear (Figure 4.4C – Ramp model) based on 10 km vertical offset between the profiles over a much larger trench-parallel distance.

Sachpazi *et al.* (2016) calculated receiver functions from a dense seismic network covering the whole Peloponnesus and central Greece. They obtained high-resolution images in which a highly segmented Hellenic slab beneath the Peloponnesus is offset vertically within a relatively short length scale, supporting the STEP model. In contrast, in another receiver functions study, Sodoudi *et al.* (2006) concluded that the slab is continuous beneath northern and southern Greece, down to ∼200 km depth, principally in agreement with the ramp model.

**Seismicity studies**

Halpaap *et al.* (2018) conducted a local earthquake tomography focusing on the area between the two seismic cross sections mentioned above. They relocated earthquakes using the double difference algorithm and combined local earthquake tomography images with published images based on scattered teleseismic waves. Earthquake and slab top depths give an indication of continental and oceanic subducting crusts align at depth, suggesting a smooth transition. However, ray density for the volume beneath the KTF and its on-land extension does not illuminate below 80 km depth, concealing the largest part of the puzzle. According to Bocchini *et al.* (2018), intermediate-depth earthquakes extending to the north of the Gulf of Corinth rules out the horizontal tear hypothesis beneath that region. Nonetheless, Bocchini *et al.* (2018) calls for detailed tomographic work to further illuminate the slab architecture beneath the region.

The suggestion by Govers and Wortel (2005) that the KTF is a STEP can thus far not be tested with existing seismological images as a result of insufficient resolution in the area of interest. We aim to improve this using full-waveform tomography.

## 4.2 Data and Methods

### 4.2.1 Tomographic inversion method

We use the S-velocity model from the full-waveform inversion of Fichtner *et al.* (2013) (see also Govers and Fichtner, 2016). In contrast to the more widely used and computationally less expensive travel time tomography, full-waveform inversion naturally exploits all three-component body and surface waves in seismic recordings. Furthermore, the complete wave propagation physics in the 3D heterogeneous, attenuating and anisotropic Earth is correctly simulated numerically, thereby largely avoiding forward-modelling artifacts. The combined effect of using full waveforms and accurate modelling is improved resolution of Earth structure, especially in the 0-200 km depth range, where the majority of lithosphere-mantle interactions occur. The waveform data used to construct the model comprise 16,837 three-component seismograms, obtained from 113 earthquakes with magnitudes from 5.0 - 6.8 that occurred between 2005 and 2011 along the tectonically active margins of the Eurasian plate. Within the eastern Mediterranean region, complete seismograms were modeled and inverted in the period range from 8–200 s, ensuring that both crustal and upper-mantle structures are jointly constrained.

Quantitative analyses of tomographic resolution (Fichtner *et al.*, 2013) indicate that S-velocity heterogeneities with a lateral extent of around 25 km or more are resolved from the surface to approximately 50 km depth. While a quantitative analysis of resolution length in vertical direction is technically more difficult, the comparison with receiver function studies suggests that vertical resolution within the upper 50 km is around 10 km (Govers and Fichtner, 2016). Below 50 km depth, where the sensitivity of surface waves decays notably, both the lateral and vertical resolution length increases gradually.

### 4.2.2 Identification of intraslab earthquakes

We use M≥4.5 earthquakes from the ISC Catalogue (2019) (Weston *et al.*, 2018; Lentas *et al.*, 2019) with the aim of constraining active deformation. The travel-time difference between direct P arrivals and the surface-reflected depth phase pP is particularly sensitive to the earthquake source depth (Lay and Wallace, 1995). For verification of the hypocentral depth relative to the regional Moho, we extracted six events with magnitude above 4.5 within a 2° radial distance from the KTF. For teleseismic distances, events with at least four pP and P readings and azimuths falling into two different quadrants

are used to determine differential times per station distance. We compute characteristic distance-time curves using the TauP toolkit (Crotwell *et al.*, 1999). The associated focal mechanism solutions are extracted from the ISC Catalogue and discussed in Section 4.4 (see also Figure 4.7).

## 4.3 Results

### 4.3.1 Tomographic images

Our tomographic model consists of anisotropic S-velocities ranging between 2500 and 4900 m $s^{-1}$. We focus on the upper 200 km of the model because here is where the most significant improvement relative to previous models may be expected. We first compute the isotropic S-velocity $v_S$ from the velocities of horizontally ($v_{SH}$) and vertically ($v_{SV}$) polarized S waves, following Babuska and Cara (1991):

$$v_s = \sqrt{\frac{2}{3}v_{SH}^2 + \frac{1}{3}v_{SV}^2}$$

We then compute relative velocity perturbations by selecting a reference mantle velocity that results in a slab structure that agrees best with the images of Bijwaard and Spakman (2000) at 150 km depth (Figure 4.5F). Our motivation for using their model to compare our results is that it captures many of the features of other tomographic models with a regional focus (e.g., Koulakov *et al.*, 2009; Zhu *et al.*, 2015). This reference mantle velocity is 4600 m $s^{-1}$, which is slightly higher than the ak135-F average S velocity of 4500 m $s^{-1}$ (Kennett *et al.*, 1995). However, it falls well within the range of average uppermost mantle velocities for the Tethyan collision zone (Govers and Fichtner, 2016). Figure 4.5D shows the S-wave perturbations at 150 km depth with the same color scale as Bijwaard and Spakman (2000). Focusing on the structures, the northeastern limit of the interface between the Hellenic slab and the mantle wedge (0% velocity anomaly) agree largely in both results. Arc-perpendicular slab widths compare well, too. The topologies of the southwestern limit of fast anomalies below the Ionian basin differ. This is likely caused by better imaging of the thick oceanic lithosphere by surface waves in our model. A significant difference —and the focus of our study— is that the northeastern part of the Hellenic slab is fragmented, whereas it was imaged as a continuous feature by BS2000 (Figure 4.5F). It should be emphasized, however, that apart from using different data and techniques, we also analyze different physical quantities, i.e., P and S velocity. For this reason, tomographic images can deviate significantly from each other. A low-velocity

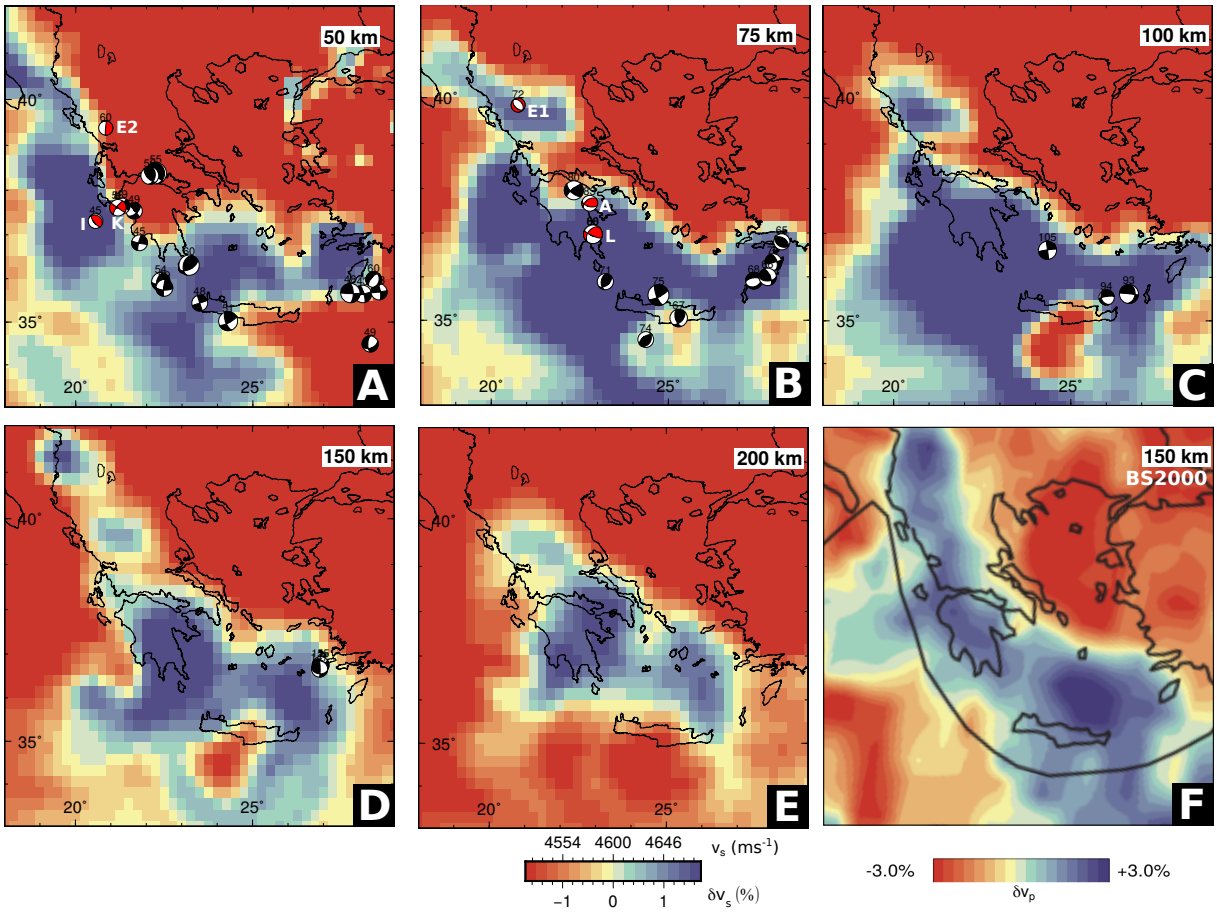


**Figure 4.5:** **(A-E)** Horizontal section at 50, 75, 100, 150 and 200 km through the isotropic S-wave velocity ($v_S$) volume. The color scale indicates perturbations from 4600 m s$^{-1}$ in percent (below). Above the color scale there are the corresponding absolute S-wave velocities **(F)** Relative P-wave velocities $v_P$ from Bijwaard and Spakman (2000) for the same region. Please refer to Figure 4.A.1 for the same cross sections with an unsaturated color scale.

gap below continental central Greece near Kefalonia suggests a discontinuity in the slab structure. Another discontinuity is imaged to the north of 40°N. Our tomographic model at 150 km depth thus suggests the existence of a separate slab fragment below Epirus.

We use the same scaling and color scale for the other depth sections. At 100 km depth (Figure 4.5C), the boundary between the slab and the mantle wedge (0% velocity anomaly) is located closer to the Hellenic trench than at 150 km depth, as is expected for a slab dipping to the northeast. The main high-speed anomaly extends to the southwest into the Ionian basin. The oceanic lithosphere of the Ionian basin is of Mesozoic age, and possibly ∼225 Myr old (Speranza *et al.*, 2012). It therefore likely is thicker than 100 km, which is why we interpret high-speed anomalies below the Ionian basin as oceanic lithosphere.

In the NW part of the Ionian basin we image a sharp transition to low-speed velocity anomalies that aligns with the strike of the KTF. The location of the transition coincides with a gradient in free-air anomalies (Supplementary Figure 4.A.4), suggesting that this represents a lithospheric property contrast. The transition is oriented roughly parallel to the KTF, and parallel to the present-day rollback direction of the trench (Nocquet, 2012). Interestingly, there is no velocity contrast across the Apulian Escarpment at this depth. A low-velocity gap below continental central Greece suggests a discontinuity in the slab structure. A slab fragment below Epirus that is separate from the Hellenic slab also appears to exist at 100 km depth.

The section at 75 km depth cuts horizontally through the surface lithospheres. The contact between the Ionian/Adriatic lithosphere and the Aegean lithosphere coincides with the slab/wedge contact at 100 km depth. The velocity contrast in the NW Ionian basin is seen at this depth also. The low-velocity gap below continental central Greece is wider than at 100 km, suggesting that the Ionian lithosphere is fragmented up-dip of the slab at 75 km depth.

The 50 km depth section cuts into continental crust at various locations (Figure 4.5A). This panel also is based on the mantle reference velocity. Both crustal regions and high-temperature mantle regions therefore show up as low-velocity regions. High-speed anomalies are absent below Epirus and the Peloponnesus. Given that oceanic lithosphere is being subducted here, our interpretation for the Peloponnesus is that the section samples the crust of the overriding plate. This interpretation is also in agreement with the receiver functions (Sachpazi *et al.*, 2016). The crustal thickness of the overriding plate is about 50 km here. The surface Adriatic lithosphere has been inferred to be continental (de Voogd *et al.*, 1992; Finetti and Del Ben, 2005), which is why we interpret low velocities in the Epirus section at 50 km depth to represent subducted continental crust, in line with Pearce *et al.* (2012). So, the contrast in our velocity anomalies is indicative of compositional variations, and we think that the Epirus is connected all the way up to the surface plate. Velocity anomalies at 50 km depth do not help to prove or disprove the existence of a lateral discontinuity related to the Epirus fragment.

At 200 km depth (Figure 4.5E), we interpret the fast velocity anomaly as the imprint of a single Hellenic slab. The wide cross-sectional dimension of the Hellenic slab gives a false impression of the actual slab thickness, given the low slab dip at 200 km depth (Bijwaard *et al.*, 1998). The slab-wedge interface is oriented NW-SE, and the edge of the Hellenic slab correlates with the Pliny-Strabo STEP Fault in the east (Özbakır *et al.*, 2013; Gov-

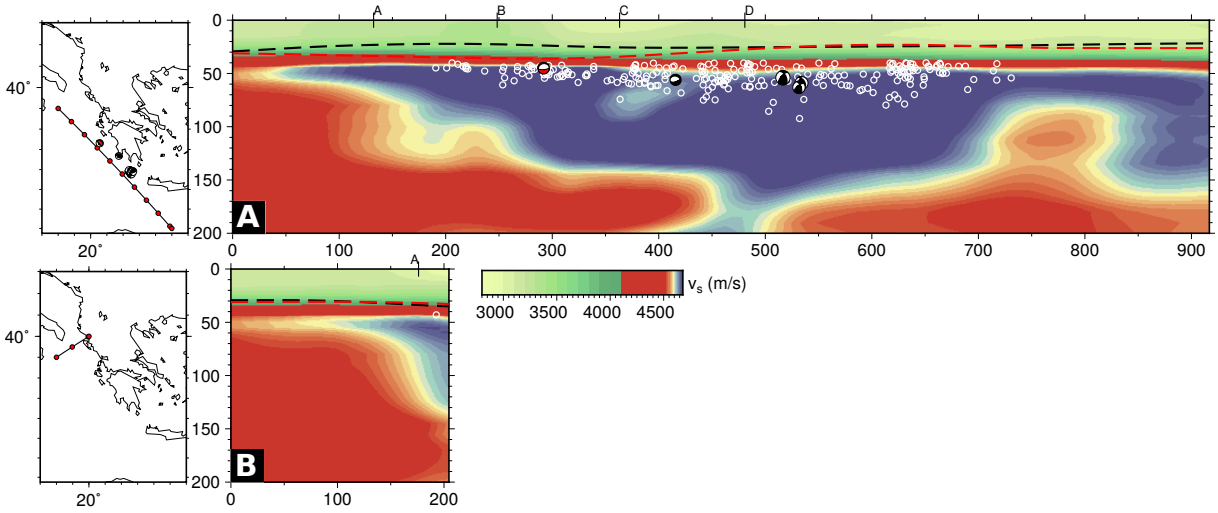


**Figure 4.6:** Vertical cross-sections through our S-velocity volume **A.** Ionian lithosphere and asthenosphere, NW left, SE right. **B.** Apulian escarpment, SW left, NE right. Letters on top of the panels indicate intersecting profiles from Figure 4.7. Red and black dashed lines show the crustal thickness variations from CRUST1.0 (Laske *et al.*, 2013) and Karabulut *et al.* (2019) respectively. Open circles and focal mechanisms represent epicenters of earthquakes within a horizontal perpendicular distance of 25 km of the cross section. Please refer to Figure 4.A.2 for the same cross sections with an unsaturated color scale.

ers and Fichtner, 2016). There is no evidence for subducted lithosphere beneath Albania. The Hellenic slab appears to be absent below the Ionian Islands and east central Greece. It is unclear whether the Epirus fragment is connected to the Hellenic slab at this depth.

Figure 4.6A shows a cross section of the Ionian lithosphere and asthenosphere. The color scale that we use for the mantle in vertical sections is identical to that for the mantle in the horizontal sections. We extended the color scale with tones of green to include low S-velocities in the crust. The thickness of the shallow low-velocity layer of ∼35 km is remarkably constant. This layer consists of both sediments of the Mediterranean Ridge (order 10 km thick, Fruehn *et al.*, 2002), and of the underlying crust. The black dashed line represents the crustal thickness from Laske *et al.* (2013), the red dashed line is the crustal thickness from (Karabulut *et al.*, 2019). The contrast that we noted in the horizontal slices at 75 and 100 km depth is clearly visible in the sub-crustal mantle in the northwestern part of the cross section. The lithospheric contrast dips to the southeast over a horizontal distance of 300 km. A simple interpretation would be that the lithospheric thickness is surprisingly small (∼50 km) in the northwest, and substantially thicker (∼150 km), which is more in line with what may be expected for Mesozoic oceanic lithosphere (Burgos *et al.*, 2014).

Figure 4.6B is a cross section across the Apulian Escarpment. The crustal thickness varies little and is about 30 km. There is a significant contrast in the lithospheric mantle structure. One interpretation of the anomalies would be that the lithosphere is thin on the Ionian side (∼50 km) and relatively thick (∼140 km) on the Tyrrhenian/Apulian side of the Apulian Escarpment. The lateral variability of this thickness contrast can be appreciated from the horizontal slice at 100 km, which shows that the contrast is absent further to the WNW; Below easternmost Apulia we find a lithospheric thickness of ∼80 km, which agrees with the result from receiver functions below onshore seismological station SCTE by Miller and Piana Agostinetti (2011).

Cross sections 4.7A-D are taken parallel to the present-day rollback direction of the trench (Nocquet, 2012). In the SSW, section 4.7A cuts into the thin surface lithosphere (c.f. Figure 4.5 at 75 km). The high velocity anomaly in the NNE (375-550 km) extends to ∼150 km depth. This anomaly represents the northwesternmost part of the Epirus fragment.

Vertical section 4.7B shows the thick lithosphere of the Ionian basin in the SSW. This lithosphere ends near the trench. Slightly slower velocities at a horizontal distance of 300 km are visible between 50 and 120 km depth. This is part of the low velocity anomaly that separates the Hellenic slab from the Epirus fragment that is visible further to the NNE between 350 and 450 km distance. The Hellenic slab as imaged previous tomographic studies at greater depths is not visibly connected to the Ionian surface plate in this section.

Cross section 4.7C shows a more pronounced separation between the Ionian lithosphere and the Epirus fragment above 130 km depth. The thick Ionian lithosphere is not continuous with the Hellenic slab at deeper levels. The NNE end of the Ionian lithosphere dips are in agreement with the Sachpazi *et al.* (2016) results.

Cross section 4.7D shows a continuous Hellenic slab. The horizontal cross sections show that subduction presently occurs between Messenia and western Crete.

Figure 4.7E is a cross section along the Hellenic trench. In the NW, it shows continental lithosphere (0-200 km distance) adjacent to the Epirus fragment (200-400 km) in the depth range 0-130 km. The NW edge of the Epirus fragments coincides with the Scutari-Pec fault zone in the overriding plate. The low-velocity region between the KTF (400 km) and the continuous part of the Hellenic slab (beyond 600 km) indicates that the Epirus fragment is a separate feature.

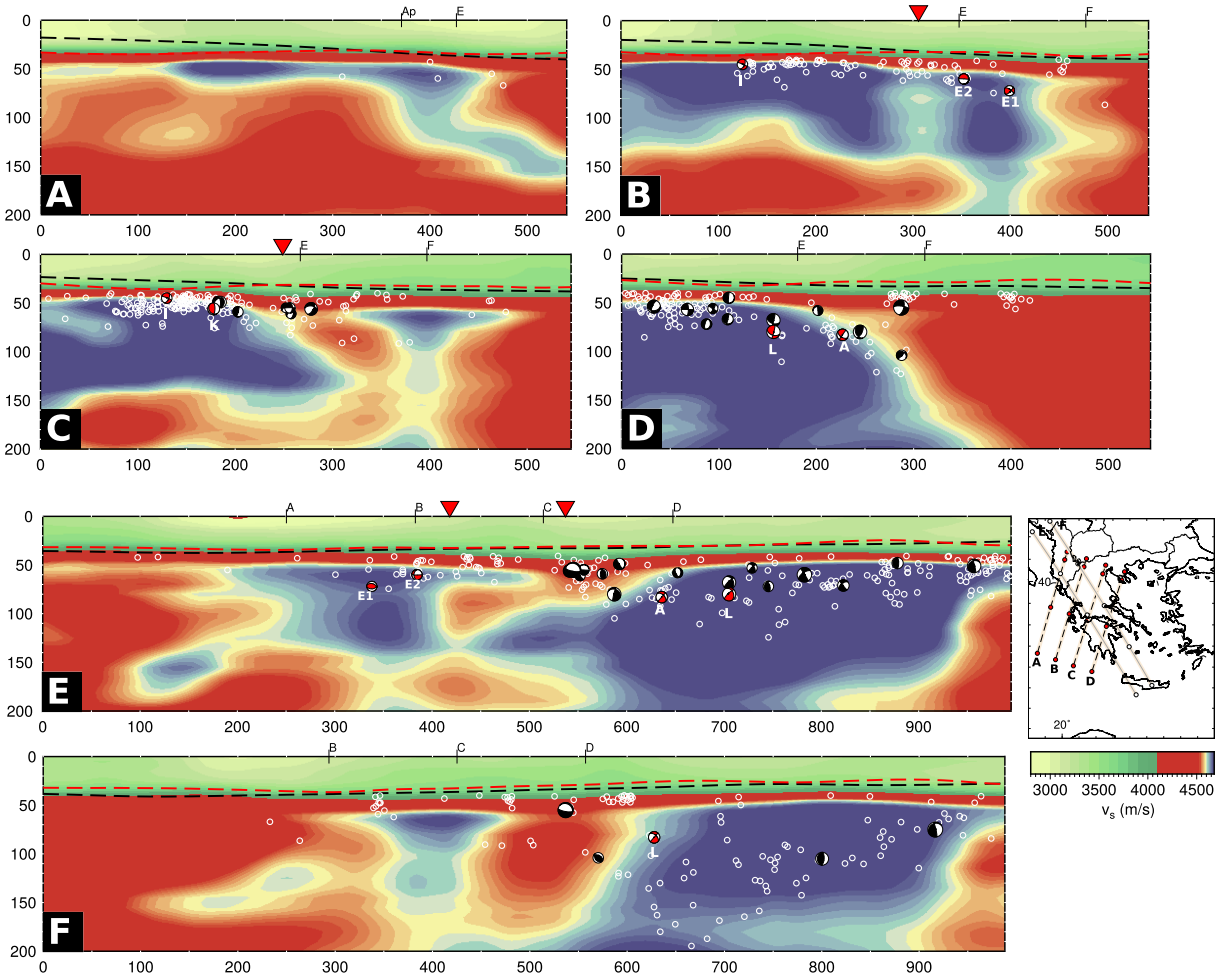


**Figure 4.7:** Vertical cross sections along the present-day rollback direction of the trench (Sections **A-D**), and in a direction that is approximately parallel to the Western Hellenic Subduction Zone (Sections **E-F**). The map panel shows where the cross sections are taken, and red and white circles on the cross section lines indicate 250 km intervals. On cross sections (A-F), red inverted triangles are used to indicate surface locations of the KTF and the Gulf of Corinth. Letters on top of the vertical cross sections refer to the labels of intersecting profiles. White open circles represent M>4 events, taken from the ISC, that have hypocenter errors (both vertical and horizontal) $\leq$10 km. Hypocenters within a swath of 50 km are projected onto the profiles. Red and black dashed lines show the crustal thickness variations from CRUST1.0 (Laske *et al.*, 2013) and (Karabulut *et al.*, 2019) respectively. Please refer to Figure 4.A.3 for the same cross sections with an unsaturated color scale.

The separation between the Epirus fragment and the Hellenic slab is even more pronounced in cross section 4.6F. It is not entirely clear whether the fast velocity anomalies merge below 150 km depth.

## 4.4 Connection between structure and kinematics

### 4.4.1 Seismicity in the slab

Focal mechanism solutions for earthquakes within the Hellenic slab (Figure 4.8) show down-dip extension (Taymaz *et al.*, 1990; Benetatos *et al.*, 2004; Shaw and Jackson, 2010). It is reasonable to assume that the extension results from slab pull that is supported by the surface lithosphere (e.g., Isacks and Molnar, 1971). The hypocenter and focal mechanism of the Mw 6.4 Leonidio earthquake (ISC Event #13328769) were constrained by Zahradnik *et al.* (2008) and Kiratzi and Benetatos (2008). Sachpazi *et al.* (2016) report a hypocentral depth of 70 km, which agrees with the pP-P travel time differences in Figure 4.8. The earthquake is located within the high-velocity region and it occurred $\sim$ 30 km below slab-top (Figure 4.5B and Figure 4.7D-F; The event is marked with "L"), which indicates a clear intraslab origin. One of the nodal planes in the vertically projected focal sphere (Figure 4.7D) is parallel to the slab dip, which corresponds to the NW dipping nodal plane in lower hemisphere projection. The strike of this nodal plane is also in agreement with the trend of intraslab seismicity (open circles, and in Halpaap *et al.* (2018)), and that of other focal mechanisms. Moreover, a NW-dipping fault plane corresponds with a slip vector with an azimuth that is approximately parallel to the direction of relative motion between Africa (Nubia) and Eurasia (Zahradnik *et al.*, 2008). We therefore suspect that the NW-dipping plane represents the fault plane. Our interpretation agrees with that of Sachpazi *et al.* (2016), which they interpret as an intraslab fault as part of fragmentation of the Hellenic slab.

The hypocenter (depth = 70$\pm$10 km) and focal mechanism of the 2008/06/18 Mw 5.0 Argos earthquake (ISC Event #11377877) were constrained by Mediterranean-Regional Moment-Tensors (Pondrelli *et al.*, 2011) and "Thales Was Right" network (Sachpazi *et al.*, 2016), and discussed by Durand *et al.* (2014) and Sachpazi *et al.* (2016). In our structural interpretation, the event is located within the slab (Figure 4.5B and Figure 4.7D-F; The event is marked with "A"), but it appears in the shallower part of the slab. The focal mechanism solution of the Argos earthquake reflects a predominantly reverse mechanism with a minor strike-slip component. One of the nodal planes (corresponding to NW-dipping nodal plane in lower hemisphere projection) lines up with the trend of local seismicity, similar to the Leonidio event. For both the Argos and Leonidio earthquakes, Sachpazi *et al.* (2016) select the NW dipping nodal planes as the intraslab fault and interpret it as a left-lateral transpressive event as part of fragmentation of the Hellenic slab. Their interpretation is based on imaging using receiver functions. Considering the high

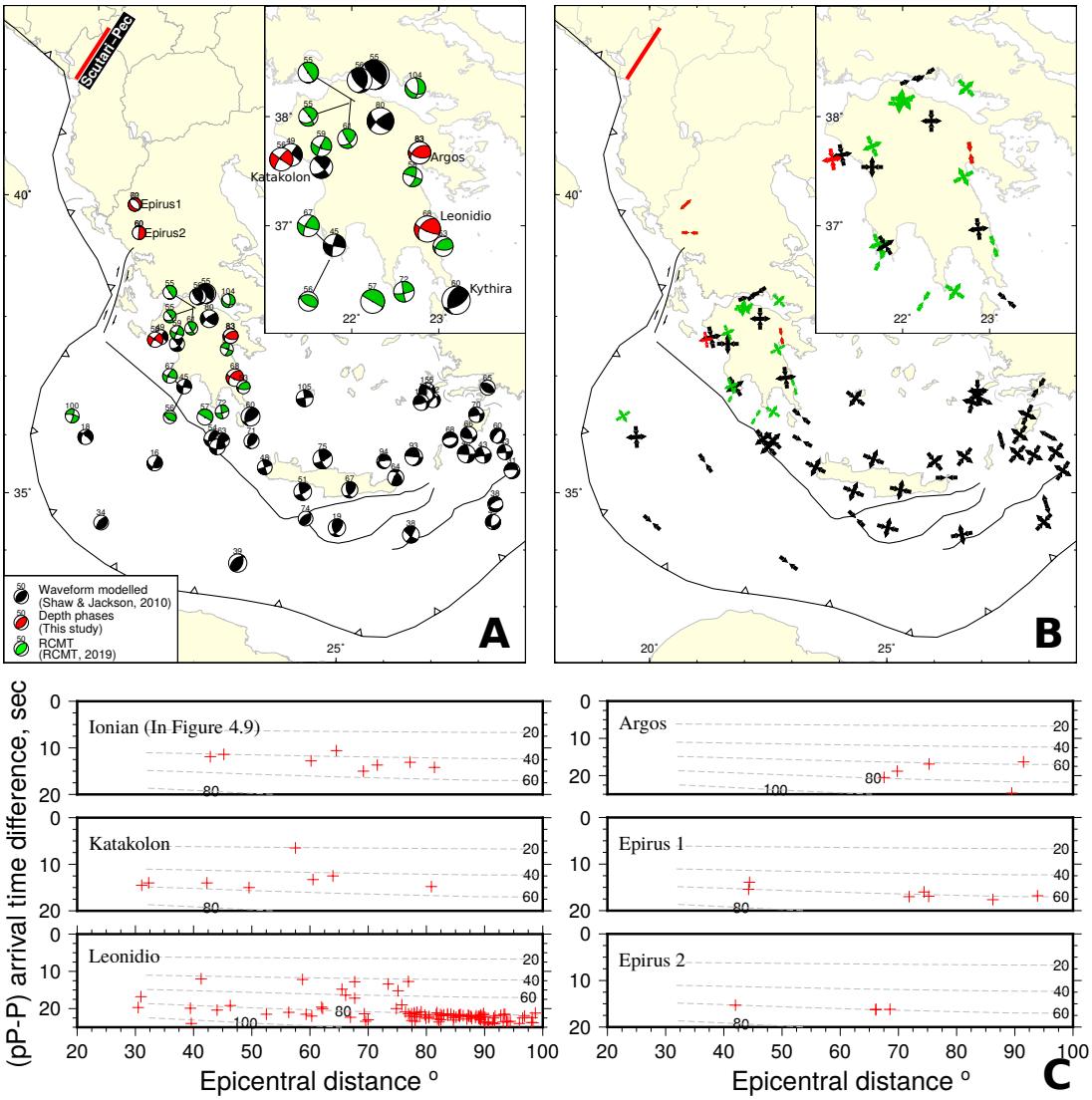


**Figure 4.8:** Synthesis of intraslab earthquakes **A.** focal mechanisms, **B.** their P- and T-axes **C.** Delay time of P- and pP-phases are plotted against distance between stations and the event (ISC event numbers are written on upper left corner of each box). Dashed gray lines show the characteristic depth at which phase difference and separation correspond. Number above beach-balls indicate centroid depths.

data quality and good station distribution of Sachpazi *et al.* (2016), the Aegean Moho and the slab Moho are well-resolved. Crustal thicknesses obtained for Peloponnesus therein are consistent with previous RF study of Sodoudi *et al.* (2006). Furthermore, similar RF patterns show up also in western Anatolia (e.g., Karabulut *et al.*, 2019). The resolution of our tomographic model is not enough to confidently image slab fragmentation because potential fault offsets are close to the resolution limit. However, we can tentatively identify trends in the intraplate seismicity, together will waveform-modelled focal mechanisms in Figure 4.7E, which support Sachpazi *et al.*'s (2016)'s interpretation of slab fragmentation.

ISC Event #13378954 corresponding to the 2008/06/30 Mw 4.6 Epirus 2 earthquake (Pondrelli et al., 2011) occurred below the Epirus region. Our plot of pP-P differential times versus epicentral distance (Figure 4.8) suggests a hypocentral depth of 60 km. This means that the event was located 20 km below the Moho of the overriding plate, along the edge between the Epirus fragment in the north, and the low-velocity anomaly in the south (Figures 4.5A-B, 7B). We suspect that the horizontal nodal plane represents the fault plane. The reason is that the vertical nodal plane aligns roughly with the seismic velocity contrast which probably also represents a strength contrast. This we consider an unlikely candidate fault plane because it is difficult to accumulate shear stresses when one block alongside a fault is weak. Our interpretation implies that this event represents westward thrusting over the Epirus fragment of the crust of the overriding plate.

ISC Event #7201105 corresponding to the 2003/12/07 Mw 4.5 Epirus 1 earthquake (Pondrelli *et al.*, 2007) occurred below the Epirus region. Our plot of pP-P differential times versus epicentral distance (Figure 4.8) suggests a hypocentral depth of 60 km. This means that the event was located well within the Epirus fragment. It corresponds to horizontal NE-SW oriented horizontal tension, or vertical compression. These principal stress directions diverge strongly from orientations for other events in the region. This suggests that the Epirus fragment experiences little slab pull, possibly indicating that it is not connected to the deeper Hellenic slab.

The June 11 1999 Mw 5.2 strike-slip earthquake occurred offshore northwestern Peloponnesus (ISC Event #1665492, denoted by Katakolon in Figure 4.8 and with letter "K" on the tomographic sections). pP-P travel time differences indicate a depth of ∼50 km (Figure 4.8). The event is therefore located in the topmost part of the underthrust Ionian lithosphere (Figures 4.5A, 4.7C). For intraplate events, the majority of the deformation is accommodated by strike-slip earthquakes. If we interpret the NE-striking nodal plane as the fault plane, the mechanism indicates left-lateral shear. This interpretation is in agreement with the mechanisms of Leonidio and Argos events, both of which exhibit sinistral slip but with a larger oblique component. Furthermore, the NE-striking nodal plane is in agreement with dominant NE-SW trending intraplate events for the western Peloponnesus (Figure 4.5; relocated seismicity from Halpaap *et al.* (2018)). Therefore, the fault plane responsible for the Katakolon earthquake should be one of the intraslab faults (F2 of Sachpazi *et al.* (2016)) as part of fragmentation of the Hellenic slab.

### 4.4.2 Seismicity along the Kefalonia Transform Fault

The KTF is commonly interpreted as bounding two segments of the Hellenic belt in the overriding plate. However, the vast majority of the strike-slip seismic activity along the KTF (Baker *et al.*, 1997) corresponds to dextral slip between the Ionian lithosphere and the forearc (Kassaras *et al.*, 2016). To the NW of the KTF, the Ionian lithosphere subducts at a substantially slower rate than the Ionian lithosphere in the SW. This interpretation agrees with an active STEP (Govers and Wortel, 2005). Near the active STEP (to the SW of the KTF) the Hellenic side would be expected to sink vertically, but the absence of vertical tearing events likely is a consequence of the predominance of rollback of the Hellenic slab. Based on the seismicity, it is uncertain whether the tear in the slab also has an expression in the overriding lithosphere. The accretionary wedge and foreland are clearly offset, but particularly the land ward continuation of the STEP fault into the overriding plate is debated. We will return to this topic in our discussion of the geological evolution of the overriding plate.

### 4.4.3 Plate boundary seismicity

Thrust faulting earthquakes occur on the subduction interface to the south and west of the Peloponnesus (Hirn *et al.*, 1996; Clément *et al.*, 2000) with slip vectors that are parallel to the relative motion direction (Figure 4.5; Shaw and Jackson, 2010). Here, the imaged top of the slab correlates with the Wadati-Benioff zone (Figure 4.6D; Hatzfeld and Martin, 1992; Papazachos *et al.*, 2000). Beneath the Ionian Islands the thrust faulting earthquakes strike oblique to the plate boundary, in a N–S direction, and their slip vectors are almost perpendicular to that of GNSS velocities (Shaw and Jackson, 2010).

The October 5 2010 Mw 4.7 earthquake in the Ionian basin, SW of Zakynthos island (ISC Event #7415293) occurred at ∼45 km depth according to pP-P travel time differences in Figure 4.8. With reference to the tomographic profiles, this event is located along the interface between the Hellenic slab and the overriding plate (Figure 4.7C, denoted by letter "I"). A swarm of seismicity delineates the plate interface, which indicates that the NE-dipping nodal plane represents the fault plane (Figure 4.9). Nevertheless, this event differs from nearby interface event because of its larger depth. Hirn *et al.* (1996) suggested that the shallow dipping interface between the Ionian lithosphere and the overriding plate beneath the Ionian Islands is at 13 km depth. Other interface events marked in Figure 4.9 corroborate Hirn *et al.*'s (1996) conclusion. However, according to Shaw

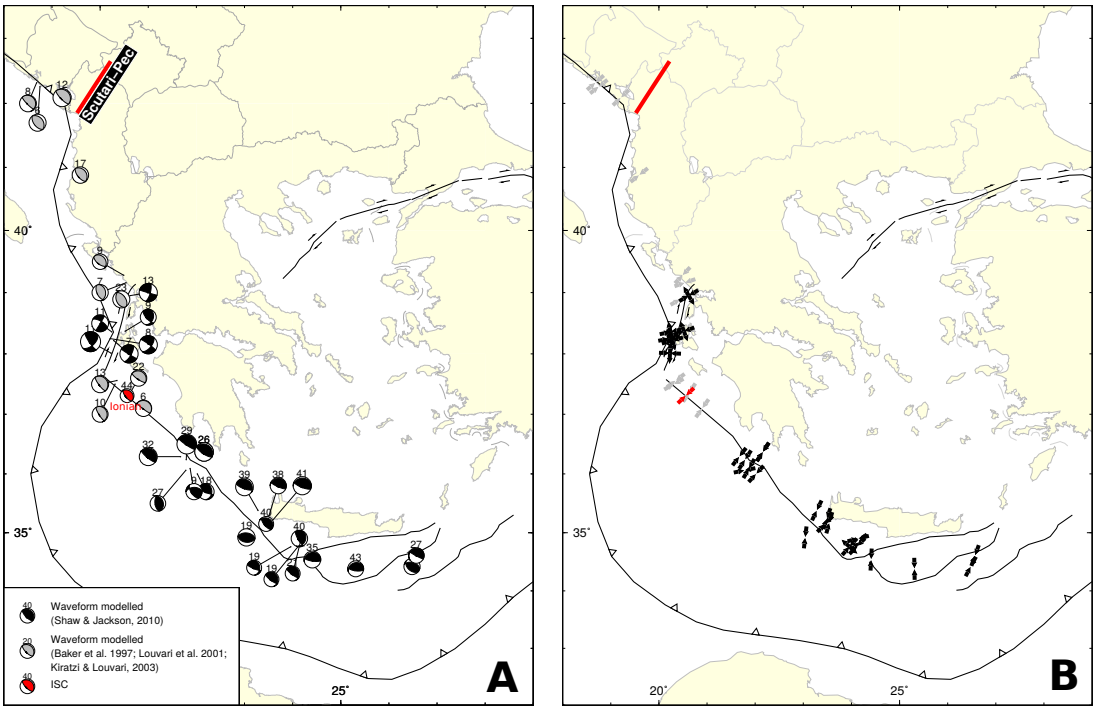


**Figure 4.9:** A synthesis of plate contact (interface) earthquakes in the larger Hellenic subduction zone. **A.** focal mechanisms, **B.** their P- and T-axes of focal mechanisms. Number above beach-balls indicates centroid depths.

and Jackson (2010), the depth of interface earthquakes can vary in a large-range, between 15 and 45 km. Therefore, we interpret this event as an interface earthquake, and it accommodates the convergence between the Ionian lithosphere and the overriding Aegean.

### 4.4.4 Active deformation of the overriding plate

In this section we review recent deformation (that is, on a time scale of a few million years) of the overriding plate with special emphasis on how differential motion between the Epirus fragment and the Hellenic slab might be accommodated in the overriding plate. In a classical and mature STEP fault system, this would involve strike-slip faulting, so we will pay special attention to transcurrent fault motions.

Figure 4.10A shows crustal seismicity and surface projections of fault planes overlying geographic regions and national boundaries of Balkan countries, modified from SHARE project (Giardini *et al.*, 2014; Basili *et al.*, 2013, Figure 4.10A). Although earthquake mislocations and distributed deformation prevents an ideal match, overall there is good correlation between faults and the seismicity. Seismic moment rate increases significantly

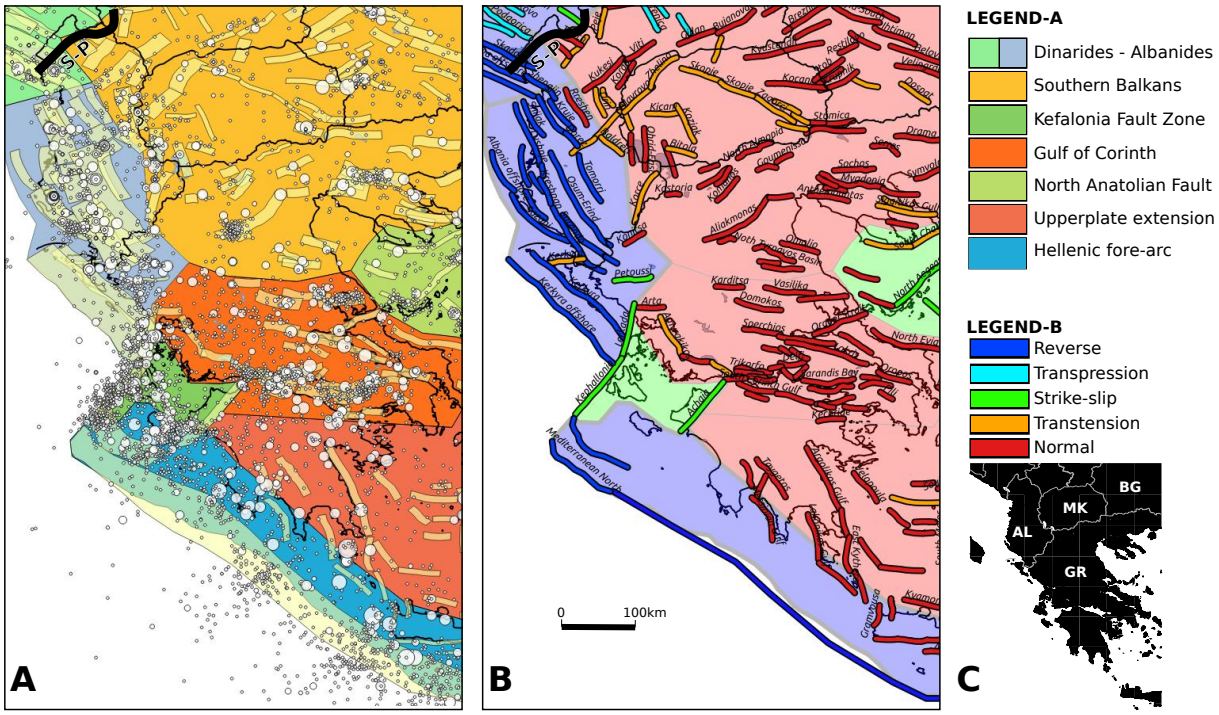


**Figure 4.10:** Map of seismic zones and active seismogenic faults modified from SHARE; The European database of Seismogenic Faults (Basili *et al.*, 2013). **A.** Seismogenic zones are shown in different colors. M4+ crustal seismicity is indicated with white circles, whose magnitudes are proportional to their radius. Faults are plotted with their surface projections in order to better illustrate limits of dipping interfaces. Thick black line label S-P indicates the Scutari-Pec line, which separates the Dinarides from the Albanides-Hellenides. **B.** Seismic zones of extension, transcurrence and compression are shown in red, green and blue shading. Fault names are taken verbatim from SHARE database. **C.** National borders of Balkan countries and Greece are mentioned in the text (GR:Greece, AL:Albania, MK: North Macedonia; BG: Bulgaria).

from the NW to the SE. Figure 4.10B shows active seismogenic faults (with their geographic names) overlying a large-scale zonation into compressional, strike-slip and extensional deformation. This zonation is based on focal mechanism solutions, on the analysis of seismicity patterns, and on the classification of mapped active faults (Basili *et al.*, 2013). Below, we discuss these tectonic zones.

We start with the southern Dinarides for context directly beyond the domain that we focus on with our tomographic model. GNSS observations (Figure 4.3) show moderate shortening (10-20 nano-strain per year) in the Dinarides (Metois *et al.*, 2015). This is likely caused by the ∼2-4 mm/yr northeastward motion of Adria and Apulia micro-plates relative to the Eurasian plate (D' Agostino *et al.*, 2008; Nocquet, 2012). Focal mechanisms of crustal events show significant components of strike-slip (Kiratzi and Dimakis, 2013). Closer to the Adriatic Sea, focal mechanisms document distributed thrusting within the

overriding plate (Baker *et al.*, 1997; Pondrelli *et al.*, 2006, 2011) with azimuths of reverse slip vectors that are consistent with GNSS-derived velocity directions (D' Agostino *et al.*, 2008). The convergence is accommodated mainly by frontal low-angle thrusts and shortening in the external Dinarides (Korbar, 2009; Biermanns *et al.*, 2019). Seismicity is correlated with surface faulting for the region close to the Adriatic (Figure 4.10A). Our tomographic results (Figure 4.5) show that there is no slab in the uppermost mantle below the southern Dinarides, suggesting that underthrusting has been limited and that Apulia-Dinarides convergence was accommodated mostly by shortening in the External Dinarides.

Figure 4.10B shows that active tectonics substantially change near the Scutari-Pec line at the transition from Dinarides to Albanides. Volumetric strain rates from GNSS velocities indicate that the region represents the boundary between compressional (N) to tensile deformation (S), and that it involves moderate clockwise vertical-axis rotation rates, and moderate bulk shear strain rates (Perouse *et al.*, 2012; Metois *et al.*, 2015). The absence of active faults and seismicity along the boundary indicates that the transition is gradual. The deeper structure (Figure 4.5) does not show lateral changes near Scutari-Pec.

Further to the SSW, neo-tectonic activity in the forearc is clustered along mapped thrust faults in Albania (Figure 4.10A). Here, NE-SW directed compression in the external Albanides and Epirus caused the Mw 6.9 1979 Montenegro earthquake. Further away from the plate contact, crustal earthquakes in the internal part of the Albanides show E-W extension (Jouanne *et al.*, 2012, Figure 4.10B). A significant horizontal dilatation rate is inferred for the eastern Albanides from GNSS data (Metois *et al.*, 2015). The Albanides separate the region of NE-ward GNSS convergent motions in the W from the region in the E with S- to SW-ward motions of the overriding plate. GNSS velocities increase in magnitude towards E and S, but the overall motion is compatible with a clockwise rotation pattern (Figure 4.3). The sub-lithospheric Epirus fragment (Figure 4.5) correlates spatially with the southern Albanides in the overriding plate. Relative to the northern Albanides, thrust activity may be more concentrated closer to the trench, signifying the SE ward transition from head-on collision to underthrusting.

The southern Balkan crust moves southward toward the Hellenic subduction zone in a Eurasian reference frame (McClusky *et al.*, 2000) at a slow rate of 3 mm/yr (Burchfiel *et al.*, 2006; Kotzev *et al.*, 2006) (Figure 4.3). GNNS-derived horizontal dilatation rates (Metois *et al.*, 2015) and neo-tectonic fault activity indicate transtension. The GNSS velocity field within the Southern Balkan zone does not vary much resulting in slow ac-

cumulation of slip deficit on regional faults. Earthquakes occur infrequently, like the Mw 6.1 1963 Skopje earthquake and the M 6.9 1904 Kresna earthquake (Dumurdzanov *et al.*, 2005). The zonation of active faults (Giardini *et al.*, 2014, Figure 4.10) corroborates the GNSS-derived deformation pattern; there is an abundance of normal faults which strike ENE to ESE, and way fewer transtensional faults with NW-SE strikes.

The Aegean upper-plate extension *zone* is confined to the area south of the NAF Zone and covers the majority of southern Peloponnesus. GNSS velocity gradients are rather low (Figure 4.3), so as the resultant dilatation and shear strain rates (Chousianitis *et al.*, 2015). Principal extension axis changes within short distance, from E-W extension in the center and south, to NE-SW in the west (Chousianitis *et al.*, 2015). NNW-striking normal faults were mapped in the field (e.g., Papanikolaou and Royden, 2007; Papanikolaou *et al.*, 2007), which agree with the seismic zone delineated in Figure 4.10. The tomographic images show that from Messenia to western Crete, the Hellenic slab is connected to the surface lithosphere, i.e., normal subduction takes place here. But to the west, the Hellenic slab is not connected to the lithosphere in the Ionian basin between the KTF and Messenia.

The near-trench forearc is characterized by shortening all along the Hellenic forearc zone. Velocities reach up to ∼40 mm/yr here (Hollenstein *et al.*, 2008), although the gradient is low. The correlation of the western end of the Hellenic slab with the boundary of the extending domain in the overriding plate supports the commonly held notion (Reilinger *et al.*, 2006) that slab roll-back is an important driver of overriding plate deformation. Well-defined compressional tectonic structures (Brooks and Ferentinos, 1984) constitute the boundary of the seismic zone to the north, between the Ionian islands and the Gulf of Patras. Compressional interface earthquakes with P-axis perpendicular to the forearc define the region as a zone of thrusting.

The transpressive KTF *zone* (Figure 4.10B) is seismically very active. The KTF and the Lefkada fault accommodate dextral slip (Baker *et al.*, 1997; Louvari *et al.*, 1999) along the northwest boundary of the KTF zone. The Achaia fault bounding the southwest of the KTF zone also accommodates dextral slip (Ganas and Parsons, 2009; Vassilakis *et al.*, 2011; Kassaras *et al.*, 2016). The KTF zone between these bounding faults is seismically much less active. Shallow seismicity (<30 km depth; Kassaras et al., 2016) along the KTF shows differential motion between the crust of the Ionian basin and the crust of the Hellenic forearc. Importantly, transpressional activity terminates abruptly to the northeast, where the Lefkada fault comes onland. This means that there is no localized,

seismically active shear zone within the overriding plate beyond the KTF. Seismicity along the Achaia fault shows an opposite behavior; the seismically active fault is restricted to the overriding plate, and does not continue into the forearc (Ganas and Parsons, 2009; Kassaras *et al.*, 2016). The northern end of the Achaia fault terminates near the GoC. Below, we discuss the downward continuity of the Achaia fault into the Hellenic slab. So, the KTF zone accommodates distributed dextral transpression between the Ionian basin and the overriding plate. Our tomographic results show that the KTF zone is located above the gap between the Epirus fragment and the Hellenic slab. Our interpretation therefore is that tearing and rollback of the Hellenic slab results in a distributed shear zone in the overriding plate, i.e., we interpret the KTF zone as a >100 km wide STEP fault.

Durand *et al.* (2014) investigated the sequence of earthquakes, beginning with the intraslab Leonidio event (6 January 2018) followed by the Methoni megathrust event (14 February 2018), and finally the Mw 6.4 Movri (8 June 2008) dextral strike-slip earthquake along the Achaia-Elia faults in the upper plate. The distribution of aftershocks of the Methoni earthquake clearly outlines the fault plane of the Movri earthquake. Hence Durand *et al.* (2014) suggested there is a link between the slab fragmentation event and overriding plate deformation. Sachpazi *et al.* (2016) extend the mechanical coupling argument of Durand *et al.* (2014) with the slab fragmentation pattern, in which coupling between the adjacent slab panels transmit stresses to the overriding plate. The Movri event coincides with the surface extension of their F2-fault. Slab fragmentation may thus be coupled to strike-slip faulting in the KTF STEP fault zone of the overriding plate (Achaia fault).

Very large strain rates (>40 nano-strain/yr) in the northern half of Peloponnesus, the Gulf of Corinth, Patras and Evvia (Chousianitis *et al.*, 2015) define the Gulf of Corinth *zone* (Figure 4.10A). The whole region is extending (Chousianitis *et al.*, 2015; Metois *et al.*, 2015). Focal mechanism solutions clearly show that normal faulting dominates within mainland Greece (Kiratzi and Louvari, 2003) and the trend of the T-axes is consistently N-S in central Greece (Baker *et al.*, 1997; Kiratzi and Louvari, 2003). The region is characterized by multitude of WNW to E-W striking normal faults (Figure 4.10; see Goldsworthy *et al.* (2002) for detailed field evidence for normal faulting). The GNSS velocity field is highly variable, resulting in a complex strain-rate field. The location of the Gulf of Corinth zone correlates in the west with the gap between the Hellenic slab and the Epirus fragment (Figure 4.5).

The North Anatolian Fault (NAF) continues in the north Aegean as the distributed dextral shear zone of the North Aegean Trough (NAT) and the Sporades (Dewey and Şengor, 1979; Lyberis, 1984; Taymaz *et al.*, 1991). The NAT separates the southern Balkan extensional zone from the Aegean upper plate extension domain. Chousianitis *et al.* (2015) report no geodetic evidence for the NAF Zone entering mainland Greece. Furthermore, the focal mechanism solutions in mainland Greece exclusively show normal faulting (Kiratzi and Louvari, 2003), no strike-slip. This is also demonstrated in the seismic zone boundaries of Figure 4.10B, where the zonation shows that the shear deformation zone does not reach the mainland.

Papanikolaou and Royden (2007) suggest that the dextral motion of the North Anatolian Fault/North Aegean Trough continues to central Greece through the transtensional "Central Hellenic Shear Zone" (CHSZ), which includes the Gulf of Corinth and ultimately joins with the Hellenic trench via the KTF. Royden and Papanikolaou (2011) proposed that this pull-apart developed following tearing of the western Hellenic slab after 4 Ma. The seismic moment release, geodetic strain rates, and faulting indeed clusters in their CHSZ. Given that there indeed is evidence for dextral slip within the overriding plate in the KTF zone, we therefore think that the CHSZ may actually form the connection to the North Aegean Trough at present.

Our review of the active horizontal deformation of the overriding plate suggests that the best candidates for accommodating the differential motion between the Epirus fragment and the Hellenic slab are the 100 km wide KTF zone (Figure 4.10B) continuing into the CHSZ in the overriding plate. The KTF STEP fault zones shares some similarities with other STEP faults worldwide; the long-lived STEP fault that constitutes the eastern plate boundary between the South America and Caribbean plates (Van Benthem *et al.*, 2013) also has major pull-apart basins in the Gulf of Paria and the Gulf of Cariaco. The STEP fault of the Pliny-Strabo trenches also is very wide. However, because particularly the KTF zone is rather wide, and slab fragmentation appears to migrate to the SE, we consider it to be a proto STEP fault (or STEP fault in the making).

### 4.4.5 Recent vertical motions of the overriding plate

In this section we review Quaternary observations of uplift and subsidence. Vertical motions may result from frictional coupling along a subduction interface (earthquake cycle effects as measured by kinematic geodesy), crustal thinning or thickening, and imprints

of changes in the subducted slab like fragmentation. In our context of connecting the imaged slab structure to overriding plate deformation, we are primarily interested in sub-lithospheric contributions related to fragmentation of the Hellenic slab. One mechanism is suggested by Le Pichon and Angelier (1981), which suggests underplating of the subducted sediments below the overriding plate as a mechanism of uplift restricted to the Hellenic forearc. So, it is noteworthy to document uplifted regions in the subsiding upper-plate extensional domain. The other mechanism involves areas of active slab tearing, where the joint effect of viscous stresses and buoyancy variations due to asthenospheric return flow produce vertical motions on the surface. This is especially pronounced next to the STEP faults, which can build kilometer-scale topography. We therefore opt to document vertical motions close to the imaged slab gap. However, as we will see below, well-documented evidence for vertical motions due to sub-lithospheric sources is scarce.

Studies of vertical deformation of the forearc region may yield opposite results depending on the time scale; short-term GNSS-velocities show subsidence of the Ionian islands (Hollenstein *et al.*, 2008), whereas paleo-bathymetry studies show uplift in Kefalonia, Zakynthos and Corfu (Van Hinsbergen *et al.*, 2006). The difference reflects the superposition of relatively fast vertical velocities during the seismic cycle (here; inter-seismic subsidence) and slower vertical velocities on the long term. Our interest here is on the long-term velocities (few Myr, Plio-Pleistocene and Holocene). These probably reflect compressional tectonics, evidenced also from reverse focal mechanisms and compressive structures both onshore and offshore (Monopolis and Bruneton, 1982; Brooks and Ferentinos, 1984) which were primarily influenced by the plate contact.

One location where the plate boundary is far and the location of the slab gap is relevant is the Gulf of Corinth. There have been many studies on vertical motions from horizontal extension in the Gulf of Corinth domain. Its southern coastal region experiences Pleistocene-Holocene rift flank uplift at rates between 0,7-1,3 mm/yr (Armijo *et al.*, 1996; Houghton *et al.*, 2003; McNeill and Collier, 2004). Considering that the majority of Quaternary marine terraces occupy foot-wall position today, it would be logical to assume that the uplift regime is fault controlled here. Armijo *et al.* (1996) showed that, after accounting for the uplift from extension, there remains a regional uplift rate of >0.2 mm/yr, which they attributed as part of the uplifting Peloponnese hinterland. We think that the required regional contribution and the location of vertical motions in the upper plate is well-correlated with the imaged slab gap and originates from the mantle structure.

According to Papanikolaou and Royden (2007), Gulf of Evia is part of the Central Hellenic

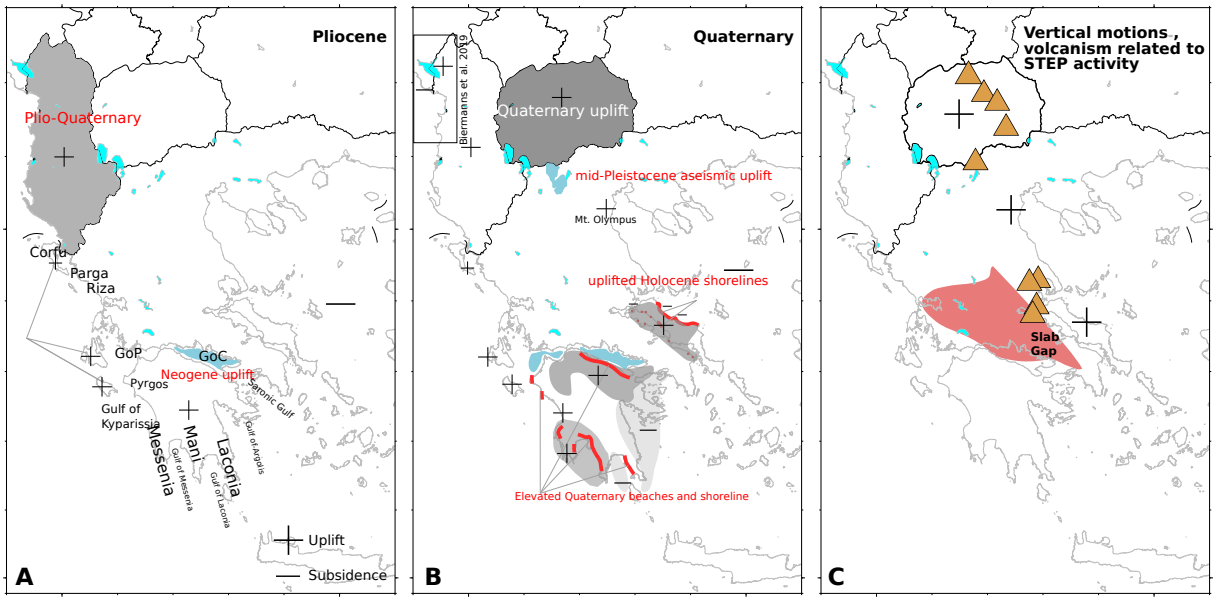


**Figure 4.11:** Vertical motions during **A.** the Pliocene; **B.** the Pleistocene. Panel **C.** shows the spatial relation of the recent uplift, the slab gap, and the location of high-K volcanic rocks.

Shear Zone, whose activity also encompasses the GoC. Uplifted Holocene shoreline within $\sim$ 40 km of the normal fault bounded region (measured from Fig 3. of Goldsworthy *et al.* (2002)) can be associated with rift flank uplift (Stiros *et al.*, 1992). Although the distance between faults suggests a short wave-length uplift, that is comparable with the effects of elastic dislocation similar to the Xylokastro fault, the position of the uplifted region over the upperplate extensional domain may indicate a sub-lithospheric regional uplift component. Tomographic images indicate that the region is underlain by the slab gap between the Epirus fragment and the Hellenic slab (Figure 4.11C). Furthermore, high-K magmatism developed in this region during the Pleistocene provides an independent evidence for the mantle origin of the uplift Pe-Piper and Piper (2007).

Dumurdzanov *et al.* (2005) correlated basin formation with late Pleistocene faulting in North Macedonia, i.e., above the NE edge of the Epirus fragment (Figure 4.11). They document that both the Pliocene and Pleistocene strata have been deeply incised and preserved as terraces in the basins. This suggests that vertical uplift occurred in North Macedonia during the Quaternary. So these vertical motions are recent, they occurred on a broader geographical region to the north an northeast of the slab fragment. The authors do not identify a possible cause of the uplift, but we suspect that it is related to the break-off of the Epirus fragment from the Hellenic slab. High-K magmatism in the uplifting region may support this conjecture (Figure 4.11; Boev and Yanev, 2001).

The southern Balkans and Greece experienced uplift since the Pliocene. Vertical motions are controlled mainly by footwall uplift on steep normal faults, but regional uplift component is prominent in the internal Hellenides, especially in North Macedonia, Mt. Olympus and Evvia. This accelerated uplift away from the plate boundary zone lends support to the mantle buoyancy origin for the vertical motions (Figure 4.11). The vertical motions show an overall uplift for the entire Peloponnesus and Albania since the Pliocene times, while the Aegean Sea experienced subsidence for a much longer period (Figure 4.11) (Le Pichon and Angelier, 1981; Aliaj *et al.*, 2001).

### 4.4.6 Synthesis

The current kinematics of the overriding plate, deformation within the slab, and along the plate interface, offer a qualitative understanding of the coupling between the Hellenic slab and the upper plate. The KTF zone is a proto-STEP fault that is situated due east of the gap between the Hellenic slab and the Epirus fragment. The KTF zone likely is part of a large pull-apart system with the CHSZ and the North Aegean Trough. The Hellenic slab may currently be in the process of fragmenting along NE-SW faults beneath the Peloponnesus (Sachpazi *et al.*, 2016). The overriding plate also deforms in response to the fragmenting slab here.

Figure 4.12 shows a synoptic view of the imaged structure. The Epirus fragment is separate from the Hellenic slab; the vertical separation is shown by our tomographic results, and the downdip end of the Epirus fragment is also not connected to the deeper Hellenic slab because it shows downdip compression, which contrasts with downdip extension due to slab pull in the continuous Hellenic slab. The NW extent of the deeper (>300 km) Hellenic slab to the northwest is limited to the Albanides (Van der Meer *et al.*, 2018). We estimate that the downward gap below the Epirus fragment is 30-60 km (Figure 4.7E). The Epirus fragment is a roughly vertical feature below the southern Albanides. Its western edge correlates with the subducted contrast within the lithospheric mantle of the Ionian Ocean basin, and its southern edge with the subducted projection of the Apulia Escarpment. Subduction of these lithospheric contrasts may thus have contributed to the separation of the Epirus fragment from the Hellenic slab. The Hellenic slab becomes narrower with depth, and the gap with the Epirus fragment wider; the resulting change in slab pull direction may contribute to rotated slip directions of interface earthquakes to the south of KTF zone.

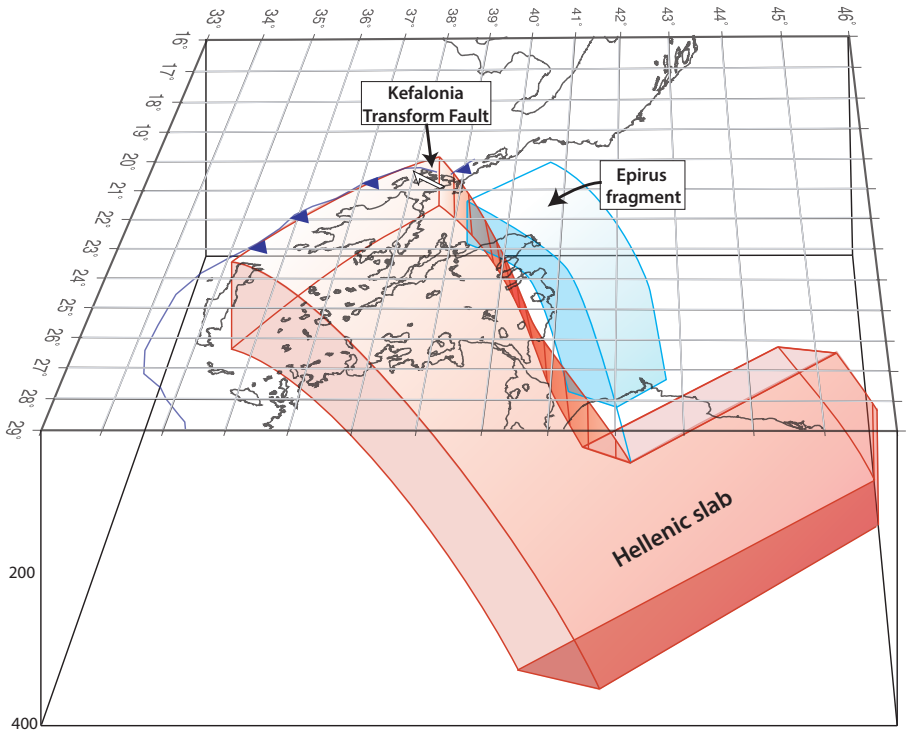


**Figure 4.12:** Summary block diagram of our interpretation of the structure of the west Hellenic subduction zone and the Epirus fragment (the eastern part is cut off here, and does not correctly display the actual structure)

The vertical size of the gap between the down dip end of the Epirus fragment and the deeper Hellenic slab can be estimated from Figure 4.7E and is 45±15 km. To estimate the time that was needed to develop this gap we assume that the Epirus fragment was connected to the deeper Hellenic slab prior to slab detachment, and that the shallow-dipping Hellenic slab subsequently rolled back to its present location. We assume also that the Epirus fragment stalled so that the slab gap was entirely caused by the roll-back of the Hellenic slab (Figure 4.12). The average trench migration rate was mm/yr during the Pliocene (taken from Royden and Papanikolaou (2011)). The average dip of the Hellenic slab dip was ∼30° - 17° in the depth range 20-100 km (Pearce *et al.*, 2012) and 45° between 100 and 180 km (Papazachos *et al.*, 2000). The time required for the development of the observed slab gap would be $\frac{45\pm15}{\tan 30\times 20\pm 3} = 3.9 \pm 1.3$ Myr.

## 4.5 Evolution of the Western Hellenic Subduction Zone

### 4.5.1 Geological evolution of the main tectonic elements in the overriding plate

The arcuate subduction boundary of the Hellenic subduction zone evolved from an initially straight geometry around ∼35 Ma (Barrier *et al.*, 2008; Royden and Papanikolaou, 2011; Van Hinsbergen and Schmid, 2012; Jolivet *et al.*, 2013). The trench curvature increased progressively as lateral variations in slab rollback became more important (Le Pichon and Angelier, 1979; Royden, 1993). The associated backarc extension of the Aegean Sea commenced in the Oligocene, as evidenced from the core-complexes (e.g., Gautier *et al.*, 1999), ocean-ward migration of the volcanic arc (Fytikas *et al.*, 1984), the chronology of high pressure rocks (Jolivet *et al.*, 2003), magmatic activity and chronology of the granitoids (Jolivet and Faccenna, 2000). Continued convergence and accretion led to the foreland-propagating nappes in the Hellenides (Underhill, 1989). Oligocene to Miocene development of a gap in the Hellenic slab below the northern and central Dinarides is commonly argued based on the absence of fast seismic velocity anomalies (Wortel and Spakman, 2000; Faccenna *et al.*, 2014; Handy *et al.*, 2015; Le Breton *et al.*, 2017). Consequently, there would have been some sort of lateral edge along the Hellenic slab to the north of Epirus during the period prior to the fragmentation of Epirus. Importantly, there is no evidence of STEP fault activity in the overriding plate during this period. As we will discuss in section 4.7, the absence of STEP faulting during the Late Miocene may be related to the predominantly dextral relative motion of Adria and Moesia.

In the northern Hellenides, tightening of the orogen continued as the Apulia continental margin collided with the European margin in the northern Hellenides, whereas in south the subduction beneath the Ionian zone continued (Royden and Papanikolaou, 2011). Paleomagnetic studies document ∼50° of clockwise rotation of the larger region from Albanides and Hellenides with respect to the Dinarides (Kissel *et al.*, 1995), of which 40° occurred between the middle to late Miocene and the remaining 10° occurred after 4 Ma (Van Hinsbergen *et al.*, 2005; Van Hinsbergen and Schmid, 2012)(Figure 4.11). Furthermore, the sense of shear and orientation of active faults in the Hellenides dramatically changed since the Miocene. In the internal part of the Hellenides of mainland Greece, NW-SE striking low-angle normal faults developed between the late Miocene, early Pliocene times, parallel to and possibly using the inherited weakness zones of the earlier nappe emplacement

(Papanikolaou and Royden, 2007). Since early Pliocene times, E-W striking high angle normal faults obliquely cut earlier nappes and low-angle normal faults (Papanikolaou and Royden, 2007). This sequence of events demonstrates that the regional stress field has rotated from dominantly NE-SW extension to N-S extension during the Plio-Pleistocene epoch (Meijer and Wortel, 1996, 1997). In the following subsections we discuss the timing of activity of major tectonic elements of the overriding plate in order to constrain the sequence of events.

**Kefalonia Transform Fault**

The age of KTF has been argued primarily on the basis of geological and paleomagnetic data. One primary age constraint is that the fault post-dates the latest stage of nappe-emplacement in western Greece. Thrust faults of Messinian age (∼5-7 Ma) are continuous in mainland Western Greece (Royden and Papanikolaou, 2011). However, west of the Ionian Thrust in Zakynthos, compressional deformation affected Messinian evaporites, which are unconformably overlain by Pliocene sediments (Underhill, 1989). Early Pliocene shortening near Lefkas, Kefalonia and Zakynthos likely reflect overthrusting of Ionian units on the Pre-Apulian zone (Clews, 1989). Underhill (1989) restored structural cross-sections in the island of Kefalonia and tentatively demonstrated that westward advancing thin-skinned tectonics continued well through the Pliocene and Pleistocene. All these evidences lend support to the early Pliocene final emplacement of the Ionian unit.

Van Hinsbergen *et al.* (2006) reported a renewed uplift of at least several hundreds of meters in the Pleistocene from paleobathymetry data and propose that the deformation along the KTF is responsible for this second phase of uplift (Figure 4.11). Furthermore, they relate ∼20° late-Pleistocene clockwise rotation (Duermeijer *et al.*, 1999), to dragging along the KTF (Van Hinsbergen and Schmid, 2012). In Zakynthos particularly no significant rotation were recorded between 8.11 and 0.77 Ma, then the island underwent a 21.6°± 7.4° clockwise rotation between 0.77 Ma and Recent (Duermeijer *et al.*, 1999). No significant paleomagnetic rotation seems to have occurred since ∼1.9 Ma along the SW coast of Kefalonia (Duermeijer *et al.*, 2000). Onshore of Zakynthos in the NW edge of the Peloponnesus, very large rotations similar in magnitude to that of Zakynthos were demonstrated (Duermeijer *et al.*, 2000).

This intensification of deformation may indicate that the localized fault should have emerged in the Pleistocene. Consistent with this interpretation, Reilinger *et al.* (2010)

suggest that ∼60 km offset on the KTF would put its age at 2 Ma, assuming present-day geodetic rates. Royden and Papanikolaou (2011), suggest a post-Messinian or early-Pliocene age for the inception of the KTF. Their geodynamic modeling results suggest an age of 4 Ma. After this, the thrust front migrated to its present location between the oceanic Ionian basin and the pre-Apulian continental shelf, thereby facilitating the latest oceanic subduction phase.

Van Hinsbergen *et al.* (2006) and Van Hinsbergen and Schmid (2012) emphasized the role of the dextral Thesprotiko fault zone, which has been considered now inactive on-land continuation of the KTF. They suggest that the Thesprotiko fault zone accommodated the deformation in western Greece relative to the stable northern parts, between 7 Ma and pre-rifting in the Gulf of Corinth. Based on DEM analysis of Jordan *et al.* (2005) and ∼20 km dextral offset of lower Miocene sediments in the Botsara syncline, Van Hinsbergen *et al.* (2006) suggested Thesprotico Fault Zone in western Greece, to be linking the strike-slip deformation of the KTF to the North Anatolian Fault via the transtensional Aliakmon fault. The strike of Thesprotico Fault Zone seems compatible with the KTF, but its continuation to Aliakmon fault places this tectonic boundary too much north of the NAF and KTF.

### The Gulf of Corinth and the North Aegean Trough

Distributed syn-rift sedimentation in the Gulf of Corinth began around ∼4 Ma, although the localized deformation started after 0,6 Ma (Armijo *et al.*, 1996; Nixon *et al.*, 2016; Gawthorpe *et al.*, 2018). There is an asymmetry between the southeastern and southwestern Gulf in terms of sedimentary facies, thickness, and the position of erosional surfaces (terraces) (Papanikolaou and Royden, 2007). Moretti *et al.* (2003) concluded that the current pattern of extension began later in the west than the east. Assuming the present-day GNSS-derived slip rates as a proxy to the geological slip-rates, Reilinger *et al.* (2010) estimate the inception of the activity in the Gulf of Evia to 3±1 Ma, the eastern Gulf of Corinth to 2 Ma and the western gulf to 1 Ma. The Gulf of Corinth thus opened simultaneous with, or shortly after the Epirus slab disconnected from the deeper Hellenic slab.

Moving eastward, Armijo *et al.* (1999) suggest that the age of westward propagation of the North Anatolian Fault into the Aegean domain is early Pliocene on the basis of an offset anticline in the Dardanelles. Yaltırak *et al.* (2000) and Şengör *et al.* (2005) dismiss

this early age due to lack of field evidence for the offset marker. Instead, Yaltırak (2002) suggest that the dextral motion of the North Anatolian Fault transferred into the Aegean domain since 4 Ma, using marine reflection studies and detailed geological mapping. This synchronicity lends support to the interpretation that there is common cause for the formation of the CHSZ-KTF proto-STEP fault system.

### 4.5.2 Our scenario for the recent evolution of the western Hellenic slab

In section 4.2 we reviewed published structural models (Figure 4.4). The seismological constraints which form the basis of these models may have been incomplete, but they have been repeatedly used to verify subsequent evolutionary scenarios. Wortel and Spakman (1992) proposed lateral migration of slab detachment from the Dinarides to Peloponnesus (Figure 4.4A). A recent regional tomographic study based on P-wave delay times (Hansen *et al.*, 2019) confirms the existence of a horizontal gap/tear in the slab in the northern Hellenic subduction zone. The scenario agrees with high/ultra-K Pleistocene magmatism beneath the Dinarides, North Macedonia, Voras mountains and Evia (Figure 4.11) (Fytikas *et al.*, 1984; Boev and Yanev, 2001; Pe-Piper and Piper, 2007; Handy *et al.*, 2015). Van Unen *et al.* (2019) attribute widespread extension to slab detachment at ∼30 Ma. Schefer *et al.* (2011) constrain the timing of the Dinarides detachment to 37-22 Ma. Given that our model also shows a vertical separation between the Epirus segment and the Hellenic slab, our model is consistent with the inferences from these other studies. Our evolutionary scenario therefore also involves lateral propagation of a horizontal slab tear.

The STEP fault model for the KTF (Figure 4.4B; Govers and Wortel, 2005) involved a free slab edge to the Hellenic slab. Royden and Papanikolaou (2011) modified the idea by suggesting that the Hellenic slab was fragmented by a vertical tear. Suckale *et al.* (2009) find seismological evidence for such tear. The scenario predicts magmatism above the tear, which may be an explanation for the magmatism in Evia (Figure 4.11). Increased rotations above the leading edge of the STEP fault agree with paleomagnetic studies (Van Hinsbergen *et al.*, 2006). We also identify a (semi-)vertical tear in our tomographic model. The previous observations and inferences thus agree with our scenario.

In section 4.5.6 we estimated the time it would require for the deep Hellenic slab to subduct deeper and create the vertical distance of ∼50 km to the base of the imaged

Epirus fragment (∼4 Myr). Our interpretation is that this gap was created by (continued) slab detachment. In the previous section we noted that this timing agrees (within uncertainty limits) with the initiation time of the KTF and CHSZ (∼4 Ma). The implication is that slab detachment and fragmentation would have occurred near-simultaneous. A similar scenario was proposed by Wortel *et al.* (2009), who suggest that the southwestern edge of the Calabria slab developed from fragmentation (vertical tearing) following slab break-off beneath the Kabylies. Near KTF it is however unclear whether the fragmentation developed from slab detachment, like they propose. Slab fragmentation potentially excites asthenospheric return flow, but seismic anisotropy around the west Hellenic slab, shows no apparent imprint of such flow (Olive *et al.*, 2014). This supports our inference that the separation of the Epirus fragment from the Hellenic slab has resulted in limited asthenospheric strain.

A continuous (smooth) transition of the Hellenic slab across the KTF was also suggested by Royden and Papanikolaou (2011) (Figure 4.4C). Pearce *et al.* (2012) showed no apparent change in slab dip between the distant seismic images and small amount of roll-back induced offset. In the depth range where Pearce *et al.* (2012) and Halpaap *et al.* (2018) have their best resolution (<100 km), the vertical offsets between the Epirus segment and the Hellenic slab are probably small. This may be the reason for their discrepant interpretation.

Our scenario combines the models associated with Figures 4.4A and B. The entry of continental Adriatic lithosphere in the WHSZ initiated slab detachment under the Dinarides from the Oligocene onward (Wortel and Spakman, 1992; Handy *et al.*, 2015; Van Unen *et al.*, 2019; Schefer *et al.*, 2011). Pliocene detachment (Figure 4.13A) triggered slab fragmentation, thereby isolating the (likely more buoyant) Epirus fragment from the Hellenic slab. The critical component for the development of the proto STEP fault may have been the redistribution of the gravitational pull, which caused the Epirus fragment to stall, and the Hellenic slab to roll back faster. This would have resulted in a significant subduction velocity difference between the two segments since the late Miocene. Direct observational constraints on this contrast in subduction rates are lacking, but in this rollback context they can be proxied by extension in the overriding plate. Papanikolaou and Royden (2007) document the change in the strikes of the normal faults from NW-SE to E-W during the late-Miocene to Pliocene. Brun *et al.* (2016) documented a Pliocene change in the direction of stretching from NE-SW to N-S in the Southern Hellenides, and an increase in the spreading rates. Meijer and Wortel (1996, 1997) discuss how tensile stress rotations can be understood as a response to slab-detachment below the Dinarides and western Greece.

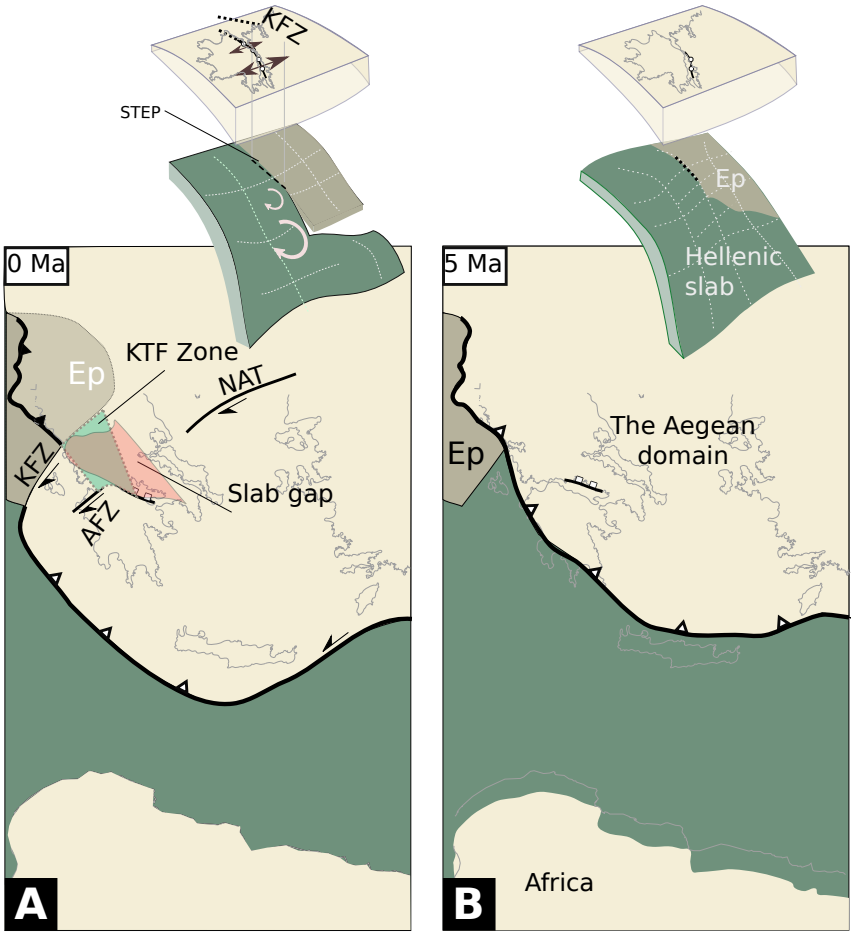


**Figure 4.13:** Tectonic evolution of the Hellenic slab and the overriding plate deformation. Circular arc with arrows indicate sagging/rotation of the subducted slab. Gray lines on 0 Ma show the plate boundary geometry of the 5 Ma setting.

This supports our interpretation of a velocity contrast between detached on attached segments. Important was that the velocity contrast between the slab fragments persisted a few Myr, long enough to initiate the proto-STEP fault in the overriding plate.

North-south extension in central Greece commenced synchronous with the isolation of the Epirus fragment from the Hellenic slab. With the development of the KTF zone, the GoC can be viewed as the feature that was necessary to connect to the already existing North Aegean Trough, i.e., localization of upper plate extension in the GoC facilitated STEP fault development.

## 4.6 Under what conditions does a STEP evolve from slab fragmentation?

Wortel *et al.* (2009) were the first to consider STEP fault initiation. These authors considered relatively simple cases of STEP fault initiation, where horizontal slab breakoff developed relatively directly into vertical tears, slab edges and STEP faults. They discuss the plate boundary reorganization that began around 20 Ma and eventually resulted in the lateral northern edge of the Tonga-Kermadec slab, and the STEP fault along the north boundary of the Lau Basin. In the Mediterranean context they discuss how Miocene slab breakoff beneath the Maghrebides (northern Africa) may have evolved into the lateral edge along the south end of the Calabria slab, and the STEP fault zone in northern Sicily and in the west of the Ionian basin.

An important further insight came from Van Benthem *et al.* (2013), who pointed out that the long-lived slab edge beneath Hispaniola (northern Caribbean) had not developed into a STEP fault in the overriding plate. Here, the relative motion is mostly transpressive with only a small trench-perpendicular motion. For the development of a STEP fault in the context of a fragmented slab, this means that a significant trench-perpendicular velocity contrast is required between the two adjacent slab fragments. The absence of STEP faulting in the Dinarides margin during the Late Miocene may be related to the predominantly dextral relative motion of Adria and Moesia.

Another step was taken by Govers and Fichtner (2016), following up on the work of Bartol and Govers (2014), on uplift of Anatolia. These authors argue that slab fragmentation below west Anatolia resulted in differential rollback between the Hellenic and Cyprus-Bitlis fragments. No well-defined STEP fault zone seems to have developed within western Anatolia during this period (35-16 Ma). Govers and Fichtner (2016) argue low mechanical coupling of the slab fragments to the overriding Anatolian surface plate. Only after the Cyprus slab rolled back from beneath the Anatolian crust did the modern Pliny-Strabo STEP fault develop (Özbakır *et al.*, 2013). The mechanical coupling of the slab fragments to the overriding thus likely plays a significant role in the development of a STEP fault.

Van Benthem *et al.* (2013) propose that the long-lived STEP fault zone that constitutes the plate boundary between the South America and Caribbean plates may have initiated ∼45 Ma due to the entry of North Andes continental fragment into the Greater Antilles Subduction. They suggest that the STEP fault activity initiated along a pre-existing weak

zone or material boundary that was inherited from the Paleocene collision. Pre-existing weakness zones or contrasts may thus facilitate the development and localization of a STEP fault. Their suggestion aligns with our inference that the North Aegean Trough may have helped localizing the strain in the proto STEP fault.

The contrast in the subduction velocity, the amount of time over which it persists, mechanical coupling to, and the deformability of, the overriding plate play a role in the initiation of a STEP fault once a slab is fragmented. These inferences should help us understand better why STEP faults did not develop above the fragmented slabs that we listed in Figure 4.1, with the idea that some of these conditions are not met here.

A lateral slab edge was identified beneath Hispaniola by Van Benthem *et al.* (2013) along the North America - Caribbean plate boundary zone. The local relative motion direction is approximately parallel to the plate boundary, and the subduction velocity is small. The absence of a STEP fault in Hispaniola thus agrees with the above conditions for its initiation.

Three distinct discontinuities have been identified within the Nazca slab; beneath the Juan Fernandez ridge in the south (Portner *et al.*, 2017; Lynner *et al.*, 2017), Carnegie Ridge in the north (Gutscher *et al.*, 1999) and Mocha Fracture Zone (Pesicek *et al.*, 2012). Beneath Juan Fernandez Ridge, there is no imaged free slab edge, but a hole in the dipping slab (Portner *et al.*, 2017). Neither of these slab discontinuities are associated with a STEP fault within the overriding plate. Within the overriding plate near Carnegie Ridge, there is some indication of convergence velocity differences across the Carnegie ridge, parallel to the proposed tear. Furthermore, the dextral Dolores-Guayaquil shear zone deforms the upper plate (Gutscher *et al.*, 1999), which might be a STEP fault candidate. Beneath the Mocha Fracture Zone, tomographic evidence (Pesicek *et al.*, 2012) confirms a free slab edge. The dip angle of the slab segments does not change in tomographic model (Pesicek *et al.*, 2012). There are no observations to document contrasts in the subduction velocity of the slab segments. There also are no observations that would suggest the existence of a STEP fault in the overriding plate.

The southern edge of the subducting Juan de Fuca plate has an edge representing the subduction of the Mendocino Fracture Zone (Furlong and Schwartz, 2004). STEP fault initiation in the overriding North America plate is not expected, however, because the region is part of the Mendocino Triple Junction so that deformation is not required from a kinematic perspective.

Levin *et al.* (2002) demonstrates the existence of a free slab edge in the Kamchatka slab where slab normal trench retreat occurs. However, there is sound evidence for independent Okhotsk and Amurian plates (Apel *et al.*, 2006), which effectively places the Kamchatka slab edge on the triple junction between Okhotsk, North America and Pacific plates. Like the Mendocino triple junction along the southern end of the Juan de Fuca plate, subduction of a free slab edge does not require (STEP fault) deformation of the overriding plate here.

Miller *et al.* (2004, 2005, 2006b) presented tomographic evidence for the Izu-Bonin slab of a deep lateral tear or hole at the transition to the N Mariana slab. There are no observational constraints indicating a subduction velocity contrast between slab segments or any transcurrent faulting on the overriding oceanic Philippine slab. For the southern end of the Mariana slab, Gvirtzman and Stern (2004) suggested a N-S trending vertical tear based on slab dip changes. Observational constraints on a subduction velocity contrast of the slab segments are lacking. Fryer *et al.* (2003) suggested N-striking sinistral faults on the overriding Philippine Sea plate west of Guam, which might be interpreted as a STEP fault zone.

The Cocos plate subducts at the Middle America Trench. For the slab beneath the Trans-Mexican volcanic belt, Dougherty *et al.* (2012) inferred a laterally discontinuous low-velocity zone across the subducted Orozco Fracture Zone, where flat to normal subduction transition occurs. The region is part of a diffuse triple junction of the Cocos, Caribbean and North American plates. In terms of kinematics, no STEP fault is therefore required in the overriding plate.

Tearing along the south end of the Japan slab has been suggested by Kennett and Furumura (2010) and Obayashi *et al.* (2009). However, the tearing occurs in the triple junction region of the Pacific, Philippine Sea and Eurasian plates, and thus is not relevant in the context of STEP fault initiation.

Lin *et al.* (2007, 2013) tomographic find evidence for vertical tearing of the Philippine Sea slab along a N-S strike near Taiwan. The relative motion between the Philippine and Eurasian plates is perpendicular to the proposed tear, which may explain the absence of observations of a STEP fault along the western edge of Okinawa backarc basin.

Tomographic evidence (Widiyantoro *et al.*, 2011) shows detachment of the Sunda slab

near Timor in the easternmost Sunda arc. No slab edge is inferred from the seismic velocity structure. This part of the trench retreats southward but the upper plate does not seem to deform accordingly (Schellart *et al.*, 2007).

Further to the north Spakman and Hall (2010) identified horizontal slab detachment. The leading edge of the tear would currently be located beneath the Seram trench. However the tomographic model does not allow the identification of Seram slab fragments.

In the eastern termination of the Makran subdution zone, global tomographic model of Bijwaard and Spakman (2000) show a marked rectangular low velocity zone at 60km depth. Earthquakes with hypocentral depths indicate pure down-dip and strike-slip focal mechanisms (Dziewonski *et al.*, 1981; Ekström *et al.*, 2012) supporting STEP hypothesis. At the northern edge of the fault (Becker and Faccenna, 2011) demonstrate a strong positive residual topography that may be related to the vertical motions due to the propagating STEP. Furthermore, the surface projection of the anomalous region corresponds to the Chaman fault, which shows a gradient in the horizontal velocity field -that may be interpreted as the STEP-fault.

Available information regarding the correlations of slab edges and vertical slab tears with STEP faults in overriding plates globally is too scarce to rigorously verify the conditions for STEP fault formation that we formulated on the basis of our inferences for the KTF. The conditions appear to agree with the absence of a STEP fault in Hispaniola.

## 4.7 Conclusions

The western end of the Hellenic slab is fragmented near the Kefalonia transform fault. The separate Epirus fragment is roughly vertical below the southern Albanides. Its western edge correlates with a newly identified major contrast within the lithospheric mantle of the Ionian Ocean basin. The southern edge of the Epirus fragment correlates with the subducted projection of the Apulia Escarpment. The Epirus fragment is laterally separated from the Hellenic slab by a low velocity zone that we interpret as a semi-vertical tear. Below 150 km depth, the Epirus fragment is separated by ∼50 km from the deeper Hellenic slab by a semi-horizontal gap. We estimate that the Epirus fragment disconnected from the Hellenic slab around 5 Ma, at about the time of opening of the Gulf of Corinth.

The Kefalonia Transform Fault zone, bounded by the dextral Kefalonia and Lefkada faults, accommodates strike-slip within the overriding plate. Together with the Central Hellenic Shear Zone and the North Aegean Trough, we interpret the Kefalonia Transform Fault zone as a proto-STEP fault that initiated simultaneous with Pliocene fragmentation of the Epirus fragment.

In the NW part of the Ionian basin we image a sharp transition to low-speed velocity anomalies that aligns with the strike of the KTF. The location of the transition coincides with a gradient in free-air anomalies.

The contrast in the subduction velocity, the amount of time over which it persists, mechanical coupling to, and the deformability of, the overriding plate play a role in the initiation of a STEP fault once a slab is fragmented. Particularly the absence of a contrast in the subduction velocity of slab fragments prevents the development of STEP faults above currently fragmented slabs. These constraints likely determined the development of the KTF proto STEP fault, and the development, or not, of other STEP faults worldwide.

## Acknowledgements

Figures are created using GMT software (Wessel and Smith, 1998). ADO was funded by the Netherlands Research Center for Integrated Solid Earth Science (ISES).

# Appendix A Supplementary Figures

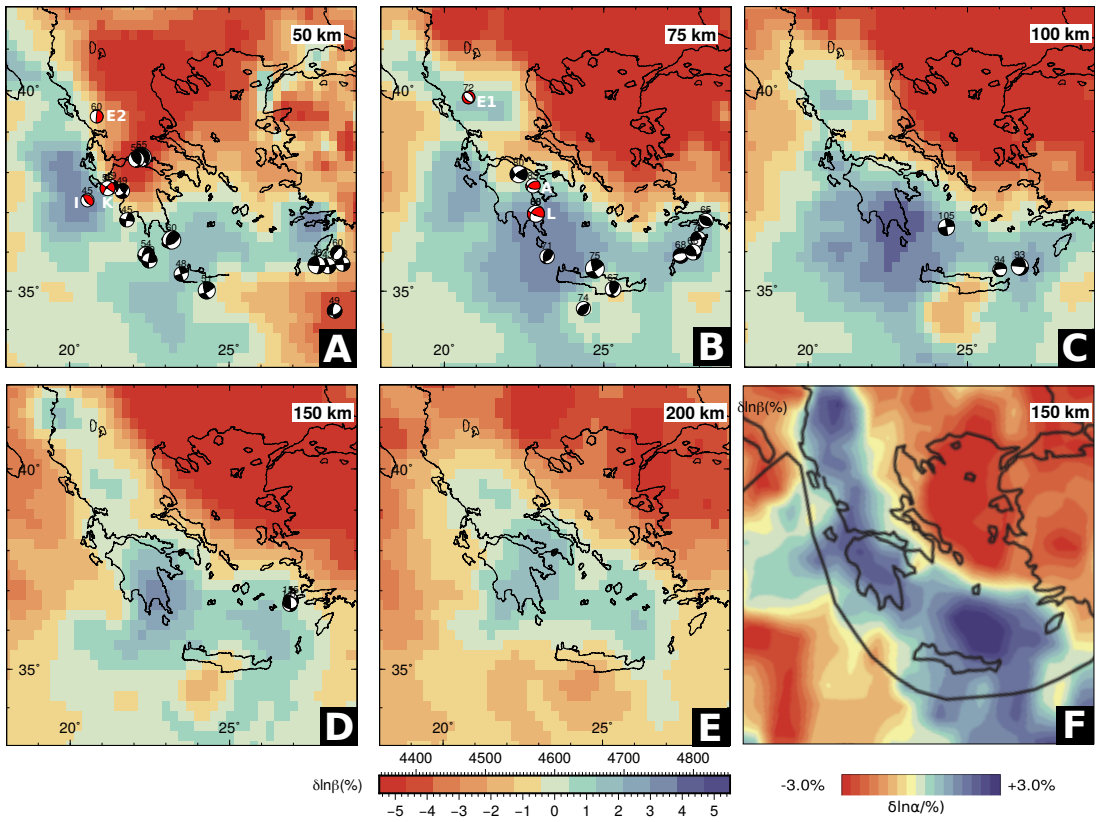


**Figure A.1:** Figure 4.S1. Figure equivalent to Fig. 4.5, i.e., horizontal cross sections through the tomographic volume, now with an unsaturated color scale.

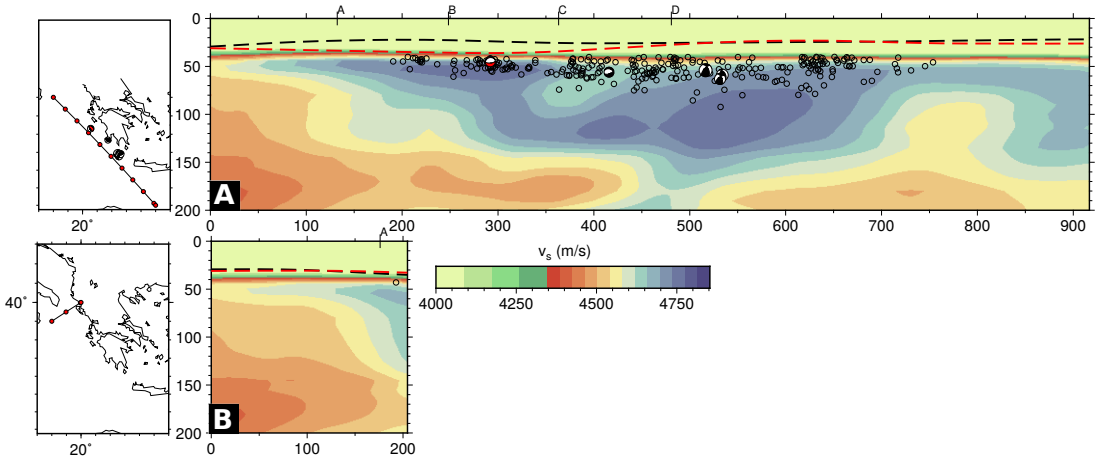


**Figure A.2:** Figure equivalent to Fig. 4.6, i.e., vertical cross sections through the tomographic volume, now with an unsaturated color scale.

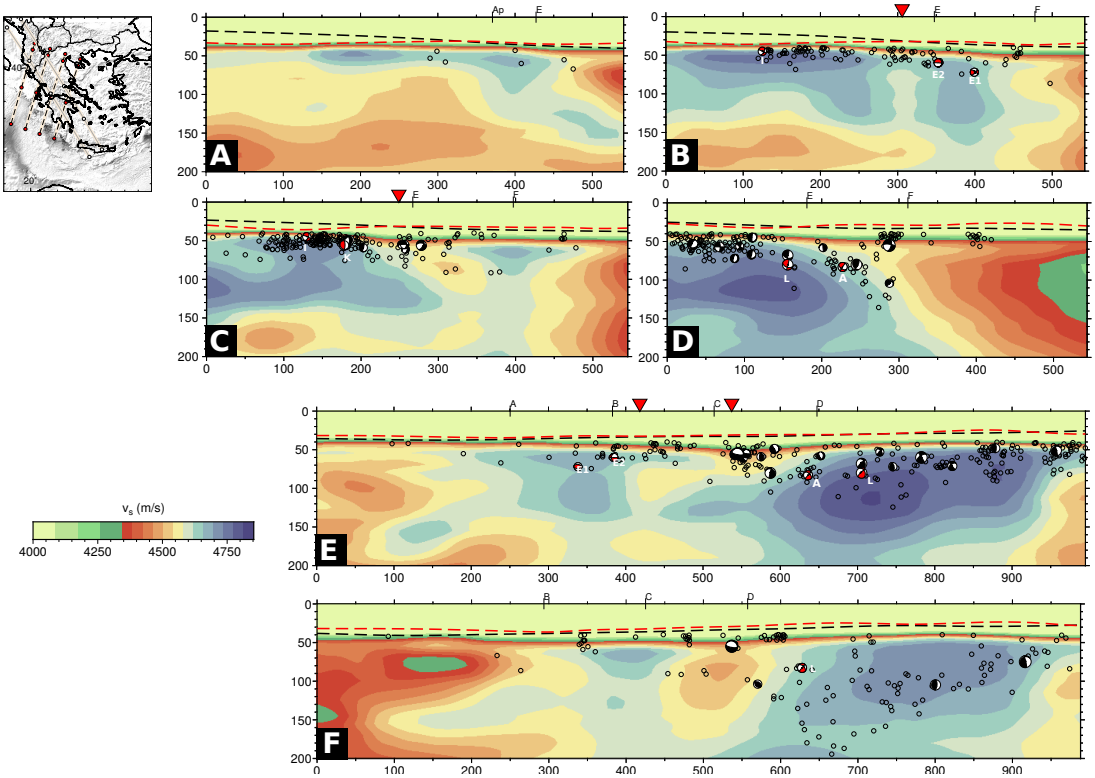


**Figure A.3:** Figure equivalent to Fig. 4.7, i.e., vertical cross sections through the tomographic volume, now with an unsaturated color scale.

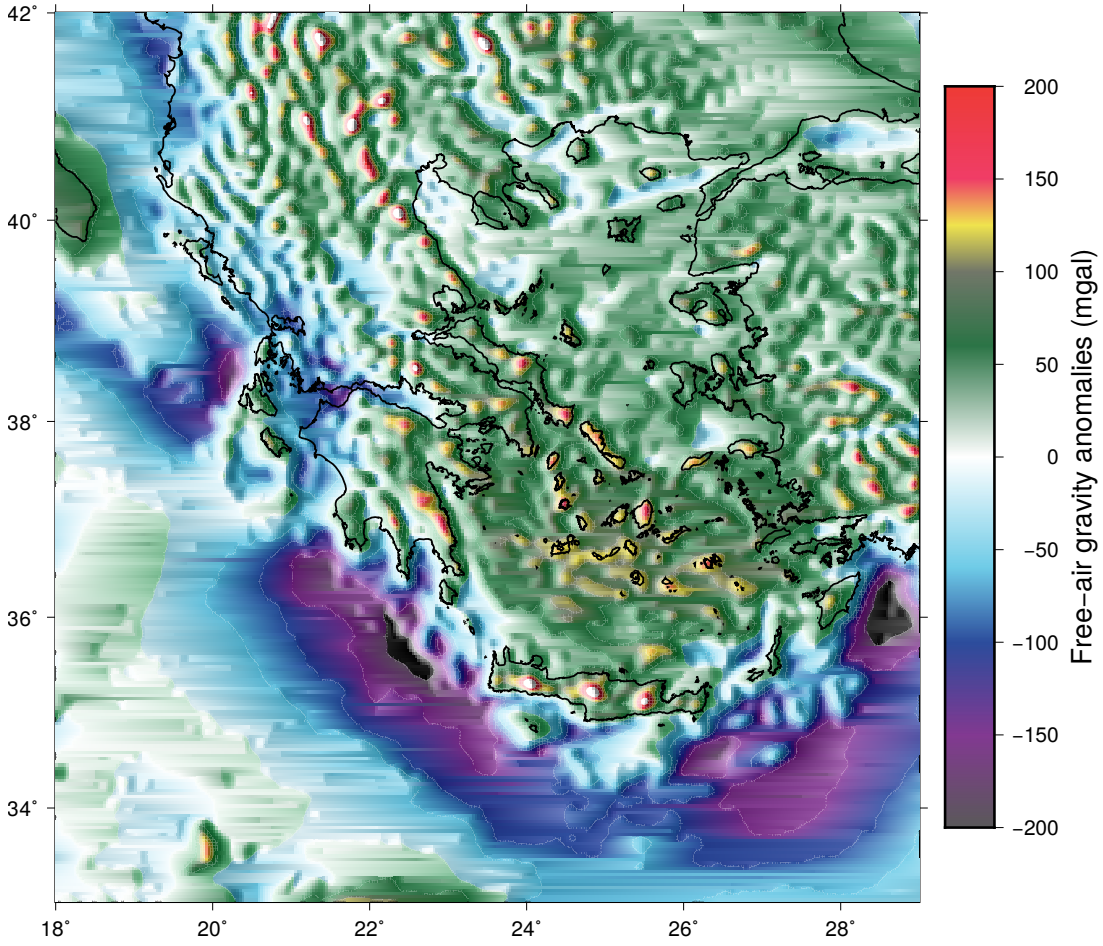


**Figure A.4:** Free-air gravity anomalies in our study area from the World Gravity Map (Bonvalot et al., 2012). The location of the SW-NE oriented 50 mgal anomaly to the SW of the KTF in the Ionian basin aligns with the velocity contrast within the Ionian lithospheric mantle (Figure 4.5B and C).

# Summary

My thesis focuses on evolving and (geologically) short-lived plate boundary segments, their segmentation processes and geological imprints in the eastern Mediterranean.

In Chapter 2, I investigate the nature/type of the plate boundary between the eastern Aegean region and the Africa plate. The work involves an integrative analysis of geological and geophysical information. I conclude that these surface observations document that the "Pliny-Strabo trench" is a predominantly strike-slip plate boundary. My interpretation is that this plate boundary represents an expression of slab tearing related to an active STEP (c.f. Figure 1.1). The paper represents the first detailed account of surface deformation related to a STEP fault, and constitutes a novel contribution to the understanding of the relation between deep processes and (near-) surface deformation, a key topic in geodynamic research.

In Chapter 3, I investigate the location and nature of currently active plate boundaries and other major faults in the southern Anatolia-Aegean region, in the transition region from the Hellenic Arc to the Cyprus Arc. The question is particularly relevant for accessing earthquake hazard. I use mechanical models based on the finite element method. I explore various options for these faults, most of them proposed in the scientific literature, to explore how they would affect the deformation at locations where there are actual observations. The (mis)fit between model predictions and observations allows us to conclude that the active plate boundary is located offshore.

The research question that I address in Chapter 4 is what the cause is of deformation in one of the seismically most active fault zones in Europe, the Kefalonia Transform Fault. I present results from a recent full-waveform tomographic model which particularly improves our understanding of the structure of the upper few hundred kilometers of the Earth. The cause of the deformation along the Kefalonia Transform Fault is likely rooted in a fragmented slab that we image for the first time. The geometry of the slab fragment leads me to conclude that it became disconnected from the larger Hellenic slab around 5 Ma, at about the time of opening of the Gulf of Corinth in the overriding plate, which suggests a highly interesting causal relation.

# Samenvatting

De tektonische platen bestaan uit koele en sterke lithosfeer, en daaronder bevindt zich warme en stroperig vervormbare asthenosfeer. Mijn proefschrift gaat vooral over de lithosfeer. Lithosfeer bestaat uit aardkorst en daaronder lithosfeermantel. Alle tektonische platen bewegen ten opzichte van elkaar. Dit veroorzaakt aardbevingen en vervorming van de korst rondom plaatgrenzen. Er zijn verschillende soorten plaatgrenzen. Subductie plaatgrenzen zijn belangrijk in dit proefschrift. Dit betekent dat twee platen convergeren en dat één plaat onder de andere schuift bij de plaatgrens. Dit verloopt relatief soepel wanneer één van de twee platen een hoog soortelijk gewicht heeft, zoals oceanische lithosfeer. Twee convergerende platen "botsen" (vervormen) wanneer ze beiden een laag soortelijk gewicht hebben, zoals continentale lithosfeer. Een ander soort plaatgrens die in 2005 opnieuw onder de aandacht kwam door een publicatie van Govers en Wortel is een zogenaamde STEP breuk. Hier breekt en scheurt een plaat voortdurend.

Plaatgrenzen in het oostelijk Middellandse Zeegebied zijn het hoofdonderwerp van het proefschrift. Hoe kan het dat dit nog het onderwerp kan zijn voor een proefschrift in 2019? Dit is opmerkelijk wanneer U zich realiseert dat de theorie van de plaattektoniek sinds de zeventiger jaren wereldwijd geaccepteerd is, en de locatie van de plaatgrenzen grotendeels bekend. De reden is dat het er lang op leek dat de bewegingen en de vervorming van de korst in het Middellandse Zeegebied zich niet liet beschrijven in de context van plaattektoniek. Twee aardwetenschappelijke innovaties van de laatste twee decennia hebben hierin grote veranderingen gebracht, GPS metingen van bewegingen van de aardkorst, en CT-scans van de asthenosfeer en de diepere aardmantel. Bij deze CT-scans worden seismologische gegevens gebruikt om de 3D-structuur van de inwendige aarde te maken.

Zo is duidelijk geworden dat plaatgrenzen in het Middellandse Zeegebied veel veranderlijker zijn dan in andere gebieden op onze planeet. Dit komt omdat de (lichte) Afrikaanse en Europese continenten elkaar dicht genaderd zijn, en vooral in het oosten al botsen. Het Middellandse Zeegebied is daardoor één grote plaatgrenszone die zich in het laatste deel van zijn levenscyclus bevindt. Gesubduceerde delen van de Afrikaanse plaat braken af, en STEP breuken zorgden voor het fragmenteren van de lithosfeer, en dit zijn oorzaken van veranderingen.

In hoofdstuk 2 gebruik ik gegevens van aardbevingen en vervorming van de oceaanbodem in combinatie met CT-scans om de aard van de plaatgrens te bepalen ten osten van het

Egeïsch gebied, van Kreta naar Rhodos. We concluderen dat dit een STEP breuk is, en het is voor de eerste keer dat de expressie van een dergelijk type breuk gedetailleerd in kaart wordt gebracht.

In hoofdstuk 3 gebruik ik GPS metingen en geologische waarnemingen voor het recente verleden om te bepalen waar de plaatgrenzen zich bevinden in het oostelijk Middellandse Zeegebied, en wat voor soort plaatgrenzen dit zijn. Ik gebruik de eindige elementen methode om de geomechanica van het gebied te modelleren. De conclusies zijn vooral belangrijk omdat ze een betere inschatting van aardbevingsrisico geven.

In hoofdstuk 4 combineer ik recente CT-scans van de lithosfeer en asthenosfeer onder het Adriatisch gebied en Griekenland met seismologische, geodetische en geologische gegevens. De CT-scans werden verkregen met een innovatieve en data- en reken-intensieve methode waarbij het merendeel van de informatie in seismogrammen werd gebruikt, en waardoor de beeldvorming van vooral de lithosfeer en asthenosfeer beter is dan van klassieke CT-scans. De onderzoekvraag draait om het breuksysteem met de meeste aardbevingen in Europa, de Kefalonia breuk. Verschillende onderzoekers hadden het vermoeden geuit dat dit een STEP breuk is, maar het bewijs hiervoor ontbrak. Wij hebben nu aanwijzingen gevonden dat dit deels juist, maar ook deels onjuist is. Uit onze CT-scans blijkt namelijk dat de gesubduceerde plaat gebroken is. Echter, de geologie van Griekenland en Albanië vertoont nog geen tekenen van een STEP breuk, en we kunnen dit verklaren doordat deze verandering pas (geologisch) onlangs begon, ca. 5 miljoen jaar geleden.

# Özet

Tektonik levhalar soğuk ve güçlü bir litosferden oluşur, ve bunun altında sıcak ve akışkan, deforme olabilen bir astenosfer yer alır. Benim tezim temel olarak litosferle ilgilidir. Litosfer, dünyanın kabuğu ve kabuğun altında yer alan litosfer mantosundan oluşur. Tüm tektonik levhalar birbirine göre hareket eder. Bu hareket levha sınırları boyunca depremlere ve kabuğun deformasyonuna neden olur. Farklı tipte levha sınırları vardır. Bu tez kapsamında dalma-batma tipi levha sınırları ön plandadır. Bu demektir ki, iki plaka birbirine yaklaşır ve, plaka sınırı boyunca biri diğerinin altına dalar. Bu iki levhadan birinin yoğunluğu okyanusal litosferde olduğu gibi daha fazlaysa nispeten sorunsuz ilerler. Yakınsayan levhalardan her ikisinin de yoğunluğu kıtasal litosferdeki gibi düşükse, bunlar "çarpışır". 2005 yılında Govers ve Wortel tarafından yayımlanan bir makaleyle yeniden dikkate alınan bir başka levha sınırı tipi de STEP fayı adıyla anılmaktadır. Burada bir levha sürekli yırtılır ve parçalanır.

Bu tezin esas konusu Doğu Akdeniz'deki levha sınırlarıdır. Peki, nasıl bu konu 2019 yılında hâlâ bir tezin konusu olabiliyor? Levha tektoniği teorisinin 1970'lerden bu yana dünya çapında kabul edildiğini, ve levha sınırlarının konumunun büyük ölçüde bilindiğini akılda tutarsak, bu şaşırtıcıdır. Bunun nedeni Akdeniz'de kabuk hareketleri ve deformasyonunun çoktan beri levha tektoniği bağlamında tarif edilememesidir. Yerbilimlerinde son yirmi yılda gerçekleşen iki teknolojik gelişme, kabuk hareketlerinin GPS ölçümleri ile astenosfer ve daha derin mantonun bilgisayarlı tomografi (BT) görüntüleri sayesinde bu alana dair bilgilerimiz de arttı. BT görüntüleri ile, sismolojik veri kullanılarak dünyanın üç boyutlu iç yapısı oluşturuldu.

Böylece Akdeniz'deki levha sınırlarının gezegenimizdeki diğer alanlardan çok daha değişken olduğu ortaya çıktı. Bunun nedeni (hafif) Afrika ve Avrupa kıtalarının birbirine yakın olması ve özellikle doğuda zaten çarpışması. Bu nedenle, Akdeniz bölgesi yaşam döngüsünün son bölümünde yer alan büyük bir yerel levha sınır bölgesidir. Afrika levhasının dalmış olan bölümü kırıldı ve litosfer STEP fayları ile parçalandı; işte meydana gelen değişimin sebepleri bunlardır.

2. bölümde, Ege Denizinin, Girit ile Rodos arasında kalan doğu kesiminde levha sınırının doğasını belirlemek için deniz tabanı araştırmaları sonucunda elde edilen deprem ve deformasyon verisi ile birlikte BT kesitlerini kullanıyorum. Bu bölgenin bir STEP fayı olduğu sonucuna vardık. Bu tür bir fayın yüzeyde oluşturduğu izi ilk kez ayrıntılarıyla etüt ettik.

3. bölümde, Doğu Akdeniz'de levha sınırlarının nerede olduğunu ve bunların ne tür levha sınırları olduğunu belirlemek için yakın geçmişe ait GPS ölçümleri ve jeolojik gözlemleri kullanıyorum. Bölgenin jeomekaniğini modellemek için sonlu elemanlar yöntemini kullanıyorum. Sonuçlarım özellikle deprem riskinin daha iyi değerlendirilmesi açısından önemlidir.

4. bölümde Adriyatik ve Yunanistan'ın altındaki litosfer ve astenosfere ait bilgisayarlı tomografi sonuçlarını sismolojik, jeodezik ve jeolojik verilerle birleştiriyorum. Bilgisayarlı tomografi, deprem dalgalalarındaki bilginin büyük bir bölümünün kullanılabildiği veri ve hesap yoğun yenilikçi bir yöntemle elde edildi, ve geleneksel tomografi yöntemlerine kıyasla özellikle listosferi daha hassas görüntülememize yardımcı oldu. Araştırma alanı ise Avrupa'da en fazla deprem olan fay sistemlerinden bir tanesini, Kefalonya Fayını konu alıyor. Çeşitli bilim insanları buranın bir STEP fayı olabileceği şüphesini dile getirmişlerdi, ancak ellerinde somut bir kanıt yoktu. Artık elimizde bu şüphenin kısmen doğru olduğuna dair göstergeler var; ancak iddiaların kısmen yanlış olduğu da ortaya çıktı. Bizim topografi sonuçlarımız dalan levhadaki yırtığı ortaya koyuyor. Ancak, Yunanistan ve Arnavutluk jeolojisi, bir STEP fayı belirtisi göstermiyor. Bu farkı, değişimin başlangıcının jeolojik olarak yeni olmasına (yaklaşık 5 milyon yıl öncesi) bağlayarak açıklıyoruz.

# Acknowledgments

I have considered myself as a decent endurance athlete for the last two decades. I know what I am capable of and what I am not -although with the help of my partners, I surprised myself several times. Obviously you cannot run an endurance race like running a short distance event; the success lies in the long-term strategy. I have prepared myself physically and mentally for many different climbs and races, from which I have built enough confidence and a sense of self. Endurance event preparations begin with a base period where body adapts to increasing volume of the exercise and learns to work efficiently. At this stage, precise knowledge of physiological thresholds is crucial, otherwise it is quite easy falling victim to over-training or under-training. The effects of the former is detrimental especially for the nervous system. Common symptoms are mild depression, absence of appetite, exhaustion, irritability and the loss of fitness. Under-training, however, as its name implies, corresponds to no-progress; for which the preparations come to a halt, motivation diminishes and eventually the athlete often surrenders to his or her comfort zone. The base period serves as a solid foundation on which subsequent specific training aims to build. These involve hill repeats, strength and interval training. The focus is on developing and harnessing the maximum power output. The result is improved records in time-trials or longer runs at the aerobic capacity -that is, effectively converting the metabolic waste into the source of energy boost. If the athlete has not developed a good foundation, he or she most likely faces injuries of various sorts. Minor injuries cure on the order of weeks, although most common for the fledgling athlete are the tendon and ligament injuries, which typically heal on the order of seasons. Finally, there is a tapering and rest period right before the endurence event. Having a good rest and nourishment is the key, as well as maintaining blood flow to the muscles, through idle running and stretching. I always thought I am in full control of my mind and body -and always counted on my perseverance. In the final analysis, I know I am fully responsible for the success and should admit the failure. Nevertheless, I find it curious to be so blind to the resemblance between endurance sports and the PhD, as if I had no experience in long-term, gradual, polarized and consistent training. Of course, I would not know if the results would be different. But still this metaphor provides me the lens rom which I can evaluate the past decade. For two things I am sure: 1) I did all the possible mistakes during my PhD – those interested in the list of mistakes can consult me in private– and receive the corresponding injuries; 2) I am not going to do a second PhD, but continue running across the mountains.

In preparation of this thesis and carrying out the research within, many people helped me. I am indebted to three gentlemen for the inception, advance and completion of my

thesis. It was under the promotorship of Prof. Rinus Wortel I began my PhD studies and he was involved and heavily contributed to my training in tectonophysics. If it would not be for Dr. Rob Govers' ardor and scientific guidance, I wouldn't have arrived this far. As my PhD research spanned over a decade, I now formally finish under the promotorship of Prof. Jeannot Trampert. I am grateful.

I would like to thank my reading committee including my opponents, Prof. Giovanni Bertotti, Prof. Douwe van Hinsbergen, Prof. Liviu Matenco, Prof. Thomas Meier, Dr. Paul Meijer, Prof. Wim Spakman, prof. Rinus Wortel; as well as peer reviewers Rob Reilinger, Jeremy Hall, and a few more anonymous scientsists, and co-authors Rinus Wortel, Rob Govers, Andreas Fichtner and Celal Şengör for their contributions to my thesis. I express my gratitude to Hayrullah Karabulut, Cengiz Zabcı, Semih Ergintav, Sinan Özeren, Ebru Bozdağ for the assistance and motivation they provide, except for the times they were excessively asking when I am going to finish. Steven van Benthem and Alper I. Duran accepted to be my paranymps, which is very meaningful for me, thank you so much! In times I needed urgent support for the IT and software troubles Joop, Theo, Lukas, and Wienand brought the electrons running in the right direction again. My sincere thanks guys! I also appreciate the support of Marjolein Mullen, Ildiko Csikos and Margot Stoete for their aid in administrative issues, thesis production details and cover design. Lastly, I thank Nalan Lom for helping me out for the logistics.

Steven, Karin and Thomas; thank you very much for your inclusive and warm friendship. I recall very often mostly fun and fulfilling moments we had together. I made many great friends in the faculty, who made life so much fun! Pasha, Robin, Bahjat, Jeroen, Marzieh, Peter, Celine, Joost, Florian, Jellie, Shalale, Gabi, Ebru, Ilaria, Come, Ahmet, Maud, thank you so much for being there. With a twist of luck, I found my dear cousin Umut in Utrecht for two years of his post-doc, which turn my life into a cozier and comforting track, thanks Q.

Finally, a big thanks goes to my family and especially my wife Burcu, without whose moral support and reassurance I certainly would not finish this thesis.

# Bibliography

**Publications of research presented in this thesis Author contributions given according to the CReDiT taxonomy (in decreasing order of contribution).**

Özbakır, A.D., Govers, R. and Fichtner, A. (in prep.). The Kefalonia Transform Fault: a STEP in the making. Conceptualization: RG; Data Curation: AF; Investigation: AO and RG; Methodology: RG; Resources and Software: RG and AO; Validation: AO; Supervision: RG; Visualization: AO; Writing: RG, AO & AF.

Özbakır, A. D., Govers, R., and Wortel, R. (2017). Active faults in the Anatolian-Aegean plate boundary region with Nubia. Turkish Journal of Earth Sciences, 26(1), 30–56. Conceptualization: RG; Data Curation: AO; Investigation: AO and RG; Methodology: AO and RG; Resources and Software: RG; Validation: AO; Supervision: RG; Visualization: AO; Writing: AO, RG and RW.

Özbakır, A. D., Şengör, A., Wortel, M., and Govers, R. (2013). The Pliny–Strabo trench region: A large shear zone resulting from slab tearing. Earth and Planetary Science Letters, 375, 188–195. Conceptualization: CS, RG, RW; Data Curation: AO; Investigation: AO&RG; Methodology: AO; Resources and Software: AO; Validation: AO; Supervision: RG; Visualization: AO&RG; Writing: AO, RG&RW.

**Other publications**

Güvercin, S., Konca, A.Ö., Özbakır, A.D., Aksarı, D., Ergintav, S. and Karabulut, H. (2019). On the Interaction between Nubia-Anatolia Plates: Segmentation, Geometry, and Kinematics of an Isolated Slab. Tectonics, submitted

Karabulut, H., Paul, A., Özbakır, A.D., Ergün, T., and Şentürk, S. (2019). A new crustal model of the Anatolia-Aegean domain: evidence for the dominant role of isostasy in the support of the Anatolian plateau. Geophys J. Int., 218, 57–73.

Öztürk, Y.K., Özel, N.M. and Özbakir, A.D. (2015). States of local stresses in the Sea of Marmara through the analysis of large numbers of small earthquakes. Tectonophysics, 665, 37-57.

Şengör, A. M. C., Özeren, M. S., Keskin, M., Sakınç, M., Özbakır, A. D., and Kayan, I. (2008). Eastern Turkish high plateau as a small Turkic-type orogen: Implications for post-collisional crust-forming processes in Turkic-type orogens. Earth Sci. Rev., 90, 1–48.

# References


Agard, P., Omrani, J., Jolivet, L., Whitechurch, H., Vrielynck, B., Spakman, W., Monie, P., Meyer, B., and Wortel, R. (2011). Zagros orogeny: a subduction-dominated process. *Geol. Mag.*, **148**, 692–725.

Aksoy, M. E., Meghraoui, M., Cakir, Z., Ferry, M., and Ucarkus, G. (2010). Short-term and long-term slip rate along the westernmost segment of the North Anatolian Fault using paleoseismic trenching and drainage offsets. *Geophysical Research Abstracts*, **12**, EGU2010–12447–1.

Aksu, A., Hall, J., and Yaltirak, C. (2009). Miocene - Recent evolution of Anaximander Mountains and Finike Basin at the junction of Hellenic and Cyprus Arcs, eastern Mediterranean. *Mar. Geol.*, **258**, 24–47.

Aksu, A. E., , Calon, T., Hall, J., Mansfield, S., and Yasar, D. (2005). The Cilicia - Adana basin complex, Eastern Mediterranean: Neogene evolution of an active fore-arc basin in an obliquely convergent margin. *Mar. Geol.*, **221**, 121–159.

Aktuğ, B., Nocquet, J. M., Cingöz, A., Parsons, B., Erkan, Y., England, P., Lenk, O., Gürdal, M. A., Kılıçoğlu, A., Akdeniz, H., and Tekgül, A. (2009). Deformation of western Turkey from a combination of permanent and campaign GPS data: Limits to block-like behavior. *J. Geophys. Res.*, **114**, B10404.

Alchalbi, A., Daoud, M., Gomez, F., McClusky, S., Reilinger, R., Romeyeh, M. A., Alsouod, A., Yassminh, R., Ballani, B., Darawcheh, R., Sbeinati, R., Radwan, Y., Masri, R. A., Bayerly, M., Ghazzi, R. A., and Barazangi, M. (2010). Crustal deformation in northwestern Arabia from GPS measurements in Syria: Slow slip rate along the northern Dead Sea Fault. *Geophys. J. Int*, **180**, 125–135.

Aliaj, S., Baldassarre, G., and Shkupi, D. (2001). Quaternary subsidence zones in Albania: some case studies. *Bull. Eng. Geol. Environ.*, **59**(4), 313–318.

Allen, M., Jackson, J., and Walker, R. (2004). Late Cenozoic reorganization of the Arabia-Eurasia collision and the comparison of short-term and long-term deformation rates. *Tectonics*, **23**, TC2008.

Alçiçek, M., Veen, J. T., and Özkul, M. (2006). Neotectonic development of the Çameli basin, south-western anatolia, turkey. *Geological Society London Special Publications*, **Tectonic development of the Eastern Mediterranean Region**(260), 591–611.

Amaru, M. (2007). *Global travel time tomography with 3-D reference models*. Ph.D. thesis, Utrecht University.

Ambraseys, N. N. (2006). Comparison of frequency of occurrence of earthquakes with slip rates from long-term seismicity data: the cases of Gulf of Corinth. Sea of Marmara and Dead Sea Fault Zone. *Geophys. J. Int.*, **165**, 516–526.

Apel, E., Bürgmann, R., Steblov, G., Vasilenko, N., King, R., and Prytkov, A. (2006). Independent active microplate tectonics of northeast Asia from GPS velocities and block modeling. *Geophysical Research Letters*, **33**(11).

Armijo, R., Meyer, B., King, G. C. P., Rigo, A., and Papanastassiou, D. (1996). Quaternary evolution of the Corinth Rift and its implications for the Late Cenozoic evolution of the Aegean. *Geophys. J. Int.*, **126**, 11–53.

Armijo, R., Meyer, B., Hubert, A., and Barka, A. (1999). Westward propagation of the North Anatolian fault into the northern Aegean: Timing and kinematics. *Geology*, **27**, 267–270.

Arpat, E. and Şaroğlu, F. (1975). Türkiye'deki bazı önemli genç tektonik olaylar. *Türkiye Jeoloji Kurumu Bülteni*, **18**(1), 91–101.

Arpat, E. and Şaroğlu, F. (1972). The East Anatolian fault system: thoughts on its development. *Bull. Miner. Res. Explor. Inst. Turk*, **78**, 33–39.

ArRajehi, A., McClusky, S., Reilinger, R., Daoud, M., Alchalbi, A., Ergintav, S., Gomez, F., Sholan, J., Bou-Rabee, F., Ogubazghi, G., Haileab, B., Fisseha, S., Asfaw, L., Mahmoud, S., Rayan, A., Bendik, R., and Kogan, L. (2010). Geodetic constraints on present-day motion of the Arabian Plate: Implications for Red Sea and Gulf of Aden rifting. *Tectonics*, **29**, TC3011.

Babuska, V. and Cara, M. (1991). *Seismic anisotropy in the Earth*, volume 10. Springer Science & Business Media.

Baes, M., Govers, R., and Wortel, M. J. R. (2011). Subduction initiation along the inherited weakness zone at the edge of a slab: Insights from numerical models. *Geophys. J. Int*, **184**, 991–1008.

Baker, C., Hatzfeld, D., Lyon-Caen, H., Papadimitriou, E., and Rigo, A. (1997). Earthquake mechanisms of the Adriatic Sea and Western Greece: implications for the oceanic subduction-continental collision transition. *Geophysical Journal International*, **131**(3), 559–594.

Barka, A. and Reilinger, R. (1997). Active tectonics of the Eastern Mediterranean region: deduced from GPS, neotectonic and seismicity data. *Ann. Geofis.*, **40**(3), 587–611.

Barrier, E., Vrielynck, B., Bergerat, F., Brunet, M.-F., Mosar, J., Poisson, A., and M.Sosson (2008). *MEBE Atlas of palaeotectonic maps of the middle east*. CCGM.

Bartol, J. and Govers, R. (2014). A single cause for uplift of the Central and Eastern Anatolian plateau? *Tectonophysics*, **637**, 116–136.

Basili, R., Kastelic, V., Demircioglu, M., Garcia Moreno, D., Nemser, E., Petricca, P., Sboras, S., Besana Ostman, G., Cabral, J., Camelbeeck, T., Caputo, R., Danciu, L., Domac, H., Fonseca, J., García-Mayordomo, J., Giardini, D., Glavatovic, B., Gulen, L., Ince, Y., Pavlides, S., Sesetyan, K., Tarabusi, G., Tiberti, M., Utkucu, M., Valensise, G., Vanneste, K., Vilanova, S., and Wössner, J. (2013). *The European Database of Seismogenic Faults (EDSF) compiled in the framework of the Project SHARE.*

Bassin, C., Laske, G., and Masters, G. (2000). The Current Limits of Resolution for Surface Wave Tomography in North America. *EOS Trans AGU*, **81**, F897.

Becker, D., Meier, T., Bohnhoff, M., and Harjes, H. (2010). Seismicity at the convergent plate boundary offshore Crete, Greece, observed by an amphibian network. *Journal of seismology*, **14**(2), 369–392.

Becker, T. and Faccenna, C. (2011). Mantle conveyor beneath the Tethyan collisional belt. *Earth and Planetary Science Letters*, **310**(3), 453–461.

Bega, Z. (2015). Hydrocarbon exploration potential of Montenegro–a brief review. *Journal of Petroleum Geology*, **38**, 317–330.

Ben-Avraham, Z., Kempler, D., and Ginzburg, A. (1988). Plate convergence in the Cyprean Arc. *Tectonophysics*, **146**, 231–240.

Benetatos, C., Kiratzi, A., Papazachos, C., and Karakaisis, G. (2004). Focal mechanisms of shallow and intermediate depth earthquakes along the Hellenic Arc. *Journal of Geodynamics*, **37**(2), 253–296.

Bevis, M., Taylor, F., Schutz, B., Recy, J., Isacks, B., Helu, S., Singh, R., Kendrick, E., Stowell, J., Taylor, B., and Calmant, S. (1995). Geodetic observations of very rapid convergence and back-arc extension at the Tonga arc. *Nature*, **374**, 249–251.

Biermanns, P., Schmitz, B., Ustaszewski, K., and Reicherter, K. (2019). Tectonic geomorphology and Quaternary landscape development in the Albania-Montenegro border region: An inventory. *Geomorphology*, **326**, 116–131.

Bijwaard, H. and Spakman, W. (2000). Non-linear global P-wave tomography by iterated linearized inversion. *Geophys. J. Int.*, **141**, 71–82.

Bijwaard, H., Spakman, W., and Engdahl, E. (1998). Closing the gap between regional and global travel time tomography. *J. Geophys. Res.*, **103**(B12), 30055–30078.

Bird, P. (2003). An updated digital model of plate boundaries. *Geochem. Geophys. Geosyst*, **4**(3), 1027.

Biryol, C., Beck, S., Zandt, G., and Özacar, A. (2011). Segmented African lithosphere beneath the Anatolian region inferred from teleseismic P-wave tomography. *Geophysical Journal International*, **1**, 16.

Bocchini, G., Brüstle, A., Becker, D., Meier, T., van Keken, P., Ruscic, M., Papadopoulos, G., Rische, M., and Friederich, W. (2018). Tearing, segmentation, and backstepping of subduction in the Aegean: New insights from seismicity. *Tectonophysics*, **734**, 96–118.

Boev, B. and Yanev, Y. (2001). Tertiary magmatism within the Republic of Macedonia: a review. *Acta Vulcuanologica*, **13**(1-2), 57–71.

Bohnhoff, M., Harjes, H. P., and Meier, T. (2005). Deformation and stress regimes in the Hellenic subduction zone from focal mechanisms. *Journal of Seismology*, **9**, 341–366.

Boray, A., Şaroğlu, F., and Emre, Ö. (1985). Isparta büklümünün kuzey kesiminde doğu-batı daralma için bazı veriler. *Jeoloji Müh*, **23**, 9–20.

Bourova, E., Kassaras, I., Pedersen, H. A., Yanovskaya, T., Hatzfeld, D., and Kiratzi, A. (2005). Constraints on absolute S velocities beneath the Aegean Sea from surface wave analysis. *Geophysical Journal International*, **160**(3), 1006–1019.

Bozkurt, E. (2001). Neotectonics of Turkey - a synthesis. *Geodinamica Acta*, **14**, 3–30.

Brooks, M. and Ferentinos, G. (1984). Tectonics and sedimentation in the Gulf of Corinth and the Zakynthos and Kefallinia channels, western Greece. *Tectonophysics*, **101**(1-2), 25–54.

Brun, J.-P. and Sokoutis, D. (2010). 45 m.y. of Aegean crust and mantle flow driven by trench retreat. *Geology*, **38**, 815–818.

Brun, J.-P., Faccenna, C., Gueydan, F., Sokoutis, D., Philippon, M., Kydonakis, K., and Gorini, C. (2016). The two-stage Aegean extension, from localized to distributed, a result of slab rollback acceleration. *Canadian journal of earth sciences*, **53**(11), 1142–1157.

Burchfiel, B. C., King, R. W., Todosov, A., Kotzev, V., Durmurdzanov, N., T, S., and Nurce, B. (2006). GPS results for Macedonia and its importance for the tectonics of the Southern Balkan extensional regime. *Tectonophysics*, **413**, 239–248.

Burgos, G., Montagner, J.-P., Beucler, E., Capdeville, Y., Mocquet, A., and Drilleau, M. (2014). Oceanic lithosphere-asthenosphere boundary from surface wave dispersion data. *Journal of Geophysical Research: Solid Earth*, **119**(2), 1079–1093.

Calon, T., Aksu, A., and Hall, J. (2005). The Neogene evolution of the Outer Latakia Basin and its extension into the Eastern Mesaoria Basin (Cyprus), Eastern Mediterranean. *Marine geology*, **221**(1-4), 61–94.

Carminati, E., Wortel, M. J. R., Meijer, P., and Sabadini, R. (1998). The two-stage opening of the western-central Mediterranean basins: a forward modeling test to a new evolutionary model. *Earth Planet. Sci. Lett.*, **160**, 667–679.

Cavalie, O. and Jonsson, J. (2014). Block-like plate movements in eastern Anatolia observed by InSAR. *Geophys. Res. Lett*, **41**, 26–31.

Çetin, H., Güneyli, H., and Mayer, L. (2003). Paleoseismology of the Palu-Lake Hazar segment of the east Anatolian fault zone, Turkey. *Tectonophysics*, **374**(3-4), 163–197.

Chamot-Rooke, N., Rangin, C., Le Pichon, X., working group, D., *et al.* (2005). *Deep Offshore Tectonics of the Eastern Mediterranean: A Synthesis of Deep Marine Data in the Eastern Mediterranean: the Ionian Basin and Margins, the Calabria Wedge and the Mediterranean Ridge*. Société géologique de France.

Chaumillon, E. and Mascle, J. (1997). From foreland to forearc domains: New multichannel seismic reflection survey of the mediterranean ridge accretionary complex (eastern mediterranean). *Mar. Geol.*, **138**, 137–259.

Chousianitis, K., Ganas, A., and Evangelidis, C. P. (2015). Strain and rotation rate patterns of mainland Greece from continuous GPS data and comparison between seismic and geodetic moment release. *Journal of Geophysical Research: Solid Earth*, **120**(5), 3909–3931.

Cianetti, S., Gasperini, P., Giunchi, C., and Boschi, E. (2001). Numerical modelling of the Aegean-Anatolian region: geodynamical constraints from observed rheological heterogeneities. *Geophys. J. Int.*, **146**, 760–780.

Clark, S., Sobiesiak, M., Zelt, C., Magnani, M., Miller, M., Bezada, M., and Levander, A. (2008). Identification and tectonic implications of a tear in the South American plate at the southern end of the Lesser Antilles. *Geochemistry, Geophysics, Geosystems*, **9**(11).

Clément, C., Hirn, A., Charvis, P., Sachpazi, M., and Marnelis, F. (2000). Seismic structure and the active Hellenic subduction in the Ionian islands. *Tectonophysics*, **329**(1-4), 141–156.

Clews, J. E. (1989). Structural controls on basin evolution: Neogene to Quaternary of the Ionian zone, Western Greece. *Journal of the Geological Society*, **146**(3), 447–457.

Cowgill, E. (2007). Impact of riser reconstructions on estimation of secular variation in rates of strike–slip faulting: Revisiting the Cherchen River site along the Altyn Tagh Fault, NW China. *Earth and Planetary Science Letters*, **254**(3-4), 239–255.

Crotwell, H. P., Owens, T. J., and Ritsema, J. (1999). The taup toolkit: Flexible seismic travel-time and ray-path utilities. *Seismological Research Letters*, **70**(2), 154–160.

D' Agostino, N., Avallone, A., Cheloni, D., D' Anastasio, E., Mantenuto, S., and Selvaggi, G. (2008). Active tectonics of the Adriatic region from GPS and earthquake slip vectors. *Journal of Geophysical Research: Solid Earth*, **113**(B12).

de Boorder, H., Spakman, W., White, S., and Wortel, M. J. R. (1998). Late Cenozoic mineralization, orogenic collapse and slab detachment in the European Alpine Belt. *Earth Planet. Sci. Lett.*, **164**, 569–575.

De Franco, R., Govers, R., and Wortel, R. (2008a). Dynamics of continental collision: influence of the plate contact. *Geophysical Journal International*, **174**(3), 1101–1120.

De Franco, R., Govers, R., and Wortel, R. (2008b). Nature of the plate contact and subduction zones diversity. *Earth and Planetary Science Letters*, **271**(1-4), 245–253.

de Lis Mancilla, F., Heit, B., Morales, J., Yuan, X., Stich, D., Molina-Aguilera, A., Azañon, J., and Martín, R. (2018). A step fault in central betics, associated with lateral lithospheric tearing at the northern edge of the gibraltar arc subduction system. *Earth Planet. Sci. Lett.*, **486**, 32–40.

de Voogd, B., Truffert, C., Chamot-Rooke, N., Huchon, P., Lallemant, S., and Pichon, X. (1992). Two-ship deep seismic soundings in the basins of the eastern Mediterranean Sea (Pasiphae cruise). *Geophysical Journal International*, **109**(3), 536–552.

DeMets, C., Gordon, R. G., and Argus, D. F. (2010). Geologically current plate motions. *Geophys. J. Int*, **181**, 1–80.

Dewey, J. and Şengor, A. (1979). Aegean and surrounding regions: Complex multiplate and continuum tectonics in a convergent zone. *Geological Society of America Bulletin*, **90**, 84–92.

Dewey, J., Helman, M., Turco, E., Hutton, D., and Knott, S. (1989). *Kinematics of the western Mediterranean.*, volume Alpine Tectonics. Geological Society of London.

Dewey, J. F., Hempton, M. R., Kidd, W. S. F., Şaroğlu, F., and Şengör, A. M. C. (1986). Shortening of continental lithosphere: The neotectonics of Eastern Anatolia – a young collision zone. **Continental Tectonics**(19), 3–36.

Dikbaş, A., Akyüz, H. S., Meghraoui, M., Ferry, M., Yalçıner, C. C., Zabcı, C., Karabacak, V., Kıyak, N., and Altunel, E. (2009). Earthquake history and slip rate of Sapanca-Akyazi segment on western part of North Anatolian fault for the past 1000 years. *62nd Geological Kurultai of Turkey*, page 1001.

Dilek, Y. and Altunkaynak, Ş. (2009). Geochemical and temporal evolution of Cenozoic magmatism in western Turkey: mantle response to collision, slab break-off, and lithospheric tearing in an orogenic belt. *Geological Society, London, Special Publications*, **311**(1), 213–233.

Dolan, J. (2009). Possible transient strain accumulation along the North Anatolian fault: Precursor or artifact. In *Proceedings of the international symposium on historical earthquakes and conservation of monuments and sites in the Eastern Mediterranean Region, 500th anniversary year of the 1509 September 10, Marmara Earthquake 10–12 September 2009*. Istanbul Technical University Istanbul, Turkey.

Dougherty, S. L. and Clayton, R. W. (2014). Seismicity and structure in central Mexico: Evidence for a possible slab tear in the South Cocos plate. *Journal of Geophysical Research: Solid Earth*, **119**(4), 3424–3447.

Dougherty, S. L., Clayton, R. W., and Helmberger, D. V. (2012). Seismic structure in central Mexico: Implications for fragmentation of the subducted Cocos plate. *Journal of Geophysical Research: Solid Earth*, **117**(B9).

Duermeijer, C., Krijgsman, W., Langereis, C., Meulenkamp, J., Triantaphyllou, M., and Zachariasse, W. (1999). A Late Pleistocene clockwise rotation phase of Zakynthos (Greece) and implications for the evolution of the western Aegean arc. *Earth and Planetary Science Letters*, **173**(3), 315–331.

Duermeijer, C., Nyst, M., Meijer, P., Langereis, C., and Spakman, W. (2000). Neogene evolution of the Aegean arc: paleomagnetic and geodetic evidence for a rapid and young rotation phase. *Earth and Planetary Science Letters*, **176**(3), 509–526.

Dumurdzanov, N., Serafimovski, T., and Burchfiel, B. C. (2005). Cenozoic tectonics of Macedonia and its relation to the South Balkan extensional regime. *Geosphere*, **1**, 1.

Durand, V., Bouchon, M., Floyd, M., Theodulidis, N., Marsan, D., Karabulut, H., and Schmittbuhl, J. (2014). Observation of the spread of slow deformation in Greece following the breakup of the slab. *Geophys. Res. Lett.*, **41**, 7129–7134.

Dziewonski, A. M., Chou, T.-A., and Woodhouse, J. H. (1981). Determination of earthquake source parameters from waveform data for studies of global and regional seismicity. *J. Geophys. Res.*, **86**, 2825–2852.

Ekström, G., Nettles, M., and Dziewonski, A. M. (2012). The global CMT project 2004-2010: Centroid-moment tensors for 13,017 earthquakes. *Phys. Earth Planet. Inter*, **200-201**, 1–9.

Emery, K. O., Heezen, B. C., and Allan, T. D. (1966). Bathymetry of the eastern Mediterranean Sea. *Deep-Sea Research*, **13**, 173–192.

Emre, Ö., Duman, T., Özalp, S., Elmacı, H., Olgun, Ş., and Şaroğlu, F. (2013). Active fault map of Turkey with explanatory text. *General Directorate of Mineral Research and Exploration Special Publication Series*, **30**.

Endrun, B., Lebedev, S., Meier, T., Tirel, C., and Friederich, W. (2011). Complex layered deformation within the Aegean crust and mantle revealed by seismic anisotropy. *Nat. Geosci.*, **4**, 203–207.

England, P. C. and McKenzie, D. P. (1982). A thin viscous sheet model for continental deformation. *J. R. Astron. Soc*, **70**, 295–321.

Eyidoğan, H. and Barka, A. (1996). The 1 October 1995 Dinar earthquake, SW Turkey. *Terra Nova*, **8**(5), 479–485.

Faccenna, C., Becker, T., Miller, M., Serpelloni, E., and Willett, S. (2014). Isostasy, dynamic topography, and the elevation of the Apennines of Italy. *Earth Planet. Sci. Lett.*, **407**, 163–174.

Fichtner, A., Trampert, J., Cupillard, P., Saygin, E., Taymaz, T., Capdeville, Y., and Villasenor, A. (2013). Multiscale full waveform inversion. *Geophysical Journal International*, **194**(1), 534–556.

Finetti, I. and Del Ben, A. (2005). Crustal tectono-stratigraphy of the Ionian Sea from new integrated CROP seismic data, Deep Seismic Exploration of the Central Mediterranean and Italy. *CROP PROJECT*, **19**, 447–470.

Fischer, K. D. (2006). The influence of different rheological parameters on the surface deformation and stress field of the Aegean-Anatolian region. *Int J Earth Sci*, **95**, 239–249.

Fitch, T. J. (1972). Plate convergence, transcurrent faults, and internal deformation adjacent to southeast Asia and the western Pacific. *J. Geophys. Res.*, **77**, 4432–4460.

Flerit, F., Armijo, R., King, G., and Meyer, B. (2004). The mechanical interaction between the propagating North Anatolian Fault and the back-arc extension in the Aegean. *Earth Planet. Sci. Lett.*, **224**, 347–362.

Floyd, M., Billiris, H., Paradissis, D., Veis, G., Avallone, A., Briole, P., McClusky, S., Nocquet, J., Palamartchouk, K., Parsons, B., *et al.* (2010). A new velocity field for Greece: Implications for the kinematics and dynamics of the Aegean. *Journal of Geophysical Research*, **115**(B10), B10403.

Forsyth, D. (1975). Fault plane solutions and tectonics of the South Atlantic and Scotia Sea. *J. Geophys. Res*, **80**, 1429–1443.

Frohlich, C. (1992). Triangle diagrams: ternary graphs to display similarity and diversity of earthquake focal mechanisms. *Phys. Earth Planet. Inter.*, **75**, 193–198.

Frohlich, C. (2001). Display and quantitative assessment of distributions of earthquake focal mechanisms. *Geophys. J. Int.*, **144**, 300–308.

Fruehn, J., Reston, T., von Huene, R., and Bialas, J. (2002). Structure of the Mediterranean Ridge accretionary complex from seismic velocity information. *Marine geology*, **186**(1-2), 43–58.

Fryer, P., Becker, N., Appelgate, B., Martinez, F., Edwards, M., and Fryer, G. (2003). Why is the Challenger Deep so deep? *Earth Planet Sc Lett*, **211**, 259–269.

Furlong, K. and Schwartz, S. (2004). Influence of the Mendocino triple junction on the tectonics of coastal California. *Annu. Rev. Earth Planet. Sci.*, **32**, 403–433.

Fytikas, M., Innocenti, F., Manetti, P., Mazzuoli, R., Peccerillo, A., and Villari, L. (1984). *Tertiary to Quaternary evolution of volcanism in the Aegean region*, volume The Geological Evolution of the Eastern Mediterranean. Geological Society London, London.

Ganas, A. and Parsons, T. (2009). Three-dimensional model of Hellenic Arc deformation and origin of the Cretan uplift. *Journal of Geophysical Research*, **114**, B06404.

Gautier, P., Brun, J.-P., Moriceau, R., Sokoutis, D., Martinod, J., and Jolivet, L. (1999). Timing, kinematics and cause of Aegean extension: a scenario based on a comparison with simple analogue experiments. *Tectonophysics*, **315**, 31–72.

Gawthorpe, R., Leeder, M., Kranis, H., Skourtsos, E., Andrews, J., Henstra, G., Mack, G., Muravchik, M., Turner, J., and Stamatakis, M. (2018). Tectono-sedimentary evolution of the Plio-Pleistocene Corinth rift, Greece. *Basin Research*, **30**, 448–479.

Ghosh, A., Holt, W. E., and Flesch, L. M. (2009). Contribution of gravitational potential energy differences to the global stress field. *Geophys. J. Int.*, **179**, 787–812.

Giardini, D., J., W., and L., D. (2014). Mapping Europe's Seismic Hazard. *EOS*, **95**, 261–262.

Goldsworthy, M., Jackson, J., and Haines, J. (2002). The continuity of active fault systems in Greece. *Geophysical Journal International*, **148**(3), 596–618.

Gong, W., Xing, J., and Jiang, X. (2018). Heterogeneous subduction structure within the Pacific plate beneath the Izu-Bonin arc. *J. Geodyn.*, **116**, 1–12.

Got, J.-L., Monteiller, V., Monteux, J., Hassani, R., and Okubo, P. (2008). Deformation and rupture of the oceanic crust may control growth of Hawaiian volcanoes. *Nature*, **451**(7177), 453.

Govers, R. and Fichtner, A. (2016). Signature of slab fragmentation beneath Anatolia from full-waveform tomography. *Earth and Planetary Science Letters*, **450**, 10–19.

Govers, R. and Meijer, P. (2001). On the dynamics of the Juan de Fuca plate. *Earth Planet. Sci. Lett.*, **189**, 115–131.

Govers, R. and Wortel, M. (2005). Lithosphere tearing at STEP faults: response to edges of subduction zones. *Earth and Planetary Science Letters*, **236**, 505–523.

Grad, M., Tiira, T., and ESC Working Group (2009). The Moho depth map of the European Plate. *Geophys. J. Int.*, **176**, 279–292.

Guillaume, B., Funiciello, F., Faccenna, C., Martinod, J., and Olivetti, V. (2010). Spreading pulses of the Tyrrhenian Sea during the narrowing of the Calabrian slab. *Geology*, **38**, 819–822.

Gutscher, M., Malavieille, J., Lallemand, S., and Collot, J. (1999). Tectonic segmentation of the North Andean margin: impact of the Carnegie Ridge collision. *Earth Planet. Sc. Lett.*, **168**, 255–270.

Gvirtzman, Z. and Stern, R. (2004). Bathymetry of Mariana trench-arc system and formation of the Challenger Deep as a consequence of weak plate coupling. *Tectonics*, **23**, TC2011.

Hall, J., Aksu, A. E., Yaltırak, C., and Winsor, J. D. (2009). Structural architecture of the Rhodes Basin: A deep depocentre that evolved since the Pliocene at the junction of Hellenic and Cyprus Arcs, eastern Mediterranean. *Mar. Geol.*, **258**, 1–23.

Hall, J., Aksu, A., Elitez, I., Yaltırak, C., and Çiftçi, G. .-. (2014). The Fethiye-Burdur Fault Zone: a component of upper plate extension of the subduction transform edge propagator fault linking Hellenic and Cyprus arcs, eastern Mediterranean. *Tectonophysics*, **635**, 80–99.

Halpaap, F., Rondenay, S., and Ottemöller, L. (2018). Seismicity, Deformation, and Metamorphism in the Western Hellenic Subduction Zone: New Constraints From Tomography. *J. Geophys. Res.*, **123**, 3000–3026.

Handy, M., Ustaszewski, K., and Kissling, E. (2015). Reconstructing the Alps–Carpathians–Dinarides as a key to understanding switches in subduction polarity, slab gaps and surface motion. *Int. J. Earth Sci.*, **104**, 1–26.

Hansen, S., Evangelidis, C., and Papadopoulos, G. (2019). Imaging Slab Detachment within the Western Hellenic Subduction Zone. *Geochemi. Geophys. Geosyst.*, **20**, 895–912.

Hatzfeld, D. and Martin, C. (1992). Intermediate depth seismicity in the Aegean defined by teleseismic data. *Earth Planet. Sci. Lett.*, **113**, 267–275.

Hatzfeld, D., Karagianni, E., Kassaras, I., Kiratzi, A., Louvari, E., Lyon-Caen, H., Makropoulos, K., Papadimitriou, P., Bock, G., and Priestley, K. (2001). Shear wave anisotropy in the upper mantle beneath the Aegean related to internal deformation. *Journal of Geophysical Research: Solid Earth*, **106**(B12), 30737–30753.

Hayes, G., Moore, G., Portner, D., Hearne, M., Flamme, H., Furtney, M., and Smoczyk, G. (2018). Slab2, a comprehensive subduction zone geometry model. *Science*, **362**, 58–61.

Heidbach, O., Tingay, M., Barth, A., Reinecker, J., Kurfeß, D., and Müller, B. (2008). The World Stress Map database release 2008: Paris, France, Commission for the Geological Map of the World, equatorial scale 1: 46,000,000, doi: 10.1594/GFZ. *WSM. Map2009*.

Heidbach, O., Tingay, M., Barth, A., Reinecker, J., Kurfess, D., and Muller, B. (2010). Global crustal stress pattern based on the World Stress Map database release 2008. *Tectonophysics*, **482**, 3–15.

Hempton, M. R. (1985). Structure and deformation history of the Bitlis suture near Lake Hazar, southeastern Turkey. *Bulletin of the Geological Society of America*, **96**, 233–243.

Herece, E. (2008). Doğu Anadolu Fayı (DAF) Atlası. *Maden Tetkik ve Arama Genel Müdürluğü, Özel Yayın Serisi*, **13**.

Herece, E. and Akay, E. (1992). Karlıova - Çelikhan arasinda Doğu Anadolu Fayı. In *Turkiye 9. Petrol Kongresi*, pages 361–362, Ankara. TMMOB Petrol Muhendisleri Odasi.

Hergert, T. and Heidbach, O. (2010). Slip-rate variability and distributed deformation in the Marmara Sea fault system. *Nature Geoscience*, **3**, 132–135.

Hessami, K., Nilforoushan, F., and Talbot, C. J. (2006). Active deformation within the Zagros Mountains deduced from GPS measurements. *J. Geol. Soc.*, **163**, 143–148.

Hirn, A., Sachpazi, M., Siliqi, R., Mc Bride, J., Marnelis, F., Cernobori, L., and STREAMERS-PROFILES (1996). A traverse of the Ionian islands front with coincident normal incidence and wide-angle seismics. *Tectonophysics*, **264**, 35–49.

Hollenstein, C., Müller, M., Geiger, A., and Kahle, H.-G. (2008). Crustal motion and deformation in Greece from a decade of GPS measurements, 1993–2003. *Tectonophysics*, **449**, 17–40.

Houghton, S., Roberts, G., Papanikolaou, I., McArthur, J., and Gilmour, M. (2003). New 234U-230Th coral dates from the western Gulf of Corinth: Implications for extensional tectonics. *Geophys. Res. Lett.*, **30**.

Howell, A., Jackson, J., Copley, A., McKenzie, D., and Nissen, E. (2017). Subduction and vertical coastal motions in the eastern Mediterranean. *Geophysical Journal International*, **211**, 593–620.

Hubert-Ferrari, A., Armijo, R., King, G., Meyer, B., and Barka, A. (2002). Morphology, displacement, and slip rates along the North Anatolian Fault, Turkey. *J. Geophys. Res.*, **107(B10)**, 2235.

Hubert-Ferrari, A., van der Woerd, J., King, G., Villa, I., and Armijo, R. (2007). New constraints on the Karliova triple junction between Arabia, Eurasia and Anatolia. *Geophysical Research Abstracts*, **9**, 06822.

Hubert-Ferrari, A., King, G., Woerd, J., Villa, I., Altunel, E., and Armijo, R. (2009). Long-term evolution of the North Anatolian Fault: new constraints from its eastern termination. *Geological Society, London, Special Publications*, **311**(1), 133.

Huchon, P., Lyberis, N., Angelier, L., Pichon, X. L., and Renard, V. (1982). Tectonics of the Hellenic trench, a synthesis of Sea-Beam and submersible observations. *Tectonophysics*, **86**, 287–300.

Huguen, C., Mascle, J., Chaumillon, E., Woodside, J. M., Benkhelil, J., Kopf, A., and Volkonskaia, A. (2001). Deformational styles of the eastern Mediterranean Ridge and surroundings from combined swath mapping and seismic reflection profiling. *Tectonophysics*, **343**, 21–47.

Huguen, C., Chamot-Rooke, N., Loubrieu, B., and Mascle, J. (2006). Morphology of a pre-collisional, salt-bearing, accretionary complex: the Mediterranean Ridge (Eastern Mediterranean). *Marine Geophysical Research*, **27**(1), 61–75.

Isacks, B. and Molnar, P. (1971). Distribution of stresses in the descending lithosphere from a global survey of focal-mechanism solutions of mantle earthquakes. *Rev. Geophys.*, **9**, 103–174.

Isacks, B., Oliver, J., and Sykes, L. R. (1968). Seismology and the new global tectonics. *J. Geophys. Res.*, **73**, 5855–5899.

Isacks, B., Sykes, L., and Oliver, J. (1969). Focal Mechanisms of Deep and Shallow Earthquakes in the Tonga-Kermadec Region and the Tectonics of Island Arcs. *Geol. Soc. Am. Bull.*, **80**, 1443–1470.

Jackson, J. and McKenzie, D. (1988). The relationship between plate motions and seismic moment tensors, and the rates of active deformation in the Mediterranean and Middle East. *Geophysical Journal*, **93**(1), 45–73.

James, D. E., Fouch, M. J., Carlson, R. W., and Roth, J. B. (2011). Slab fragmentation, edge flow and the origin of the Yellowstone hotspot track. *Earth and Planetary Science Letters*, **311**(1-2), 124–135.

Jimenez-Munt, I. and Sabadini, R. (2002). The block-like behavior of anatolia envisaged in the modeled and geodetic strain rates. *Geophysical Research Letters*, **29**, 39–1.

Jimenez-Munt, I., Sabadini, R., Gardi, A., and Bianco, G. (2003). Active deformation in the Mediterranean from Gibraltar to Anatolia inferred from numerical modeling and geodetic and seismological data. *J. Geophys. Res*, **108**(B1), 2006.

Jolivet, L. and Faccenna, C. (2000). Mediterranean extension and the Africa-Eurasia collision. *Tectonics*, **19**, 1095–1106.

Jolivet, L., Faccenna, C., Goffe, B., Burov, E., and Agard, P. (2003). Subduction tectonics and exhumation of high-pressure metamorphic rocks in the mediterranean orogens. *Am. J. Sci.*, **303**, 353–409.

Jolivet, L., Faccenna, C., Huet, B., Labrousse, L., Le Pourhiet, L., Lacombe, O., Lecomte, E., Burov, E. nd Denèle, Y., Brun, J.-P., Philippon, M., Paul, A., Salaün, G., Karabulut, H., Piromallo, C., Monié, P., Gueydan, F., Okay, A., Oberhänsli, R., Pourteau, A., Augier, R., Gadenne, L., and Driussi, O. (2013). 2013. Aegean tectonics: Strain localisation, slab tearing and trench retreat. *Tectonophysics*, **597**, 1–33.

Jongsma, D. (1977). Bathymetry and shallow structure of the Pliny and Strabo trench, south of the Hellenic arc. *Geological Society of America Bulletin*, **88**, 797 – 805.

Jordan, G., Meijninger, B., Van Hinsbergen, D., Meulenkamp, J., and Van Dijk, P. (2005). Extraction of morphotectonic features from DEMs: Development and applications for study areas in Hungary and NW Greece. *Int. J. Appl. Earth Obs.*, **7**, 163–182.

Jouanne, F., Mugnier, J.L. nd Koci, R., Bushati, S., Matev, K., Kuka, N., Shinko, I., Kociu, S., and Duni, L. (2012). GPS constraints on current tectonics of Albania. *Tectonophysics*, **554**, 50–62.

Karabacak, V., Altunel, E., Meghraoui, M., and Akyüz, H. (2010). Field evidences from northern Dead Sea Fault Zone (South Turkey): New findings for the initiation age and slip rate. *Tectonophysics*, **480**, 172–182.

Karabulut, H., Paul, A., Özbakır, A., Ergün, T., and Şentürk, S. (2019). A new crustal model of the Anatolia-Aegean domain: evidence for the dominant role of isostasy in the support of the Anatolian plateau. *Geophys J. Int.*, **218**, 57–73.

Kassaras, I., Kapetanidis, V., and Karakonstantis, A. (2016). On the spatial distribution of seismicity and the 3D tectonic stress field in western Greece. *Physics and Chemistry of the Earth, Parts A/B/C*, **95**, 50–72.

Kearey, P., Klepeis, K. A., and Vine, F. J. (2008). *Global Tectonics*. Wiley-Blackwell.

Kennett, B. and Furumura, T. (2010). Tears or thinning? Subduction structures in the Pacific plate beneath the Japanese Islands. *Phys. Earth Planet. In.*, **180**, 52–58.

Kennett, B., Engdahl, E., and Buland, R. (1995). Constraints on seismic velocities in the earth from traveltimes. *Geophys. J. Int.*, **122**, 108–124.

Keskin, M. (2003). Magma generation by slab steepening and breakoff beneath a subduction-accretion complex: An alternative model for collision-related volcanism in Eastern Anatolia, Turkey. *Geophys. Res. Lett*, **30**(24), 8046.

Ketin, I. (1948). Über die tektonisch-mechanischen Folgerungen aus den großen Anatolischen Erdbeben des letzten Dezenniums. *Geologische Rundschau*, **36**(1), 77–83.

Kiratzi, A. and Benetatos, C. (2008). The 6 January 2008 (Mw6.2) Leonidio (southern Greece) intermediate depth earthquake: teleseismic body wave modelling. Technical report, EMSC.

Kiratzi, A. and Dimakis, E. (2013). Focal mechanisms and slip models of moderate size earthquakes in Albania and adjacent countries. *Ital. J. Geosci.*, **132**, 186–193.

Kiratzi, A. and Louvari, E. (2003). Focal mechanisms of shallow earthquakes in the Aegean Sea and the surrounding lands determined by waveform modelling: a new database. *J. Geodyn.*, **36**, 251–274.

Kiratzi, A. and Papazachos, C. (1995). Active crustal deformation from the Azores triple junction to the Middle East. *Tectonophysics*, **243**(1-2), 1–24.

Kiratzi, A. A. (1993). A study on the active crustal deformation of the North and East Anatolian fault zones. *Tectonophysics*, **225**, 191–203.

Kissel, C., Speranza, F., and Milicevic, V. (1995). Paleomagnetism of external southern and central Dinarides and northern Albanides: Implications for the Cenozoic activity of the Scutari-Pec Transverse Zone. *J. Geophys. Res.*, **100**, 14999–15007.

Kondo, H., Ozaksoy, V., and Yildirim, C. (2010). Slip history of the 1944 Bolu-Gerede earthquake rupture along the North Anatolian fault system: Implications for recurrence behavior of multisegment earthquakes. *J. Geophys. Res.*, **115**, B04316.

Kontogianni, V. A., Tsoulos, N., and Stiros, S. C. (2002). Coastal uplift, earthquakes and active faulting of Rhodes Island (Aegean Arc): modeling based on geodetic inversion. *Marine Geology*, **186**, 299 – 317.

Kopf, A. (2002). Significance of mud volcanism. *Rev. Geophys.*, **40**, 1–2–2–52.

Korbar, T. (2009). Orogenic evolution of the External Dinarides in the NE Adriatic region: a model constrained by tectonostratigraphy of Upper Cretaceous to Paleogene carbonates. *Earth-Sci. Rev.*, **96**, 296–312.

Kotzev, V., Nakov, R., Georgiev, T., Burchfiel, B. C., and King, R. W. (2006). Crustal motion and strain accumulation in western Bulgaria. *Tectonophysics*, **413**, 127–145.

Koulakov, I., Kaban, M., Tesauro, M., and Cloetingh, S. (2009). P-and S-velocity anomalies in the upper mantle beneath Europe from tomographic inversion of ISC data. *Geophys. J. Int.*, **179**, 345–366.

Kozacı, O., Dolan, J., Finkel, R., and Hartleb, R. (2007). Late Holocene slip rate for the North Anatolian Fault, Turkey, from cosmogenic 36Cl geochronology: Implications for the constancy of fault loading and strain release rates. *Geology*, **35**, 867–870.

Kozacı, O., Dolan, J., and Finkel, R. (2009). A late Holocene slip rate for the central North Anatolian fault, at Tahtakopru, Turkey, from cosmogenic 10BE geochronology: Implications for fault loading and strain release rates. *J. Geophys. Res.*, **114**, B01405.

Koçyiğit, A., Ünay, E., and Saraç, G. (2000). Episodic graben formation and extensional neotectonic regime in west Central Anatolia and the Isparta Angle: a case study in the Akşehir-Afyon Graben, Turkey. In E. Bozkurt, J. Winchester, and J. Piper, editors, *Tectonics and Magmatism in Turkey and the Surrounding Area*, volume 173, pages 405–421. Geological Society, London, Special Publications.

Kreemer, C., Holt, W., and Haines, A. (2003). An integrated global model of present-day plate motions and plate boundary deformation. *Geophys. J. Int.*, **154**, 8–34.

Kuran, U. (1980). The location magnitude and long-term time prediction of damaging earthquake along Anatolian faults and Levant coast. *Bulletin of the Geophysical Congress of Turkey*, pages 151–163.

Lallemand, S., Liu, C., and Font, Y. (1997). A tear fault boundary between the Taiwan orogen and the Ryukyu subduction zone. *Tectonophysics*, **274**, 171–190.

Langstaff, M. A. and Meade, B. J. (2013). Edge-driven mechanical microplate models of strike-slip faulting in the Tibetan Plateau. *Journal of Geophysical Research: Solid Earth*, **118**(7), 3809–3819.

Laske, G., Masters, G., Ma, Z., and Pasyanos, M. (2013). Update on CRUST1. 0—A 1-degree global model of Earth's crust. *Geophys. Res. Abstr*, **Vol. 15**, 2658. EGU General Assembly Vienna, Austria.

Lay, T. and Wallace, T. C. (1995). *Modern global seismology*. Academic Press.

Le Breton, E., Handy, M., Molli, G., and Ustaszewski, K. (2017). Post-20 Ma motion of the Adriatic plate – new constraints from surrounding orogens and implications for crust-mantle decoupling. *Tectonics*, **36**, 3135–3154.

Le Pichon, X. (1982). *Land-locked oceanic basins and continental collision: the Eastern Mediterranean as a case example*. Academic Press.

Le Pichon, X. and Angelier, J. (1979). The Hellenic arc and the trench system: A key to the neotectonic evolution of the Eastern Mediterranean area. *Tectonophysics*, **60**, 1–42.

Le Pichon, X. and Angelier, J. (1981). The Aegean Sea [and Discussions]. *Phil. Trans. R. Soc. Lond. A*, **300**(1454), 357–372. Extensional Tectonics Associated with Convergent Plate Boundaries.

Le Pichon, X., Angelier, J., Aubouin, J., Lyberis, N., Monti, S., Renard, V., Got, H., *et al.* (1979). From subduction to transform motion: a seabeam survey of the Hellenic trench system. *Earth and Planetary Science Letters*, **44**(3), 441–450.

Le Pichon, X., Chamot-Rooke, N., Lallemant, S., Noomen, R., and Veis, G. (1995). Geodetic determination of the kinematics of central Greece with respect to Europe, implications for eastern Mediterranean. *J. Geophys. Res.*, **100**, 12675 – 12690.

Le Pichon, X., Şengör, A., Demirbağ, E., Rangin, C., Imren, C., Armijo, R., Görür, N., Çağatay, N., De Lepinay, B. M., Meyer, B., *et al.* (2001). The active main marmara fault. *Earth and Planetary Science Letters*, **192**(4), 595–616.

Leite, O. and Mascle, J. (1982). Geological structures on the south Cretan continental margin and Hellenic Trench (eastern Mediterranean). *Marine Geology*, **49**, 199–223.

Lentas, K., Di Giacomo, D., Harris, J., and Storchak, D. A. (2019). The ISC Bulletin as a comprehensive source of earthquake source mechanisms. *Earth Syst. Sci. Data*, **11**, 565–578.

Levin, V., Shapiro, N., Park, J., and Ritzwoller, M. (2002). Seismic evidence for catastrophic slab loss beneath Kamchatka. *Nature*, **418**(6899), 763.

Lin, J., Hsu, S., Sibuet, J., Lee, C., and Liang, C. (2013). Plate tearing in the northwestern corner of the subducting Philippine Sea Plate. *J. Asian Earth Sci.*, **70**, 1–7.

Lin, J.-Y., Sibuet, J.-C., Lee, C.-S., Hsu, S.-K., and Klingelhoefer, F. (2007). Origin of the southern Okinawa Trough volcanism from detailed seismic tomography. *J. Geophys. Res.*, **112**, B08308.

Louvari, E., Kiratzi, A., and Papazachos, B. (1999). The Cephalonia transform fault and its extension to western Lefkada island (Greece). *Tectonophysics*, **308**(1-2), 223–236.

Loveless, J. P. and Meade, B. J. (2011). Partitioning of localized and diffuse deformation in the Tibetan Plateau from joint inversions of geologic and geodetic observations. *Earth and Planetary Science Letters*, **303**(1-2), 11–24.

Lundgren, P., Giardini, D., and Russo, R. M. (1998). Geodynamic framework for eastern Mediterranean kinematics. *Geophys. Res. Lett.*, **25**(21), 4007–4010.

Lyberis, N. (1984). *Tectonic evolution of the North Aegean trough*, volume 17. Geological Society London.

Lynner, C., Anderson, M., Portner, D., Beck, S., and Gilbert, H. (2017). Mantle flow through a tear in the Nazca slab inferred from shear wave splitting. *Geophys. Res. Lett.*, **44**, 6735–6742.

Mardia, K. V. (1972). *Statistics of directional data*. Academic press.

Mascle, J., Quellec, P. L., Leite, O., and Jongsma, D. (1982). Structural sketch of the Hellenic continental margin between the western Peloponnesus and eastern Crete. *Geology*, **10**, 113–116.

Mascle, J., Cleac'h, A., and Jongsma, D. (1986). The eastern Hellenic margin from Crete to Rhodes: example of progressive collision. *Marine geology*, **73**(1-2), 145–168.

Mascle, J., Benkhelil, J., Bellaiche, G., Zitter, T., Woodside, J., Loncke, L., and Party, P. I. S. (2000). Marine geologic evidence for a Levantine-Sinai plate, a new piece of the Mediterranean puzzle. *Geology*, **28**, 779–782.

Masson, F., Djamour, Y., Gorp, S. V., Chéry, J., Tatar, M., Tavakoli, F., Nankali, H., and Vernant, P. (2006). Extension in NW Iran driven by the motion of the South Caspian Basin. *Earth Planet. Sci. Lett.*, **252**, 180–188.

McClusky, S., Balassanian, S., Barka, A., Demir, C., Ergintav, S., Georgiev, I., Gurkan, O., Hamburger, M., Hurst, K., Kahle, H., Kastens, K., Kekelidze, G., King, R., Kotzev, V., Lenk, O., Mahmoud, S., Mistin, A., Nadariya, M., Ouzounis, A., Paradissis, D., Peter, Y., Prilepin, M., Reilinger, R., Sanli, I., Seeger, H., Tealeb, A., Toksoz, M., and Veis, G. (2000). Global Positioning System constraints on plate kinematics and dynamics in the eastern Mediterranean and Caucasus. *J. Geophys. Res.*, **105**(B3), 5695–5719.

McKenzie, D. (1970). Plate tectonics of the Mediterranean region. *Nature*, **226**(5242), 239.

McKenzie, D. (1972). Active tectonics of the Mediterranean Region. *Geophys. J. R. Astr. Soc.*, **30**, 109–185.

McKenzie, D. (1976). The east anatolian fault: A major structure in eastern turkey. *Earth Planet. Sci. Lett.*, **29**, 189–193.

McNeill, L. and Collier, R. (2004). Uplift and slip rates of the eastern Eliki fault segment, Gulf of Corinth, Greece, inferred from Holocene and Pleistocene terraces. *J Geol Soc, London*, **161**, 81–92.

Meade, B., Hager, B., McClusky, S., Reilinger, R., Ergintav, S., Lenk, O., Barka, A., and Ozener, H. (2002). Estimates of seismic potential in the Marmara Sea region from block models of secular deformation constrained by Global Positioning System measurements. *Bulletin of the Seismological Society of America*, **92**(1), 208.

Meghraoui, M., Aksoy, M. E., Akyüz, H. S., Ferry, M., Dikbaş, A., and Altunel, E. (2012). Paleoseismology of the North Anatolian fault at Güzelköy (Ganos segment, Turkey): Size and recurrence time of earthquake ruptures west of the Sea of Marmara. *Geochemistry, Geophysics, Geosystems*, **13**(4).

Meijer, P. T. and Wortel, M. J. R. (1996). Temporal variation in the stress field of the Aegean region. *Geophysical Research Letters*, **23**(5), 439–442.

Meijer, P. T. and Wortel, M. J. R. (1997). Present-day dynamics of the Aegean region: A model analysis of the horizontal pattern of stress and deformation. *Tectonics*, **16**(6), 879–895.

Meijers, M. J. M., Van Hinsbergen, D. J. J., Dekkers, M. J., Altiner, D., Kaymakci, N., and Langereis, C. G. (2011). Pervasive Palaeogene remagnetization of the central Taurides fold-and-thrust belt (southern Turkey) and implications for rotations in the Isparta Angle. *Geophysical Journal International*.

Melosh, H. and Raefsky, A. (1981). A simple and efficient method for introducing faults into finite element computations. *Bulletin of the Seismological Society of America*, **71**(5), 1391.

Melosh, H. J. and Williams, C. A. (1989). Mechanics of graben formation in crustal rocks: a finite element analysis. *J. Geophys. Res.*, **94**, 13961–13973.

Metois, M., D' Agostino, N., Avallone, A., Chamot-Rooke, N., Rabaute, A., Duni, L., Kuka, N., Koci, R., and Georgiev, I. (2015). Insights on continental collisional processes from GPS data: Dynamics of the peri-Adriatic belts. *J. Geophys. Res.*, **120**, 8701–8719.

Millen, D. and Hamburger, M. (1998). Seismological evidence for tearing of the Pacific plate at the northern termination of the Tonga subduction zone. *Geology*, **26**(7), 659–662.

Miller, M. and Piana Agostinetti, N. (2011). Erosion of the continental lithosphere at the cusps of the Calabrian arc: Evidence from S receiver functions analysis. *Geophys. Res. Lett.*, **38**.

Miller, M., Kennett, B., and Lister, G. (2004). Imaging changes in morphology, geometry, and physical properties of the subducting Pacific plate along the Izu–Bonin–Mariana arc. *Earth Planet. Sci. Lett.*, **224**, 363–370.

Miller, M., Gorbatov, A., and Kennett, B. (2005). Heterogeneity within the subducting Pacific slab beneath the Izu–Bonin–Mariana arc: Evidence from tomography using 3D ray tracing inversion techniques. *Earth and Planetary Science Letters*, **235**(1-2), 331–342.

Miller, M., Kennett, B., and Toy, V. (2006a). Spatial and temporal evolution of the subducting Pacific plate structure along the western Pacific margin. *Journal of Geophysical Research: Solid Earth*, **111**(B2).

Miller, M., Gorbatov, A., and Kennett, B. (2006b). Three-dimensional visualization of a near-vertical slab tear beneath the southern Mariana arc. *Geochem. Geophys. Geosyst.*, **7**.

Molnar, P. (1988). Continental tectonics in the aftermath of plate tectonics. *Nature*, **335**, 131–137.

Monopolis, D. and Bruneton, A. (1982). Ionian Sea (Western Greece): its structural outline deduced from drilling and geophysical data. *Tectonophysics*, **83**, 227–242.

Moretti, I., Sakellariou, D., Lykousis, V., and Micarelli, L. (2003). The Gulf of Corinth: an active half graben? *Journal of Geodynamics*, **36**(1-2), 323–340.

Muller, R., Sdrolias, M., Gaina, C., and Roest, W. (2008). Age, spreading rates, and spreading asymmetry of the world's ocean crust. *Geochemistry Geophysics Geosystems-G3*, **9**.

Naylor, M., Mandl, G., and Supesteijn, C. (1986). Fault geometries in basement-induced wrench faulting under different initial stress states. *Journal of Structural Geology*, **8**, 737–752.

Neely, J. S. and Furlong, K. P. (2018). Evidence of displacement-driven maturation along the San Cristobal Trough transform plate boundary. *Earth and Planetary Science Letters*, **485**, 88–98.

Nicolosi, I., Speranza, F., and Chiappini, M. (2006). Ultrafast oceanic spreading of the Marsili Basin, southern Tyrrhenian Sea: Evidence from magnetic anomaly analysis. *Geology*, **34**, 717–720.

Nixon, C. W., McNeill, L., Bull, J., Bell, R., Gawthorpe, R., Henstock, T., Christodoulou, D., Ford, M., Taylor, B., Sakellariou, D., G., F., G., P., M.R., L., Collier, R., Goodliffe, A., Sachpazi, M., and Kranis, H. (2016). Rapid spatiotemporal variations in rift structure during development of the Corinth Rift, central Greece. *Tectonics*, **35**, 1225–1248.

Nocquet, J. (2012). Present-day kinematics of the Mediterranean: A comprehensive overview of GPS results. *Tectonophysics*, **579**, 220–242.

Nur, A. and Helsley, C. (1971). Paleomagnetism of Tertiary and recent lavas of Israel. *Earth and Planetary Science Letters*, **10**(3), 375–379.

Nyst, M. and Thatcher, W. (2004). New constraints on the active tectonic deformation of the Aegean. *J. Geophys. Res*, **109**, B11406.

Obayashi, M., Yoshimitsu, J., and Fukao, Y. (2009). Tearing of stagnant slab. *Science*, **324**, 1173–1175.

Ocakoğlu, N. (2012). Investigation of Fethiye-Marmaris Bay (SW Anatolia): seismic and morphologic evidences from the missing link between the Pliny Trench and the Fethiye-Burdur Fault Zone. *Geo-Marine Letters*, **32**, 17–28.

Oldroyd, D. R. (1996). *Thinking about the Earth: A history of ideas in geology*. Harvard University Press.

Olive, J.-A., Pearce, F., Rondenay, S., and Behn, M. D. (2014). Pronounced zonation of seismic anisotropy in the Western Hellenic subduction zone and its geodynamic significance. *Earth and Planetary Science Letters*, **391**, 100–109.

Özbakır, A. D., Şengör, A., Wortel, M., and Govers, R. (2013). The Pliny–Strabo trench region: A large shear zone resulting from slab tearing. *Earth and Planetary Science Letters*, **375**, 188–195.

Özbakır, A. D., Govers, R., and Wortel, R. (2017). Active faults in the Anatolian-Aegean plate boundary region with Nubia. *Turkish Journal of Earth Sciences*, **26**(1), 30–56.

Özeren, M. and Holt, W. (2010). The dynamics of the eastern Mediterranean and eastern Turkey. *Geophysical Journal International*, **183**(3), 1165–1184.

Özeren, M. S. (2012). Crust-mantle mechanical coupling in Eastern Mediterranean and Eastern Turkey. *Proceedings of the National Academy of Sciences*, **109**(22), 8429–8433.

Papanikolaou, D., Fountoulis, I., and Metaxas, C. (2007). Active faults, deformation rates and Quaternary paleogeography at Kyparissiakos Gulf (SW Greece) deduced from onshore and offshore data. *Quat. Int.*, **171**, 14–30.

Papanikolaou, D. J. and Royden, L. H. (2007). Disruption of the Hellenic arc: Late Miocene extensional detachment faults and steep Pliocene-Quaternary normal faults—Or what happened at Corinth? *Tectonics*, **26**(5).

Papazachos, B., Karakostas, V., Papazachos, C., and Scordilis, E. (2000). The geometry of Wadati-Benioff zone and lithospheric kinematics of the Hellenic arc. *Tectonophysics*, **319**, 275 – 300.

Papazachos, C. and Nolet, G. (1997). P and S deep velocity structure of the Hellenic area obtained by robust nonlinear inversion of travel times. *Journal of Geophysical Research: Solid Earth*, **102**(B4), 8349–8367.

Parlak, O. (2004). *Çelikhan - Erkenek arasinda Doğu Anadolu fayının özellikleri*. Master's thesis, Istanbul Teknik Universitesi, Avrasya Yer Bilimleri Enstitusu, ITU Ayazaga.

Pe-Piper, G. and Piper, D. J. W. (2007). Neogene backarc volcanism of the Aegean: New insights into the relationship between magmatism and tectonics. *Geological Society of America Special Papers*, **418**, 17–31.

Pearce, F., Rondenay, S., Sachpazi, M., Charalampakis, M., and Royden, L. (2012). Seismic investigation of the transition from continental to oceanic subduction along the western Hellenic Subduction Zone. *Journal of Geophysical Research: Solid Earth*, **117**(B7).

Perouse, E., Chamot-Rooke, N., Rabaute, A., Briole, P., Jouanne, F., Georgiev, I., and Dimitrov, D. (2012). Bridging onshore and offshore present-day kinematics of central and eastern Mediterranean: implications for crustal dynamics and mantle flow. *Geochemistry, Geophysics, Geosystems*, **13**(9).

Pesicek, J., Engdahl, E., Thurber, C., DeShon, H., and Lange, D. (2012). Mantle subducting slab structure in the region of the 2010 M 8.8 Maule earthquake (30–40 S), Chile. *Geophys. J. Int.*, **191**, 317–324.

Peterek, A. and Schwarze, J. (2004). Architecture and Late Pliocene to recent evolution of outer-arc basins of the Hellenic subduction zone (south-central Crete, Greece). *Journal of Geodynamics*, **38**(1), 19–55.

Peters, J. and Huson, W. (1985). The Pliny and Strabo trenches (eastern Mediterranean): integration of seismic reflection data and seabeam bathymetric maps. *Marine Geology*, **64**(1-2), 1–17.

Piper, J. D. A., Gursoy, H., Tatar, O., Beck, M. E., Raoa, A., Kocbulut, F., and Mesci, B. L. (2010). Distributed neotectonic deformation in the Anatolides of Turkey: A palaeomagnetic analysis. *Tectonophysics*, **488**, 31–50.

Piromallo, C. and Morelli, A. (2003). P wave tomography of the mantle under the Alpine-Mediterranean area. *J. Geophys. Res*, **108**(B2), 2065.

Plattner, C., Malservisi, R., and Govers, R. (2009). On the plate boundary forces that drive and resist Baja California motion. *Geology*, **37**, 359–362.

Polonia, A., Gasperini, L., Amorosi, A., Bonatti, E., Bortoluzzi, G., Cagatay, N., Capotondi, L., Cormier, M. H., Gorur, N., McHugh, C., and Seeber, L. (2004). Holocene slip rate of the North Anatolian fault beneath the Sea of Marmara. *Earth Planet. Sci. Lett.*, **227**, 411–426.

Pondrelli, S., Salimbeni, S., Ekström, G., Morelli, A., Gasperini, P., and Vannucci, G. (2006). The Italian CMT dataset from 1977 to the present. *Phys. Earth Planet. Int.*, **159**, 286–303.

Pondrelli, S., Salimbeni, S., Morelli, A., Ekström, G., and Boschi, E. (2007). European-Mediterranean Regional Centroid Moment Tensor catalog: Solutions for years 2003 and 2004. *Phys. Earth Planet. Int.*, **164**, 90–112.

Pondrelli, S., Salimbeni, S., Morelli, A., Ekstrom, G., Postpischl, L., Vannucci, G., and Boschi, E. (2011). European-Mediterranean Regional Centroid Moment Tensor Catalog: solutions for 2005-2008. *Physics of the Earth and Planetary Interiors*.

Portner, D., Beck, S., Zandt, G., and Scire, A. (2017). The nature of subslab slow velocity anomalies beneath South America. *Geophys. Res. Lett.*, **44**, 4747–4755.

Portner, D., Delph, J., Biryol, C., Beck, S., Zandt, G., Özacar, A., Sandvol, E., and Türkelli, N. (2018). Subduction termination through progressive slab deformation across Eastern Mediterranean subduction zones from updated P-wave tomography beneath Anatolia. *Geosphere*, **14**, 907–925.

Price, S. P. and Scott, B. (1994). Fault-block rotations at the edge of a zone of continental extension; southwest Turkey. *Journal of Structural Geology*, **16**(3), 381–392.

Provost, A.-S., Chery, J., and Hassani, R. (2003). 3D mechanical modeling of the GPS velocity field along the North Anatolian fault. *Earth Planet. Sci. Lett.*, **209**, 361–377.

Pucci, S., Martini, P. M. D., and Pantosti, D. (2008). Preliminary slip rate estimates for the Duzce segment of the North Anatolian Fault zone from offset geomorphic markers. *Geomorphology*, **97**, 538–554.

Ramsay, J. and Huber, M. (1983). *The techniques of modern structural geology, vol. 1*. Academic Press.

Ranalli, G. (1987). *Rheology of the Earth*. Allen & Unwin, 1st edition.

Reilinger, R., McClusky, S., Vernant, P., Lawrence, S., Ergintav, S., Cakmak, R., Ozener, H., Kadirov, F., Guliev, I., Stepanyan, R., Nadariya, M., Hahubia, G., Mahmoud, S., Sakr, K., ArRajehi, A., Paradissis, D., Al-Aydrus, A., Prilepin, M., Guseva, T., Evren, E., Dmitrotsa, A., Filikov, S., Gomez, F., Al-Ghazzi, R., and Karam, G. (2006). GPS constraints on continental deformation in the Africa-Arabia-Eurasia continental collision zone and implications for the dynamics of plate interactions. *J. Geophys. Res*, **111**, B05411.

Reilinger, R., McClusky, S., Paradissis, D., Ergintav, S., and Vernant, P. (2010). Geodetic constrains on the tectonic evolution of the Aegean region and strain accumulation along Hellenic subduction zone. *Tectonophysics*, **488**, 22–30.

Robertson, A. (1998). Tectonic significance of the Eratosthenes Seamount: a continental fragment in the process of collision with a subduction zone in the Eastern Mediterranean (Ocean Drilling Program Leg 160). *Tectonophysics*, **298**, 63–82.

Rosenbaum, G., Gasparon, M., Lucente, F. P., Peccerillo, A., and Miller, M. S. (2008). Kinematics of slab tear faults during subduction segmentation and implications for italian magmatism (doi 10.1029/2007tc002143). *Tectonics*, **27**, TC2008.

Royden, L. (1993). Evolution of retreating subduction boundaries formed during continental collision. *Tectonics*, **12**(3), 629–638.

Royden, L. and Papanikolaou, D. (2011). Slab segmentation and Late Cenozoic disruption of the Hellenic arc. *Geochemistry Geophysics Geosystems*, **12**(3), Q03010.

Russo, R. (2012). Source-side shear-wave splitting and upper-mantle flow beneath the Arakan slab, India-Asia-Sundalind triple junction. *Geosphere*, **8**, 158–178.

Russo, R., Speed, R., Okal, E., Shepherd, J., and Rowley, K. (1993). Seismicity and tectonics of the southeastern Caribbean. *Journal of Geophysical Research: Solid Earth*, **98**(B8), 14299–14319.

Sachpazi, M., Laigle, M., Charalampakis, M., Diaz, J., Kissling, E., Gesret, A., Becel, A., Flueh, E., Miles, P., and Hirn, A. (2016). Segmented Hellenic slab rollback driving Aegean deformation and seismicity. *Geophysical Research Letters*, **43**(2), 651–658.

Salaün, G., Pedersen, H. A., Paul, A., Farra, V., Karabulut, H., Hatzfeld, D., Papazachos, C., Childs, D. M., Pequegnat, C., and Team, S. (2012). High-resolution surface wave tomography beneath the Aegean-Anatolia region: constraints on upper-mantle structure. *Geophysical Journal International*, **190**(1), 406–420.

Şaroğlu, F., Emre, Ö., and Boray, A. (1987). Turkiye'nin diri faylari ve depremsellikleri. Unpublished 8174, MTA, Ankara.

Şaroğlu, F., Emre, Ö., and Kuşçu, I. (1992). The East Anatolian fault zone of Turkey. *Annales Tectonicae*, **Special Issue-Supplement to Volume VI**, 99–125.

Schefer, S., Cvetković, V., Fügenschuh, B., Kounov, A., Ovtcharova, M., Schaltegger, U., and Schmid, S. (2011). sCenozoic granitoids in the Dinarides of southern Serbia: age of intrusion, isotope geochemistry, exhumation history and significance for the geodynamic evolution of the Balkan Peninsula. *International Journal of Earth Sciences*, **100**, 1181–1206.

Schellart, W. P., Freeman, J., Stegman, D. R., Moresi, L., and May, D. (2007). Evolution and diversity of subduction zones controlled by slab width. *Nature*, **446**, 308–311.

Schindler, C. (1997). Geology of northwestern turkey: results of the marmara poly-project. *Active Tectonics of Northwestern Anatolia-The MARMARA Poly-Project*, pages 329–374.

Şengör, A. M. C. (1987). Cross-faults and differential stretching of hanging walls in regions of low-angle normal faulting: examples from western turkey. *Geological Society of London, Special Publications*, **28**(1), 575–589.

Şengör, A. M. C. (1983). *Levha tektoniği*. İTÜ Maden Fakültesi.

Şengör, A. M. C. (1990). Plate tectonics and the orogenic research after 25 years: synopsis of a tethyan perspective. *Earth Sci. Rev.*, **27**, 1–201.

Şengör, A. M. C. and Yılmaz, Y. (1981). Tethyan evolution of turkey: a plate tectonic approach. *Tectonophysics*, **75**, 181–241.

Şengör, A. M. C., Tüysüz, O., Imren, C., Sakınç, M., Eyidoğan, H., Görür, N., Le Pichon, X., and Rangin, C. (2005). The North Anatolian Fault: A new look. *Annu. Rev. Earth Planet. Sci.*, **33**, 37–112.

Şengör, A. M. C., Özeren, M. S., Keskin, M., Sakınç, M., Özbakır, A. D., and Kayan, I. (2008). Eastern Turkish high plateau as a small Turkic-type orogen: Implications for post-collisional crust-forming processes in Turkic-type orogens. *Earth Sci. Rev.*, **90**, 1–48.

Severinghaus, J. and Atwater, T. (1990). sCenozoic geometry and thermal state of the subducting slabs beneath western North America. Basin and range extensional tectonics near the latitude of Las Vegas, Nevada. *Geological Society of America Memoir*, **176**, 1–22.

Seymen, I. and Aydin, A. (1972). Bingol deprem fayi ve bunun kuzey anadolu fayi ile iliskisi. *MTA Dergisi*, **79**, 1 – 8.

Seyrek, A., Demir, T., Pringle, M. S., Yurtmen, S., Westaway, R. W. C., Beck, A., and Rowbotham, G. (2007). *Kinematics of the Amanos Fault, southern Turkey, from Ar/Ar dating of offset Pleistocene basalt flows: transpression between the African and Arabian plates*, volume Tectonics of Strike-Slip Restraining and Releasing Bends. Geological Society London Special Papers.

Shaw, B. and Jackson, J. (2010). Earthquake mechanisms and active tectonics of the Hellenic subduction zone. *Geophys. J. Int.*, **181**, 966–984.

Sigloch, K., McQuarrie, N., and Nolet, G. (2008). Two-stage subduction history under North America inferred from multiple-frequency tomography. *Nature Geoscience*, **1**(7), 458.

Sodoudi, F., Kind, R., Hatzfeld, D., Priestley, K., Hanka, W., Wylegalla, K., Stavrakakis, G., Vafidis, A., Harjes, H., Bohnhoff, M., *et al.* (2006). Lithospheric structure of the Aegean obtained from P and S receiver functions. *J. geophys. Res*, **111**, B12307.

Sodoudi, F., Brüstle, A., Meier, T., Kind, R., Friederich, W., and Group, E. W. (2015). Receiver function images of the Hellenic subduction zone and comparison to microseismicity. *Solid Earth*, **6**, 135–151.

Spakman, W. and Hall, R. (2010). Surface deformation and slab–mantle interaction during Banda arc subduction rollback. *Nature Geoscience*, **3**(8), 562.

Spakman, W., Wortel, M. J. R., and Vlaar, N. J. (1988). The Hellenic subduction zone: A tomographic image and its geodynamic implications. *Geophys. Res. Lett.*, **15**(1), 60–63.

Spakman, W., van der Lee, S., and van der Hilst, R. (1993). Travel-time tomography of the European-Mediterranean mantle down to 1400 km. *Phys. Earth Planet. Inter.*, **79**(1-2), 3–74.

Speranza, F., Minelli, L., Pignatelli, A., and Chiappini, M. (2012). sThe Ionian Sea: The oldest in situ ocean fragment of the world? *J. Geophys. Res.*, **117**.

Stein, C. and Stein, S. (1992). A model for the global variation in oceanic depth and heat flow with lithospheric age. *Nature*, **359**(6391), 123–129.

Stiros, S., Arnold, M., Pirazzoli, P., Laborel, J., Laborel, F., and Papageorgiou (1992). Historical coseismic uplift on Euboea Island, Greece. *Earth Planet. Sci. Lett.*, **108**, 109–117.

Suckale, J., Rondenay, S., Sachpazi, M., Charalampakis, M., Hosa, A., and Royden, L. H. (2009). High-resolution seismic imaging of the western Hellenic subduction zone using teleseismic scattered waves. *Geophys. J. Int.*, **178**, 775–791.

Tapponnier, P., Ryerson, F. J., Van Der Woerd, J., Mériaux, A.-S., and Lasserre, C. (2001). Long-term slip rates and characteristic slip: keys to active fault behaviour and earthquake hazard. *Comptes Rendus de l'Académie des Sciences-Series IIA-Earth and Planetary Science*, **333**(9), 483–494.

Taymaz, T. and Price, S. (1992). The 1971 May 12 Burdur earthquake sequence, SW Turkey: a synthesis of seismological and geological observations. *Geophysical Journal International*, **108**(2), 589–603.

Taymaz, T., Jackson, J. A., and Westaway, R. (1990). Earthquake mechanisms in the Hellenic Trench near Crete. *Geophys. J. Int.*, **102**, 695 – 732.

Taymaz, T., Jackson, J. A., and McKenzie, D. (1991). Active tectonics of the north and central Aegean Sea. *Geophys. J. Int.*, **106**, 433 – 490. Tara!

Tchalenko, J. S. (1970). Similarities between shear zones of different magnitudes. *Bulletin of the Geological Society of America*, **81**, 1625–1639.

Ten Veen, J. and Kleinspehn, K. (2003). Incipient continental collision and plate-boundary curvature: Late Pliocene - Holocene transtensional Hellenic forearc, Crete, Greece. *Journal of the Geological Society*, **160**, 161–181.

Ten Veen, J. H., Woodside, J., Zitter, T., Dumont, J., Mascle, J., and Volkonskaia, A. (2004). Neotectonic evolution of the Anaximander Mountains at the junction of the Hellenic and Cyprus arcs. *Tectonophysics*, **391**, 35–65.

Tesauro, M., Kaban, M. K., and Cloetingh, S. A. P. L. (2009). A new thermal and rheological model of the European lithosphere. *Tectonophysics*, **476**, 478–495.

Thatcher, W. (2009). How the continents deform: the evidence from tectonic geodesy. *Annu. Rev. Earth Planet. Sci.*, **37**, 237–262.

Tiryakioğlu, İ., Floyd, M., Erdoğan, S., Gülal, E., Ergintav, S., McClusky, S., and Reilinger, R. (2013). GPS constraints on active deformation in the Isparta Angle region of SW Turkey. *Geophysical Journal International*, **195**(3), 1455–1463.

Turan, M. (1993). Some important tectonic structures in the surroundings of Elazığ and their meaning in the geological evolution in the region. In *Proceedings of Suat Erk Symposium, Ankara University, Ankara-Turkey*, pages 193–204.

Underhill, J. (1989). Late Cenozoic deformation of the Hellenide foreland, western Greece. *Geological Society of America Bulletin*, **101**, 613–634.

Ustaszewski, K., Schmid, S., Fügenschuh, B., Tischler, M., Kissling, E., and Spakman, W. (2008). A map-view restoration of the Alpine-Carpathian-Dinaridic system for the Early Miocene. *Swiss Journal of Geosciences*, **101**, 273–294.

Van Benthem, S. and Govers, R. (2010). The Caribbean plate: Pulled, pushed, or dragged? *J. Geophys. Res*, **115**.

Van Benthem, S., Govers, R., Spakman, W., and Wortel, R. (2013). Tectonic evolution and mantle structure of the Caribbean. *Journal of Geophysical Research: Solid Earth*, **118**(6), 3019–3036.

Van der Meer, D., Van Hinsbergen, D., and Spakman, W. (2018). Atlas of the underworld: Slab remnants in the mantle, their sinking history, and a new outlook on lower mantle viscosity. *Tectonophysics, 723, 309-448.*

Van Dongen, P., Van der Voo, R., and Raven, T. (1967). Paleomagnetism and the Alpine tectonics of Eurasia III:: Paleomagnetic research in the Central Lebanon Mountains and in the Tartous area (Syria). *Tectonophysics*, **4**(1), 35–53.

Van Hinsbergen, D. J. and Schmid, S. M. (2012). Map view restoration of Aegean–West Anatolian accretion and extension since the Eocene. *Tectonics*, **31**(5).

Van Hinsbergen, D. J. J., Langereis, C. G., and Meulenkamp, J. E. (2005). Revision of the timing, magnitude and distribution of Neogene rotations in the western Aegean region. *Tectonophysics*, **396**, 1–34.

Van Hinsbergen, D. J. J., Van der Meer, D. G., Zachariasse, W. J., and Meulenkamp, J. E. (2006). Deformation of western Greece during Neogene clockwise rotation and collision with Apulia. *Int J Earth Sci*, **95**, 463–490.

Van Unen, M., Matenco, L., Nader, F., Dernault, R., Mandic, O., and Demir, V. (2019). Kinematics of Foreland-Vergent Crustal Accretion: Inferences From the Dinarides Evolution. *Tectonics*, **38**, 49–76.

Vassilakis, E., Royden, L., and Papanikolaou, D. (2011). Kinematic links between subduction along the Hellenic trench and extension in the Gulf of Corinth, Greece: A multidisciplinary analysis. *Earth Planet. Sci. Lett.*, **303**, 108–120.

Vernant, P., Reilinger, R., and McClusky, S. (2014). Geodetic evidence for low coupling on the Hellenic subduction plate interface. *Earth Planet Sc Lett*, **385**, 122–129.

Vidal, N., Alvarez-Marron, J., and Klaeschen, D. (2000). The structure of the Africa-Anatolia plate boundary in the Eastern Mediterranean. *Tectonics*, **19**, 723–739.

Warners-Ruckstuhl, K. N., Govers, R., and Wortel, M. J. R. (2012). Lithosphere-mantle coupling and the dynamics of the Eurasian plate. *Geophys. J. Int.*, **189**, 1253–1276.

Warners-Ruckstuhl, K. N., Govers, R., and Wortel, R. (2013). Tethyan collision forces and the stress field of the Eurasian Plate. *Geophysical Journal International*, **195**(1), 1–15.

Watts, A. and Zhong, S. (2000). Observations of flexure and the rheology of oceanic lithosphere. *Geophysical Journal International*, **142**(3), 855–875.

Wdowinski, S., Ben-Avraham, Z., Arvidsson, R., and Ekstrom, G. (2006). Seismotectonics of the Cyprian Arc. *Geophysical Journal International*, **164**, 176–181.

Wessel, P. and Smith, W. H. F. (1998). New, improved version of Generic Mapping Tools released. *EOS Trans. Amer. Geophys. U.*, **79**, 579.

Westaway, R. (1994). Present-day kinematics of the Middle East and eastern Mediterranean. *J. Geophys. Res.*, **99**, 12071–12090.

Westaway, R. and Arger, J. (1996). The Gölbaşı basin, southeastern Turkey: a complex discontinuity in a major strike - slip fault zone. *Journal of the Geological Society*, **153**(5), 729.

Weston, J., Engdahl, E., Harris, J., Di Giacomo, D., and Storchak, D. (2018). ISC-EHB: reconstruction of a robust earthquake data set. *Geophys. J. Int.*, **214**, 474–484.

Widiyantoro, S., Pesicek, J., and Thurber, C. (2011). Subducting slab structure below the eastern Sunda arc inferred from non-linear seismic tomographic imaging. *Geological Society, London, Special Publications*, **355**(1), 139–155.

Wilson, J. T. (1965). A new class of faults and their bearing on continental drift. *Nature*, **207**(4995), 343.

Woodside, J., Mascle, J., Huguen, C., and Volkonskaia, A. (2000). The Rhodes Basin, a post-Miocene tectonic trough. *Mar. Geol.*, **165**, 1–12.

Woodside, J., Mascle, J., Zitter, T., Limonov, A., Ergun, M., and Volkonskaia, A. (2002). Shipboard scientists of PRISMED II expedition, 2002. The Florence Rise, the western bend of the Cyprus arc. *Mar. Geol.*, **185**, 177–194.

Wortel, M. J. R. and Spakman, W. (1992). Structure and dynamics of subducted lithosphere in the Mediterranean region. *Proceedings of the Koninklijke Nederlandse Akademie van Wetenschappen*, pages 325–347.

Wortel, M. J. R. and Spakman, W. (2000). Subduction and Slab Detachment in the Mediterranean-Carpathian Region. *Science*, **290**, 1910–1917.

Wortel, R., Govers, R., and Spakman, W. (2009). Continental collision and the STEP-wise evolution of convergent plate boundaries: from structure to dynamics. *Subduction Zone Geodynamics*, pages 47–59.

Wright, T. J., Parsons, B., England, P. C., and Fielding, E. J. (2004). InSAR observations of low slip rates on the major faults of western Tibet. *Science*, **305**(5681), 236–239.

Yaltırak, C. (2002). Tectonic evolution of the Marmara Sea and its surroundings. *Mar. Geol.*, **190**, 493–529.

Yaltırak, C., Sakinç, M., and Oktay, F. (2000). Westward propagation of North Anatolian fault into the northern Aegean: Timing and kinematics: Comment and Reply. *Geology*, **28**(2), 187.

Yogodzinski, G., Lees, J., Churikova, T., Dorendorf, F., Wöerner, G., and Volynets, O. (2001). Geochemical evidence for the melting of subducting oceanic lithosphere at plate edges. *Nature*, **409**(6819), 500.

Yönlü, Ö., Altunel, E., Karabacak, V., and Akyüz, H. S. (2013). Evolution of the Gölbaşı basin and its implications for the long-term offset on the East Anatolian Fault Zone, Turkey. *Journal of Geodynamics*, **65**, 272–281.

Zabcı, C. (2012). *The 5 ka morphochronological slip-rate history and the paleoseismicity of the Ilgaz - Karlıova section of the North Anatolian Fault, Turkey*. Ph.D. thesis, İstanbul Technical University.

Zachariasse, W., van Hinsbergen, D., and Fortuin, A. (2008). Mass wasting and uplift of Crete and Karpathos during the early Pliocene related to initiation of south Aegean left-lateral, strike-slip tectonics. *GSA Bulletin*, **120**(7-8), 976–993.

Zahradnik, J., Gallovic, F., Sokos, E., Serpetsidaki, A., and Tselentis, A. (2008). Quick fault-plane identification by a geometrical method: Application to the Mw 6.2 Leonidio earthquake, 6 January 2008, Greece. *Seismol. Res. Lett.*, **79**, 653–662.

Zhu, H., Bozdağ, E., and Tromp, J. (2015). Seismic structure of the european upper mantle based on adjoint tomography. *Geophys. J. Int.*, **201**, 18–52.

Zitter, T., Woodside, J., and Mascle, J. (2003). The Anaximander Mountains: a clue to the tectonics of southwest Anatolia. *Geol. J.*, **38**, 375–394.

# Curriculum Vitae

| | |
|---|---|
| **26 Jul 1980** | Born in İstanbul |
| **1999 - 2003** | B.Sc in Mining Engineering,<br>Istanbul Technical University, Turkey<br>*cum laude* |
| **2002 - 2005** | B.Sc in Geological Engineering,<br>Istanbul Technical University, Turkey |
| **2003 - 2006** | M.Sc in Geodynamics,<br>Istanbul Technical University, Turkey |
| **2006 - 2007** | Researcher,<br>Eurasia Institute of Earth Sciences, Turkey |
| **2007 - 2012** | Ph.D student in Tectonophysics group,<br>Utrecht University, the Netherlands |
| **2012 - 2014** | Engineer,<br>Boğaziçi University, Turkey |
| **2004 - 2018** | Manager<br>Turkish Foundation for Combating Soil Erosion, Reforestation and Protection of Natural Habitats, Turkey |